



HAL
open science

Competition between normal and transformed cells

Sarah Moitrier

► **To cite this version:**

Sarah Moitrier. Competition between normal and transformed cells. Physics [physics]. Paris Sciences et Lettres, 2017. English. NNT: . tel-04058138

HAL Id: tel-04058138

<https://hal.science/tel-04058138v1>

Submitted on 4 Apr 2023

HAL is a multi-disciplinary open access archive for the deposit and dissemination of scientific research documents, whether they are published or not. The documents may come from teaching and research institutions in France or abroad, or from public or private research centers.

L'archive ouverte pluridisciplinaire **HAL**, est destinée au dépôt et à la diffusion de documents scientifiques de niveau recherche, publiés ou non, émanant des établissements d'enseignement et de recherche français ou étrangers, des laboratoires publics ou privés.

THÈSE DE DOCTORAT

de l'Université de recherche Paris Sciences et Lettres
PSL Research University

Préparée à l'Institut Curie

Compétition entre populations de cellules normales et transformées

Ecole doctorale n°564

Physique en Ile-de-France

Spécialité Physique

Soutenue par **Sarah MOITRIER**
le 1^{er} décembre 2017

Dirigée par **Isabelle BONNET & Pascal SILBERZAN**

COMPOSITION DU JURY :

M. BORGHI Nicolas
CR CNRS, Rapporteur

M. CAPPELLO Giovanni
DR CNRS, Rapporteur

Mme WILHELM Claire
DR CNRS, Présidente du jury

Mme PIDDINI Eugenia
University of Bristol, Membre du jury

M. DESTAING Olivier
CR CNRS, Membre invité

M. SILBERZAN Pascal
DR CNRS, Directeur de thèse

Mme BONNET Isabelle
MCU UPMC, Co-directrice de thèse



Résumé

Lors du développement d'une tumeur au sein d'un tissu, les cellules cancéreuses se retrouvent entourées par les cellules saines. Les interactions entre ces deux types cellulaires, transformé et normal, jouent un rôle important dans le devenir de la tumeur, mais restent à ce jour mal comprises. L'objectif de cette thèse a été de mettre en place des systèmes *in vitro* qui permettent d'étudier les interactions entre une population de cellules normales et une population de cellules transformées.

Nous avons tiré profit d'une lignée de cellules épithéliales sensibles à la lumière, élaborée par Olivier Destaing (IAB, Grenoble). Lorsqu'elles sont exposées à la lumière bleue, ces cellules suractivent la protéine Src, connue pour être surexprimée dans de nombreux cancers. Sinon, elles gardent un phénotype normal. L'utilisation de ces cellules, appelées "OptoSrc", combinée à un dispositif optique, permet de créer des tissus mosaïques dans lesquels le motif des cellules mutées est déterminé par le motif d'illumination bleue. Notre système présente plusieurs avantages : le contrôle dans le temps et dans l'espace du motif de cellules transformées, mais aussi l'activation graduelle et réversible de l'oncoprotéine.

Nous avons montré qu'en illuminant dans le bleu un îlot circulaire de cellules au sein d'une monocouche OptoSrc, les cellules activées s'extrudent collectivement, donnant naissance à un agrégat tri-dimensionnel cohésif surplombant la monocouche. Nous pouvons contrôler la taille et le temps d'apparition de ce sphéroïde en ajustant respectivement l'aire éclairée et la fréquence d'illumination. De plus, ce phénomène d'extrusion collective est réversible lorsque le stimulus de lumière bleue s'arrête. Finalement, nous avons montré que la formation de cet agrégat s'accompagne d'une diminution des E-cadhérines à la membrane, et de l'apparition de la vimentine, pour les cellules éclairées. Nos résultats suggèrent qu'un groupe de cellules surexprimant la protéine Src, au sein d'une monocouche de cellules normales, subit une transition épithéliale-mésenchymateuse partielle.

Abstract

During the development of a tumour in a tissue, the cancer cells are surrounded by healthy cells. The interactions between these two cell types, transformed and normal, play an important role in the tumour stability, but remain to this day poorly understood. The aim of this thesis was to establish *in vitro* assays to study the interactions between populations of normal and transformed cells.

We benefited from a light-sensitive cell line, constructed by Olivier Destaing (IAB, Grenoble). When they are exposed to blue light, these cells overactivate the protein Src, which is known to be overexpressed in many cancers. Otherwise, they keep a normal phenotype. Using these cells, called "OptoSrc", in combination with an optical setup, we are able to create mosaic tissues in which the pattern of mutated cells is determined by the blue illumination pattern. Our system has several advantages: a selective control in time and space of the group of transformed cells, and a gradual and reversible activation of the oncoprotein.

We have shown that when we illuminate a circular islet of cells from a monolayer of OptoSrc cells, the activated cells were collectively extruded, resulting in a cohesive three-dimensional aggregate on top of the monolayer. We can control the size and appearance time of this spheroid by tuning, respectively, the area and frequency of illumination. Besides, this collective extrusion is reversible when the blue light stimulation is stopped. Finally, we have shown that the formation of this three-dimensional aggregate coincides with the loss of E-cadherin at the membrane, as well as the apparition of vimentin, for the illuminated OptoSrc cells. Our results suggest that a group of cells overexpressing the protein Src, in a monolayer of normal cells, undergoes a partial epithelial-to-mesenchymal transition.



Acknowledgements

This work would not have been possible without the guidance of my thesis supervisor Dr Isabelle Bonnet, the help of my colleagues and the support of my family and friends. A PhD thesis is about so much more than just science, and I want to take the opportunity here to thank all the people who contributed to making it a rich and fruitful experience.

I would first like to thank Pascal for welcoming me in the team, supervising my internship, and giving me the opportunity to stay for my PhD, under the supervision of Isabelle.

I am grateful to Isabelle in many ways, which I will have to summarize in the interest of space (and dignity). I want to thank her for designing this great project from scratch, for trusting me to take on the challenge, and for guiding me these past three years. I particularly appreciated her straightforward ways, and our discussions on many topics, which taught me a great deal about both scientific research and life in general. Isabelle has shown a curiosity, a determination, and an efficiency at work I will strive to emulate in the future. It has been an honor to be her first PhD student.

The members of the PBME team have contributed immensely to my personal and professional time in the lab. Besides Pascal and Isabelle, I would like to thank Axel for his sharp and relevant comments in group meetings, as well as his technical expertise on the bench, Sylvie for her kind help, and all my fellow PhD students, post-docs and interns, for creating a unique and enjoyable work environment. I am especially grateful to Simon, Guillaume and Hannah, who constituted the team during my internship and the beginning of my PhD. They not only trained me, but also made these trying and uncertain times a pleasure to come to work every day.

I am grateful to the members of my thesis advisory committee, Mathieu Coppey, Martial Baland, and Olivier Destaing, for their time, interest, and helpful advice along the way.

I would like to thank the members of my jury, Nicolas Borghi, Giovanni Cappello, Claire Wilhelm, and Eugenia Piddini, for reviewing this manuscript and for a stimulating discussion at the defense. There are still many questions to answer on this project (and many more to ask!), and it is exciting to know that this is only the beginning.

On this note, I would like to thank Nastassia for deciding to join the team to follow up on this project, and also for proofreading this manuscript.

I gratefully acknowledge our collaborators from IAB Grenoble, who designed and constructed the OptoSrc cell line: Adèle, Christiane, and especially Olivier. The joy and enthusiasm he has for his research was contagious and motivational all along these three years. Thanks also for enlightening us physicists on the biological aspects of the project.

My time at Curie was made enjoyable in large part due to the many friends and colleagues I made along the way, and to the stimulating discussions we had, on a professional as well as

a personal level. I would thus like to thank all my fellow labmates from UMR 168, including but not limited to: Céline, Simon, Perrine, Mélanie, Anne-Marie, Sarah Jr, John, Tatiana, Mohamed, Chiara, Quentin, Bastien, Floriana, Patricia, Alicia, Laura, Valentina, Aude, Floriane and many more. Special mention to my office-mates, Antoine & Ajay, and to my ballet-mate Marie.

The Curie Institute is a truly exceptional environment to do research in, not least because of the access we have to great equipment and expertise. I gratefully acknowledge Fanny for her guidance on cell culture, Olivier & Olivier from the BDD imaging platform, for their invaluable help with the microscopes and Imaris software, Eric & Rémy of the mechanical workshop for their frequent and very efficient help with all things mechanical.

I would like to thank my microscopes for working properly whenever they did, and for teaching me how to fix a microscope, whenever they didn't. I would also like to thank Andor for their valuable demonstration that self-reliance is sometimes the best option.

I am especially indebted to the Institut Pierre-Gilles de Gennes (IPGG) for providing me with funding, lab equipment, and a friendly work environment.

I greatly acknowledge the whole administrative crew from both Curie and IPGG, especially Laurence, Brigitte, Karen, Agnès, Perrine, Mériam, and Manon. Their help navigating the legendary French bureaucracy is deeply appreciated, and saves us precious time as we are eager to go back to our research.

I would like to thank all my friends, particularly friends from ESPCI, who went through this adventure either before me (promotion 128) and provided me with hindsight and encouragement, or alongside myself (promotion 129), and lived through the good, the bad, and the ugly times of it with me — without forgetting our beloved non-doctors who had to endure all the PhD talk these past three years. A special thank you to Charlotte & Hugo for an impromptu defense rehearsal.

I would like to thank all the people who somehow contributed to my ending up here, teachers and mentors, and I would like to mention specifically: Simon Sutter, Hervé Delime, Emmanuel Bougnol, Anabelle Legrix, Sophie Pezet.

I am grateful to my family, especially to my parents, who have always been supportive of my career goals and have made it all possible. I would also like to take this opportunity to thank my new family for welcoming me among them.

Finally, I am infinitely grateful to my husband, Rémi. Everything is made better by sharing it with you, and this PhD thesis was no exception.

List of Abbreviations

4-AP 4-aminopyridine

Aam Acrylamide

ADP Adenosine diphosphate

AMA Antagonistic Migration Assay

ATP Adenosine triphosphate

BIS N,N- methylene bisacrylamide

BSA Bovine Serum Albumin

CAAX Cysteine, Aliphatic Amino acid, any amino acid (X)

DAH Differential adhesion hypothesis

ddH₂O double distilled water

DMD Digital Micromirror Device

DMEM Dulbecco's Modified Eagle's Medium

DMSO Dimethyl sulfoxide

ECM Extracellular Matrix

EDTA Ethylenediaminetetraacetic acid

EGTA Ethylene glycol-bis(β -aminoethyl ether)-N,N,N',N'-tetraacetic acid, also known as egtazic acid

EMT Epithelial to Mesenchymal Transition

FBS Fetal Bovine Serum

FOV Field of view (of a camera)

GFP Green Fluorescent Protein

HEK Human Embryonic Kidney

iRFP near-infraRed Fluorescent Protein

LED Light-emitting diode

MDCK Madin-Darby Canine Kidney

PBS Phosphate Buffered Saline

PDMS Polydimethylsiloxane

PDT Population doubling time

PEG Polyethylene glycol

PI Propidium iodide

PIV Particle Image Velocimetry

pMLC phospho-Myosin Light Chain

ROCK Rho-associated protein kinase

ROI used here for **Region of Illumination** (can otherwise mean Region of Interest)

RSV Rous Sarcoma Virus

SFK Src Family of Kinases

SH2-SH3 Src homology domain 2 (resp. 3)

TFM Traction Force Microscopy

wt wild type

ZO1 Zonula Occludens-1

Foreword

The general context of this project is the study of the interactions between normal and transformed cell populations. In particular, we focused on the creation of an interface between normal and transformed cells in a controlled manner. The current manuscript presents the work that was done in the scope of this thesis, and is divided in five chapters:

- **Chapter 1** is a general introduction setting the framework of this thesis: we first describe epithelial tissues, our model system, and their constituent parts. We then delve into carcinogenesis, the process of cancer formation in epithelia, as well as some of the genes involved in cancer. Finally, we give an account of previous studies on the interactions between normal and transformed cells.
- The experimental techniques used for this project can be found in **Chapter 2**. In particular, we present the optical set-up, dedicated to optogenetics, that was established in the course of this thesis.
- A first approach used to study cell competition between two cell types is presented in **Chapter 3**: we describe the Antagonistic Migration Assay (AMA), in which two cell populations initially separated are confronted in a competition for space.
- **Chapter 4** focuses on the use of a light-inducible oncoprotein to study cell competition. We present the optogenetics-inspired system that was developed during this thesis as a way to create a precisely controlled interface between normal and transformed cell populations. We then show that the overactivation of the protein Src in a subset of cells from a monolayer gives rise to a collective extrusion phenomenon. We investigate this phenomenon, and present evidence that Src-activated cells might be undergoing a partial Epithelial-to-Mesenchymal transition.
- In the last part, **Chapter 5**, we discuss various observations we have made, in order to improve our understanding of the collective extrusion phenomenon.



Contents

1	Introduction	1
1.1	Context of the study	2
1.2	Epithelial tissues and their functions	3
1.2.1	The cytoskeleton	3
1.2.2	Epithelial sheets	5
1.2.3	The apico-basal polarity	5
1.2.4	Cell junctions and adhesions	7
1.2.5	<i>In vitro</i> model of epithelia: monolayer of cultured cells	8
1.3	Carcinogenesis	11
1.3.1	Hallmarks of cancer cells	12
1.3.2	Cancer is a multistep process	12
1.3.3	Genes implicated in cancer	13
1.3.4	Src and Ras	15
1.4	Interactions between normal and transformed cells	18
1.4.1	Cell segregation	18
1.4.2	Cell competition	20
1.4.3	Interactions between normal and transformed cells <i>in vivo</i>	22
1.4.4	Use of an inducible oncogene to create an interface between normal and transformed cells <i>in vitro</i>	23
1.4.5	Interactions between normal and transformed cell populations <i>in vitro</i> : confrontation assay	25
2	Materials and Methods	29
2.1	Cell biology	30
2.1.1	Cell lines	30
2.1.2	Cell culture	31
2.2	Antagonistic migration assays (AMA)	32
2.3	Surface treatment	33
2.3.1	Fibronectin coating	33
2.3.2	Adhesive patterns for cell confinement	33

2.4	Drug inhibitors and inducers	35
2.5	Fluorescence labelling	36
2.5.1	Live cell assays	36
2.5.2	Live F-actin labelling	36
2.5.3	Immunofluorescence staining	37
2.6	Image acquisition	38
2.6.1	Videomicroscopy	38
2.6.2	Confocal microscopy	39
2.7	Photoactivation	39
2.8	Image analysis	42
2.8.1	Mixing index computation	42
2.8.2	PIV	43
2.8.3	Statistical analyses	44
2.9	Traction Force Microscopy	44
3	Antagonistic migration assay	47
3.1	Characterization of the HEK cell lines	49
3.1.1	Population doubling time	49
3.1.2	Traction forces	49
3.1.3	HEK cells develop into monolayers	50
3.2	No spontaneous cell sorting in co-cultures	51
3.3	Antagonistic Migration Assay	53
3.3.1	Free migration of the two populations before the meeting	53
3.3.2	After the meeting, the Ras^{V12} population moves forwards and the wt population goes backwards	57
3.4	What affects the evolution of the interface?	60
3.4.1	Effect of the initial density	60
3.4.2	Effect of the proliferation	60
3.4.3	Effect of the traction forces	62
4	Using optogenetics to study <i>in vitro</i> cell competition	67
4.1	Optogenetics: a control of cell activity using light	69
4.1.1	Why optogenetics?	69
4.1.2	Optogenetic systems	69
4.1.3	The CRY2/CIBN system	71
4.2	MDCK OptoSrc: a cell line expressing a light-inducible Src	74
4.2.1	The OptoSrc system	74
4.2.2	Behaviour of a MDCK OptoSrc cell at the cellular scale	76
4.2.3	Migratory properties of a monolayer of MDCK OptoSrc cells	78

4.2.4	Effect of the blue light stimulus on cell division and cell extrusion	80
4.3	Competition between normal and OptoSrc cells	81
4.3.1	Single OptoSrc cell in a wt monolayer	81
4.3.2	Group of OptoSrc cells in a wt monolayer	83
4.4	OptoSrc & patterned light: optical control of local Src activation	84
4.4.1	Local Src activation in the OptoSrc monolayer	84
4.4.2	Control, in space, of the collective extrusion	95
4.4.3	Control, in time, of the collective extrusion	97
4.4.4	Effect of the initial density on the collective extrusion	101
4.4.5	Molecular basis of the collective extrusion	103
4.4.6	Does the collective extrusion require a frontier between two distinct src-level populations?	105
4.4.7	Is the collective extrusion associated with an Epithelial-Mesenchymal Transition?	107
5	Discussion	111
5.1	MDCK OptoSrc cells' response to a light stimulus is context-dependent	112
5.2	Possible origins of the collective extrusion	113
5.2.1	Do cells follow the light?	114
5.2.2	The mechanical hypothesis	117
5.2.3	The molecular hypothesis	123
	Appendices	129
	A List of Movies	130
	B French Abstract	133

Chapter 1

Introduction

“The most exciting phrase to hear in science, the one that heralds new discoveries, is not “Eureka!” (I found it!), but “That’s funny...”

Isaac Asimov

Contents

1.1	Context of the study	2
1.2	Epithelial tissues and their functions	3
1.2.1	The cytoskeleton	3
1.2.2	Epithelial sheets	5
1.2.3	The apico-basal polarity	5
1.2.4	Cell junctions and adhesions	7
1.2.5	<i>In vitro</i> model of epithelia: monolayer of cultured cells	8
1.3	Carcinogenesis	11
1.3.1	Hallmarks of cancer cells	12
1.3.2	Cancer is a multistep process	12
1.3.3	Genes implicated in cancer	13
1.3.4	Src and Ras	15
1.4	Interactions between normal and transformed cells	18
1.4.1	Cell segregation	18
1.4.2	Cell competition	20
1.4.3	Interactions between normal and transformed cells <i>in vivo</i>	22
1.4.4	Use of an inducible oncogene to create an interface between normal and transformed cells <i>in vitro</i>	23
1.4.5	Interactions between normal and transformed cell populations <i>in vitro</i> : confrontation assay	25

1.1 Context of the study

During the initial stages of cancer, one or several cells undergo a mutation making them precancerous. In most cases, they can be eliminated, if the surrounding tissue recognizes and eliminates this threat to tissue integrity. But they can also go on proliferating, competing with the healthy cells for space and resources, to form a precancerous mass. It is now well admitted that the interactions between tumour cells and their wild-type neighbours are key regulators in tumour progression [1,2]. The aim of this thesis work is thus to study the interactions between normal and transformed cells in a controlled manner. Our model is the monolayer of cells *in vitro*.

In this opening chapter we describe epithelial tissues, as well as some specificities of using epithelial cell monolayers *in vitro*. We then present the process of carcinogenesis, and some of the genes involved in cell transformation. Finally, we give an account of previous studies dealing with interactions between normal and transformed cells.

1.2 Epithelial tissues and their functions

Epithelial tissues are one of the four basic types of tissues constituting the animal body, along with connective, muscle, and nervous tissues. Epithelia line organs and cavities within the body. They form a dynamic barrier to protect these different compartments from each other, or from the external environment. Their other functions include selective absorption, secretion and transport of fluids, as well as sensory responses. In order to perform all these functions, the cells in epithelial tissues adopt a characteristic structure: they are strongly cohesive and display a well-established polarity between their inner and outer sides, called the apico-basal polarity. We will first present the internal architecture of epithelial cells before describing their specific tissue-scale structure.

1.2.1 The cytoskeleton

Although we mention only epithelial cells, the cell architecture described here is common to almost all animal cells.

The ability of epithelial cells to maintain their shape and internal organization depends on their cytoskeleton: a set of protein filaments that extends throughout the cytoplasm. This intricate network of filaments also provides the mechanical support that enables the cells to carry out essential functions, such as division and movement. The cytoskeleton is a highly dynamic structure, constantly rearranging itself in response to changes in the state of the cell. It attaches to the cell environment through substrate adhesions and cell-cell junctions (section 1.2.4).

The three types of protein filaments that form the cytoskeleton are: actin filaments, intermediate filaments, and microtubules (Figure 1.1):

- Actin filaments are formed through the polymerization of actin monomers into polar helical filamentous structures. These are dynamic structures that grow by polymerization at one end (called the (+), or barbed, end) and shrink by depolymerization at the other end (called the (-), or pointed, end). Actin filaments can also assemble into larger structures with the help of cross-linking proteins which organize actin into gel-like networks and bundles. The dynamic organization of actin filaments mediates cell migration by forming protrusive structures at the leading edge. These protrusions are composed of armlike structures called lamellipodia and filopodia. Reviewed in [3].
- Intermediate filaments are made of many long strands of proteins twisted together, giving them high tensile strength. These strong rope-like structures form a network throughout the cytoplasm, around the nucleus and out to the cell periphery, playing a major role in the stability of the cytoskeleton. They enable cells to withstand the mechanical stress that occurs when cells are stretched. Reviewed in [4].

- Microtubules are hollow tubes of tubulin that can rapidly disassemble in one location and reassemble in another. They are typically nucleated from a small structure near the center of the cell called the centrosome, which is the microtubule organizing center. They grow out from this center toward the cell periphery, and create a system of tracks within the cell, along which vesicles, organelles, and other cell components can be transported by motor proteins: kinesins and dyneins. Microtubules also play a crucial role throughout the cell cycle, notably positioning the cell's chromosomes along the mitotic spindle and splitting them into two sets. Reviewed in [5].

The structure and position of these protein filaments in cells are represented in Figure 1.1. All three types of filaments are made of thousands of protein subunits assembled into long threads.

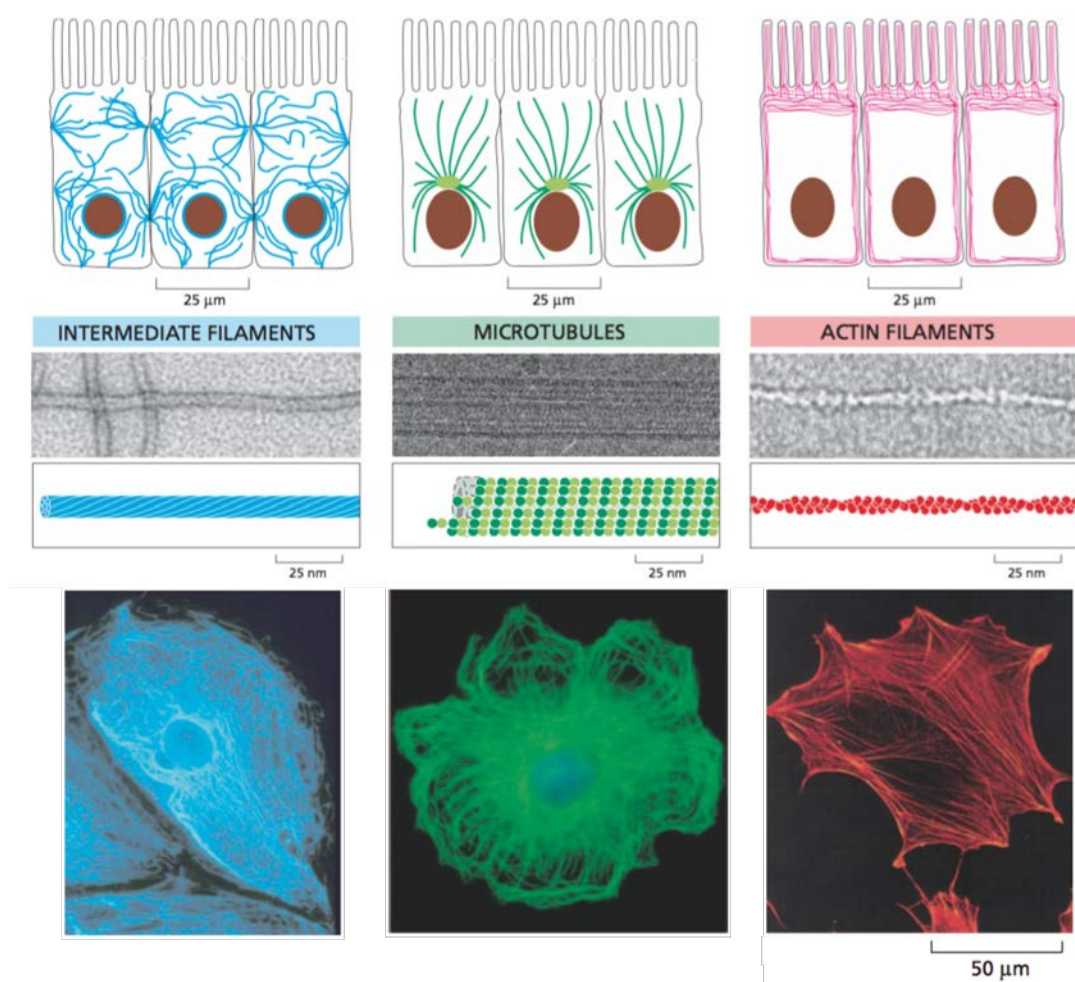


FIGURE 1.1: **The three types of protein filaments that form the cytoskeleton** differ in their composition, mechanical properties, and roles inside the cell. They are depicted here in epithelial cells, but they are found in almost all animal cells. From [6].

1.2.2 Epithelial sheets

Epithelial cells are organized into multicellular sheets, in which the cells are joined together side by side [7]. This sheet can be a simple epithelium, *i.e.* one-cell thick, such as the lining of the gut, or cells can be piled up across several layers in a stratified epithelium, as in the epidermis. The cells themselves can take various forms: they can be tall and columnar, squat and cuboidal, or flat and squamous (Figure 1.2). A given cell sheet contains cells of either a single cell type, or a mixture of different types, surrounded by extracellular matrix.

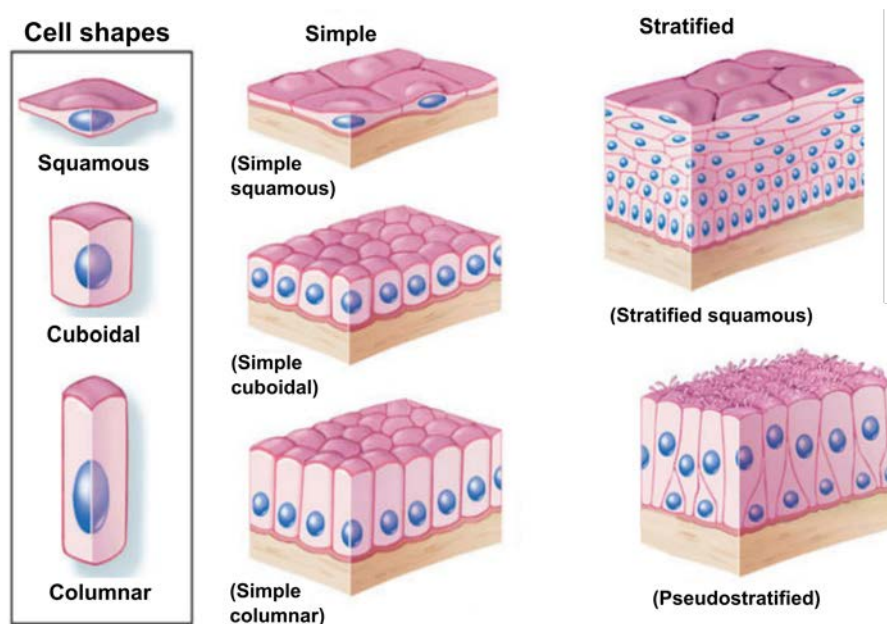


FIGURE 1.2: Different ways of arranging cells to form an epithelial sheet. From [7].

The **extracellular matrix** (ECM) is the non-cellular component present within all tissues and organs, made of extracellular molecules that cells secrete around themselves. The main components of the ECM are water, proteins, and polysaccharides, but each tissue has its own specific composition. The various functions of the ECM include: providing support to the cells, segregating tissues from one another, and regulating intercellular communication. [8]

1.2.3 The apico-basal polarity

Epithelial tissues are characterized by their top and bottom (or inner and outer) faces: the apical surface is in contact with either liquid or air, and the basal surface rests on a layer of connective tissue called the basal lamina. These two faces are intrinsically different, as they serve different functions.

The **apical side** constitutes an exchange interface with other parts of the body. As such, it contains most of the proteins needed for the organs specific roles, such as secretion and absorp-

tion. In order to facilitate these transfers, the exchange surface of some epithelia is enhanced by means of microvilli (Figure 1.3). Most epithelia also bear hair-like structures called **cilia** on their apical side, which can be either motile or nonmotile. Nearly every mammalian cell bears a single nonmotile primary cilium, which acts as an antenna for sensing signals from other cells or fluids nearby [9]. Besides, numerous epithelia in vertebrates are covered with motile cilia, that wave back and forth to move particles out of the body, for example to flush dirt-containing mucus out of the respiratory tract [10].

The **basal side** lies on a basement membrane that separates the epithelium from other tissues. The basal membrane is made up of a thin layer of extracellular matrix, that provides structural support to cells, and influences their behaviour by transmitting external cues, such as chemical and mechanical cues. It also constitutes a reservoir for growth factors, which play an important role in the physiological or pathological remodeling of the basement membrane. The main components of the basal membrane are collagen I and IV, laminin, and fibronectin [11].

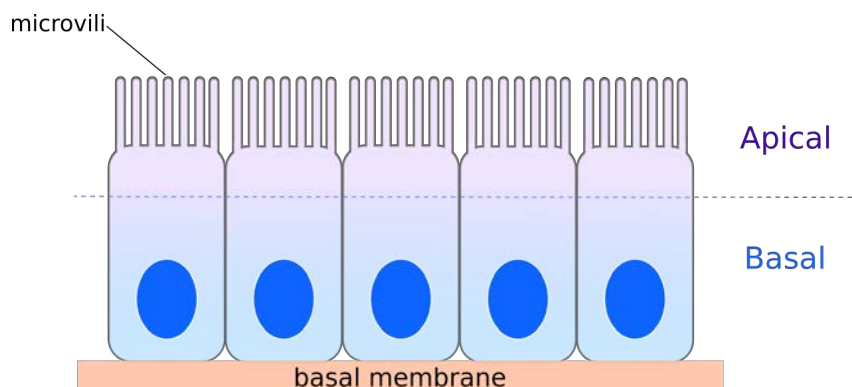


FIGURE 1.3: **Apico-basal polarity.** Schematic of an epithelium arranged in a monolayer, with an apical side in contact with liquid or air, and a basal side lying on the basal lamina.

The establishment and maintenance of apico-basal cell polarity is a complex mechanism, through which cells autonomously build separated specialized domains on their plasma membrane and in their cytoplasm [12]. The preservation of correct cell polarity is crucial for normal cell physiology and tissue homeostasis. Loss of polarity can indeed be observed in pathological situations, such as kidney diseases [13] and cancer [14,15]. In particular, loss of epithelial polarity is involved in Epithelial to Mesenchymal Transition (EMT): a process which can contribute to tumour progression through increased motility and enhanced invasiveness of cells. EMT will be discussed further in section 4.4.7.

In addition to this external organization, this well-established polarity is also reflected in the internal organization of each individual cell: for instance, epithelial cells have distinct molecular components distributed along their vertical axis (Figure 1.4).

1.2.4 Cell junctions and adhesions

A cell is connected to its surrounding environment by direct cell-cell junctions, as well as adhesions to the substrate through the extracellular matrix.

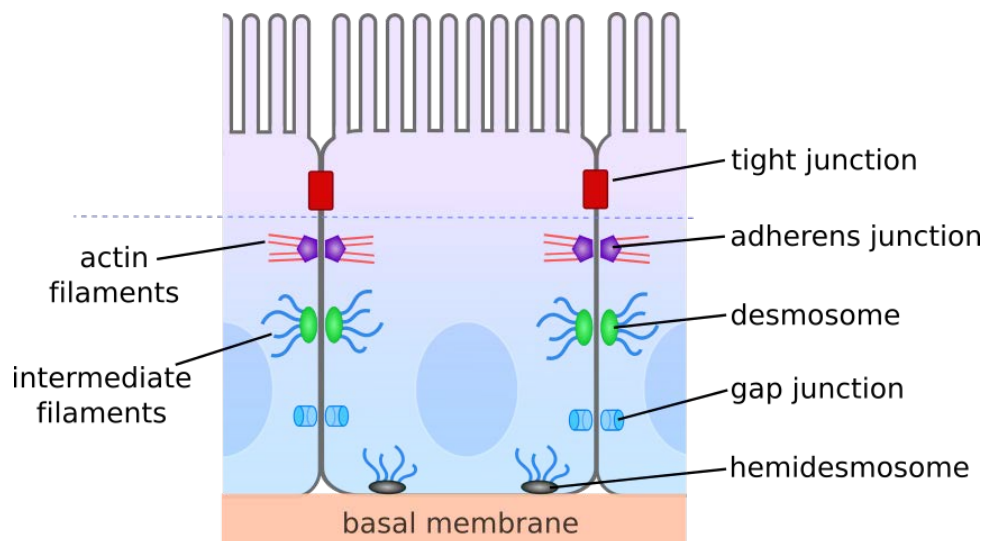


FIGURE 1.4: The different types of cell junctions along the apico-basal polarity axis of an epithelial cell.

Cell-cell junctions

Closest to the apical side of the cells are occluding junctions, or tight junctions (Figure 1.4). They seal the gaps between cells in order to make the tissue impermeable — or selectively permeable. Their role is crucial to form strongly cohesive epithelial tissues that execute their function as barriers in the body. Below these are two types of anchoring junctions: adherens junctions and desmosomes, that connect actin filaments and intermediate filaments, respectively, from one cell to the next. This connection enables them to transmit stress between adjacent cells. Then gap junctions, or more generally communicating junctions, enable cellular communication through chemical or electrical signalling [6].

The main mediators of cell-cell attachment are proteins from the cadherin family: a large family of transmembrane or membrane-associated proteins that mediate cell-cell adhesion in a Ca^{2+} -dependent manner [16–18]. The classical cadherins are E (epithelial)-, N (neural)- and P (placental)-cadherins. Epithelial cells contain large amounts of E-cadherin along their lateral surfaces, chiefly — but not exclusively — at adherens junctions. The structure of a typical epithelial adherens junction is shown on Figure 1.5. The extracellular domain of E-cadherin from two adjacent cells assemble in Ca^{2+} -dependent homophilic bonds. The cytosolic domain of E-cadherin interacts with the actin cytoskeleton by a variety of cytosolic adapter proteins. In one such linkage, the intracellular domain of the E-cadherin binds to β -catenin, which then binds to

α -catenin, itself attached to the actin filaments of the cytoskeleton. More than just a “biological glue”, cadherins regulate force transduction signals between cells [19, 20], and influence many cellular processes. In particular, E-cadherin has a central role in epithelial cell behaviour, tissue formation, cell sorting, and cancer [21–23].

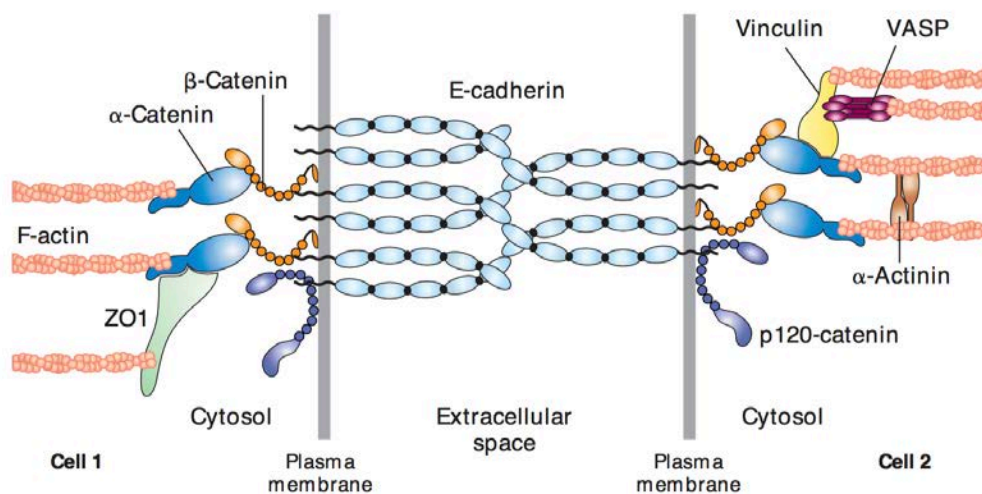


FIGURE 1.5: **Typical adherens junctions.** The cytoplasmic domains of E-cadherin bind directly or indirectly to several adapter proteins that connect the junctions to actin filaments of the cell cytoskeleton. From [24], previously adapted from [25].

Cell-substrate adhesion

As was previously mentioned, epithelia lie on a thin mat called the basal lamina, made up of extracellular matrix (ECM). Cells form adhesions with this underlying ECM through adherens junctions and hemidesmosomes. Cell attachment to the matrix is chiefly mediated by adhesion structures called focal adhesions, which contain proteins of the integrin family [26]. As with cell-cell contacts, adherens junctions tie a cell to its substrate by anchoring actin filaments to the extracellular matrix, this time *via* transmembrane integrin receptors. Hemidesmosomes form contacts between cell and substrate by anchoring intermediate filaments from the cell to the ECM.

1.2.5 *In vitro* model of epithelia: monolayer of cultured cells

Collective cell behaviours are prevalent in living organisms, be it for their development, healing, or even in pathological situations [27]. For these reasons, many studies have been dedicated to understanding how groups of epithelial cells interact and migrate collectively. However, the complexity of these processes make their direct study *in vivo* particularly challenging, not least because potential interactions with the rest of the organism are difficult to uncouple. Thus, *in vitro* strategies on cell lines or primary cells are also employed, as they allow more controlled and systematic experimental conditions.

Advantages and limitations of *in vitro* studies

The major advantage of *in vitro* studies is that it provides a simplified system, making it possible to focus on a subpart of a complex living organism. For example, it can allow researchers to isolate a specific cell line from the various cell types present in the body, or to characterize intermediary steps to a complicated process.

Another advantage of *in vitro* models is that they can be used for high-throughput screening. This can be particularly useful in the context of pharmacology or toxicology: tens of thousands of molecules can be tested as potential drugs for a specific target, using only *in vitro* assays. This has crucial financial benefits as it reduces the number of potentially ineffective preclinical trials conducted on animals or humans.

Besides, *in vitro* techniques can also enable us to directly study human cells, instead of having to extrapolate results from *in vivo* studies on animals.

It must be noted that 2D *in vitro* models differ from *in vivo* situations in several ways, though. For one thing, the various artificial culture substrates can differ from cells natural substrates in their rigidity or their biochemistry, for example. In particular, the glass or plastic substrates often used in culture are more rigid than naturally occurring ECM. But the main limitation of *in vitro* studies is that cells are examined out of their natural environment. The results obtained that way usually cannot be transposed as is to predict their behaviour in a whole organism. But several steps can be taken to cross the gap between the data gathered from *in vitro* experiments and predictions for *in vivo* systems. For example, *in vitro* models can be gradually complexified to include more and more components of the organism, as with organ-on-chip studies [28]. Also, the complexity of complete organisms can be approached with mathematical models, which will be sharpened and quantified by results obtained *in vitro* [29].

Ultimately, 2D *in vitro* systems are a very useful tool, not least because they are flexible and provide simple ways to break down complex systems into individual components. In the present work, we have used mainly the Madin-Darby Canine Kidney (MDCK) cell line [30]. It is a prototypical polarised epithelial cell line, which is widely used as a model to study epithelia. Indeed, they have the benefits of having clear apico-basal polarity, well defined cell junctions, and a rapid growth rate. Plus they are very robust and will polarise both in 2D and 3D cell culture [31]. One drawback of MDCK cells is their canine origin, since it prevents us from using genetic tools that are specific to human cells.

Contact inhibition

In order to fulfill their role as a barrier, epithelial tissues need to be continuous. In cell culture, cells are said to be **confluent** when they cover the culture surface entirely, and there are no

more gaps in the monolayer. They are then subject to **contact inhibition**, a term that refers to two distinct phenomena.

Contact inhibition of locomotion was first described by Abercrombie and Heaysman in the 1950s [32]. They observed that when two cells come into contact, they stop and adjust their direction of migration: they end up moving away from each other to avoid future collision. This is due to the transitory creation of adherens junctions between the two colliding cells, which prevents them from creating protrusion in the area of contact. Protrusions are therefore created outside of this contact zone, leading to migration in another direction [33,34]. Although this description of contact inhibition of locomotion is accurate for isolated cells coming into contact, it is not entirely suitable to the case of a confluent epithelium. When cells occupy the entire surface, there is no free space left for cells to migrate away from each other: contact between cells is unavoidable. Hence, any internal movement should disappear in the monolayer, which is not the case. Instead, the velocity inside a confluent monolayer decreases as cell density increases, but some cellular motion is still observed [35].

Contact inhibition of proliferation Once the cells have reach confluence, the epithelial monolayer can fulfill its function as a barrier, and must then self-regulate in order to preserve its integrity, or homeostasis [36]. One classic mechanism involved in maintaining epithelial homeostasis is called contact inhibition of proliferation, whereby cells stop growing altogether. In fact, cells do not stop dividing right after reaching confluence, but only when they reach a specific size limit. In some cell types, this type of contact inhibition is not due to the cell-cell contacts themselves, but to the local density of cells on the substrate [37]. Another homeostatic mechanism is the extrusion of cells from the monolayer, or delamination, to balance crowding in the tissue and keep the cell density constant [38].

Interestingly, some cells can evade contact inhibition of proliferation, such as cancer cells for example [39,40]. Even when the monolayer has reached confluence, and they are in contact with neighbouring cells all around, cancer cells do not stop proliferating or start to delaminate to maintain tissue integrity. Instead, they continue to divide and grow on top of each other (Figure 1.6).

“Normal” and “transformed” cells

For our study, we have used immortalised cell lines. An immortalised cell line is a population of cells that have evaded normal cellular senescence because of mutations, and are thus able to divide indefinitely. These mutations can occur naturally, or be deliberately induced in cells for research purposes. For example, the HeLa cell line was naturally immortalised and obtained from a cervical cancer, while the HEK 293 cell line was generated by introduction of two viral genes partially deregulating the cell cycle (*hTERT* and *large-T*). Such cell lines are useful for

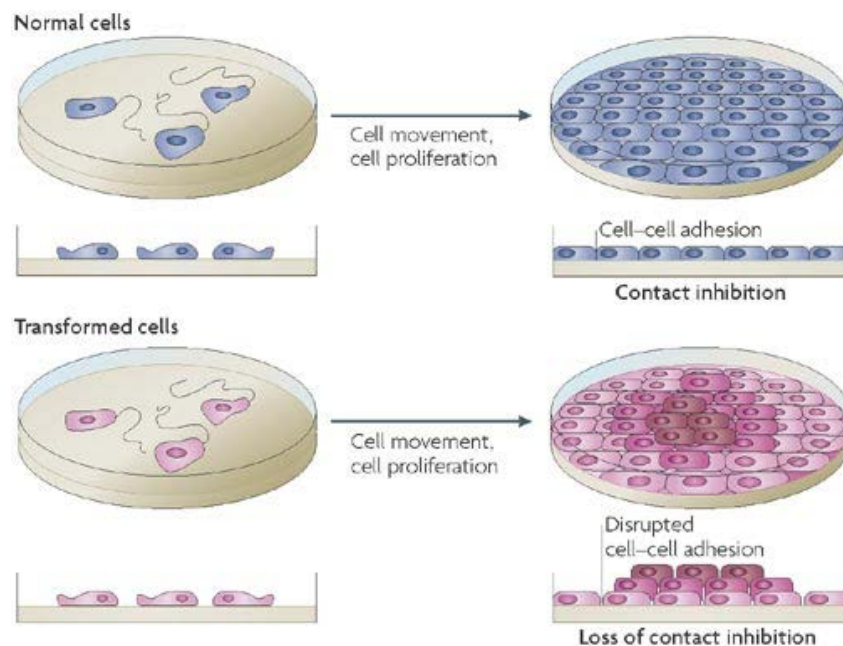


FIGURE 1.6: **Contact inhibition of proliferation.** Normal cells stop dividing when they occupy the entire surface available, but transformed cells continue growing in an uncontrolled manner and pile up on top of the monolayer. From [41].

experimental research, since they can be grown indefinitely in culture, as opposed to primary cells, which have a limited lifetime. The downside is that the biology of these cells is likely altered by the mutations they have undergone to become immortal. It should therefore be kept in mind that the cells we consider as “normal cells” are not strictly “normal”, but an immortalised version of normal cells. This distinction is not so critical since we do not focus on the absolute characteristics of one cell type, so much as in the interactions taking place between these “normal” cells with cells that have undergone another mutation responsible for cell transformation. Cell transformation refers to the process leading to a change in the phenotype of a cell, usually due to genetic alterations. Possible characteristics of transformed cells are genetic instability, immortalisation, aberrant growth control, and tumorigenicity. Indeed, cell transformation usually leads to neoplastic cells, *i.e.* cells that can ultimately become malignant tumour cells, which we will now describe.

1.3 Carcinogenesis

In humans, more than 80% of cancers originate from epithelial tissues such as lung, colon, cervix, and mammary glands [42]. Cancers that develop from epithelial cells are called carcinomas. We will now introduce the process of carcinoma formation, called carcinogenesis, and some of the genes that can be involved in it.

1.3.1 Hallmarks of cancer cells

Cancer cells behave differently than normal cells in the body. Hanahan & Weinberg identified six essential physiological alterations characteristic of tumour cells: the hallmarks of cancer [40,43].

- **Sustaining proliferative signalling.** While normal cells need growth-promoting signals in order to proliferate, cancer cells prove to be self-sufficient in growth signals. For instance, normal cells stop dividing in a growth factors-depleted medium, whereas cancer cells divide even in the absence of growth factors. They can manage this by increasing their own growth factor production, by stimulating their neighbouring normal cells to provide them with growth factors, or by increasing their own levels of receptor proteins, making them hyper-responsive to low amounts of ambient growth factors.
- **Evading growth suppressors.** Cancer cells have the ability to evade programs that negatively regulate cell proliferation. Failure to obey contact inhibition of proliferation, as previously mentioned, is one example of this ability.
- **Resisting cell death.** Cancer cells fail to undergo programmed cell death, or apoptosis, under conditions when normal cells would, such as in the case of DNA damage beyond repair.
- **Enabling replicative immortality.** In general, human cells can only go through about 40 to 60 division cycles before they become senescent, *i.e.* before they lose the ability to divide, and ultimately die. Indeed, repeated cell divisions shorten telomeres, which are the caps protecting the end of chromosomes. When telomeres are too short to protect the chromosomes correctly, senescence or apoptosis can be induced, stopping the cell from dividing [44]. Cancer cells, on the other hand, can potentially replicate indefinitely. They do this by overexpressing telomerase, an enzyme that maintains telomere length.
- **Inducing angiogenesis.** Tumours are able to induce the development of new blood vessels in their vicinity, in order to attract nutrient and oxygen to sustain themselves.
- **Activating invasion and metastasis.** Finally, cancer cells acquire the ability to detach from a tumour and invade other tissues of the body. There, they can settle down again and potentially start new tumour masses, called metastases.

1.3.2 Cancer is a multistep process

Cancer is a genetic disease. But while most other genetic diseases arise from a single mutation, cancer requires the accumulation of several mutations. This is known as the ‘multi-hit’ model of cancer induction, which was first described by Vogelstein *et al.* about 25 years ago [45].

In this model, the first step is **initiation**, where a mutation first occurs in a single cell. In

the following step, called **promotion**, the growth and proliferation of this mutated cell can be enhanced by compounds called promoters. This creates a colony of daughter cells that carry the original mutation. One of these descendant cells later undergoes a second mutation, which can give rise to a small benign tumour. One cell from this benign tumour will then acquire a third mutation, which will be passed on to an even larger group of progeny cells. This accumulation of mutations is referred to as tumour **progression**, a step during which the tumour, still benign, expands in size. Eventually, one cell will accumulate enough mutations, or hits, to make it malignant. This results in a malignant tumour: a group of cells dividing excessively, able to invade surrounding tissues and metastasize to other organs, a process called **metastasis**. This multistep model of carcinogenesis explains, in particular, why the frequency of most cancers increases with age: age merely provides the time necessary for an individual to accumulate enough mutations to cause malignant tumours.

To further understand this multistep process, *in vitro* studies were carried out in an attempt to reproduce cell transformation. In particular, gene transfer experiments provided evidence that cells cannot be transformed by any kind of combinations of gene mutations: these have to act in complementary ways. This is due to the fact that cells employ several pathways in a redundant manner to regulate their growth, so that damage in more than one pathway is necessary to induce abnormal growth [46]. Thus, two gene mutations disrupting two distinct pathways can be complementary and trigger cell transformation, whereas two genes acting on the same pathway might not. For example, overexpression of the oncogene *c-myc* in cells can induce neoplastic growth, but causes cells to undergo apoptosis in serum starved conditions. However, when these cells also overexpress *bcl-2*, a gene regulating apoptosis, they can be rescued from such premature death. *c-myc* and *bcl-2* are thus said to have synergistic effects for cell transformation [47, 48]. Figure 1.7 shows a simplified illustration of a series of mutations acting on distinct cell cycle pathways, resulting in a cancerous transformation.

There are three main types of mutations implicated in cancerous transformation, which we will describe now.

1.3.3 Genes implicated in cancer

The genes involved in cancer induction belong to three main classes: proto-oncogenes, tumour-suppressor genes, and genome maintenance genes [24]. These genes encode many types of proteins that help control cell growth and proliferation.

Proto-oncogenes are positive cell cycle regulators: their normal function is to promote cell survival or proliferation. These genes can be overactivated in cancer, thus allowing unregulated cell proliferation and survival. The overactive forms of proto-oncogenes are called **oncogenes**. For example, the *ras* gene is a proto-oncogene encoding a protein Ras that promotes cell division,

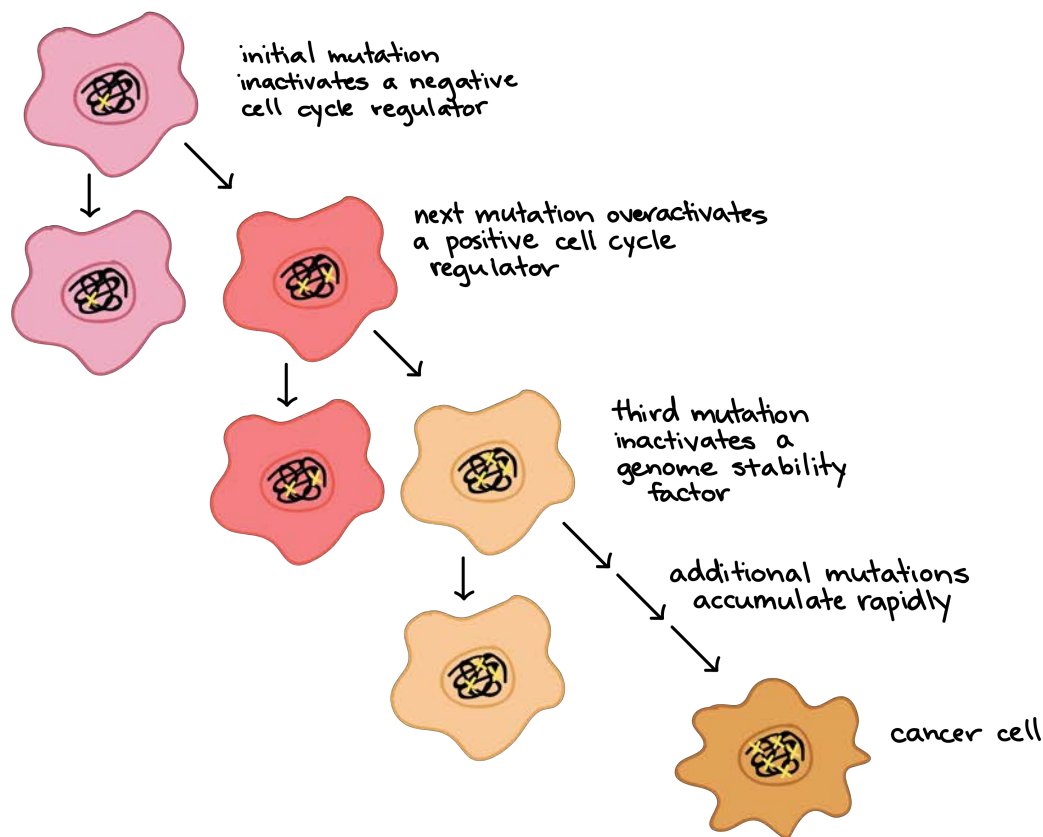


FIGURE 1.7: Hypothetical series of mutations leading to cancer. From [49].

and a mutant called Ras^{V12} derived from *ras* is an oncogene whose protein product leads to uncontrolled proliferation-promoting signals [50].

Tumour-suppressor genes are negative cell cycle regulators: their normal function is to inhibit cell survival or proliferation. A down-regulation of these genes can be observed in cancer cells, allowing them to grow in an uncontrolled way. Tumour suppressor genes generally inhibit cell cycle progression or induce apoptosis when they recognize that a cell is not healthy or fit. One of the most notorious tumour suppressors is **p53**, which is a key player in the cellular response to DNA damage. Its function is to detect DNA damage and, if need be, halt the cell cycle for as long as it takes to repair the cell's DNA. If the DNA is damaged beyond repair, p53 then triggers apoptosis so that the damaged DNA does not get transmitted to the daughter cells. If p53 is faulty, a cell with damaged DNA may continue proliferating, and mutations due to unrepaired DNA get passed on to the progeny cells [51].

Genome maintenance genes encode enzymes that repair DNA, or maintain the integrity of the chromosomes, following DNA damage. Mutations in these genes can lead to uncontrolled cell proliferation and accumulation of additional mutations.

The cell lines that were provided by our collaborators for this thesis work involve two oncogenes: *src* and *ras*, coding for the proteins Src and Ras.

1.3.4 Src and Ras

Src

In 1911, Peyton Rous first described a virus that appeared to cause transmissible growth of tumours in chicken [52], an idea that was controversial because, by then, cancers were not thought to be caused by infectious agents. These doubts were resolved in the 1950s when it was demonstrated that a Rous sarcoma virus (RSV)-induced tumour could indeed produce infected tumour cells [53–55]. An RSV gene named *v-src* was then identified in the 1970s in the genome of this virus [56, 57]. The cellular counterpart of this oncogene, *c-src* [58], is involved in a wide range of human cancers [59]. The protein product of the *c-src* gene, Src, belongs to the Src Family of Kinases (SFKs), a group of non-receptor tyrosine kinases [60, 61], and is expressed ubiquitously in all cell types. Each Src family protein contains an N-terminal membrane anchor, a unique region specific to each protein, an SH2 and an SH3 domain (Src Homology 2 and 3), a tyrosine kinase domain (or catalytic domain), and a C-terminal region (Figure 1.8) [62].

The activity and biological function of Src are regulated by phosphorylation in two major tyrosine sites, called Tyr416 and Tyr527 (also referred to as Y416 and Y527). While phosphorylation of Tyr416 results in activation of Src, phosphorylation of Tyr527 results in its inhibition (Figure 1.8) [63–65].

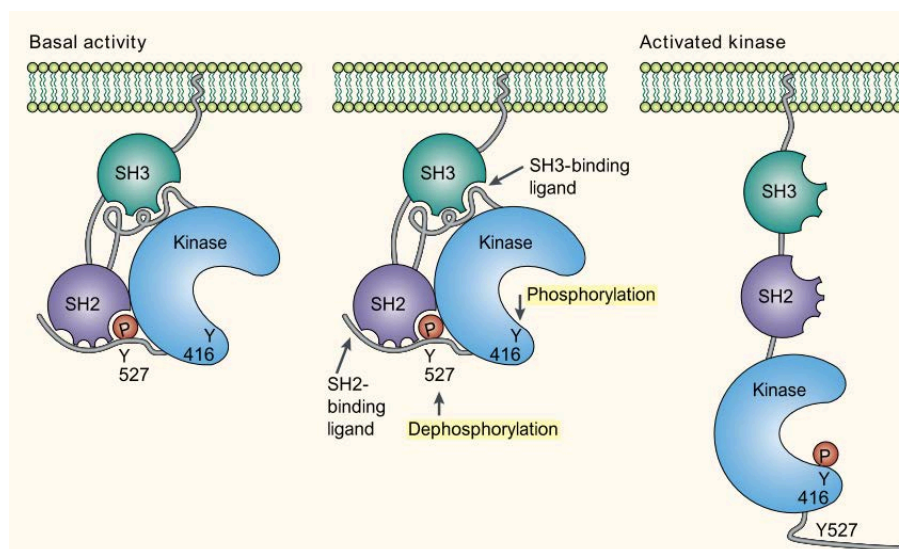


FIGURE 1.8: **Activation of c-Src.** **Left:** inactive conformation of Src. Tyr527 interacts with the SH2 domain, positioning the SH3 domain to interact with the linker between the SH2 and catalytic domains. **Middle:** Different mechanisms involved in the activation of Src, such as phosphorylation of Tyr416 and dephosphorylation of Tyr527. **Right:** open, or active conformation of Src. From [66].

Src is involved in a wide range of cellular processes, so de-regulation of Src can induce drastic changes in cell phenotype. For instance, increased Src activity has been shown to reduce adhesion between cells [67], to increase the growth rate of cells [68], as well as to regulate actin dynamics [69]. This affects cell migration and can, in turn, facilitate invasion and increase metastatic potential of cells [70]. In particular, v-Src activity is associated with disruption of cadherin-mediated cell-cell adhesions in epithelial cells. For instance, v-Src activity in MDCK cells leads to loss of epithelial organization and gain of invasive potential [71]. In general, considerable evidence implicates elevated expression and/or activity of Src in cancer development [72]. A selection of different mechanisms through which Src activity affects cancer cells is presented in Figure 1.9.

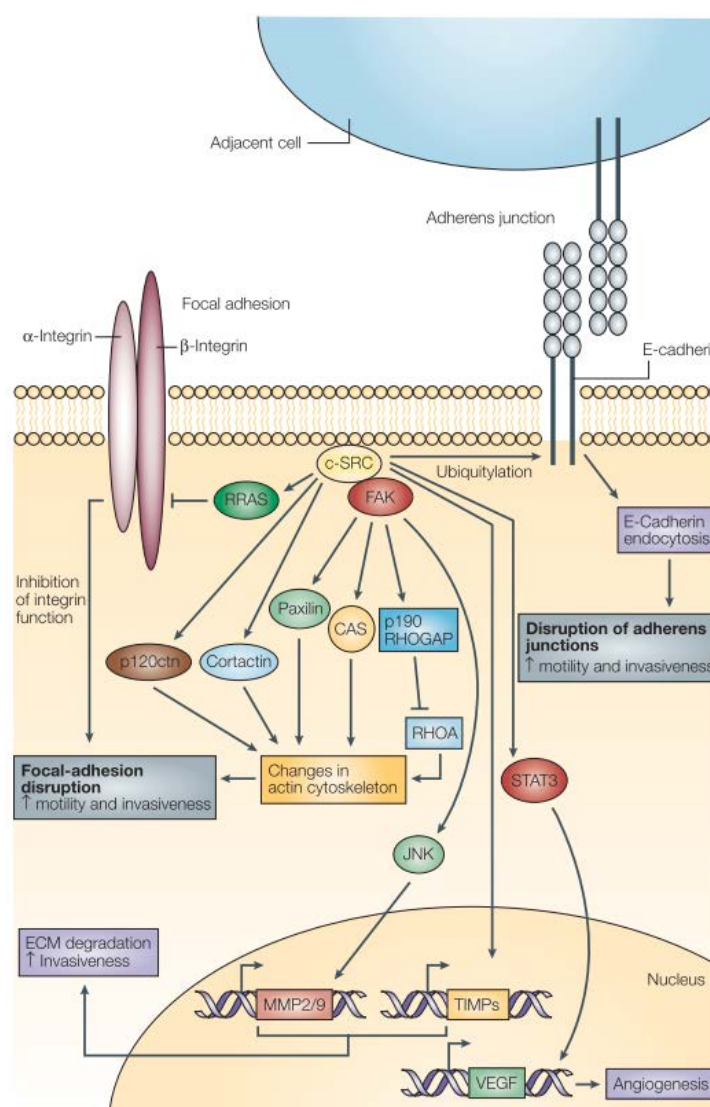


FIGURE 1.9: **Effect of c-Src on tumour-cell behaviour.** c-Src exerts its effects on tumour-cell behaviour through a range of mechanisms mediated by interactions with various substrates and binding partners. A selection of these mechanisms is illustrated here. From [60].

Ras

In 1964, Jennifer Harvey found that another virus was able to induce sarcomas in mice and rats [73]. Discoveries made in the late 1970s and early 1980s found other such retroviruses, and revealed that the transforming activities of the rat-derived Harvey and Kirsten murine sarcoma retroviruses contribute to cancer pathogenesis through a common set of genes, dubbed *ras* (for rat sarcoma) [73–75]. The *ras* genes were then identified as key players in experimental transformation, as well as in human tumour pathogenesis [76, 77]. For example, oncogenic *ras* mutations are found in about 90% of pancreatic cancers [78]. The three closely related mammalian *ras* genes, H-*ras*, K-*ras* and N-*ras*¹, are found mutated in about a quarter of human tumours [50, 79]. In human tumours, mutation at residue 12 is the most common point mutation. Therefore, one of the most studied mutation is the replacement of glycine in position 12 with a valine, also called *Ras*^{V12}. In this study, we have used a cell line bearing the oncogenic mutation *Ras*^{V12} of the H-*ras* gene (section 2.1.1).

The Ras proteins are involved in signal transmission within cells. They belong to a class of proteins called small GTPases, which are enzymes capable of binding and hydrolysing guanosine triphosphate (GTP) into guanosine diphosphate (GDP) [80]. Ras is bound to the cytoplasmic face of the plasma membrane, and acts as a binary switch between an active state (GTP-bound) and an inactive state (GDP-bound). Extracellular signals such as growth factors or hormones can activate receptor tyrosine kinases (RTK), which subsequently switches Ras to its activated state. Activated Ras then regulates several downstream signalling pathways, ultimately influencing cell behaviour (Figure 1.10). Through this process, Ras proteins play a role in the regulation of proliferation, differentiation, apoptosis, and in the cytoskeleton organisation [81, 82].

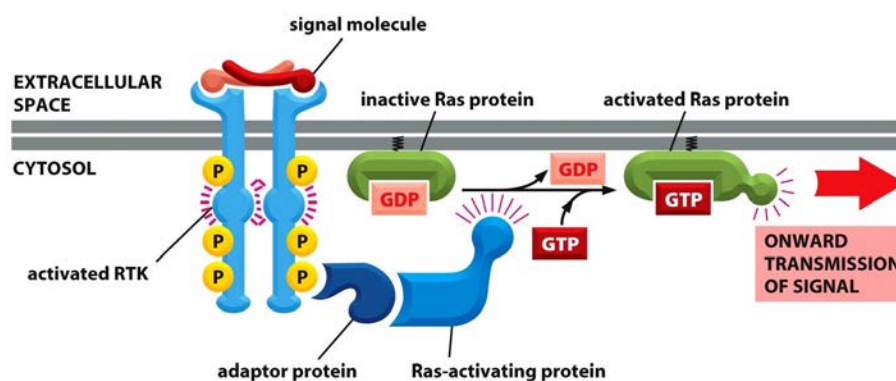


FIGURE 1.10: **Ras proteins are involved in signal transmission within cells.** Extracellular signalling molecules activate receptor tyrosine kinases (RTK), which stimulates Ras to exchange its bound GDP for GTP. The activated Ras protein in turn stimulates several downstream signalling pathways. From [6].

¹H-*ras* and K-*ras* for their respective discoverer Harvey and Kirsten, and N-*ras* for its initial identification in human Neuroblastoma cells.

As we have seen, tumorigenesis rests on several factors. Oncogenes are involved in a wide range of cellular processes, so an oncogenic mutation can upset normal cellular behaviours. But it is now known that these internal factors alone cannot explain the tumour cell phenotype [2, 83]. It is important to study the non cell-autonomous parameters that also come into play. We therefore need to broaden the scope of study to the cell environment and the interactions at the interface between cells of different genotype.

1.4 Interactions between normal and transformed cells

The effects of the mutations in oncogenes and tumour suppressor genes on the phenotype of a cell have been broadly studied [72, 84]. Yet, the properties of entire groups of cells can only be partially described by summing up those of individual cells. A comprehensive understanding of these effects requires to look beyond the single cell level, to integrate the interconnections between cells. Indeed, we should bear in mind that actual cell transformation occurs within normal epithelial sheets and that the transformed cells grow while being surrounded by untransformed epithelial cells. It is now widely accepted that the interactions between transformed cells and their environment, including their neighbouring normal cells, play a crucial role in the evolution of the tumours [1, 2]. The rest of this chapter gives an account of previous studies of interactions between different cell types.

1.4.1 Cell segregation

Putting two different populations of cells in contact generally leads to a phenomenon called cell segregation, or cell sorting, which is a fundamental process in tissue organization [85]. Indeed cell segregation plays an important role in pattern formation, the developmental process through which cells acquire different identities, or fates, depending on their relative position in the embryo. During the development of an embryo, its cells differentiate and acquire their specific functions, to ultimately form distinct organs. The complex arrangement of these organs to form a functioning organism requires a precise organisation of the different tissues and cell types within it. This spatial organisation is achieved in part through cell-cell signalling to guide the building blocks to their designated location. Then, the control of cell movements at the borders between tissue subdivisions is crucial to maintain tissue homeostasis in adult organisms.

Classic studies on the formation of these frontiers lead to the first observations of cell segregation *in vitro* [86–88]. When cells from two distinct tissues were dissociated, mixed together, and allowed to reaggregate, they were found to systematically segregate from each other. The phenomenon of cell segregation has since been widely observed, both in 2D cell monolayers [88, 89] and in 3D cell aggregates [90–92], and can take several forms (Figure 1.11).

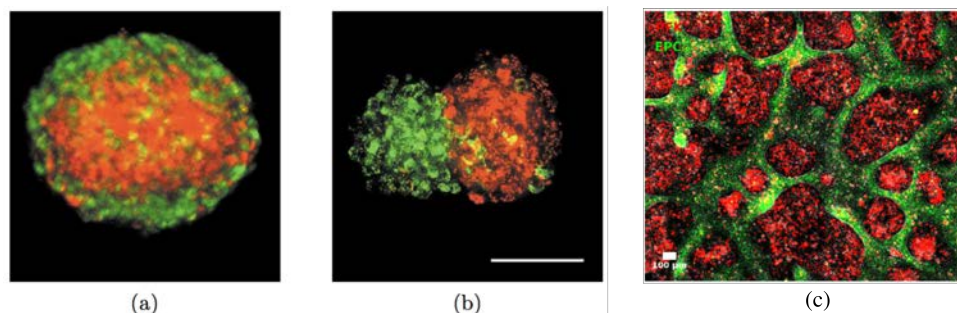


FIGURE 1.11: **Different conformations of cell segregation.** (a)-(b) In 3D aggregates, cells can segregate radially, one cell type surrounding the other (a), or one cell type can form a mound partially capping a mass of the second cell type (b). Scale bar: 100 μm . From [91]. (c) In 2D cultures, cell segregation usually takes the form of clusters of one cell type surrounded by the second cell type (c). Scale bar: 100 μm . From [89].

Early on, studies using this cell reaggregation assay led to the formulation of the Differential Adhesion Hypothesis (DAH) [93]. According to this hypothesis, if adhesions between cells of the same cell type (homotypic adhesions) are stronger than adhesions between two different cell types (heterotypic adhesions), each cell would strive to replace weaker adhesions with stronger ones, by surrounding themselves with cells of the same cell type. Such rearrangements ultimately maximize the total cell-cell binding strength, giving rise to large domains of each cell type, in a conformation minimizing interfacial free energy. The difference in adhesion between two cell types was confirmed to have a strong role to play in cell segregation, in particular *via* cell adhesion molecules from the cadherins family. In particular, both the level of expression of cadherins and their type appear crucial: cell lines expressing different types or different levels of cadherins were shown to spontaneously segregate from each other [91, 94]. Beyond differences in adhesive properties, other mechanisms have since been found to promote cell segregation. For instance, cell segregation can be driven by tension generated by the contraction of actomyosin in the cell cortex [95, 96]. Indeed, Krieg *et al.* have found that actomyosin-dependent cell-cortex tension played an important role in cell sorting in zebrafish embryos [97]. All in all, these studies show that the principal effect leading to cell segregation is an effective **surface tension** between the two cell populations.

In addition to the interfacial tension, another mechanism found to influence cell segregation is collective motion. Belmonte *et al.* have studied cell sorting *in silico* using a self-propelled particle model, and showed that collective motion facilitates cell segregation, compared to a situation in which only the surface tension is considered [98]. Furthermore, Méhes *et al.* have looked at the role played by differences in cell motility. Using keratocytes from distinct animal species in 2D culture, they showed that the relative motility of the two mixed cell types influenced greatly the size and speed of cluster formation [89]. Their results have since been corroborated in a theoretical study by Yang *et al.* [99].

1.4.2 Cell competition

The phenomenon of cell competition was first described in 1975 by Morata and Ripoll in *Drosophila melanogaster* [100], when studying the development of cells bearing a genetic mutation called *Minute* in the imaginal wing disc. They first observed that these mutated cells divided slower than their wild-type counterparts, but ultimately formed a normal-sized organism. Surprisingly, although these slower-dividing cells were viable on their own, they were eliminated when grown in a wild-type fly wing, through what was later shown to be an active process of apoptosis [101]. This phenomenon was named **cell competition**, and has been defined as the short-range elimination by apoptosis of slow-dividing cells (“loser” cells) when in contact with faster growing cells (“winner” cells) (Figure 1.12 (a)). It is important to note that the slow-dividing cells are otherwise viable in a homotypic environment, so that winner and loser cells need to be in contact, or at least in close proximity, and perceive each other to trigger the outcome of the competition. Cell competition has since been described for other genetic mutations and in several other systems, such as mammals, both *in vivo* and *in vitro* [102, 103].

Although the first definition of cell competition was linked to cell proliferation, it has since been shown that differential proliferation is not necessary, nor is it sufficient, to trigger such selection phenomena [104]. For example, clones mutant for the apicobasal polarity component *lgl* (lethal giant larvae) are eliminated from the *Drosophila* wing disc, even though they do not display significant changes in their proliferation rate [105]. Similarly, differences of expression of the *flower* (*fwe*) gene between two cell types can trigger cell elimination without influencing the proliferation [106].

A specific attribute of cell competition is that it is based on the comparison of relative fitness between two neighbouring cell types, and therefore requires a way for cells to communicate their fitness status to each other. This **cellular fitness** is broadly defined as the replicative success relative to competing organisms, *i.e.* the ability of a cell to thrive in a given environment [103, 107, 108]. In particular, the transmembrane protein Flower has been proposed to be a marker for relative cell fitness [106]. Indeed, the expression of several isoforms of the *flower* (*fwe*) gene, such as *loseA* and *loseB*, can act as “fitness fingerprints”, to define the winner or loser status of neighbouring cell types [109].

Cell competition was also linked to cancer formation, since a correlation between cancer genes and competitive cell interactions was observed. In particular, some mutations were shown to provide cells with a proliferative advantage over wild-type cells, a process termed **super-competition** [110]. As opposed to classical competition, in which a mutation reduces the cell fitness, a super-competitor mutation increases the cell fitness compared to normal cells (Figure 1.12 (b)). One of the first contenders for this class of “super-competitor”-inducing genes was the

myc oncogene. Moreno *et al.* studied populations with different levels of dMyc — the *Drosophila* homolog of the human proto-oncogene product cMyc — in the epithelium of the fly wing [111]. They found that competition induced by dMyc is context specific: cells expressing physiological levels of dMyc (*i.e.* normal cells) act as “winner” cells when in contact with cells displaying lower levels of dMyc, but they act as “loser” cells if they are flanked by cells overexpressing dMyc. Therefore, it is not the absolute, but the relative level of dMyc between cells that is a source of competition: cells with lower levels of dMyc are eliminated by apoptosis, whereas cells with higher levels of dMyc overproliferate. These results suggested that dMyc could indeed transform cells into “super-competitors”. Super-competition was thus seen as a tumour-promoting phenomenon, potentially giving cancerous cells the ability to kill normal cells around them and proliferate in their stead [112].

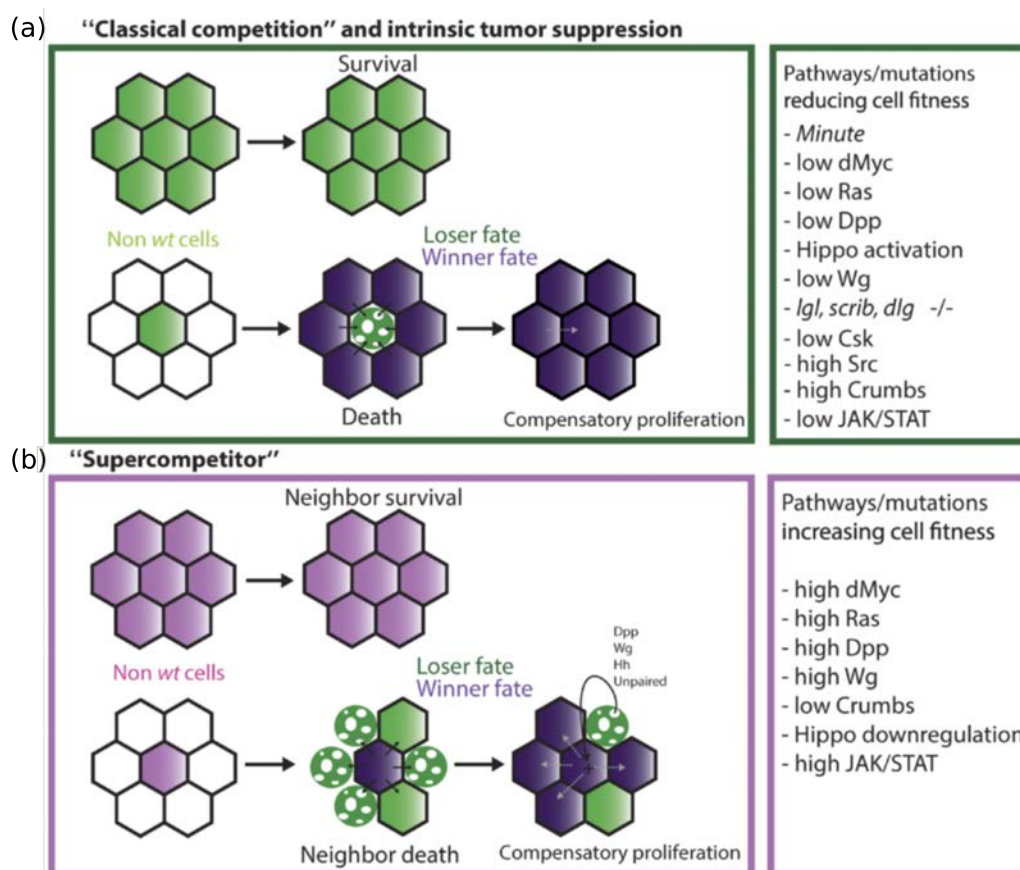


FIGURE 1.12: **Principle of cell competition and super-competition.** (a): “Classical” cell competition. Mutated cells (green) survive in a homotypic environment. If they are surrounded with non-mutated cells (white), they are eliminated and replaced with faster proliferating, or fitter, cells (identified as winner cells, in purple). (b): Super-competition. In a homotypic environment, mutated cells (light purple) do not induce apoptosis of their neighbouring cells. When surrounded with wild-type cells (white), they become the winner cells (dark purple): they eliminate and replace wt cells. From [102].

The notion of **homeostatic pressure** was then introduced to describe theoretically the competition for space between two cell populations [113]. When a cell population grows in a confined space, it will reach a steady state when cell division balances apoptosis. The pressure in the tissue at this steady state defines the homeostatic pressure. In this article, Basan *et al.* show that the ability of one tissue to compete for space with another one, for example in the case of a tumor invading a healthy tissue, is determined by the difference in their homeostatic pressures. They also find that there is a critical size above which a tumour tends to grow, and below which it is more likely to shrink.

On the other hand, several studies have found that cells bearing a pre-cancerous mutation could be eliminated by neighbouring normal cells. Competitive interactions can therefore also hold a tumor-suppressive role, by actively eliminating transformed cells from a healthy tissue, a process called epithelial defence against cancer [114, 115]. Such cases include mutations in proto-oncogenes like Ras [116] and Src [117] (described in section 1.4.4), or tumour-suppressors like Mahjong [118] and p53 [119]. Most of these studies were made with epithelial cells.

These conflicting views of cell competition suggest that normal and transformed cells engage in a bidirectional tug of war, that can lead to either tumour progression or suppression [2]. The interactions between tumour cells and their wild-type neighbours thus appear as key regulators in tumour progression, and have been studied in various systems: both *in vivo* and *in vitro*, at the single cell level as well as on a broader scale. Some of these systems will now be described.

1.4.3 Interactions between normal and transformed cells *in vivo*

In order to create situations where mutated cells are surrounded by a normal tissue, most *in vivo* studies induce the expression of a mutation in a mosaic manner in an embryo (for example in *Drosophila* or zebrafish). This technique consists in inducing genetic modifications in only a subset of cells in a single organism, which allows the study of these genetic changes without being lethal to the organism [120].

In *Drosophila*, Vidal *et al.* [121] showed that single Src-activated cells surrounded by wild-type cells were basally extruded and died by apoptosis (Figure 1.13 (a)). Similarly, Kajita *et al.* [117] showed that extrusion of isolated v-Src expressing cells also occurred in the zebrafish, this time in an apical manner (Figure 1.13 (b)). This was the first *in vivo* demonstration in vertebrates that Src-transformed cells are extruded from the apical side of a normal epithelial monolayer. Also in Fujita's group, Hogan *et al.* expressed Ras^{V12} in a mosaic manner in *Drosophila*, and found that Ras^{V12} -expressing cells were apically extruded from the surrounding normal monolayer [116].

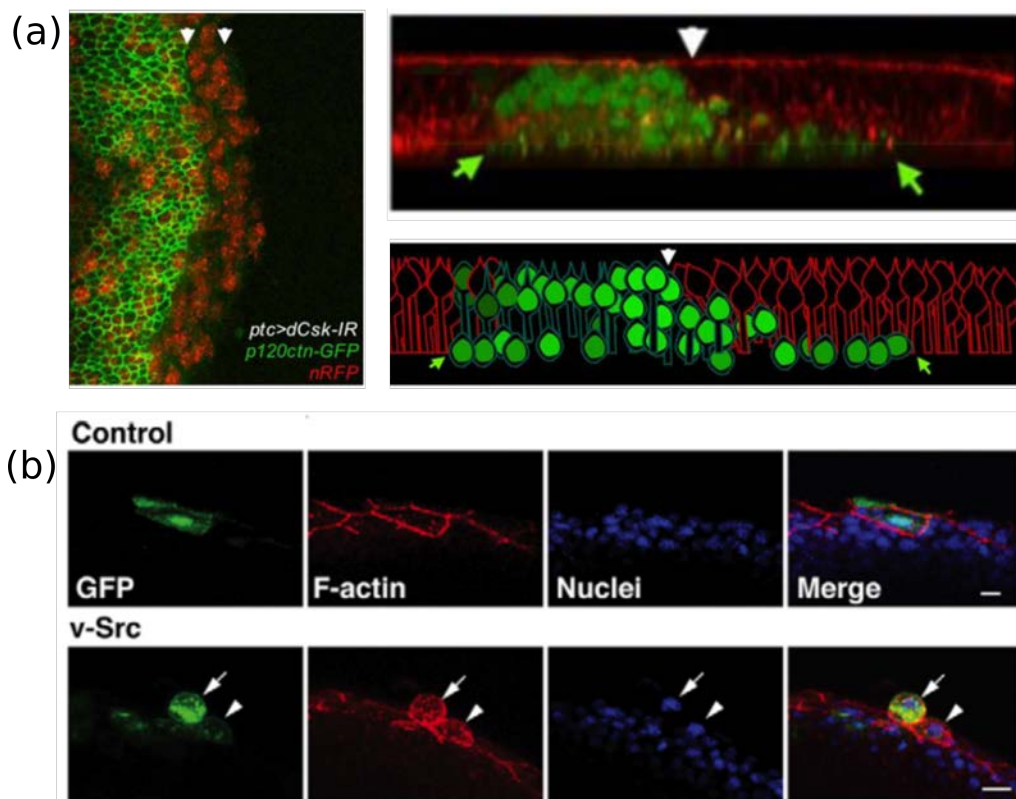


FIGURE 1.13: **Single Src-activated cells are extruded from a wild-type tissue *in vivo*.** (a): Cells deficient in Csk, a negative regulator of the Src family tyrosine kinase, are basally excluded from the boundary layer of a *Drosophila* wing disc. **Left:** Csk-deficient, hence Src-activated, cells (green) are basally excluded and migrate away from the boundary. Normal cells are in red. **Right:** Confocal section (top) and schematic drawing (bottom) of the wing-disc boundary layer, showing Src-activated cells (green) basally excluded from the normal cells of the boundary (red). From [121] (scale bar not provided). (b): Immunofluorescence images of zebrafish embryos injected with the control (top) or v-Src-expressing vector (bottom), stained with phalloidin (red) and Hoechst (blue). An isolated v-Src-expressing cell (green) is apically extruded (arrow). Scale bar: 10 μm . From [117].

1.4.4 Use of an inducible oncogene to create an interface between normal and transformed cells *in vitro*

In parallel, studies of single transformed cells in wild-type tissues were also carried out in cell monolayers *in vitro*. This method makes use of inducible oncogenes: oncogenes that can be induced by an external stimulus such as a temperature shift or antibiotics. The main strategy to create an interface between two different cell types in culture is thus based on statistical mixtures of cells. Cells containing the inducible oncogene are mixed with normal cells at a ratio of 1:100 and cultured until a monolayer is formed. The oncogene activation is then triggered by the appropriate stimulus, revealing a subset of transformed cells in a normal tissue.

Following this technique, Hogan *et al.* used MDCK cell lines expressing constitutively active oncogenic Ras^{V12} in a tetracyclin-inducible manner [116]. Ras^{V12} cells were first labelled with a fluorescent dye and mixed with non-transfected normal MDCK cells at a ratio of 1:100. The mixture of the cells was cultured on a collagen matrix in the absence of tetracycline to form a monolayer. The expression of GFP- Ras^{V12} was then induced by adding the tetracycline, which resulted in isolated Ras^{V12} cells in the monolayer. The authors found that 80% of these single Ras^{V12} cells were apically extruded from the monolayer of normal cells, and that this occurred in an apoptosis-independent manner. Importantly, apical extrusion was not observed when Ras^{V12} cells were cultured homogeneously, suggesting that activation of autonomous Ras signalling pathways alone is not sufficient to induce apical extrusion of Ras^{V12} cells, but that the interaction with the surrounding normal cells is also required. The authors showed that Ras^{V12} cells recognized that they were surrounded by normal cells and modulated their cell shape and cytoskeleton accordingly: increased cell height, accumulated intercellular F-actin, higher levels of phosphorylated myosin light chain (pMLC) of myosin-II. The 20% of Ras^{V12} cells that were not extruded apically formed large, dynamic basal protrusions beneath the surrounding normal cells and eventually delaminated basally and invaded the collagen matrix. This protrusion formation also occurred in a non cell-autonomous fashion.

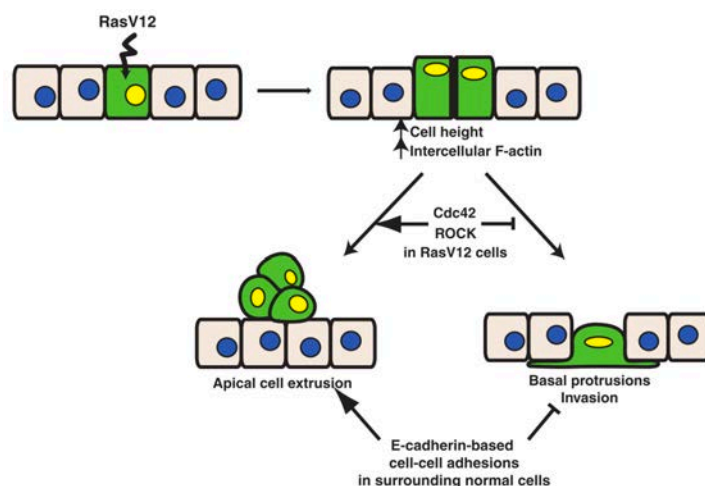


FIGURE 1.14: **Interactions between normal and Ras^{V12} epithelial cells.** Isolated Ras^{V12} cells in a monolayer of normal cells are either apically extruded from the monolayer, or form basal protrusions underneath their neighbouring cells. The fate of the transformed cells is influenced by the activity of Cdc42 and ROCK in the Ras^{V12} cells and by E-cadherin-based cell-cell adhesion in the surrounding normal cells. From [1, 116].

When Ras^{V12} cells were surrounded by E-cadherin-deficient cells, the frequency of basal protrusion and basal delamination of Ras^{V12} cells increased while that of apical extrusion decreased. These results suggest that the fate of Ras^{V12} cells is influenced by E-cadherin-based cell-cell contacts in the surrounding normal cells.

In a similar manner, Kajita *et al.* studied phenomena occurring at the interface between normal and Src-transformed epithelial cells, using MDCK cells that expressed a temperature-sensitive mutant of v-Src (ts-Src) [117]. In this cell line, Src activation is tightly controlled by temperature shifts: the activity of Src is suppressed at the non-permissive temperature (40.5°C), but enhanced at the permissive temperature (35°C). As described for Ras^{V12} cells, Src cells were stained with a fluorescent dye, mixed with normal MDCK cells at a ratio of 1:100 and cultured at 40.5°C (non-permissive temperature) until a monolayer was formed. When Src activation was induced at 35°C, 80% of isolated Src cells were also apically extruded from the monolayer. Importantly, Src cells were not extruded when they were surrounded by an homologous Src monolayer, suggesting that the presence of surrounding normal cells is also required for apical extrusions of Src cells.

In these two studies from Fujita's group, apical extrusion of Src-activated and Ras^{V12} cells shared several common characteristics [122]:

- Apical extrusion of transformed cells occurs only when transformed cells are surrounded by normal cells.
- Apical extrusion of transformed cells occurs in an apoptosis-independent manner.
- Cell height of transformed cells increases before they are extruded from a monolayer.
- Myosin-II is activated in transformed cells surrounded by normal cells and this activation is involved in apical extrusion.

However, Src cells did not form the basal protrusions that were observed in Ras^{V12} cells. These results suggest that these two systems share some common signalling pathways, but other distinct signalling pathways also come into play.

These studies show that a single mutated cell gets extruded from the tissue, but what about a group of cells? What would be the influence of the number of transformed cells, or the group geometry?

1.4.5 Interactions between normal and transformed cell populations *in vitro*: confrontation assay

Wound healing assay

One basic strategy used to place different cell types in contact at a multicellular level is to create a removable physical barrier between two populations. This is usually done through microfabrication of a polydimethylsiloxane (PDMS) stencil. This protocol is based in the injury-free wound healing assay described in [123]: a microstencil contains holes of controlled size and shape, in which cells can be grown until they reach confluence. The stencil is then removed,

thereby releasing new areas for the cells to migrate on (Figure 1.15). Similar stencils are now commercially available from Ibidi (Culture-Inserts 2-Well, described in section 2.2).

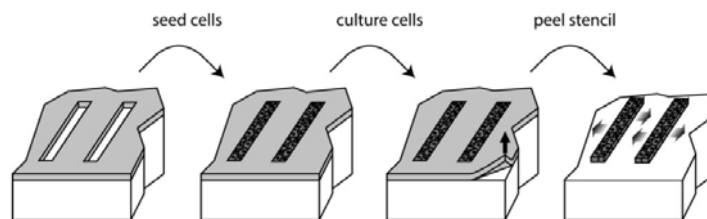


FIGURE 1.15: **Principle of the injury-free wound healing assay.** Cells are cultured on a microfabricated PDMS thin elastic film. When they reach confluence, this microstencil is removed to allow cells to migrate collectively. From [91].

Cell confrontation assay

Such a wound healing assay can be adapted to the antagonistic migration assay of two cell populations. Each cell type is seeded into one of the compartments of a cell culture insert separated by a fixed gap. When the culture insert is removed, cells migrate to close the gap: opposing cells then collide and interact with each other. This cell confrontation assay was used to study the interactions between normal and GFP- Ras^{V12} MDCK cells [124].

In this study, Porazinski *et al.* showed that when Ras^{V12} and normal cells collided, the Ras^{V12} cells collapsed and were repulsed backward, while normal cells continued to migrate forward (Figure 1.16). Besides, after the collision with normal cells, Ras^{V12} cells adopted a contractile morphology and did not mix with normal cells at the border. As a control, the confrontation of two populations of Ras^{V12} cells did not give rise to any repulsion, and cells at the border mingled together, showing that the interaction of two different cell types is needed to trigger a displacement of the interface. Porazinski *et al.* attributed this repulsion phenomenon to an ephrin-dependent mechanism: normal cells are able to detect transformed Ras^{V12} cells through interactions between ephrin-A and its receptor EphA2. These differences in ephrin-A-EphA2 signalling then induce the repulsion of the Ras^{V12} cells. The authors also point out that E-cadherin is involved upstream of ephrin signalling. In particular, they showed that cell repulsion did not occur when Ras^{V12} cells collided with E-cadherin-depleted cells, and that the interface between the two tissues was less well-defined than with normal cells (Figure 1.16). This suggested that the contraction and segregation observed when Ras^{V12} cells collided with normal cells was dependent on E-cadherin-based cell-cell adhesion.

In a recent paper, Taylor *et al.* focused on the role of Eph receptor and ephrin signalling in the repulsion between two cell types, using both computer simulations and experimental assays

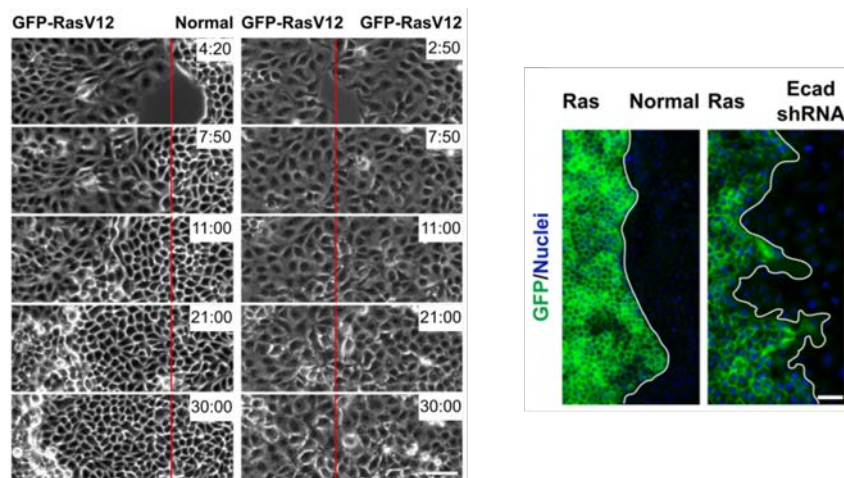


FIGURE 1.16: **Cell confrontation assay between normal and Ras^{V12} cells.** **Left:** Ras^{V12} cells display a backward repulsion when confronted to normal cells but not to another population of similar Ras^{V12} cells. **Right:** Ras^{V12} cells were not repulsed by E-cadherin-depleted cells, and the two tissues interpenetrated each other, instead of forming a clear frontier, as they did with normal cells. Scale bar: 20 μm . From [124].

— such as a confrontation assay between two cell types expressing the EphB2 receptor and its ligand ephrinB1, respectively — [125]. They showed that the repulsive interactions between two cell types drives cell segregation and border sharpening more efficiently than a low level of heterotypic adhesion. They also found that N-cadherin enhanced homotypic cohesion, and must therefore be present in both cell types to promote cell segregation and border sharpening.

In an even more recent paper, from the group of Xavier Trepats, a similar confrontation assay between the same two cell types (expressing either EphB2 or ephrinB1) was used to study the mechanical interactions between these two populations [126]. They highlighted oscillatory traction patterns, which pull cell-substrate adhesions away from the border, and trigger a gradient of intercellular stress. They also observed that deformation waves were generated at the interface between the two cell types and propagated across the populations.

All of these studies on cell confrontation suggest, in every sense, that the interactions between tumour cells and their wild-type neighbours are key regulators in tumour progression. But the precise contribution of these interactions remains poorly understood. In order to study the interactions at the interface between normal and transformed cells, we first need to create situations where these two cell types coexist in a controlled manner. We could then evaluate how different parameters of the environment influence the dynamics of these interfaces. In the following chapters, we will describe the two main strategies we have used to create such controlled interfaces: the antagonistic migration assay (Chapter 3), and the use of a light-inducible oncogene (Chapter 4). We first present the materials and methods used in this thesis work.

Chapter 2

Materials and Methods

“On peut rater une expérience mille fois.
On peut rater mille expériences une fois.
Mais on ne peut pas rater mille expériences mille fois.”

Adapted from La Cité de la Peur

Les nuls.

Contents

2.1	Cell biology	30
2.1.1	Cell lines	30
2.1.2	Cell culture	31
2.2	Antagonistic migration assays (AMA)	32
2.3	Surface treatment	33
2.3.1	Fibronectin coating	33
2.3.2	Adhesive patterns for cell confinement	33
2.4	Drug inhibitors and inducers	35
2.5	Fluorescence labelling	36
2.5.1	Live cell assays	36
2.5.2	Live F-actin labelling	36
2.5.3	Immunofluorescence staining	37
2.6	Image acquisition	38
2.6.1	Videomicroscopy	38
2.6.2	Confocal microscopy	39
2.7	Photoactivation	39
2.8	Image analysis	42
2.8.1	Mixing index computation	42
2.8.2	PIV	43
2.8.3	Statistical analyses	44
2.9	Traction Force Microscopy	44

2.1 Cell biology

2.1.1 Cell lines

Most of the cell lines used in this thesis were acquired thanks to collaborations: the HEK cell lines used in Chapter 3 came from the team of Jaques Camonis (U830 INSERM and Institut Curie), and the optogenetic constructions used in Chapter 4 have been stably expressed in our MDCK cells by Olivier Destaing (IAB, Inserm U 1209, CNRS UMR 5309 et Université Grenoble Alpes).

HEK cell lines The experiments described in Chapter 3 were conducted on HEK cell lines (*Human Embryonic Kidney*, precise cell type unknown), immortalized by ectopic expression of large-T and hTERT genes for the normal cell line, and additionally with the *Ras*^{V12} mutation — more precisely H-RAS^{G12V} —, for the transformed cell line [127]. The first two mutations are

associated with resistance to hygromycin and geneticin, respectively, and the Ras^{V12} mutation is associated with resistance to puromycin. In this thesis, we have used the two following clonal cell lines:

- The HEK-HT GFP, or HEK GFP: a variant transduced to express the green fluorescent protein GFP. We refer to this cell line as the “normal” cell line thereafter.
- The HEK-HT Ras^{V12} -mCherry, or HEK Ras^{V12} -mCherry: a transformed cell line carrying the H-RAS^{G12V} mutation, also referred to as Ras^{V12} , and transduced to express mCherry fluorescent protein.

Although they are not *a priori* epithelial, these cell lines form monolayers in culture.

MDCK cell lines Madin-Darby canine kidney (MDCK) cells are an immortalised epithelial cell line which forms monolayers in culture. MDCK wild type (wt) cells were used, as well as modified photoactivable versions, in Chapter 4. The following cell lines were used:

- MDCK OptoSrc: OptoSrc-mCherry, LifeAct-iRFP and CIBN-GFP-CAAX
- MDCK OptoSrc devoid of CIBN: OptoSrc-mCherry, LifeAct-iRFP and GFP-CAAX
- MDCK OptoSrc devoid of CIBN-CAAX-GFP: OptoSrc-mCherry and LifeAct-iRFP

The OptoSrc constructs associated to these cell lines will be described in more detail in Chapter 4. The two cell lines devoid of CIBN or CIBN-CAAX-GFP were used as controls for the OptoSrc cell line. We note that the LifeAct-iRFP labelling was very weak, so it was not useable in our experiments.

2.1.2 Cell culture

All cells were cultured in Dulbecco’s Modified Eagle’s Medium (DMEM GlutaMAX, Gibco) supplemented with penicillin-streptomycin (Gibco) and fetal bovine serum (FBS, Gibco) — respectively 1% and 10% vol/vol — at 37°C, 5% CO₂ and 95% relative humidity.

In the case of the HEK cell lines, the medium was also supplemented with selection antibiotics according to their specific resistance features, namely with hygromycin B (100 µg/mL, Gibco) and geneticin (400 µg/mL, Gibco) for both cell lines, and with additional puromycin (0.5 µg/mL, Gibco) for the Ras^{V12} cell line.

Cells were maintained in plastic cell culture flasks and passaged using Trypsin-EDTA (Gibco) every 3 to 4 days, and were used for experiments to a maximum of 25 passages. They were tested for mycoplasma every month. In the event of contamination, cells were trashed and a new mycoplasma-free batch was defrosted.

For live experiments, cells were seeded on plain glass bottom plates and left to attach for a few hours or overnight. In order to optimize fluorescence imaging, DMEM was sometimes (specified in section 4.4.1) replaced with FluoroBrite DMEM (Gibco), similarly supplemented with penicillin-streptomycin and FBS. We note that FluoroBrite medium does not contain GlutaMAX (contrary to DMEM), which translates into a decrease of cell proliferation during experiments.

To estimate the population doubling time of the HEK cell lines, cells from each cell line were seeded in 8 wells of a plastic bottom 24-well plate. Twice a day, for 4 consecutive days, the cells from one well were resuspended using Trypsin-EDTA and counted using a KOVA Glasstic Slide 10 with Grids (KOVA). In the case of the MDCK cell lines, cells from each cell type were seeded in a glass-bottom 6-well plate, and placed under a videomicroscope. Cells were either not exposed to blue light, or exposed to blue light every 5 minutes using the Mosaic (see 2.7). Cells were counted by hand on the images acquired for 6 timepoints between 0 and 60 h. The number of cells as a function of time after seeding followed the relation: $n(t) = n_0 \cdot 2^{t/PDT}$. The population doubling time PDT was then linked to the slope of the $\ln(n) = f(t)$ curve by: $PDT = \ln(2)/slope$.

2.2 Antagonistic migration assays (AMA)

The antagonistic assay was designed to place different cell populations in opposition; it is based on the use of a removable barrier between two cell populations.

The first strategy to do this is based on the expertise of the team to create silicone ‘microstencils’ of polydimethylsiloxane (PDMS) to conduct injury-free “wound healing” assays [123]. The main advantage of these custom-made stencils is that they can be designed to follow a wide range of geometries and sizes. They have indeed originally been used to set precise initial conditions for migration or wound healing experiments [35,123]. Another strategy to carry out a wound healing experiment is based on magnetically attachable stencils. These are magnetite-containing PDMS stencils that can be attached to the culture substrate by placing magnets right underneath the surface. It is also a versatile technique, that can be used on dry or wet surfaces [128].

Ultimately, we decided to use commercially available PDMS-based stencils. Although they were less versatile in terms of geometry and size – linear, 400 μm -wide gap – Culture-Inserts 2 Well (Ibidi) were a convenient solution to create competition situations with reproducible initial conditions. Indeed, they are ready to use, functionalized on one side to adhere to the substrate, and can be used several times if washed properly (for as long as the adhesive treatment is effective). These Culture-Inserts are made of 2 wells separated by a barrier: two cell populations can thus be easily seeded in the two separated compartments, as illustrated in Figure 2.1. Once the cells are attached, the Culture-Insert is removed, revealing two monolayers set apart by a 400 μm

gap of free substrate. The antagonistic migration of the two monolayers before and after their contact can then be observed over time (Chapter 3).

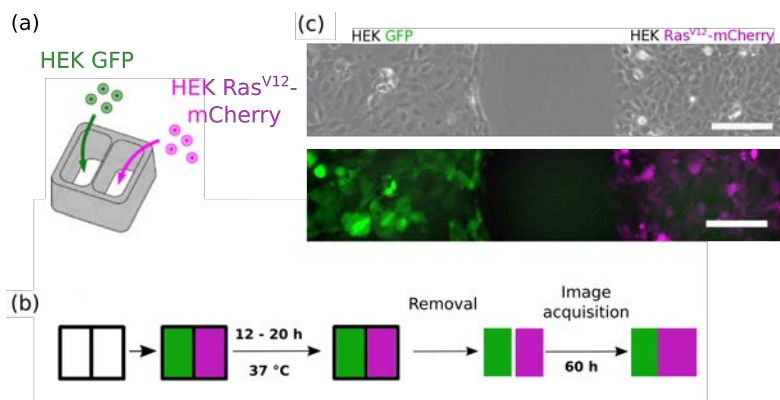


FIGURE 2.1: **Principle of the Antagonistic Migration Assay (AMA).** (a) Culture-Inserts 2 Well (Ibidi) used for antagonistic migration assays. The outer dimensions of the chamber are 9 mm x 9 mm, and each well covers a surface of 22 mm². (b) Schematic of the AMA experiment steps. (c) Starting point: phase contrast (top) and fluorescence images (bottom) of the cell monolayers after insert removal, here with HEK GFP (green) and HEK Ras^{V12}-mCherry (magenta) cell lines, separated by a 400 μm gap. The fluorescence image shows the GFP and mCherry channels merged, in false colours. Scale bar: 200 μm.

2.3 Surface treatment

2.3.1 Fibronectin coating

Fibronectin is a protein of the extracellular matrix involved in cell adhesion: it facilitates cell attachment to a culture substrate. Occasionally, this coating was used to assess the influence of the cell-substrate adhesion, by comparison with our standard plain glass condition (sections 3.4.3 and 4.4.5). For fibronectin coating, glass slides were incubated with a solution of Fibronectin Bovine Protein (Gibco) in Phosphate Buffer Saline (PBS) at 25 μg/mL for 30 minutes at 37°C. It was rinsed with PBS three times and immersed in culture medium. Cells were then seeded on the treated substrate.

2.3.2 Adhesive patterns for cell confinement

We used a patterning technique to confine cell monolayers according to a specific geometry, either stripes in Chapter 3 or discs in Chapter 4. This was done by creating precise patterns of adhesive and non-adhesive areas: the adhesive areas correspond to plain glass and the non-adhesive ones are made of a thin layer of non-adhesive polymers (acrylamide and polyethylene glycol).

The detailed protocol for adhesive patterns can be found in [130, 131]. Briefly, clean glass substrates were first uniformly coated with a protein-repellent layer formed by interpenetrated networks of polyacrylamide and polyethylene glycol (Aam-PEG, Figure 2.2.(1)). A photoresist mask was then structured directly on top of the layer by classical photolithography methods, and air plasma was used to locally etch the protein-repellent coating through this mask. The photoresist was then removed, yielding a cell repellent substrate on which domains where cells can adhere and proliferate have been etched (Figure 2.2.(2)).

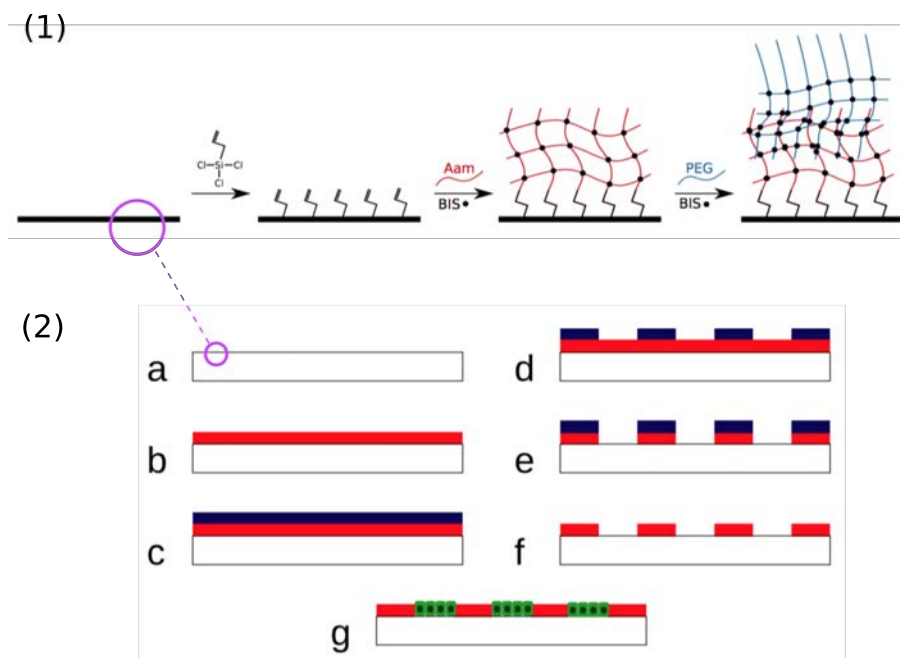


FIGURE 2.2: **Micro-patterning technique for monolayer confinement:** (1) The different steps of the Aam-PEG based surface treatment. First step: Grafting of the allyltrimethylchlorosilane. Second step: Polymerization of the acrylamide gel. Third step: Polymerization of the PEG gel (Aam: acrylamide, BIS: N,N- methylene bisacrylamide, PEG: polyethylene glycol). (2) The different steps of the Aam-PEG based micro-patterning protocol: **a.** Plain glass slide. **b.** Glass slide coated with the repellent gel (red) obtained in (1). **c.** Coating of a layer of positive photoresist (blue) on top of the repellent layer. **d.** Photolithography and developing of the resist. **e.** Plasma etching of the repellent layer that is not protected by the photoresist. **f.** Dissolution of the photoresist layer. **g.** Seeding of the cells (green) on the pattern (not to scale). Adapted from Maxime Deforet's thesis [132].

When experiments were performed on adhesive patterns, the cells were seeded on top of the patterns and left to adhere for about 1-2 hours. The medium was delicately rinsed twice, in order to flush the non-attached cells, otherwise they might manage to create enough extracellular matrix to slightly adhere to the repellent substrate. When AMA were performed on stripes, cells were seeded in the culture insert compartments placed on top of the adhesive stripes. When the cells had started to attach in the patterns, the medium was rinsed delicately twice, before they were left overnight to grow and fill the patterns inside the compartments.

2.4 Drug inhibitors and inducers

The molecular basis of the collective extrusion formation (Chapter 4) was examined through inhibition and induction experiments. Cells were seeded on a glass-bottom 6-well plate as usual and left to attach for a few hours or overnight. The medium was changed to FluoroBrite 1 to 4 hours prior to the start of illumination. The drugs were added during this medium change and left in the medium for the duration of the experiment ($\sim 60 - 70$ h). For drugs dissolved in DMSO, the same volume of the vehicle was added to another well of the 6-well plate as a control, so that the two experiments were run in parallel, to account for the effect of the DMSO.

Src inhibitors To inhibit Src, PP2 (Sigma) and Src Inhibitor n°5 (Biaffin GmbH) were used at concentrations $10 \mu\text{M}$ and 10 nM , respectively [133–135]. The drugs were first dissolved in DMSO at concentrations 10 mM and $10 \mu\text{M}$, respectively, and stored at -20°C . They were then added to the cell medium to reach the desired final concentration.

PP2 inhibits Src Family Kinases by binding to their ATP-binding site¹, or ATP pocket. However, the general features of this ATP pocket are well conserved across most known kinases, which is why PP2 can inhibit protein kinases other than SFKs [136–138]. Src Inhibitor n°5 is part of an anilinoquinazoline series of compounds. The particular conformation of these molecules enables them to bind more specifically to the ATP binding site of SFKs, due to steric interactions [134].

Blebbistatin is an inhibitor of myosin II contractility. It keeps myosin in an actin-detached state, by blocking the myosin heads in a complex with low actin-binding affinity, and thus prevents rigid actomyosin cross-linking [139]. We attempted to use it to assess the effect of a decreased contractility on the experiments from Chapter 4. Unfortunately, blebbistatin is phototoxic [140,141], and experiments of localised illumination in presence of blebbistatin ($10 \mu\text{M}$, Sigma) merely resulted in localised cell death. We then attempted to use *para*-Nitroblebbistatin, a less cytotoxic myosin II inhibitor [142], but the outcome was not conclusive, as it was delicate to properly uncouple the residual phototoxicity from the actual effect of the drug.

Y27632 is a ROCK-inhibitor, and was used to decrease cell cortical tension [143]. This compound inhibits ROCK kinases by competing with ATP for binding to the catalytic site of the kinases [144]. It was dissolved in water and used at a concentration of $10 \mu\text{M}$ (Sigma).

Calyculin A is a protein phosphatase inhibitor known to induce cell contractility. This compound inhibits myosin-light-chain phosphatase from dephosphorylating myosin, which results in hyperactivated myosin [145,146]. It was dissolved in DMSO and used at a concentration of 1 nM (Life Technologies).

¹The ATP binding site is the place in which ATP catalytically activates the protein, while being hydrolyzed to ADP.

Mitomycin C is an inhibitor of cell division. It binds DNA by alkylation reactions, resulting in the inhibition of DNA synthesis, and cell cycle arrest [147]. It was used at a concentration of $0.5 \mu\text{g}/\text{mL}$ (Sigma). However, Mitomycin C shows signs of toxicity on MDCK cells after several hours (for instance 12h in [123]). The main cause of this cytotoxicity is likely the formation of interstrand DNA-DNA crosslinks [148]. Thus, it could not be used for long term experiments. We note that most of the live experiments described in Chapter 4 were conducted in FluoroBrite medium, which does not contain GlutaMAX, therefore the proliferation is already somewhat hindered.

EGTA The calcium chelator Ethylene Glycol Tetraacetic Acid (EGTA) was dissolved in water and used at 2 mM (Euromedex), to disrupt cell-cell contacts [149]. EGTA binds extracellular Ca^{2+} cations, which are necessary to maintain cell-cell junctions [150].

4-aminopyridine We used the potassium channel inhibitor 4-aminopyridine (4-AP, Sigma), which blocks the early stage of apoptosis in epithelial cells [151]. A direct cause and effect relationship has been found between the level of K^+ and the apoptotic activity [152], and 4-aminopyridine blocks K^+ channels in their open state [153], thus inhibiting apoptosis. 4-AP was dissolved in water and used at a concentration of 1 mM.

2.5 Fluorescence labelling

2.5.1 Live cell assays

Hoechst labelling of the nuclei was done using NucBlue ReadyProbes Reagent (Life technologies). It was added at 1 drop/mL of medium and left to incubate for 30 minutes before acquiring images.

In order to evaluate apoptotic activity in the cells, we used a fluorescent marker of Caspase-3/7 (CellEvent Caspase-3/7 Green ReadyProbes, Invitrogen): 2 drops were added per mL of media, and incubated for 30-60 minutes. This reagent is intrinsically non-fluorescent, and can emit green fluorescence ($\sim 530 \text{ nm}$) only when caspase-3/7 is activated, *i.e.* in apoptotic cells. Propidium iodide (PI, Propidium Iodide ReadyProbes Reagent, Invitrogen) was used to stain the nucleus of apoptotic cells in far red (emission $\sim 617 \text{ nm}$), since PI cannot cross the cell membrane of viable cells. Two drops were added to a well (recommandation is 2 drops/ 10^6 cells), and incubated for 15 - 30 minutes.

2.5.2 Live F-actin labelling

In order to label F-actin in cells for live experiments, we used an SiR-Actin Kit (Spirochrome). About 4 hours before an experiment, SiR-Actin (100 nM) and verapamil (10 μM) were added

to the cell medium. These were left in the medium for the duration of the experiment (~ 60 h) and the images were acquired with the far red channel (Cy5 filter set).

2.5.3 Immunofluorescence staining

For immunofluorescence staining, cells were fixed with 4% paraformaldehyde (Euromedex) for 10 minutes and thoroughly washed with PBS. Unless otherwise mentioned, they were permeabilized for 4 minutes using 0.1% Triton X-100 in PBS with 0.1% BSA and rinsed with PBS. The cells were then blocked in a solution of 2.5% normal goat serum in PBS-BSA for 1 hour, incubated with the selected primary antibody (Table 2.1) for 1 hour and washed with PBS three times. They were then incubated with the secondary antibody (Table 2.2) for 30 minutes, washed with PBS three times, Hoechst-labelled with NucBlue ReadyProbes Reagent and mounted on glass slides using ProLong Gold mounting agent (Invitrogen). All steps were carried out at room temperature.

Primary Antibody	Reference	Provider	Species	Concentration
E-cadherin	cat#610181	BD Biosciences	mouse	1:100
E-cadherin	cat#13-1900	Invitrogen	rat	1:100
Vimentin	cat#M0725	Dako	mouse	1:300
α -catenin	cat#C2081	Sigma	rabbit	1:100
ZO1	cat#339100	Invitrogen	mouse	1:100
ZO1	cat#61-7300	Invitrogen	rabbit	1:100
p-MLC	cat#3674	Cell Signaling	rabbit	1:100

TABLE 2.1: Primary Antibodies

Secondary Antibody	Reference	Provider	Conjugated	Concentration
Goat anti-mouse	A21050	Molecular Probes	Alexa Fluor 633	1:1000
Goat anti-rat	A21247	Invitrogen	Alexa Fluor 647	1:1000
Goat anti-rabbit	SAB4600141	Sigma	CF 633	1:1000

TABLE 2.2: Secondary Antibodies

Images were acquired on a confocal microscope (Zeiss LSM780 or LSM880 NLO), with a 40x/1.3 OIL/DIC II PL APO VIS-IR or a 63x/1.4 OIL/DIC II PL APO objective (Zeiss, see section 2.6.2).

2.6 Image acquisition

2.6.1 Videomicroscopy

Time-lapse experiments were acquired using automated inverted videomicroscopes equipped with temperature, humidity, and CO₂ regulation. The motorized stage and the image acquisition with a CCD camera were controlled using Metamorph (Molecular Devices) software. Unless otherwise specified, the typical delay between two successive images of the same field of view was set to 15 minutes.

Most experiments of **antagonistic migration assays** (AMA, Chapter 3) were made on a DM IRB inverted microscope (Leica) with a H117 motorized stage (Prior Scientific), and a 10x objective (HCX PL Fluotar, 10x/0,30 Ph1, Leica). The CCD camera was either a CoolSnap EZ (Photometrics) or a Retiga 6000 (Qimaging). The fluorescent source was a Lumen 200pro (Prior). The integrated transmitted light illumination unit consisted of a 12 V, 100 W, halogen lamp housing.

All experiments using **patterned illumination** (Chapter 4) were made on an Axiovert 200M inverted microscope (Zeiss) equipped with a Mosaic 2 module from Andor. The motorized stage was a SCAN IM 130x100, with a TANGO 3 controller (both from Marzhauser), and the CCD camera used was either a CoolSnap HQ2 (Photometrics) or a Retiga R6 (Qimaging). Unless otherwise specified, the images were taken with a 40x objective (UplanFLN 40x/0.75 Ph2 from Olympus). The fluorescent source was a pE-300^{white} (CoolLed) and the transmitted light for phase contrast images was a pE-100 (CoolLed).

Each microscope was enclosed in an incubator maintained at 37°C with “The Cube & The Box” system (Life Imaging Services), and the atmosphere around the sample was kept at 5% CO₂ and 95% humidity with “The Brick” system (Life Imaging Services). In order to avoid excitation of CRY2 *via* transmitted light, but also to protect the cells from toxic wavelengths (UV-blue and infrared), the transmitted light sources from both microscopes were filtered to keep only wavelengths between 610 - 710 nm (filters: FGS900S and RG610, Thorlabs). In particular, cryptochrome responds to UVA light and blue light with a peak at 450 nm, and weakly above 500 nm [154, 155].

Occasionally, videomicroscopes from the Institut Pierre Gilles de Gennes (IPGG) imaging platform (Leica microscopes) or the Nikon Imaging Center from Institut Curie were also used.

2.6.2 Confocal microscopy

Immunostaining pictures and 3D images were acquired on confocal microscopes. Three such microscopes were used:

- LSM880 NLO (Zeiss) from the Pict-BDD imaging platform at Institut Curie
- LSM780 (Zeiss) from the Pict-Pasteur imaging platform at Institut Curie
- DMI8 (Leica) from the imaging platform at Institut Pierre-Gilles de Gennes

2.7 Photoactivation

For photoactivation of the MDCK OptoSrc cells (Chapter 4), the periodic illumination consisted of 200 ms-pulses of blue light separated by an interval Δt . Unless otherwise specified, the interval between two pulses was $\Delta t = 5 \text{ min}$ (Figure 2.3). This ensured an almost continuous activation (see section 4.1.3).

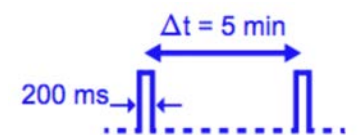


FIGURE 2.3: **Illumination sequence for photoactivation.** The standard illumination consisted in a 200 ms-pulses of blue light every 5 minutes, for the duration of the experiment (about 60 hours).

Targeted photoactivation of the MDCK OptoSrc cells was done using a Mosaic 2 (Andor) coupled to a X-Cite XLED (Lumen Dynamics, BDX led, emission: 450-495 nm) *via* an excitation filter (450-490 nm) and controlled with the “Mosaic Targeted Illumination” plugin on MetaMorph. The photoactivation parameters (region size, frequency and duration of the blue pulse) were controlled using custom MetaMorph journals. The Mosaic uses a digital micromirror device (DMD) to pattern the light coming from the XLED: a DMD is an array of micromirrors that can be individually positioned towards or away from the light path (Figure 2.4). A light pattern can thus be created by tilting each micromirror in its ON or OFF state, which corresponds to lit or dark pixels in the image. The patterned light coming from the Mosaic and the light from the pE-300^{white} fluorescence source both enter the microscope’s epifluorescence port through a 50/50 beamsplitter.

The DMD of the Mosaic 2 is a 800 x 600 grid and each mirror is 16 μm square, with a 1 μm gap between each mirror. The maximum area of illumination available with the Mosaic 2 was a 160 x 120 μm^2 rectangle with our 40x objective (Figure 2.5), which is smaller than the field of view of the camera (320 x 262 μm^2 for the Retiga R6, 235 x 175 μm^2 for the CoolSnap HQ2). Unless otherwise mentioned, the blue-light illuminated region was a disk of diameter 70 μm .

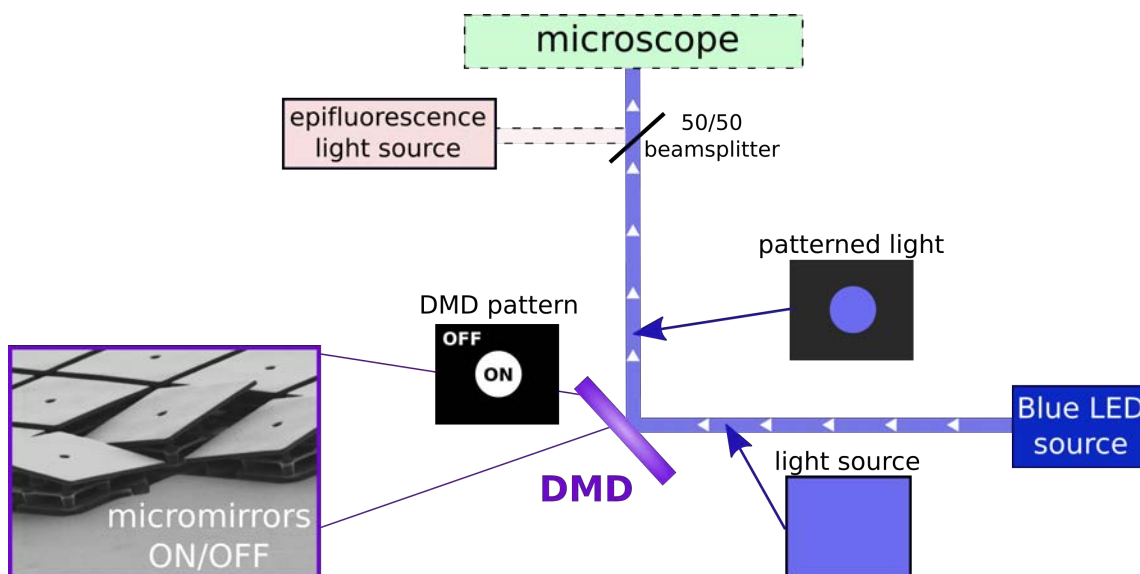


FIGURE 2.4: **Light path for targeted illumination using a DMD.** The light beam from the LED source is first reflected on the DMD: the light is only reflected on the micromirrors that are in the ON state. The DMD pattern thus defines the illumination pattern, which then enters the microscope and illuminates the sample. SEM image of the micromirrors from [156] (no scale bar provided, the size of a micromirror is usually a few μm^2).

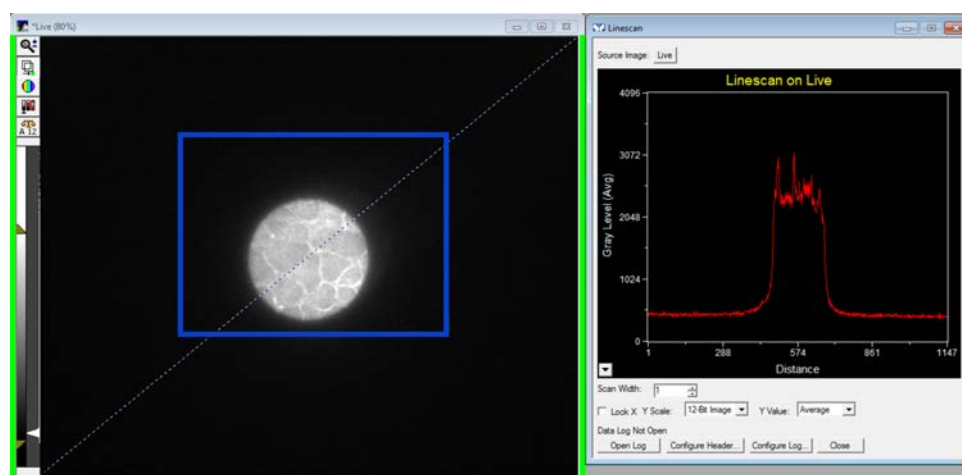


FIGURE 2.5: **Targeted illumination using the Mosaic 2.** (Metamorph software screenshots) **Left:** Illumination of a $70\ \mu\text{m}$ diameter disc of MDCK OptoSrc (CIBN-GFP fluorescence signal). The blue rectangle represents the available area of illumination with the Mosaic 2, which is a subset of the field of view of the camera (black window). **Right:** Illumination profile corresponding to the dashed line on the left image. The baseline value corresponds to the default offset of the Metamorph software (which coincides with the value measured when the room is in complete darkness).

The light power was measured after the objective, with a PM30 Optical Power Meter (Thorlabs), to be $20 \mu\text{W}$ for a $70 \mu\text{m}$ disk, which is in a similar range as was previously reported for optogenetic manipulations in other systems [157].

Illumination of the entire field of view The GFP fluorescent channel was used to illuminate the entire field of view of the camera, in the case of the statistical mixture method (section 4.3.1), or the antagonistic migration assays of MDCK OptoSrc cells against MDCK wt cells (section 5.2.2). In that case, the pE-300^{white} was used in combination with the Filter Set 10 (Zeiss) for GFP (excitation 450-490 nm). For this optical set-up, we measured a light power of 4 mW for the entire field of view, *i.e.* about an order of magnitude higher than with the XLED and the Mosaic.

Global illumination of an entire culture well For global illumination of cells in view of immunofluorescence labelling, we designed and used a custom-made “illuminator” (Figure 2.6), based on an original idea by M. Balland and built with the help of F. Saiag. This illuminator consisted of 6 blue LEDs (XREBLU-L1-0000-00K01, Farnell), to illuminate each well of a 6-well plate, controlled by an Arduino Leonardo board (Arduino). Cells were seeded in either a glass-bottom 6-well plate, or a plastic² 6-well plate containing 6 glass coverslips. The 6-well plate was mounted on the illuminator holder and maintained in an incubator (37°C , 5% CO_2), in the dark, for the duration of the experiment (24 to 48 h). The intermittent illumination of the LEDs consisted of a 200 ms-pulse of blue light every 5 minutes.

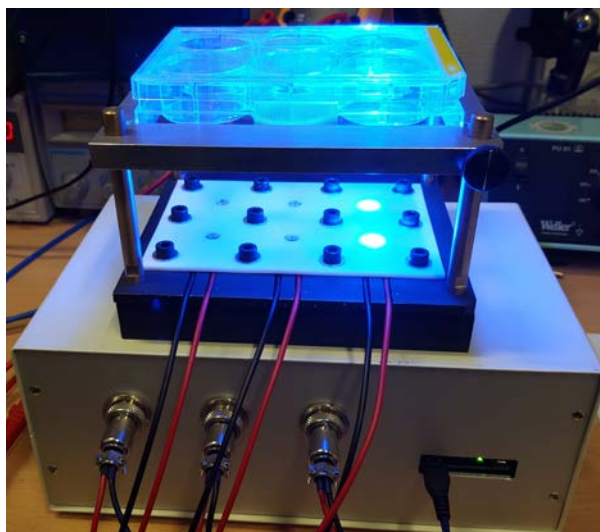


FIGURE 2.6: **Custom-made “illuminator” for global illumination of entire culture wells.** On the picture, only the two LEDs on the right are on. To prevent blue light from a given LED to “leak” into an adjacent well, we added a custom-made black cache that funnels the light of each LED to its associated well (not shown here).

²We first ascertained that the blue light power measured on top of the plate was not impacted in the case of a plastic substrate.

Quantification of the extrusion rate in a cell monolayer In order to quantify the effect of the photoactivation on the extrusion rate in a monolayer, cells were either kept in the dark or subjected to illumination (200-ms pulse of blue light every 5 minutes) of the entire field of view using the GFP channel of a videomicroscope, as previously described. We then counted the number of extrusions from the monolayer in $150 \times 150 \mu\text{m}^2$ sample squares, for 6 squares (same experimental well), for a duration of 40 ± 3 h after confluence. The extrusion rate is then given in $\text{cells}/\mu\text{m}^2/\text{h}$.

2.8 Image analysis

Images were handled using ImageJ. In particular, macros were used to automatically process large numbers of images for stitching, merging channels and assembling movies. Image analysis was mainly done with custom-made scripts on Matlab (Mathworks). Three-dimensional confocal images were reconstructed with Imaris software (Bitplane), which was also used for nuclei counting: we counted the number of cells in a 3D structure (section 4.4.1) using the *Surfaces* tool of the Imaris software to automatically detect the nuclei in the 3D confocal images.

2.8.1 Mixing index computation

To assess the homogeneity in a 2-cell type mixture (section 3.2), we have been inspired by literature dealing with process analytical technologies and we decided to compute the Poole Index [158–160] which is equal to zero when the two components of a mixture are completely segregated (unmixed situation) and approaches unity if the mixture is perfectly mixed. These analyses were implemented with the Matlab software (The Mathworks, Mass., USA).

Image pre-processing Each color-channel (typically, GFP and mCherry) is independently processed as a greyscale image in the range 0-1. If needed (when the fluorescence signal is weak), a rolling ball-type background subtraction is performed (with a ball of radius ~ 20 pixels). We then adjust the histogram of the color channel of lowest mean value to match the histogram of the other color image (*imhistmatch* function). Finally, these two “standardized” color images are combined to create an RGB image, whose blue component is null for a red and a green fluorescent channel (Figure 2.7 (a)).

Color-based segmentation using K-means clustering We transform the RGB images to the L^*a^*b space: L is the luminosity layer, and all the color information is in the a^*b layers: a indicates where color falls along the red-green axis and the b layer indicates where the color falls along the blue-yellow axis. The K-means algorithm [161], based on squared Euclidean distance, is used to cluster objects present in a^*b layers into two domains using the Euclidean distance metric: we thus get a binary image for our mixture of two components (Figure 2.7 (b)).

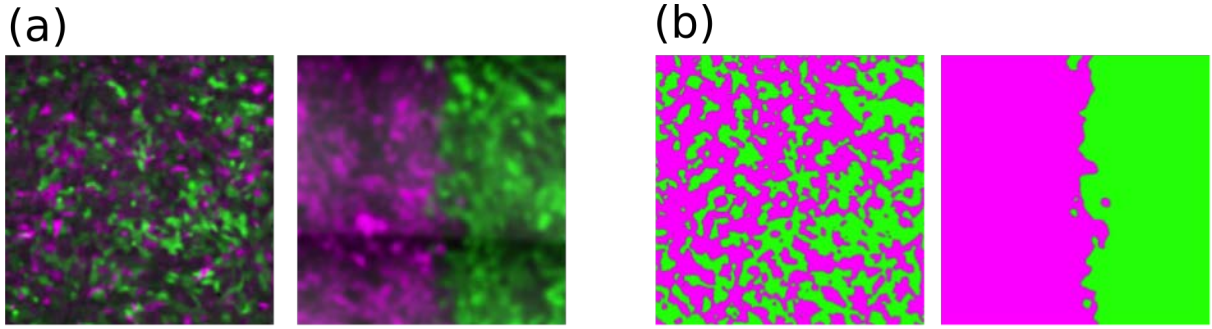


FIGURE 2.7: **Mixing index computation.** (a): Image pre-processing of two different mixing situations: HEK cells (wt in green, Ras^{V12} in magenta) either seeded together (left), or separately using a Culture-Insert 2-Well (right). (b): Color-based segmentation of these two images using K-means clustering.

Heterogeneity analysis: the Poole index

In 1964, Poole suggested an index defined as: $M = \frac{\sigma_0}{\sigma_R}$, where σ_0 is the observed standard deviation of the composition of the mixture, while σ_R is the standard deviation of a complete random mixture [162]. To measure homogeneity in the binary image, we use macropixel analysis: the image is split into non-overlapping square sub-windows from which mean and standard-deviation are extracted. Adapted to image analysis, M becomes $M_P = \frac{\overline{M_{sd}}}{\overline{M_{sd-rnd}}}$, where $\overline{M_{sd}}$ is the average of standard deviations of macropixels for the real image, and $\overline{M_{sd-rnd}}$ is the average of standard deviations of macropixels for its randomized image. A randomized image of a binary image contains the same pixels that have been randomly arranged. Consequently, M_P tends to unity for totally random images.

2.8.2 PIV

The velocity field in a cell monolayer was mapped by particle image velocimetry (PIV) analysis, as previously done in the team [35, 163]. Stacks of images were analysed with a custom-made PIV algorithm based on the MatPIV toolbox for Matlab. The PIV algorithm computes the cross-correlation between successive sub-windows and returns the average displacement for each sub-window between the two time steps. In our case, the time between successive analysed images was set to 15 min.

The velocity field $\mathbf{V}(i, j, t)$ was measured by correlating two successive images, at times t and $t + \Delta t$ separated by $\Delta t = 15$ min, and by performing a sliding average over a time window of a few hours (depending on the experiment) to improve the signal to noise ratio without loss of information. The window size was usually set to 64 pixels (unless in experiments with the 10x objective, for which it was set to 32 pixels), with an overlap of 0.25. The velocity field \mathbf{V} was represented with *arrows*, expressed in $\mu\text{m}\cdot\text{h}^{-1}$. Differentiating the velocity field yields the

velocity gradient matrix, ∇V , which is expressed in h^{-1} :

$$\nabla V = \begin{pmatrix} \frac{\partial V_x}{\partial x} & \frac{\partial V_y}{\partial x} \\ \frac{\partial V_x}{\partial y} & \frac{\partial V_y}{\partial y} \end{pmatrix} \quad (2.1)$$

The divergence is given by $\text{divergence} = \frac{\partial V_x}{\partial x} + \frac{\partial V_y}{\partial y}$. The convergence (opposite of the divergence) was then averaged inside the ROI.

2.8.3 Statistical analyses

All data were analysed using Matlab (Mathworks). P-values for determining statistical significance were calculated by a two-sample Student's t-test, and p values less than 0.05 were considered significant. Different levels of significance are shown with asterisk on the graphs: *: $p \leq 0.05$; **: $p \leq 0.01$.

Unless otherwise mentioned, the error bars represent the standard error of the mean (SEM).

The probability of observing a collective extrusion (section 4.4) was defined as $P_{bud} = \frac{k}{n}$, where k is the number of occurrences of the collective extrusion observed over n experiments. We consider the binomial distribution with parameters n and P_{bud} . The uncertainty on P_{bud} is thus $\Delta p = \sqrt{\text{var}(p)} = \sqrt{\frac{p(1-p)}{n}}$. Therefore: $P_{bud} = p \pm \sqrt{\frac{p(1-p)}{n}}$.

2.9 Traction Force Microscopy

The traction forces exerted by the cells on the substrate were measured using Traction Force Microscopy [164, 165]. The protocol was adapted from [166]. All steps were done in the clean room, and all chemicals were handled under the fume hood.

Coverslips (#1.5, 30 mm diameter, Harvard Apparatus) were cleaned in a plasma cleaner for 10 minutes, incubated in a solution of 3-aminopropyltrimethoxysilane (2% vol/vol in isopropanol, Sigma) for 10 minutes, and cleaned thoroughly with ddH₂O (4 exchanges of water). They were then incubated in glutaraldehyde (1% vol/vol in ddH₂O, Sigma) for 30 minutes, thoroughly washed, and dried using compressed air. These coverslips are referred to as "activated".

Independently, microscope glass slides were incubated with a solution of Fibronectin Bovine Protein (Gibco) in PBS at 25 $\mu\text{g}/\text{mL}$ for 30 minutes at room temperature. They were rinsed with PBS three times and left to air dry. A stock solution of acrylamide/bis-acrylamide mix was made according to the desired stiffness of the gel [167]. For a gel of ~ 10.6 kPa, the stock solution was made with 2.5 mL of 40% acrylamide solution (Bio-Rad), 0.5 mL of 2% bis-acrylamide solution (Bio-Rad), and 7 mL of water. Fluorescent beads were added to this mix (1% vol/vol, FluoSpheres 0.2 μm dark red fluorescent (660/680), Life technologies). To start the polymerization of the acrylamide gel, ammonium persulfate (1% vol/vol, Bio-Rad) and TEMED (1%

vol/vol, Bio-Rad) were added to the acrylamide/bis-acrylamide mix containing the beads. This solution was mixed well by pipetting 3-4 times, then 30 μL was applied on the fibronectin-coated glass slide immediately once these were dry, and an activated coverslip was placed on top. During the polymerization, the gel attaches covalently to the activated surface on one side, and attaches to the fibronectin proteins on the other side. This step, inspired by the deep-UV patterning technique [168], enables us to directly coat the surface of the gel with fibronectin. This technique is faster, more reliable, and more cost-effective than the commonly employed use of a cross-linker: Sulfo-SANPAH [166,167,169,170], or Sulfo-LC-SDA [171]. Indeed, the protocol for both compounds requires additional steps (including an overnight reaction), an extra cost for the molecule (several hundreds of euros), and in our experience is not as successful in attaching cells to the acrylamide gel.

The completion of polymerization could be assessed by observing the remaining mix solution in the eppendorf tube. When the polymerization was complete, the sandwiched gel was immersed in PBS, and the fibronectin-coated glass slide was carefully detached from the surface of the gel using a razor blade and tweezers. The gel was then incubated in culture medium for 45 minutes at 37°C, before the cells could be seeded on its surface, and were left to adhere overnight. The coverslip bearing the gel was then placed in a POCmini-2 cell cultivation system (Pecon GmbH), and under the microscope. The images were acquired as usual, with the added far red channel to image the beads. The software autofocus from Metamorph is used for the far red channel, to focus on the fluorescent beads, and prevent any drift in the z-axis.

At the end of the experiment, the reference image of the beads in the gel at rest (without the cells) are needed for the computation: without moving the gel, the medium was removed, the cells were rinsed with PBS, and incubated in trypsin (still under the microscope). An image of the beads was then taken without any cell attached to the gel (gel at rest).

To compute the traction forces, we used both the Fiji plugins developed by Qingzong Tseng³ [172], and the TFM Matlab package from Danuser Lab⁴ [173].

³available at <https://sites.google.com/site/qingzongtseng/tfm>

⁴available at <http://www.utsouthwestern.edu/labs/danuser/software/>

Chapter 3

Competition for space: antagonistic migration assay (AMA)

Contents

3.1	Characterization of the HEK cell lines	49
3.1.1	Population doubling time	49
3.1.2	Traction forces	49
3.1.3	HEK cells develop into monolayers	50
3.2	No spontaneous cell sorting in co-cultures	51
3.3	Antagonistic Migration Assay	53
3.3.1	Free migration of the two populations before the meeting	53
3.3.2	After the meeting, the Ras^{V12} population moves forwards and the wt population goes backwards	57
3.4	What affects the evolution of the interface?	60
3.4.1	Effect of the initial density	60
3.4.2	Effect of the proliferation	60
3.4.3	Effect of the traction forces	62

This chapter describes the use of an antagonistic migration assay to study the competition for space between two cell lines that differ only in the expression of an oncogene. The strategy we adopted here was the removal of a physical barrier between the two initially separated cell populations.

This project was originally started by Simon Garcia [174] and Isabelle Bonnet, in the team. Thanks to our collaborators in the team of Jacques Camonis (U830, Institut Curie, Paris), we had access to two HEK cell lines: a normal — or wild-type (wt) — cell line, and a cell line transformed by an oncogenic Ras^{V12} mutation. This appeared as a good starting point to study the competition for space between two cell types. This approach holds the advantage of creating a reproducible interface between two populations, in a very straightforward way. The physical barrier is rectangular, so that the interface created adopts a roughly linear geometry, with the two populations on either side of it. Besides, we can then witness the evolution of this interface once the two monolayers have met, after a period of “free migration”. We first characterize basic aspects of the two cell types, before describing what happens in these Antagonistic Migration Assays (AMA).

The two cell lines were fluorescently labelled in order to distinguish them: HEK wt with GFP and HEK Ras^{V12} with mCherry. We have used green and magenta as fake colours for GFP and mCherry signals.

3.1 Characterization of the HEK cell lines

3.1.1 Population doubling time

We estimated the population doubling time (PDT) by counting the cells manually at various time points, up to 4 days after seeding. We found a doubling time of 16 ± 3 h for HEK GFP and 16 ± 1 h for HEK Ras^{V12} -mCherry (Figure 3.1). The transforming mutation does not seem to affect the doubling time of the cells. We can thus consider that the cell cycle duration of both cell lines is identical.

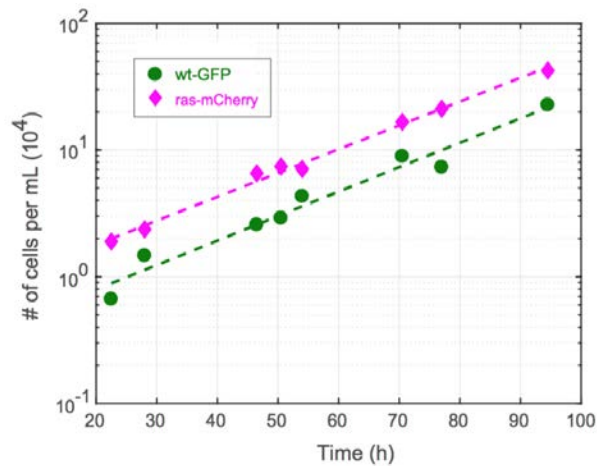


FIGURE 3.1: **Estimation of the population doubling time (PDT) of both HEK cell lines.** Both HEK cell lines, wt (green circles) and Ras^{V12} (magenta diamonds), were cultured in 24-well plates. Twice a day, for 4 days, one well of each cell line was trypsinized and the cells were counted. The PDT was estimated to be about 16 h for both cell lines.

3.1.2 Traction forces

We used Traction Force Microscopy (TFM) to investigate the amplitude of traction forces exerted by isolated HEK cells on the substrate. Strain energy (in J) was calculated by multiplying the traction forces by the displacements of the beads, and integrating it over the whole area of an individual cell. We also computed the strain energy density (in $J.m^{-2}$), which is the strain energy of a cell normalized by its area, since the two cell types differ in size (Figure 3.2). We found that strain energy density, which reflects the work per unit area exerted by a cell to deform the substrate, was about 3 times higher for wt cells compared to Ras^{V12} cells: $1.3 \pm 0.2 \times 10^{-5} J.m^{-2}$ and $0.4 \pm 0.08 \times 10^{-5} J.m^{-2}$, respectively (SEM, $n = 14$ and $n = 13$). This indicates that wt cells apply stronger traction forces on the substrate compared to Ras^{V12} cells. This is consistent with the common observation that cancer cells are softer than normal cells [175–177]. This seems contradictory to the observation that tumours are rigid masses, which are often felt as lumps. But in fact, it is now believed that it is the increased stiffness

of the extracellular matrix, not of the cells themselves, that gives a tumour its rigidity [178–180].

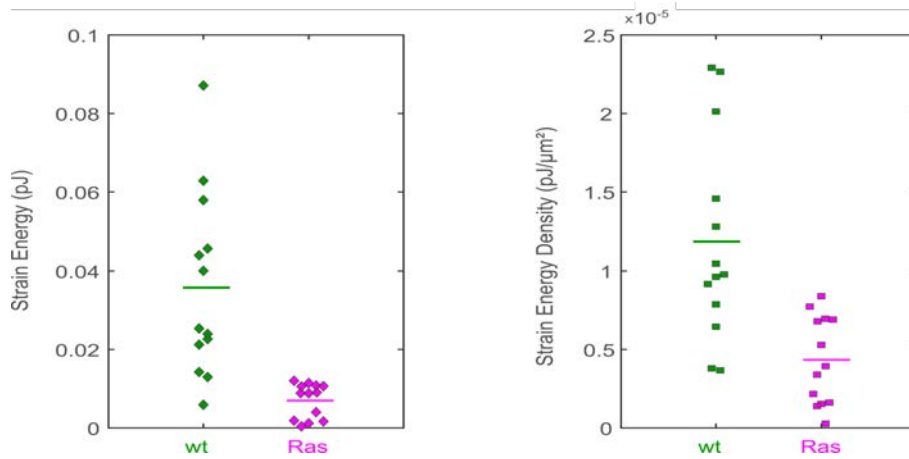


FIGURE 3.2: **Strain energy (pJ, left) and strain energy density (pJ.m⁻², right) of single HEK cells.** HEK wt cells (green) exert higher traction forces on the substrate than HEK *Ras*^{V12} cells (magenta).

3.1.3 HEK cells develop into monolayers

HEK cells are derived from human embryonic kidney cells grown in tissue culture. Their precise cell type is unknown, and they have proved difficult to characterize, not least because embryonic kidneys are a mix of almost all the types of cells present in the body [181]. Although most cells derived from an embryonic kidney would be endothelial, epithelial, or fibroblast, several researchers have speculated that HEK cells may be of neuronal origin. Besides, HEK cells were shown to express both epithelial cell markers, such as E-cadherin (albeit at low levels), zonula occludens (ZO)-1 and occludin, as well as mesenchymal cell markers, such as N-cadherin and vimentin (also at low levels) [182]. Even though HEK cells might not be strictly speaking an epithelial cell type, we have observed that both the HEK wt and the HEK *Ras*^{V12} cell lines form monolayers in culture (Figure 3.3). Looking at the internal movements in a developing monolayer of each cell type, the HEK GFP population appears more cohesive than the HEK *Ras*^{V12}-mCherry one, in which the cells behave more individually within the monolayer.

We also note that the HEK wt cells are twice as large as the HEK *Ras*^{V12} cells: we measured a mean area of $3100 \pm 300 \mu\text{m}^2$ for an isolated wt cell, and $1600 \pm 100 \mu\text{m}^2$ for an isolated *Ras*^{V12} cell (SEM, $n = 14$). This implies that, for a given area, a confluent monolayer of *Ras*^{V12} cells comprises about twice as many cells as a confluent monolayer of wt cells: $d^{wt} = 385 \pm 20$ cells/mm² and $d^{Ras^{V12}} = 785 \pm 50$ cells/mm² at confluence (Figure 3.3). These values give an estimate of the mean area of each cell type in a confluent monolayer: $2600 \mu\text{m}^2$ for a wt cell, and $1300 \pm 100 \mu\text{m}^2$ for a *Ras*^{V12} cell. This would correspond to a diameter of $60 \mu\text{m}$ and $40 \mu\text{m}$ for a wt or a *Ras*^{V12} “circular” cell in a confluent monolayer, respectively. After confluence,

this value decreases as the monolayer densifies and cells are compressed.

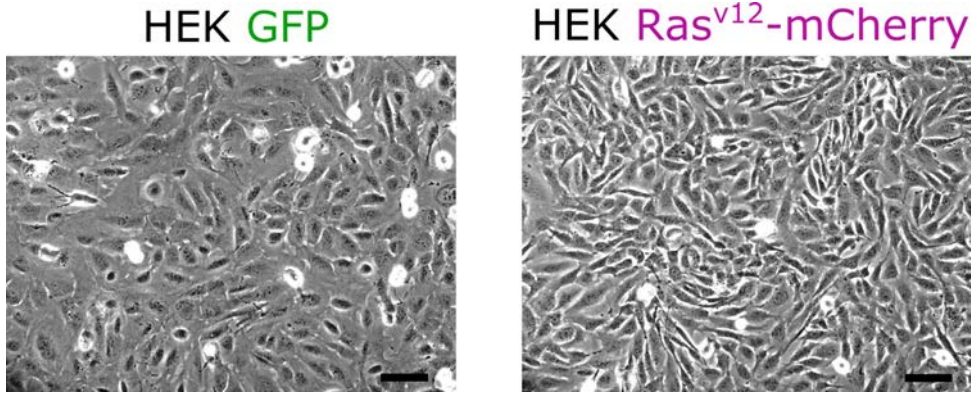


FIGURE 3.3: **Phase contrast images of monolayers of HEK cells at confluence.** **Left:** HEK GFP cells. **Right:** HEK Ras^{V12} -mCherry cells. Scale bar: 100 μm .

3.2 No spontaneous cell sorting in co-cultures

We mentioned in the first chapter the phenomenon of cell segregation (section 1.4.1), in which two cell types spontaneously segregate when cultured together, usually due to a difference in adhesion [93]. In our case, when the HEK GFP and HEK Ras^{V12} -mCherry cells are mixed and seeded together on a substrate at low density, they do not exhibit large-scale segregation, even 2 to 3 days after seeding, and the two populations remain well mixed (Figure 3.4).

In order to determine precisely the level of mixing of the two populations, we have computed an heterogeneity index, namely the Poole index, described in section 2.8.1. Briefly, it consists in comparing the standard deviation of different subregions in a binary image, as a function of the size of these subregions, called macropixels. Figure 3.5 shows the Poole index of the mixed situation, 60 h after seeding, as a function of the macropixel size: this index tends to 1, which corresponds to a completely mixed situation, for a macropixel of about 80 px, that is 60 μm . This indicates that the size of the clusters of one specific cell type is around 60 μm , *i.e.* about 2-3 cells (depending on the cell type), which is likely due to cell division. We can thus conclude that HEK GFP and HEK Ras^{V12} -mCherry stay well mixed when cultured together.

However, Ranft *et al.* showed that this situation did not exclude competition if the two cell types are put face to face [183]. In this paper, the authors study numerically the evolution of two cell populations initially in contact along a linear interface. The two populations differ only in their homeostatic pressure [113]. They show that the evolution of this interface is driven by cell division and cell death, which are themselves influenced by mechanical forces in the tissue. They find that a difference in homeostatic pressure is enough to move the frontier between the two cell types: this represents situations of invasion of one population into the other.

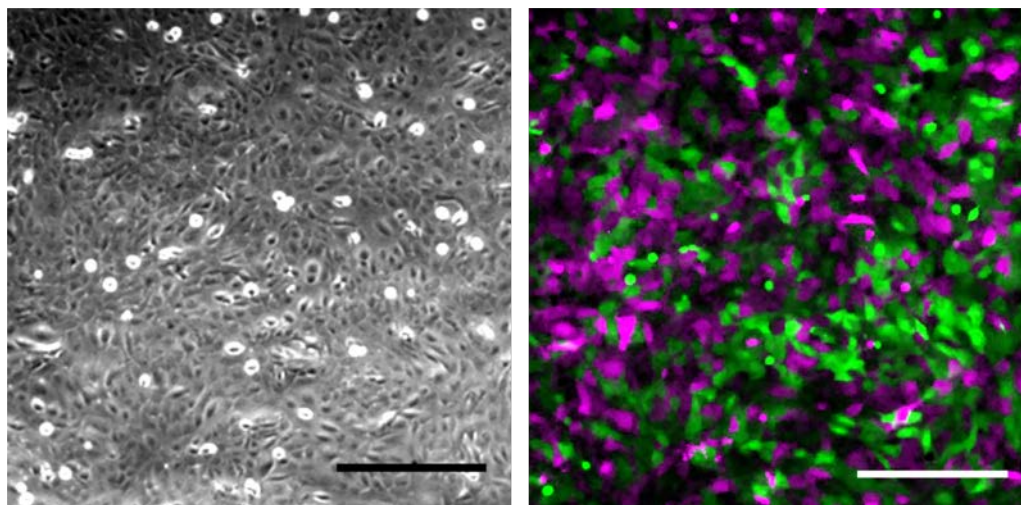


FIGURE 3.4: **Absence of spontaneous sorting between HEK GFP and HEK Ras^{V12} -mCherry cells.** Phase contrast (left) and fluorescence images (right, false colours) of HEK GFP (green) and HEK Ras^{V12} -mCherry cells (magenta), 60 hours after seeding. When they are seeded together, these two cell types stay well-mixed. Scale bar: 100 μm .

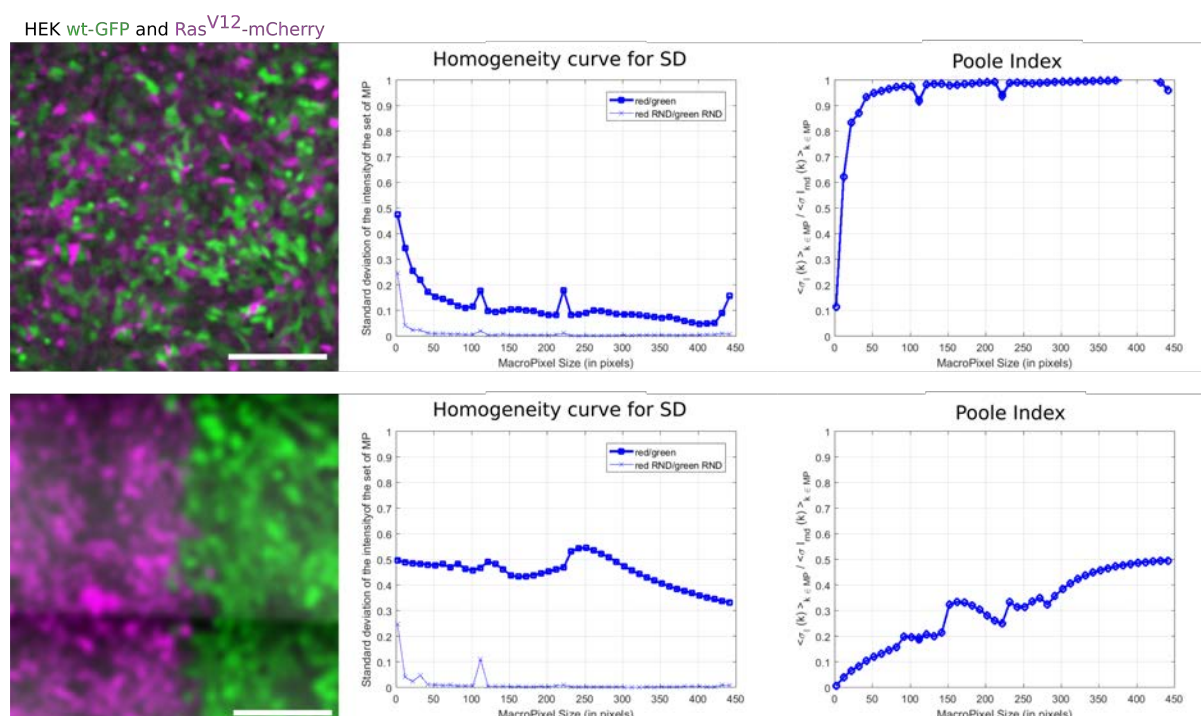


FIGURE 3.5: **Poole index computation.** **Top:** mixing experiment (showed in Figure 3.4), 60 hours after seeding. The Poole index reaches 1 (random mixing) for a macropixel size of about 80 pixels, indicating that the typical size of the clusters of a specific population is about 60 μm , *i.e.* just a few cells. This shows that the two cell types are well mixed. **Bottom:** a control situation where the two cell populations are separated. In such a situation, the Poole index tends towards 0.5 for larger values of the macropixel size, meaning that the “cluster size” must exceed 450 pixels ($\sim 350 \mu\text{m}$). This implies a well-segregated mix. Scale bars: 100 μm .

We then reproduce a geometry for which the two cell types are on either side of a linear interface, facing each other. Experimentally, it is not as easy to place two different cell types in direct contact, though. There is now a way to grow two cell monolayers on either side of a removable microfilament, in order to initially place them in close proximity [184]. But we haven't been able to use this technique yet. For now, we have been using a method for which the two cell populations are initially separated by a $\sim 400 \mu\text{m}$ free space, and then brought into contact, using the antagonistic migration assay (AMA).

3.3 Antagonistic Migration Assay

The description of this assay can be found in section 2.2. Briefly, the two cell types are seeded in two compartments separated by a physical wall, and left overnight until they form monolayers. The physical separation is removed, leaving a free space of about $400 \mu\text{m}$ between the two monolayers, which can then migrate towards each other to close this gap. We follow this antagonistic migration over 3 days by acquiring images in 3 channels: phase contrast, GFP (to see HEK wt cells) and mCherry (to see HEK Ras^{V12} cells).

3.3.1 Free migration of the two populations before the meeting

After removal of the culture insert, the two populations start migrating toward each other in the free space between them. The two populations meet roughly 15 hours after the removal of the barrier, and the gap closes completely within about 30 hours.

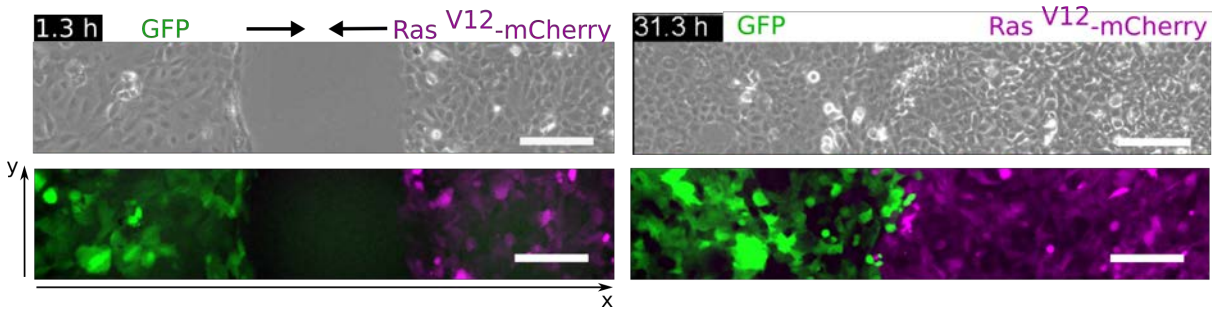


FIGURE 3.6: **Free migration of the two populations before the meeting.** **Left:** Starting point: phase contrast (top) and fluorescence images (bottom) of the cell monolayers after insert removal, with HEK GFP (green) and HEK Ras^{V12} -mCherry (magenta) cell lines, separated by a $400 \mu\text{m}$ gap. The cell populations migrate along the x direction. **Right:** Gap closure, about 31 h after removal of the barrier. Scale bars: $200 \mu\text{m}$.

Due to the symmetry of the system, we reason in 1-dimension, by averaging the quantities over the y -axis (perpendicular to the direction of migration). We can visualize the evolution in time of this assay using a kymograph (Figure 3.7). Each image is averaged over the y -axis, giving one line for each time point. The resulting kymograph therefore gives the evolution over time of the x -axis (*i.e.* the direction of migration). We first look at the migration profile of the two

tissues over time before they meet. The downward-pointing black triangle represents the initial free space being colonized as time goes by. The lowest point of the black triangle represents the first contact between the two populations, for which we define the coordinates (X_{meet}, T_{meet}) .

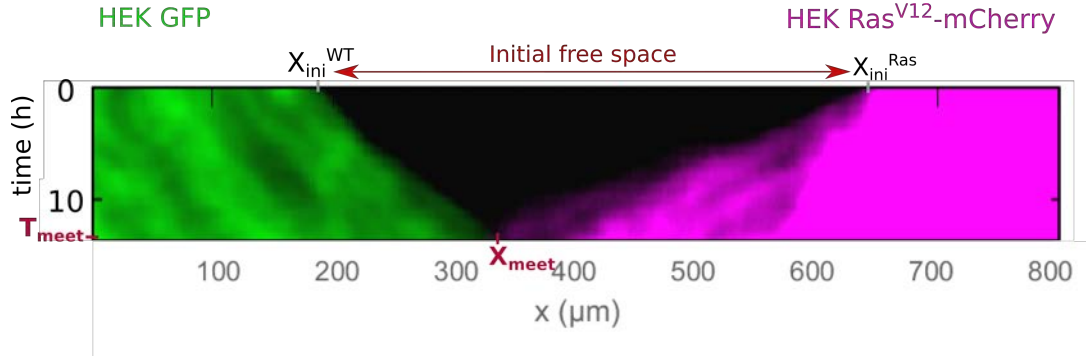


FIGURE 3.7: **Typical 1D kymograph of an AMA experiment during the gap closure.** Each horizontal line represents the y -axis average, for one time point, of the fluorescent channels (merged): green for HEK GFP cells and magenta for HEK Ras^{V12} -mCherry cells. We define X_{ini}^{wt} and X_{ini}^{Ras} as the initial position of each migration front, and (X_{meet}, T_{meet}) as the first meeting point. The time reference $t = 0$ h is set when the physical barrier is removed.

Before the meeting (T_{meet}), we see the 1D migration front of each tissue. We can estimate the migration velocity of each population from the slope of the migration fronts (Figure 3.8 (b)). The Ras^{V12} -mCherry and the GFP monolayers appear to migrate with comparable front velocities: $V_{front}^{Ras} = 18 \pm 2 \mu\text{m/h}$ and $V_{front}^{wt} = 16 \pm 2 \mu\text{m/h}$ (SEM, $n = 13$). We also estimate the velocity of the gap closure: $V_{gapclosure} = 18 \pm 1.4 \mu\text{m/h}$. The time of complete gap closure, $T_{closure}$, is taken on the phase contrast images. The speed of the gap closure can vary, in particular due to differences in cell density: for higher initial densities, cells tend to migrate faster towards the free space, and therefore close the gap faster than with lower initial densities.

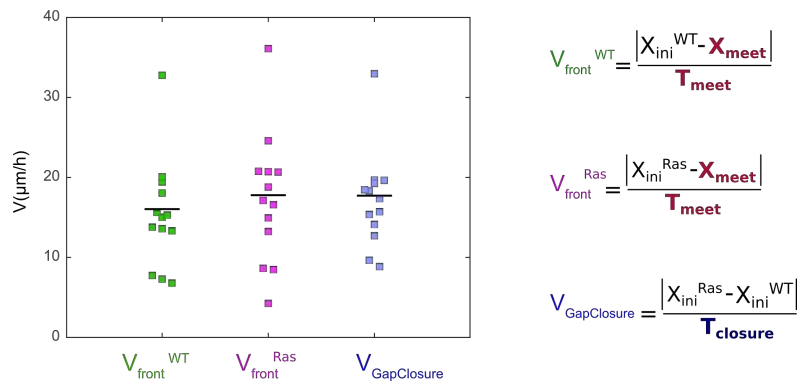


FIGURE 3.8: **Velocities of the migration front and of the gap closure.** The Ras^{V12} and wt populations have roughly similar front velocities before the meeting.

Velocity fields computed on phase contrast images

The velocity field of the tissues were computed using Particle Image Velocimetry (PIV) on the phase contrast images (see section 2.8.2). We have computed two averaged values of the velocity field, $\langle v_x \rangle$ and v_{rms} , defined as follows:

$$\langle v_x \rangle(x, t) = \left\langle \vec{v}(x, y, t) \cdot \vec{u}_x \right\rangle_y \quad \text{and} \quad v_{rms}(x, t) = \sqrt{\left\langle \vec{v}(x, y, t)^2 \right\rangle_y}$$

These values give us two different types of information: $\langle v_x \rangle$ is a measure of the velocity component in the direction of migration x , and translates the effective motion forward, *i.e.* towards the free surface of the opposing population. This velocity is represented in blue when positive, *i.e.* when cells migrate towards the right, and in orange when negative, *i.e.* when cells migrate towards the left (Figure 3.9). On the other hand, v_{rms} represents the average velocity of the cells in the tissue regardless of their direction, and can be seen as an activity. In the example shown in Figure 3.9, the gap closes 21 hours after the barrier removal (see phase contrast panel).

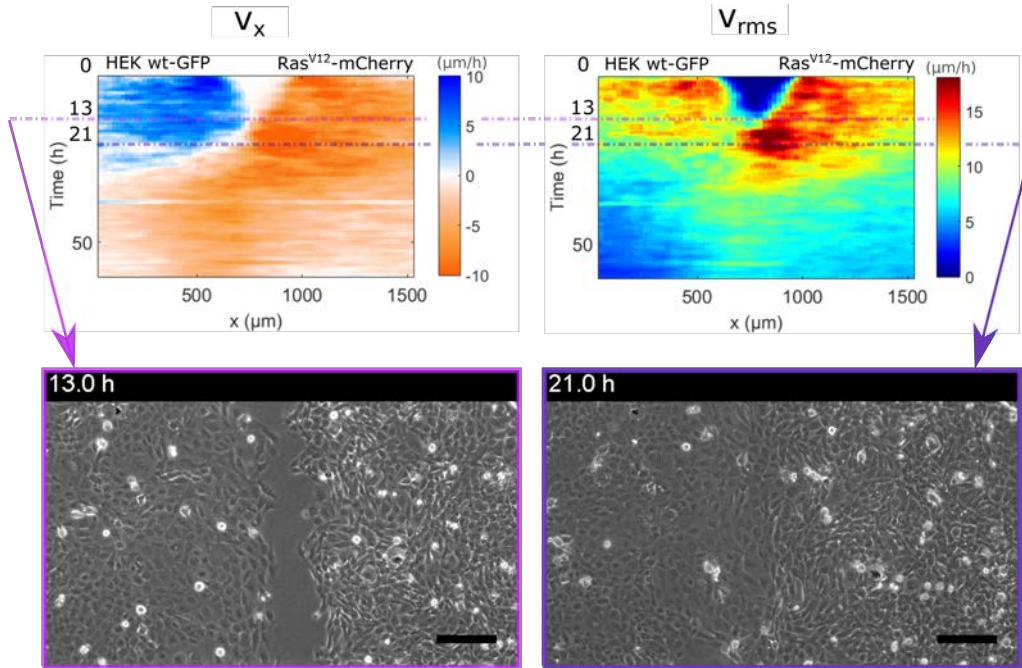


FIGURE 3.9: **Kymographs of $\langle v_x \rangle$ and v_{rms} of an AMA.** $\langle v_x \rangle$ and v_{rms} are averaged along the y -axis, and color-coded. The velocity along the x -axis, $\langle v_x \rangle$, appears blue for motion towards the right, and orange for motion towards the left. Note that the velocity kymographs do not strictly represent the position of the migrating front: they are calculated as the average of the velocity field along the y -axis, so only a few cells are needed to make the average non null. On this example, 13 hours after the barrier removal (pink line), the velocities in the center are non null, but the gap between the two populations is not yet closed (phase contrast image, left panel). The non-zero values come from the roughness of the migration front: cells do not migrate in a straight line, but rather in a wavy front, so that there are non-zero values at the center even if the cells do not yet touch each other. Scale bar: 200 μm .

We also computed the distributions of the velocities in each population before the meeting (Figure 3.10). We note that the velocities of the two populations in the x direction are roughly similar. The velocities along the y -direction are close to zero, consistent with the fact that the populations migrate primarily in the direction of the free surface (wound). The norm of the velocity is slightly higher for the Ras^{V12} population, which translates a higher internal motion in the monolayer. Besides, the angle distribution of the velocities indicates that the wt population migrates in a more directed manner than the Ras^{V12} one, a characteristic that was studied more extensively in Simon Garcia's thesis manuscript [174].

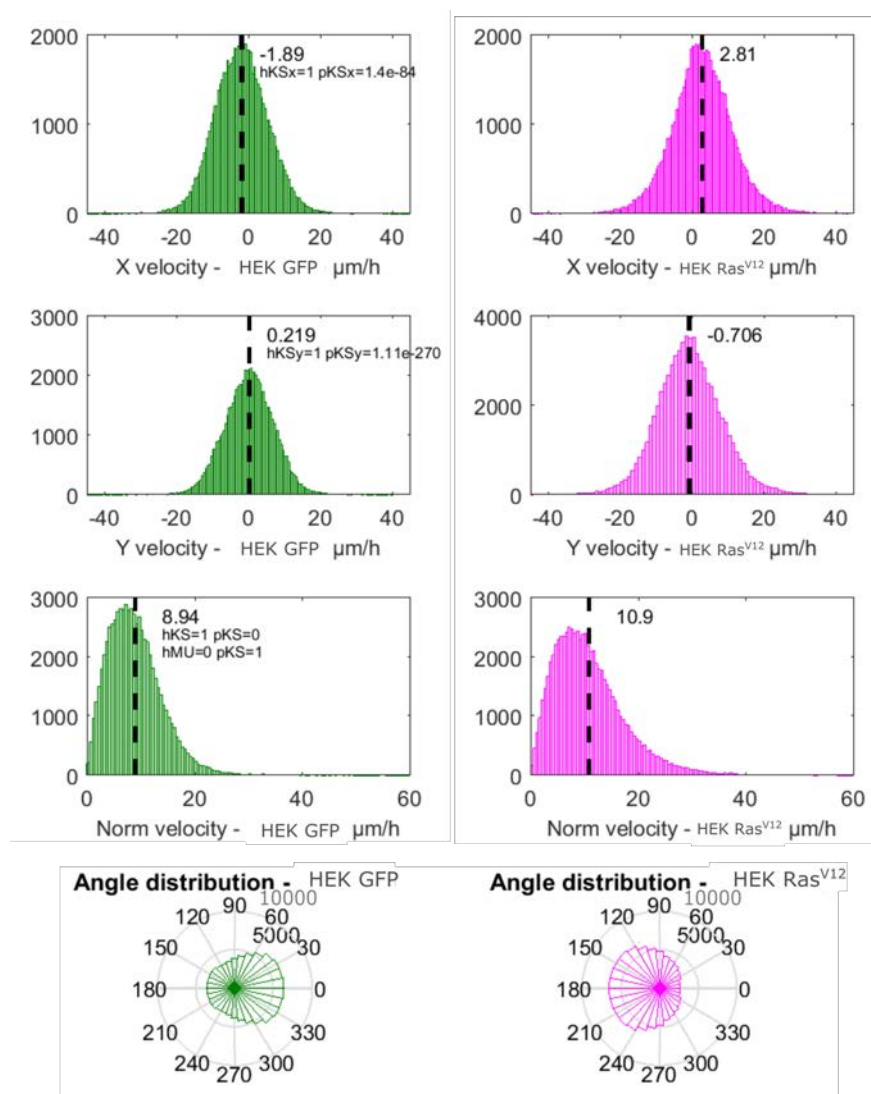


FIGURE 3.10: **Velocity distributions of each cell population computed before the meeting, on one example of AMA.** The velocities in both direction, as well as the norm of the velocity, were obtained by PIV on the phase contrast images, in the bulk of each population, before their meeting. The velocity of both populations in the x -direction is roughly similar, and the velocity in the direction perpendicular to the wound closure (y) is close to zero. The Ras^{V12} population displays a slightly larger velocity norm, and appears less directed along the x -direction than the wt population.

3.3.2 After the meeting, the Ras^{V12} population moves forwards and the wt population goes backwards

After the gap closes, the migration does not come to a halt, and a competition for space arises between the two populations (Figure 3.11). The Ras^{V12} monolayer continues to advance, while the wt population moves backwards. To illustrate this, we draw the typical kymographs for the entire duration of the experiment, for the GFP and mCherry signal intensity, as well as the overlay of the two signals (Figure 3.13).

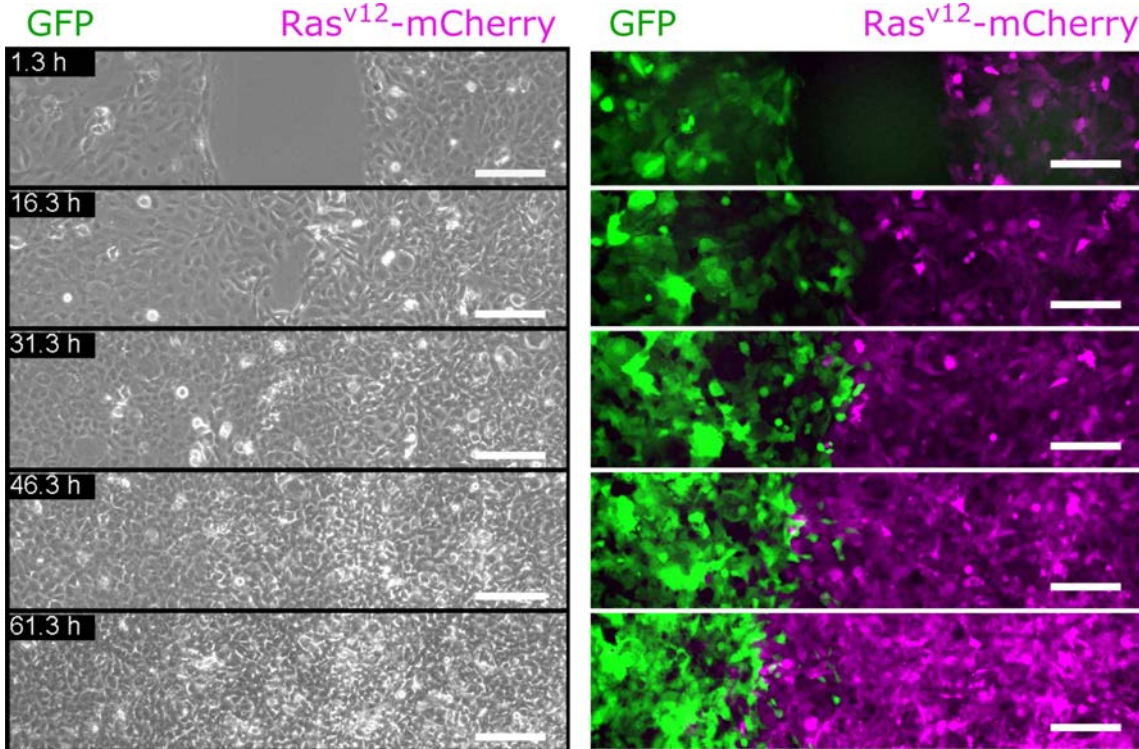


FIGURE 3.11: **An example of AMA on plain glass showing the backward migration of the GFP population after the meeting.** Phase contrast images (left) and fluorescence images (right) of an AMA between HEK GFP cells (green) and HEK Ras^{V12} -mCherry cells (magenta). Once the gap is closed, the transformed Ras^{V12} -mCherry population continues moving forwards, while the normal GFP population goes backwards. The time reference $t = 0$ h is set when the physical barrier is removed. Scale bar: $200 \mu\text{m}$.

Besides, we see on the velocity kymographs (Figure 3.9) that $\langle v_x \rangle$ becomes mostly negative (orange), as Ras^{V12} cells continue migrating forwards, but wt cells start going backwards, *i.e.* towards the left. In both the $\langle v_x \rangle$ and v_{rms} kymographs, the velocity values naturally decrease after the meeting, as the cells migrate more and more slowly as their density increases. Note that the phase contrast images do not allow us to distinguish between the two cell types after the meeting, so the velocity values measured after the gap has closed give a global view of the movement of the whole monolayer.

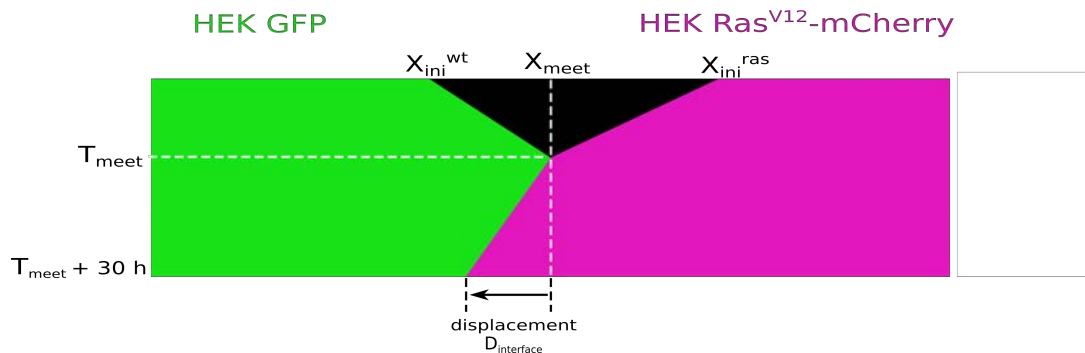


FIGURE 3.12: **Schematic representation of the 1D fluorescence kymographs.** We represent X_{ini}^{wt} , X_{ini}^{Ras} , X_{meet} and T_{meet} , as previously described, as well as the displacement of the interface $D_{interface}$ 30 h after the meeting.

AMA kymographs on fluorescence channels

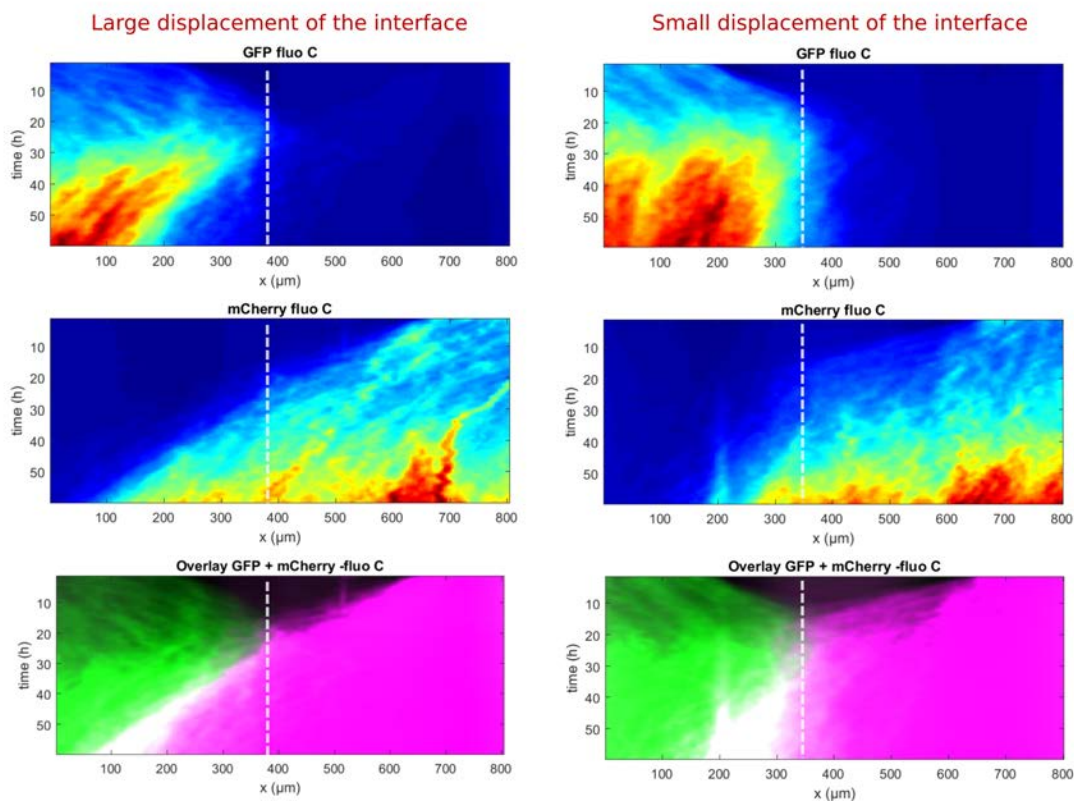


FIGURE 3.13: **Typical examples of 1D fluorescence kymographs of the AMA.** Antagonistic migration assay of HEK GFP and HEK Ras^{V12} -mCherry cells (in green and magenta, respectively) results in a large (left) or small (right) recoil of the wt population from the Ras^{V12} population. Kymographs of the GFP (top) and mCherry (middle) signal intensity averaged over the y -axis. **Bottom:** Overlay of the two signals.

To quantify the recoil of the wt population, we measured the displacement of the interface between the two populations 30 hours after the first meeting T_{meet} . It ranges from an almost static interface (only a few micrometers) to more than 100 μm (*i.e.* the width of about 10 cells), with an average of $76 \pm 18 \mu\text{m}$ (SEM, $n = 13$)¹. The velocity of the interface was deduced from this displacement (Figure 3.14). The average interface velocity is $2.7 \pm 0.5 \mu\text{m/h}$ (SEM, $n = 13$), which is non-negligible, considering that there is no free space anymore. We have only encountered the case of transformed Ras^{V12} cells moving forward and the wt backward, never the opposite.

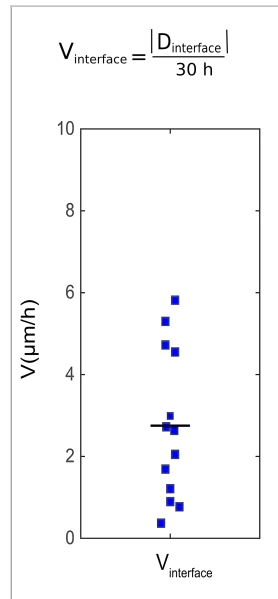


FIGURE 3.14: **Velocity of the interface between the two populations after the meeting.** The average interface velocity is $2.7 \pm 0.5 \mu\text{m/h}$ (SEM, $n = 13$).

Note that this behaviour is reminiscent of that observed by Porazinski *et al.* in their cell confrontation assay between MDCK wt and Ras^{V12} populations [124]. However, in our case of HEK wt and Ras^{V12} cells, the situation is reversed: here, it is the front of the wild-type population that regresses while the Ras^{V12} keep on marching forward. Porazinski *et. al* attributed the phenomenon they observed to an ephrin-dependent mechanism described in section 1.4.5, which, by extension, is affected by E-cadherin. It is therefore not surprising that our system does not follow the same mechanism, given that HEK cells have low levels of E-cadherin [182].

¹These results were pooled from the data collected by Simon Garcia and myself.

Given that both cell types remain well mixed when seeded together, we could have expected the two populations to interweave as they met after closing the gap. This is observed only to a limited extent, as some cells from each population locally penetrate the opposite one. But the two cell populations essentially stay separated after the gap closure, forming a visible frontier between the two cell populations (Figure 3.11). This counter-intuitive behaviour raises several questions: what is the mechanism underlying the forward motion of Ras^{V12} and the backward motion of wt cells? Are the Ras^{V12} cells actively pushing on the wt cells, and if so, how? Is there a parameter in the initial conditions that could predict the evolution of the system?

3.4 What affects the evolution of the interface?

3.4.1 Effect of the initial density

The first parameter that comes to mind as a potential factor in the AMA is the density of the cell monolayers. Even though the cells are counted before seeding, it is quite hard to precisely control the initial density of the monolayers in these kinds of experiments. Even within one compartment, the cells do not spread homogeneously, so that some areas of the monolayer end up more or less crowded than others. Therefore, we cannot rely on the number of cells calculated before seeding: we need to estimate the cell density based on the first images taken after the culture insert removal.

Initial cell density was thus measured by manual counting on the phase contrast images within 2 hours of the barrier removal. We were surprised to see that the initial densities did not provide a way to predict how the frontier between the two populations would evolve. Neither the absolute initial densities, the ratio between the densities on either side, nor their difference, gave any indication of how the antagonistic migration assay would unfold (Figure 3.15).

3.4.2 Effect of the proliferation

To account for the evolution of cell density over time, we then examined cell proliferation. This is a critical parameter in the homeostatic pressure theory [113], and one we need to consider in our experiments: the displacement of the interface arises about 40 hours after the culture insert removal, which is slightly more than twice the doubling time of the cells.

Our first approach was to block cell division altogether to see how this would differ from the control experiments. It was challenging to use mitomycin C to block proliferation, as it is toxic for cells at high concentrations, and likely to lose its efficacy over long periods of time at low concentrations. The preliminary experiments ($n = 2$) yielded a displacement of the interface similar to those observed in the control condition: $59 \pm 4 \mu\text{m}$ (SEM, $n = 2$), but we observed that cells had started to divide again after a few hours, revealing a drop in the drug efficiency

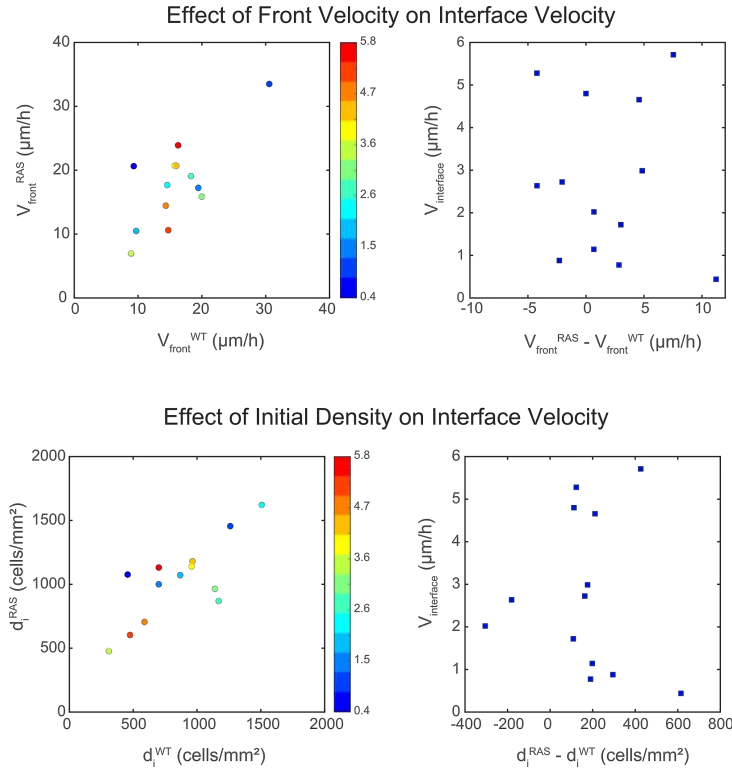


FIGURE 3.15: **Effect of the front velocities and initial densities on the motion of the interface between the HEK-GFP and HEK Ras^{V12} -mCherry populations.** Neither the initial front velocity (top), nor the initial density (bottom), of the populations seems to affect the displacement of the interface between the two populations after meeting.

and making these experiments not fully exploitable. One solution to keep blocking proliferation would be to inject, at low concentrations, fresh mitomycin C regularly during the experiment.

We have also tried to deplete the medium of serum (0.2 % vol/vol instead of the usual 10 %) in order to stop cells from proliferating, but this stopped them from migrating altogether, and thus prevented the meeting between the two populations. All in all, we did not find a proper experimental solution to block proliferation without disturbing the AMA experiment too much. We are more inclined to think that a theoretical model could answer this question.

Another approach would be to count the number of cells as a function of time. The usual ways of counting cells are based on nuclear labelling. But the classical Hoechst staining cannot be used over long periods of time², as it is toxic for cells [185]. There now exists a less toxic dye to label cell nuclei, SiR-DNA (or SiR-Hoechst [186], Spirochrome), that we have used to account for cell proliferation over time for the most recent experiments, which remain to be analyzed.

²The AMA experiments typically last 4 days.

3.4.3 Effect of the traction forces

We then set to evaluate the forces exerted by the cells on the substrate using TFM, to see how forces were involved during the antagonistic migration assay.

Effect of the substrate

The TFM experiments are done on soft acrylamide gels, which need to be coated with fibronectin, a protein of the extracellular matrix, to enable adhesion of the cells to the substrate. Since we generally carry out experiments on plain glass, we first wanted to evaluate the effect of a fibronectin-coated substrate on the antagonistic migration assay. We thus coated the glass with fibronectin at $25 \mu\text{g}\cdot\text{mL}^{-1}$ and conducted the antagonistic migration assay as previously described.

We observed slight differences between the plain glass and fibronectin-coated substrates. First of all, we noted that the cells migrated faster on a fibronectin-coated substrate, so that the gap was closed earlier than in the plain glass experiments: 22 ± 3 h on average on fibronectin (SEM, $n = 8$), against 29 ± 2 h on average on glass (SEM, $n = 13$). Second, the interface created between the two populations was less well defined than previously observed: cells intermingle more at the border, and especially single *Ras*^{V12} penetrate further in the wt tissue (notably for low cell density). Ultimately, we observed that the fibronectin coating gives rise to a more individual migration, as was previously described [187], and that this favors the interpenetration on the two populations at their interface, instead of a cohesive front as seen on plain glass. This interpenetration is also helped by the potentially lower cell density of the monolayers on fibronectin, which leaves more room for cells to migrate within their own population and, crucially, the opposing population. But the fibronectin coating only slightly reduced the amplitude of the displacement of the interface between the two populations after the meeting: we measured a mean displacement of $51 \pm 11 \mu\text{m}$ (SEM, $n = 4$), compared to $76 \pm 18 \mu\text{m}$ (SEM, $n = 13$) for a plain glass substrate. Thus cell adhesion to a fibronectin-coated substrate does not appear as a critical parameter in the outcome of the AMA, so it is unlikely to disturb TFM experiments.

Preliminary TFM results

Doing the AMA experiment on soft polyacrylamide gels revealed quite tricky, especially since the hydrogels have to be kept hydrated at all times, and the Culture Insert 2-wells is specifically treated to adhere to a glass or plastic substrate in dry conditions. We have finally managed to couple the two experimental techniques, by taking advantage of a short window of time in which the gel is dry enough that the insert will attach, but not too dry that it starts to crack.

The preliminary results, in the first hours of migration of the monolayers, show that the wt population displays higher forces on the substrate than the Ras^{V12} population (Figure 3.16). This is consistent with the values we have obtained with TFM for single cells (section 3.1.2), knowing that the value of the traction forces scales with the size of the cell population [188]. We haven't yet been able to carry out this experiments at longer times, though. When we do, we expect to gain a better understanding of the forces at play, and thus on the mechanical interactions at the interface between the two populations.

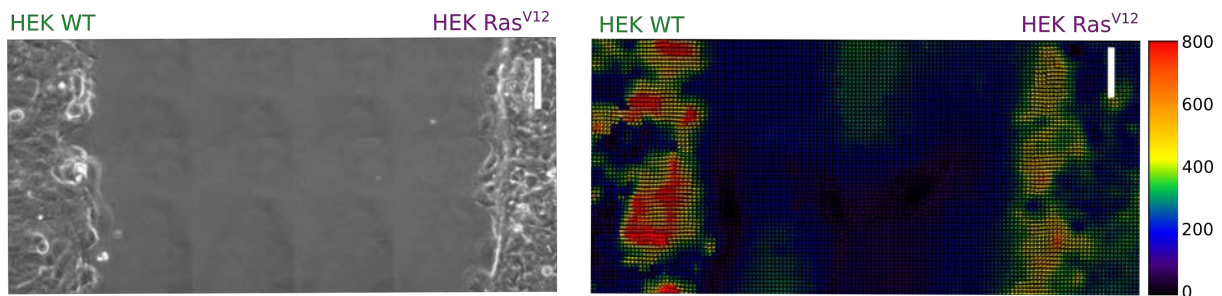


FIGURE 3.16: **Traction forces displayed at the beginning of an AMA.** **Left:** phase contrast images. **Right:** Traction forces measured for the two populations in the first few hours of the AMA. This experiment was done by Tobias Martin, intern in the team. Scale bar: 75 μm .

We suspect the mechanical interactions between the two populations to be a crucial parameter in the outcome of the AMA. Interestingly, Blanch-Mercader *et al.* came up with a model that is able to accurately characterize the behaviour of a cell monolayer in migration, only taking into account the velocities and traction forces involved [189]. We could thus adapt this model to the situation of two cell monolayers migrating face to face, in order to model the AMA. This suggests that we could potentially describe the outcome of this experiment using only the velocities and traction forces.

Discussion

In this chapter, we have described the use of the Antagonistic Migration Assay to study the confrontation of two cell populations initially separated: HEK wt and HEK Ras^{V12} . This work is the continuation of a project started by Simon Garcia [174]. He had previously established that an interface is created between the two populations when they come into contact, and that this interface moves along the direction of migration of the transformed cell type. His velocity analyses showed that the transformed population displays a higher activity, but a lower persistence and polarization than the normal cell type, translating a poorer migration efficiency of the Ras^{V12} cells. Yet, this cell type still manages to gain ground on the normal cell type in this competition for space.

We have since tried to identify which parameters played a role in the outcome of this competition. We have shown that the initial density of the two monolayers did not affect the displacement of the interface after the meeting. Neither proliferation nor substrate biochemistry seemed to influence too much the global migration of the two populations, and of the interface between them. Based on our preliminary experiments, we suspect the traction forces at play between the two populations to be critical in this assay.

Effect of the size of the interface between the two cell types

The fact that these two cell types stayed mixed when seeded together, but formed a border at the population level when initially separated, suggests that the size of the contact area between the two cell types could play a role in the evolution of the system after the meeting. To test this hypothesis, we varied the size of the interface between the two populations by confining them in stripes of different width. Adhesive patterns were made, following the protocol described in Chapter 2 (section 2.3.2), in the shape of stripes of various width, ranging from 50 μm to 500 μm (Figure 3.17). By performing the antagonistic migration assay on these stripes, we could therefore control the width of the interface, varying the approximate number of cells from each cell type that will come into contact with each other.

Our preliminary results seemed to indicate that confining the populations on adhesive stripes hindered the displacement of the interface between the wt and Ras^{V12} cells. We noticed that the interface between the two populations was less well defined than in the unconfined situation, and that the two populations tended to interpenetrate more around the meeting border, especially for stripes narrower than 100 μm . This made it more difficult to define a proper “frontier” between the two populations, and to study a potential displacement of this frontier. Besides, confining cells in stripes not only limits the size of the monolayers, it also introduces physical borders to the area of migration. Indeed, the cells closest to the border migrated faster along the side of the stripes, giving rise to shapes that diverged greatly from the mostly linear migration front that we observe in the unconfined case (Figure 3.17 (b)). Hence, it seems more appropriate to adopt a different geometry in order to avoid these challenges when varying the size of the interface: for example a circular geometry. By creating a circular patch of transformed cells in a normal tissue, we can tune the size of the circular patch without introducing physical borders (*i.e.* confinement).

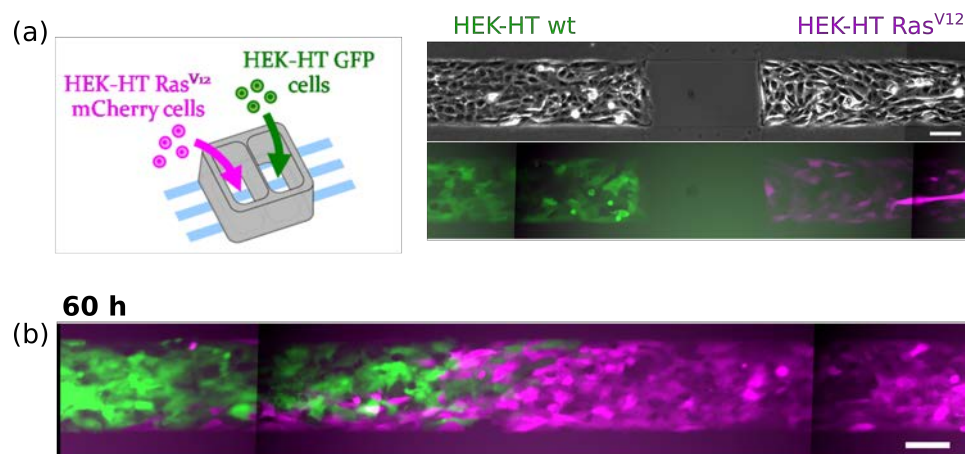


FIGURE 3.17: **Principle of AMA on stripes.** (a) **Left:** The culture insert was placed on the patterned substrate, with its border perpendicular to the adhesive stripes. Cells were then seeded in both compartments as usual. **Right:** Phase contrast and fluorescence images of monolayers of HEK GFP and HEK *Ras*^{V12}-mCherry cells confined in a 200 μm-wide stripe, after culture insert removal. (b) The AMA on a confined stripe is clearly affected by the physical borders 60 h after removal: the interface between the two population is tilted, and the two populations interpenetrate each other around this border. Scale bars: 100 μm.

The use of a physical barrier to place two different cell populations in contact is very convenient, not least because it is straightforward and can be used with any two populations of cells. The main limit of this system is that it lacks flexibility in the shape and size of the interface created. Another shortcoming of this method is that it implies a phase of migration in a free space before the two populations come into contact. In order to draw nearer to biological situations, in which there is no such free space, **the interface between cell populations can be created *in situ***. This can be done using an inducible oncogene, *i.e.* an oncogene whose expression can be triggered using a specific stimulus. In this respect, we have used an optogenetics-based system to study cell competition using a light-inducible oncogene, presented in the following chapter.

Chapter 4

Using optogenetics to study *in vitro* cell competition

“Happiness can be found in the darkest of times,
if one only remembers to turn on the light.”

Dumbledore, in *Harry Potter*
and *the Prisoner of Azkaban* by JK Rowling

Contents

4.1	Optogenetics: a control of cell activity using light	69
4.1.1	Why optogenetics?	69
4.1.2	Optogenetic systems	69
4.1.3	The CRY2/CIBN system	71
4.2	MDCK OptoSrc: a cell line expressing a light-inducible Src	74
4.2.1	The OptoSrc system	74
4.2.2	Behaviour of a MDCK OptoSrc cell at the cellular scale	76
4.2.3	Migratory properties of a monolayer of MDCK OptoSrc cells	78
4.2.4	Effect of the blue light stimulus on cell division and cell extrusion	80
4.3	Competition between normal and OptoSrc cells	81
4.3.1	Single OptoSrc cell in a wt monolayer	81
4.3.2	Group of OptoSrc cells in a wt monolayer	83
4.4	OptoSrc & patterned light: optical control of local Src activation	84
4.4.1	Local Src activation in the OptoSrc monolayer	84
4.4.2	Control, in space, of the collective extrusion	95
4.4.3	Control, in time, of the collective extrusion	97
4.4.4	Effect of the initial density on the collective extrusion	101
4.4.5	Molecular basis of the collective extrusion	103
4.4.6	Does the collective extrusion require a frontier between two distinct src-level populations?	105
4.4.7	Is the collective extrusion associated with an Epithelial-Mesenchymal Transition?	107

In real situations of carcinogenesis, the cells undergoing mutations are already in contact with the surrounding healthy tissue. This type of situation is therefore the most relevant to reproduce *in vitro*. Our goal in the present project is to develop a new *in vitro* tool to work on a model situation: we wish to create a cluster of transformed cells embedded in a monolayer of healthy cells “on demand”.

The key to creating this type of model situation properly is to achieve a good control of the initial conditions in time and space (*e.g.* in terms of density and geometry). Our strategy thus consists in a precise tuning in time and space of the oncogene transformation, and, ultimately, its level. We propose a solution based on optogenetics, which appears to be the appropriate tool to induce such a controlled perturbation in a given group of cells.

4.1 Optogenetics: a control of cell activity using light

4.1.1 Why optogenetics?

To decipher a complex biological process, one needs tools to perturb the various players involved, in order to evaluate their relative importance. In general, three steps have to be followed: identify which players are involved, determine the ones that are necessary, and figure out if they are sufficient. The first step often implies direct visualization, which could be done using fluorescent reporters, for example. The second step consists in blocking the different conditions to see if they are necessary. This can be done with the usual disruptive tools based on genetics or chemicals.

- Genetic perturbations – such as knock-out techniques, siRNA, shRNA, and mutations – are good at identifying the proteins involved in a specific process. But the effect induced can be slow (at least 24 hours for siRNA) and wide-ranging. They might also be difficult to modulate. Recently, the powerful technique CRISPR-Cas9 has made gene editing easier, but it requires several steps of refinement to be successful [190].
- Chemical perturbations, usually drugs, can rapidly switch off a function (from seconds to a few hours). But they often have unspecific effects and do not allow a spatial control. Plus, their effect is sometimes limited in time, and they can prove to be toxic for cells.

Hence, these tools are useful to establish necessary conditions, but not to assess their sufficiency. In order to fulfill this third step, one needs to alter the conditions in a controlled manner: localised and transient perturbations are therefore required. Optogenetic tools present themselves as the most adapted way to control gene or protein expression in both space and time.

4.1.2 Optogenetic systems

Optogenetics combines genetic and optical methods to achieve gain or loss of function of well-defined events in specific cells of living tissue [191]. The field of optogenetics emerged during the last decade, and was dubbed “Method of the Year” 2010 by the journal *Nature Methods*. Optogenetic tools are based on photosensitive proteins, and have the advantages of being non-invasive, highly specific, and to allow precise spatio-temporal control of biological processes. They also trigger a fast response (within minutes), and are often reversible. The first optogenetic tools exploited opsins, a group of light-sensitive proteins found in visual systems of animals, and were originally employed in the field of neuroscience.

The optogenetic toolbox was then expanded, with a new generation of light-activated proteins, mainly based on plants and bacteria photoreceptors. The most famous ones are light-oxygen-voltage (LOV) domains, cryptochromes, and phytochromes. One of the main advantages of these systems is their reversibility. Besides, they are fully encoded, as well as fast and reliable.

Table 4.1 presents the activation wavelength and reversibility time scale of these photosensitive systems.

	Activation wavelength	Characteristic time of reversibility	Reference
LOV domain	Blue light ~ 450 nm	\sim min in dark	Yazawa <i>et al.</i> 2009 [192]
CIB1 and cryptochrome 2	Blue light $\sim 405 - 530$ nm	\sim min in dark	Kennedy <i>et al.</i> 2010 [157]
Phytochrome B and PIF6	Activated by red (650 nm) and inactivated by infra red (750 nm)	\sim s upon exposure \sim h in dark	Liu <i>et al.</i> 2008 [193]
Dronpa	Inhibition of a protein by activation of Dronpa at 390 nm Reversion at 490 nm	\sim s upon exposure \sim min in dark	Zhou <i>et al.</i> 2010 [194]
iLID	Blue light ~ 488 nm	\sim min in dark	Guntas <i>et al.</i> 2015 [195]

TABLE 4.1: Light-activated proteins.

Through the manipulation of processes affecting cell signalling, these optogenetic systems can help address many biological questions. The general strategies employed to manipulate intracellular signals with optogenetic proteins are depicted in Figure 4.1.

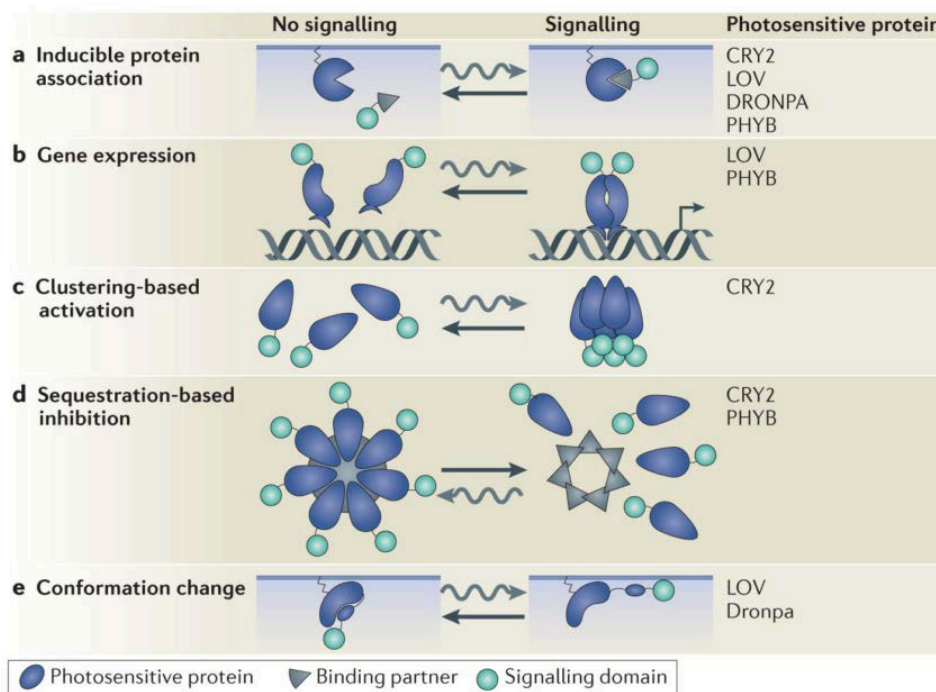


FIGURE 4.1: **Main optogenetic strategies to optically control gene or protein expression.** System reversion occurs either in the dark or can be stimulated with light, depending on the system used. From [196].

4.1.3 The CRY2/CIBN system

We opted for the CRY2/CIBN light-sensitive protein couple as the basis for our light-inducible system. CRY2 and CIBN are two plant proteins which bind upon exposure to blue light, but otherwise dissociate when blue illumination is switched off [157]. Cryptochromes are active principally in the range from 365 to 550 nm, with a maximal response between 390 and 480 nm, and a broad peak around 450 nm [154, 155].

One application of this system consists in associating the CIBN protein to the membrane, often *via* a CAAX group¹, and fusing CRY2 to a protein of interest that is inactive in the cytosol but active at the membrane. Thus, light-induced dimerization of the pair results in relocalization at the membrane of CRY2 (Figure 4.2 (a)), and of the protein of interest linked to it. Figure 4.2 (b) shows the localisation of the GFP-labelled CIBN fragment, when attached to the cell membrane, and of the mCherry-labelled CRY2 fragment before and after light excitation: respectively in the cytoplasm and at the cell membrane [157]. In the absence of blue light, the CRY2/CIBN dimer splits up following a dissociation rate k_d . The CRY2 fragment thus detaches from the membrane and diffuses back to the cytoplasm, with a characteristic time τ_d of a few minutes. Several studies have found: a dissociation time $\tau_d = 1/k_d \approx 180 \pm 40$ s, a half-life time of $\sim 6 \pm 1$ min, and a complete dissociation time of ~ 12 min ([197, 198] and [157], resp.). A new pulse of blue light can again induce the recruitment of CRY2 to the membrane.

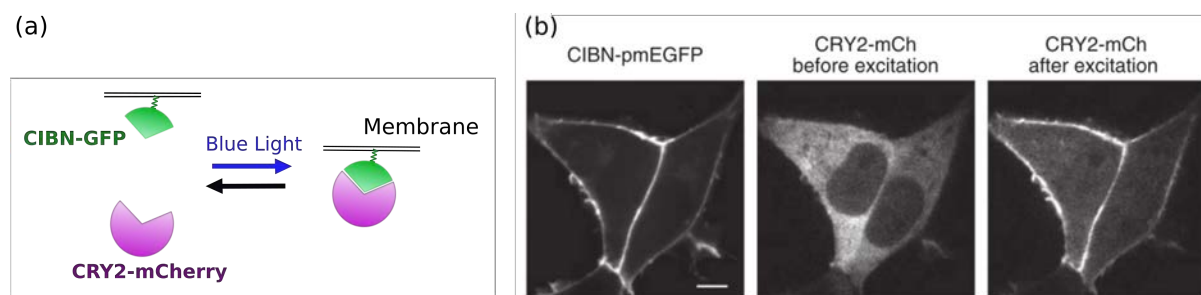


FIGURE 4.2: **Light-triggered translocation of CRY2 at the membrane in HEK293T cells.** (a) Schematic of the CRY2/CIBN proteins dimerization under blue light, which is reversible in the absence of blue light. (b) Confocal fluorescence images of CIBN-GFP and CRY2-mCherry co-expressed in HEK293T cells. CRY2-mCherry is in the cytoplasm before light excitation, and at the membrane 20 s after a 100-ms pulse of blue light (488 nm, 25 μ W). Scale bar: 5 μ m. From [157].

A significant property of the CRY2-CIBN dimerization is its reversibility, which is a typical feature of most optogenetic systems. This reversibility can be used to our advantage as it provides an additional control parameter: the frequency of illumination, which influences the residency

¹The “CAAX box” is the most common prenyl site in proteins; prenyl groups facilitate protein attachment to the cell membrane.

time at the membrane of the protein fused to CRY2. Plus, the transfection of the plasmids is easy and very stable in MDCK cells, and there is relatively little CRY2 homo-oligomerization (see box), as opposed to other cells, such as HeLa cells.

CRY2 oligomerization The behaviour of CRY2 under blue light is complex: it can either undergo heterodimerization by binding to CIBN, or homo-oligomerization by forming clusters of CRY2 [199]. This clustering process can be used on its own to create clusters of a protein, by fusing it to CRY2 [200], but it is also in competition with the heterodimerization necessary for using the CRY2/CIBN optogenetic system. However, the cytoplasmic wild-type CRY2 was found ineffective in forming clusters [201,202], so it should not, *a priori*, hinder the CRY2/CIBN dimerization upon blue light, in our cells.

The main practical inconvenience of the CRY2/CIBN system is that it is responsive to wavelengths comprised in 405 - 530 nm, which prohibits the use of CFP, GFP or YFP reporters, whose excitation wavelengths overlap with this range. Also, it requires the transfection of two different plasmids. Besides, the dissociation of the CRY2/CIBN dimer cannot be triggered: it occurs naturally in the absence of light. Finally, the blue light required for the photoactivation of CRY2/CIBN has to be kept as low as possible to avoid potential toxic effects [203,204].

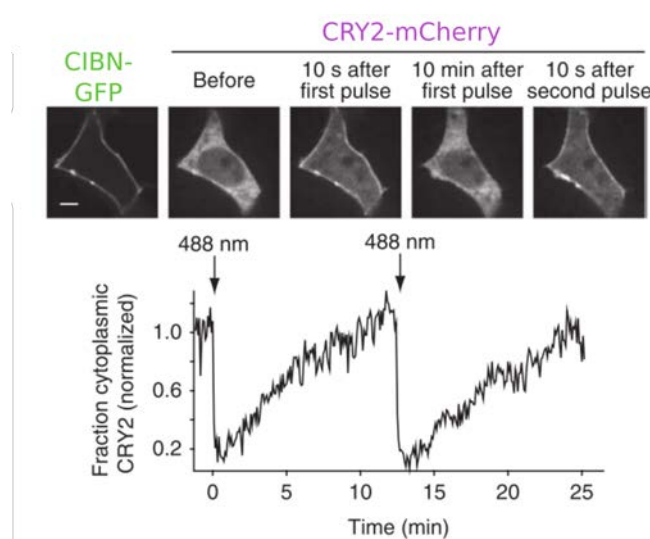


FIGURE 4.3: Light-induced CRY2/CIBN dimerization is reversible. Top: Fluorescence images of cells expressing a CIBN-GFP/CRY2-mCherry system, before and after delivery of two 100-ms pulses of blue light ($25 \mu\text{W}$) spaced 12.5 minutes apart. The CIBN fragment is localised at the cell membrane. CRY2, initially cytosolic, is rapidly ($\sim\text{s}$) translocated to the membrane due to a blue light pulse, in a reversible manner. **Bottom:** Quantification of cytoplasmic CRY2-mCherry, with blue light pulses (arrows) delivered at 0 and 12.5 minutes. The amount of CRY2 in the cytoplasm drops dramatically after a blue-light pulse, as it gets recruited to the membrane, then steadily increases in the absence of light, translating the release of the protein from the membrane. A second light pulse induces similar effects. Scale bar: $5 \mu\text{m}$. From [157].

Previous uses of the CRY2/CIBN system Some signaling pathways have already been targeted using CRY2/CIBN: *e.g.* regulation of the small GTPases Rac/Cdc42, phosphoinositides and Erk activity [198, 205, 206].

Use of a light-induced oncogene to study tumor induction Recently, the group of David Bensimon presented a new light-inducible tumor model in the zebrafish [207]. They can activate an oncogene “*kRASG12V*” in the zebrafish embryo in a non-reversible manner: by decaying a ligand (cyclofen) using light. Although this system allows them to trigger *kRASG12V* in a localized way using targeted light, they mostly show results for the illumination of entire embryos. They find that the constitutive activation of this oncogene was not efficient in inducing tumors in the fish.

Using optogenetics to study cell competition Our strategy is to use optogenetics to create a precisely controlled interface between normal and transformed cells. We use the CRY2/CIBN system to control the activity of an oncoprotein in cells using light. The idea is to select which cells will become transformed using targeted illumination, allowing us to generate groups of transformed cells of any geometry and size in a cell monolayer (Figure 4.4). We also have a dynamic control of the activation of the oncogene, thanks to the reversibility of the CRY2/CIBN system.

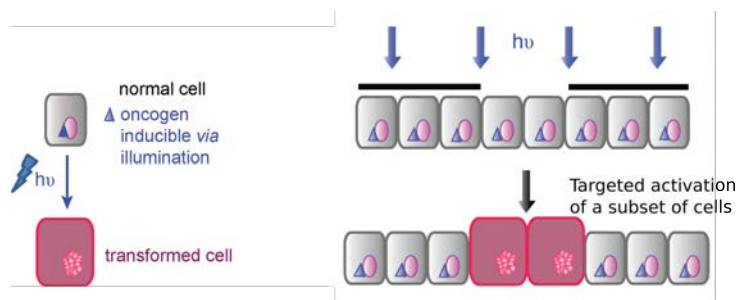


FIGURE 4.4: **Strategy to create an interface *in-situ*:** combination of a light-inducible oncogene with targeted illumination. Normal cells (grey) contain a light-inducible oncogene. Targeted illumination triggers the activation of this oncogene in selected cells (pink).

4.2 MDCK *OptoSrc*: a cell line expressing a light-inducible Src

With its combined approach using light and genetics, optogenetics provides us with a direct control of the activity of an oncogenic protein in space and time. Given that mutations activating Src are among the most common genetic alterations detected in human cancers [59], we chose to elaborate the first photosensitive Src oncogene.

4.2.1 The *OptoSrc* system

Our collaborator, Olivier Destaing (IAB Grenoble), developed the first optogenetic probe to control the tyrosine kinase Src in space and time, named *OptoSrc*. Based on the CRY2-CIBN optogenetic set-up, *OptoSrc* is a potentially active mutant that can notably phosphorylate its natural substrates after its plasma membrane relocation in a light-dependent manner. Note that in normal conditions, activation of Src is induced by both the release of intramolecular bounds (Y527, resulting in the opening of the molecule) and the unfolding of the kinase domain (Y416, leading to its autophosphorylation) [60].

The principle of the *OptoSrc* light-inducible system is depicted in Figure 4.5. CRY2-mCherry is fused to a Src mutant that is cytosolic and potentially active (open conformation), and the CIBN fragment is anchored to the cell membrane *via* a CAAX-GFP group. Specifically, the *OptoSrc* system has undergone three modifications: (a) the membrane anchoring domain has been removed, to make the protein fully cytosolic, (b) the Y527 site has been mutated in order to lock the protein in its open conformation, and (c) the SH2 domain is dead, to prevent localization of the protein in adhesive sites of the cells.

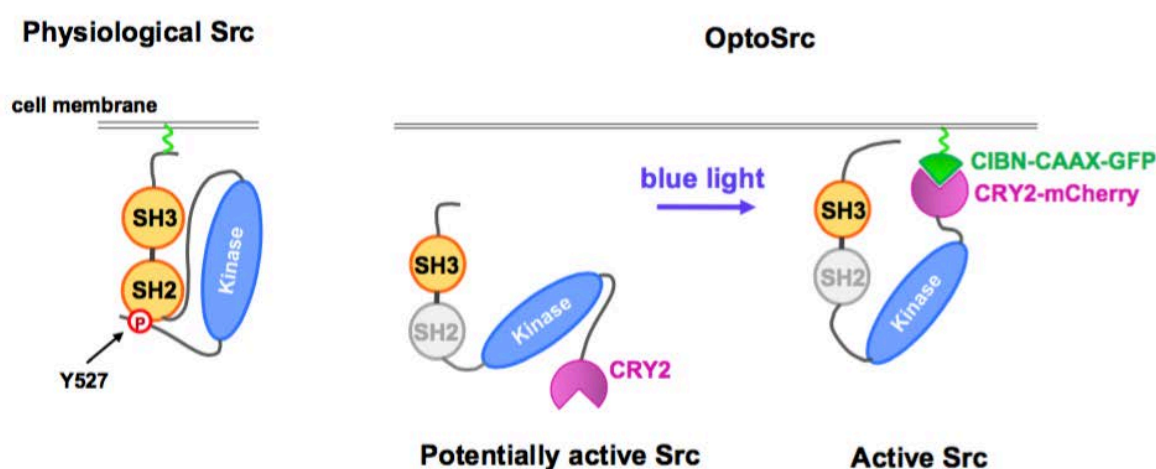


FIGURE 4.5: **Principle of the *OptoSrc* light inducible system:** activation of Src kinase is mediated *via* its recruitment to the membrane using the light-sensitive system CRY2-CIBN.

A pulse of blue light (typically $\lambda \sim 488$ nm) is sufficient to induce the dimerization of CRY2-CIBN, thereby translocating CRY2-Src to the membrane where its natural substrates are, and it is thus able to phosphorylate them (cf. Figure 4.6). Hence, we can induce the activation of the Src kinase in a cell with a blue light stimulus. In the dark, the CRY2/CIBN dimer splits up: the OptoSrc is free to diffuse back to the cytoplasm, away from its natural substrate, and stays inactive.

Our OptoSrc is:

- fully cytosolic
- ready to be translocated to the membrane
- susceptible to phosphorylate its substrates

This OptoSrc system was stably expressed in a MDCK cell line. From now on, we use the term “MDCK OptoSrc”, or simply “OptoSrc cells”, to refer to this stable cell line expressing the light-inducible Src oncogene.

Since stable cell lines of OptoSrc were obtained by a cotransfection (double or triple) of MDCK cells, one should note that there remains the endogenous Src, which is not sensitive to blue-light, in all the MDCK OptoSrc cells. Consequently, the effect of blue light illumination must be viewed as an over-activation of Src compared to the situation where the cells are in the dark. It is difficult to estimate the proportion of OptoSrc over the endogenous Src. The expression of pY416A (autophosphorylation) in OptoSrc cells displayed a 7-fold increase after blue-light illumination, compared to cells kept in the dark.

The OptoSrc system was validated using western blots. This technique enables one to detect specific proteins in a sample using fluorescently-labeled antibodies and a gel electrophoresis [208]. The amount of phosphorylated p130^{Cas}, a major substrate of Src, was detected in MDCK OptoSrc cells that had been exposed, or not, to blue light. Indeed, phosphorylation of p130^{Cas} has been found to correlate strongly with v-Src transformation [209]. The resulting western blot (Figure 4.6) shows that MDCK OptoSrc cells exposed to blue light display a higher level of phosphorylated p130^{Cas} than non-exposed cells, demonstrating an increased Src activity upon blue illumination. Besides, the amount of phosphorylated p130^{Cas} dramatically dropped with the addition of the Src inhibitor PP2. Taken together, these results show that membrane relocalisation of Src *via* blue light exposure is sufficient to increase the phosphorylation of p130^{Cas} in a PP2-dependent manner. These western blot analyses were made by Adèle Kerjouan and Olivier Destaing (manuscript in preparation).

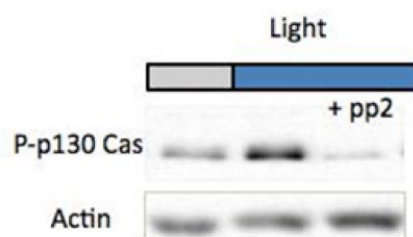


FIGURE 4.6: **Validation of the OptoSrc system by western blot:** recruitment of Src to the membrane using blue-light exposure increased the phosphorylation of p130^{Cas} in a PP2-dependent manner. The actin band is the loading control. Courtesy of A. Kerjouan and O. Destaing.

Our optogenetic approach presents numerous advantages, chief among them is the spatio-temporal control of an oncogenic transformation. Besides, our system is specific, non-invasive, reversible, and versatile. It can even be used in association with other types of inducers, such as chemical drugs, or other oncogenes (for example Ras or Myc).

We first studied the behaviour of the OptoSrc cells by themselves, to confirm that effects consistent with Src activation could indeed be induced by blue-light stimulation, and that these effects were reversible.

4.2.2 Behaviour of a MDCK OptoSrc cell at the cellular scale

OptoSrc is recruited to the membrane upon blue-light illumination

Partial illumination was used on a cluster of MDCK OptoSrc cells using the Mosaic 2 DMD module, to confirm that we could induce the recruitment of CRY2-Src at the membrane of selected cells (Figure 4.7). We checked that this relocalisation was reversible when the blue light was switched off, as described in the literature [157]. Figure 4.7 shows that CRY2-Src is recruited to the membrane in the cells contained in the illumination area, and diffuses back to the cytoplasm in the absence of light. The mCherry signal in cells outside of the exposed area is not impacted, with a spatial resolution of $\sim 15 \mu\text{m}$.

Membrane ruffling Src signalling is known to be involved in ruffle formation [210, 211], a process due to actin rearrangement. Indeed, upon blue illumination, OptoSrc cells started exhibiting membrane ruffling. When the light was turned off, this membrane ruffling rapidly stopped. When cycles of light and dark were conducted, the ruffling was turned on and off accordingly. Figure 4.8 shows the GFP signal (activation channel), as well as the phase contrast images and the mCherry (CRY2) channel, in an MDCK OptoSrc cell. The kymograph on the right shows the cross-section (purple line) of the mCherry signal in a cell over time. We can visualize the membrane ruffling of the cell, which is only present during the times of illumination (blue rectangles).

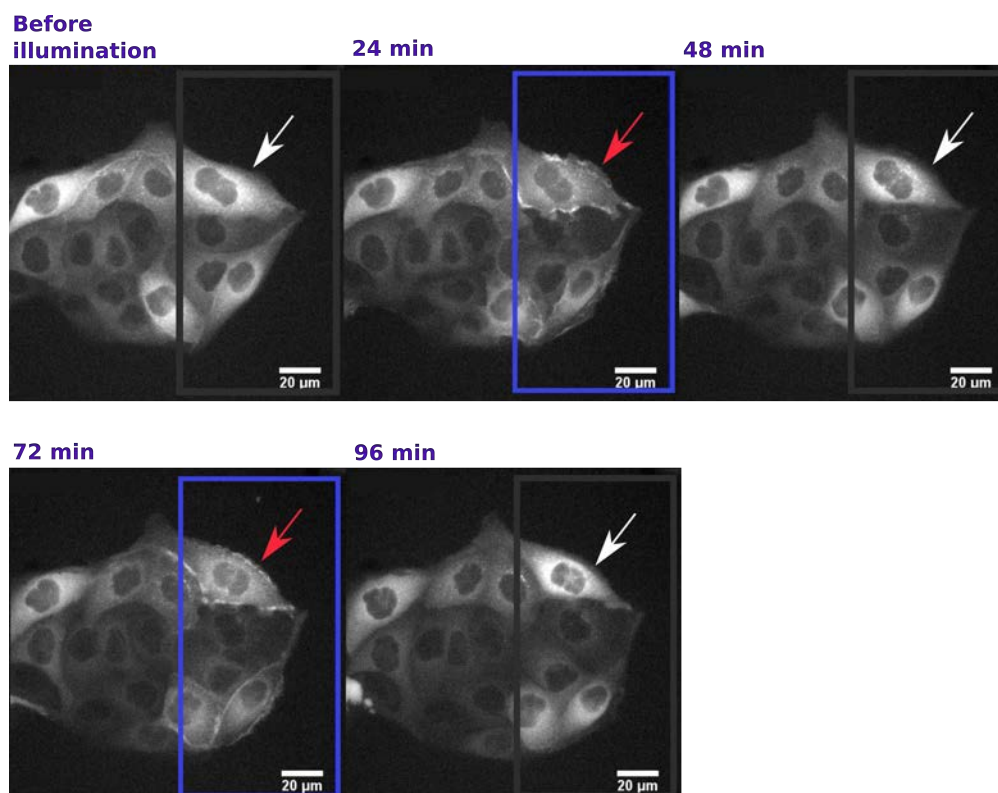



FIGURE 4.7: **CRY2** relocalization upon blue light illumination in MDCK OptoSrc cells. In this experiment, 200-ms light pulses were induced every 20 seconds for 20 minutes, followed by 20 minutes in the dark. This cycle was repeated once more. The epifluorescence CRY2-mCherry signal shows the recruitment at the membrane of CRY2 (red arrows) in illuminated OptoSrc cells (blue rectangles). When left in the dark, CRY2 diffuses back to the cytoplasm (white arrows). Scale bar: 20 μm .  [Movie 4.7](#)

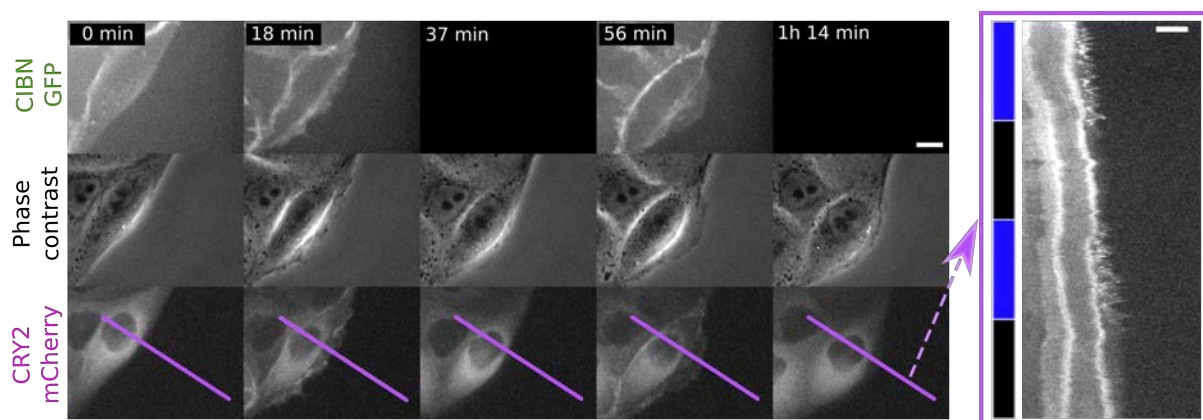



FIGURE 4.8: **Membrane ruffling** upon light activation of Src. **Left:** CIBN-GFP, Phase contrast and CRY2-mCherry images of cells going through two light/dark cycles. **Right:** Kymograph of a section of cell (purple line) over 80 minutes, showing membrane ruffling upon blue illumination (blue rectangles). Scale bar: 10 μm .  [Movie 4.8](#)

4.2.3 Migratory properties of a monolayer of MDCK OptoSrc cells

We then studied the effect of Src photoactivation at the monolayer level using a wound healing assay. OptoSrc cells were cultured in two wells separated by a physical barrier, using a Culture Insert (Ibidi) as in the previous chapter. When cell monolayers had formed in both compartments, the frontier was removed and the cells were free to migrate in the available space. Figure 4.10 shows the gap closure of OptoSrc cell monolayers in the absence (left) or presence (right) of blue light.

In the case of non-activated cells, the migration front is well defined and displays finger-like structures (left, $t = 20$ h), as previously described for MDCK wt cells [123]. In the case of Src over-activated cells, however, the cells at the edge behave in a less cohesive manner. The migration front is less well defined, and we can see individual cells detaching from the monolayer to migrate in the free space on their own (detailed on Figure 4.9), which we have as yet never observed in the case of a confluent monolayer of MDCK wt cells. We also note that the Src-activated cells migrate faster than the non-activated cells, as exemplified by the gap closing time: 31 ± 1 h in the case of exposed cells as opposed to 37 ± 1 h for non-exposed cells. Kymographs of the root mean square velocity (v_{rms}), as well as the velocity in the direction of migration ($\langle v_x \rangle$) were established as described in Chapter 2, and are shown in Figure 4.10. We observe that Src-activated cells exhibit both a higher v_{rms} and a higher $\langle v_x \rangle$, especially in the first few hours of migration, which explains the faster gap closure.

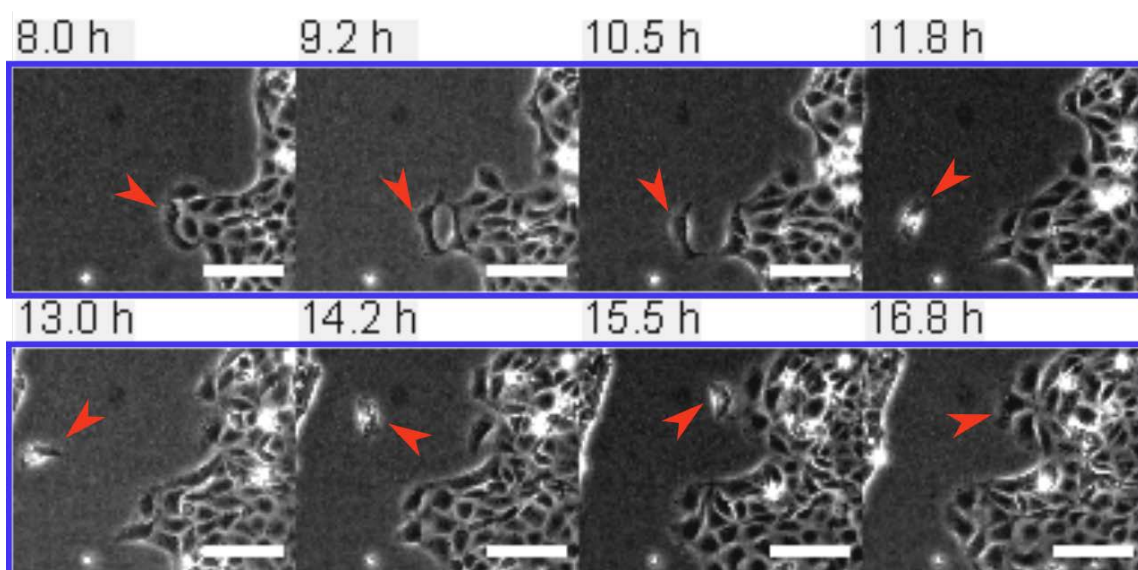


FIGURE 4.9: An OptoSrc cell detaches from the monolayer to explore the free space (red arrows), during a wound healing assay. Blue-light illumination: 200-ms pulse every 5 minutes. Scale bar: $100 \mu\text{m}$.

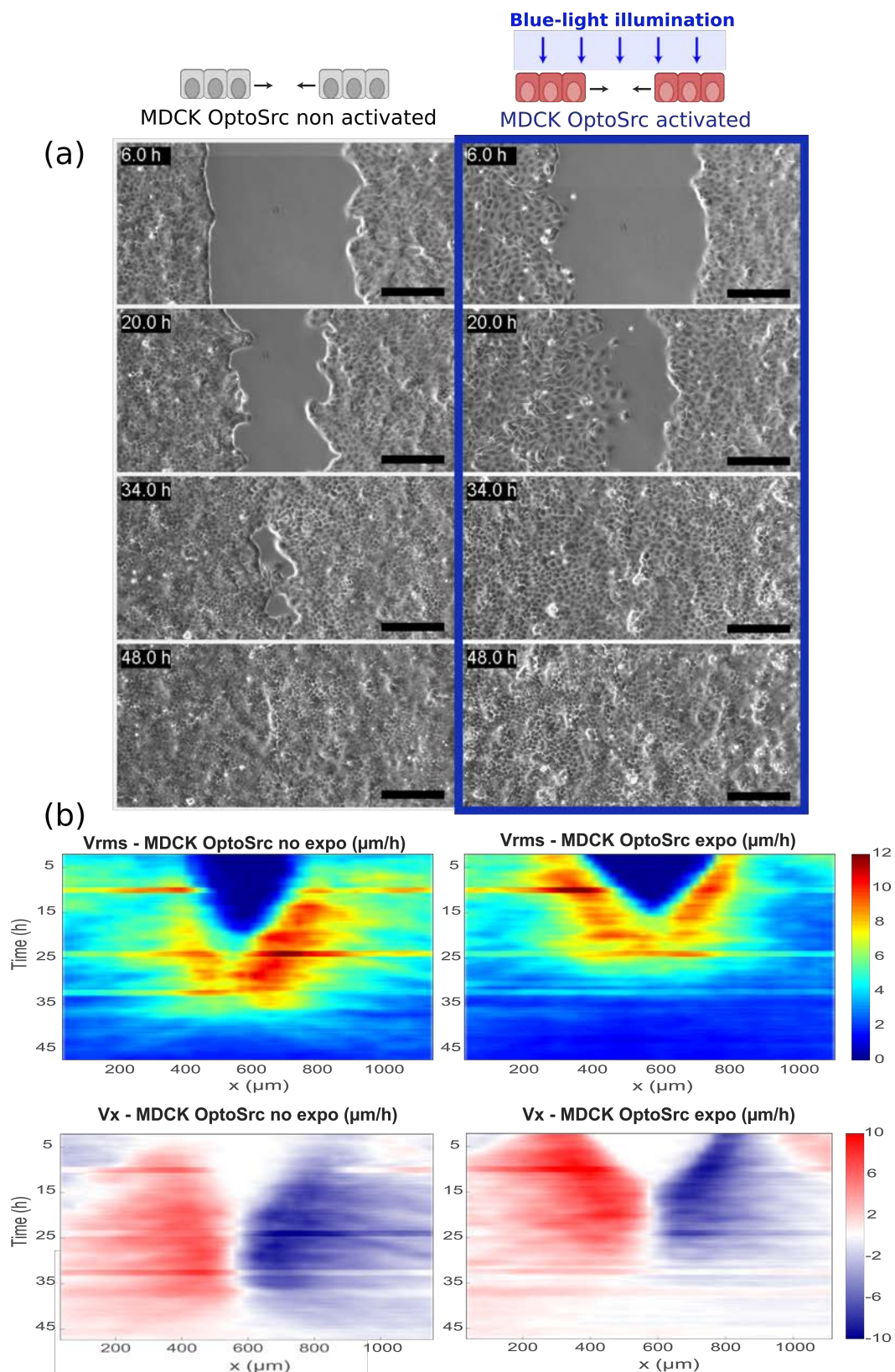


FIGURE 4.10: **Wound healing assay on OptoSrc cells.** (a): phase contrast images. **Left:** Without intermittent blue light, the migration front is well defined, and the gap takes longer to close. **Right:** With intermittent blue light (200-ms pulse every 5 minutes), Src activated cells display a less coherent migration front. Scale bar: 200 μm . (b): Velocity kymographs $\langle v_x \rangle$ and v_{rms} . [Movie 4.10](#)

4.2.4 Effect of the blue light stimulus on cell division and cell extrusion

We have evaluated the effect of the blue light stimulus on the cell division, as well as the extrusion rate in a monolayer, for both the MDCK wt and OptoSrc cell lines. Monolayers of either MDCK wt or MDCK OptoSrc were subjected to the same conditions of illumination, 200-ms pulse of blue light every 5 minutes, and we measured both the population doubling time and the extrusion rate, as described in section 2.7.

We found no significant difference in either the population doubling time or the cell extrusion rate, between the four conditions, as seen in table 4.2. The amount of blue light used for photoactivation does not seem to disturb cell division in these cell lines, nor does it foster cell extrusions from the monolayer.

	MDCK wt dark	MDCK wt blue light	MDCK OptoSrc dark	MDCK OptoSrc blue light
PDT	16.6 ± 0.8 h	16.1 ± 0.4 h	20.2 ± 0.8 h	24.8 ± 2.3 h
Extrusion rate (cells/mm ² /h)	8.1 ± 1.8	8.5 ± 2.0	7.7 ± 1.8	7.1 ± 0.8

TABLE 4.2: Population doubling time of MDCK wt and OptoSrc cells with and without blue-light illumination.

We now have a stable cell line of genetically modified cells containing a photo-activable oncogenic protein: the MDCK OptoSrc cell line. We have shown that illumination of these cells does induce an over-activation of Src (Western blot). We have observed that light stimulation induces a recruitment of CRY2-Src to the cell membrane in a reversible manner. Finally, we have identified phenotypical specificities of the illuminated OptoSrc cells, namely membrane ruffling, a higher motility, and a more individualistic behaviour than non-illuminated OptoSrc cells, which behave like normal MDCK cells do. The next step is to place the MDCK OptoSrc population in contact with an MDCK wt population to study the competition between these two cell types.

4.3 Competition between normal and OptoSrc cells

The simplest strategy to place MDCK wt and MDCK OptoSrc cells in contact is to mix them and to apply a global illumination. When applying this light stimulus, only the OptoSrc cells will be transformed. This generates a cell monolayer containing both cell types, in proportions matching the ratio selected for the mixing, and gives rise to random patches of transformed cells in a normal monolayer. The main advantage of this technique is that it doesn't require a specific optical setup to pattern illumination: it can be done with any microscope equipped with a blue fluorescent light source (*e.g.* GFP). We thus started by studying the behaviour of OptoSrc cells in a wt monolayer, first with a single OptoSrc cell, then with a larger group of cells.

4.3.1 Single OptoSrc cell in a wt monolayer

We used the MDCK OptoSrc cell line to reproduce the extrusion of single transformed cells as previously observed in the literature [116, 117], and described in section 1.4.4. We followed the same statistical mixture protocol: MDCK OptoSrc cells were mixed with MDCK wt cells in a proportion 1:100 and seeded on a glass-bottom plate, until they formed a monolayer of wt cells containing a few isolated OptoSrc cells (discernible thanks to the mCherry labelling). Upon blue illumination of the whole monolayer, only the OptoSrc cells were responsive to the light stimulus (200-ms pulse of blue light every 5 minutes). This resulted in isolated transformed cells in a wt monolayer. Figure 4.11 shows the evolution of a single OptoSrc cell in a MDCK wt monolayer with or without blue-light stimulation.

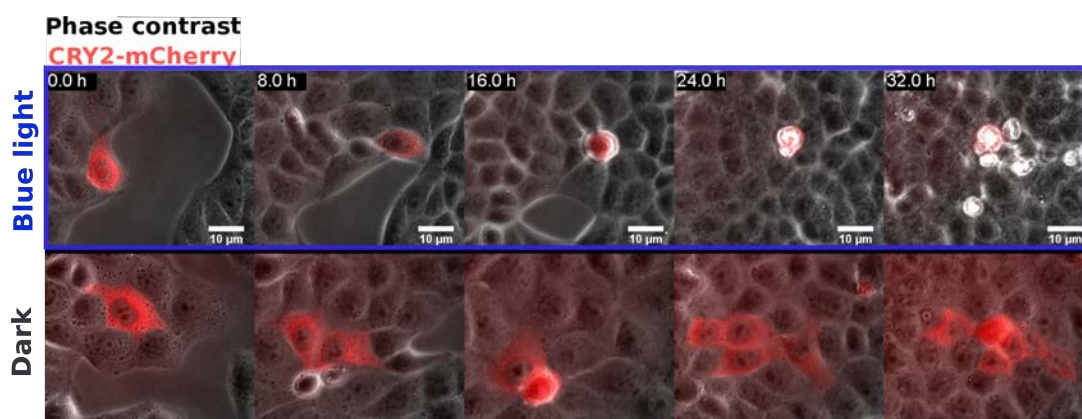


FIGURE 4.11: **Single OptoSrc cell in a monolayer of MDCK wt cells.** **Top:** A single Src-activated cell (mCherry-labelled, red) grown in a wt monolayer is extruded within the first 24 hours of illumination. **Bottom:** Without blue light stimulation, the single OptoSrc cell proliferates normally in the monolayer, akin to the surrounding wt cells. Scale bar: 10 μm .

The single photo-activated OptoSrc cells were found to be extruded from the monolayer within 48 hours of illumination in 46% of the cases ($n = 54$). In the absence of blue light, single OptoSrc

cells proliferated normally in the wt monolayer for more than 48 hours, and were extruded in only 3% of the cases ($n = 20$). A preliminary series of experiments suggested that the addition of Src inhibitor PP2 ($20 \mu\text{M}$) strongly suppressed the extrusion of Src cells: only 21% of extrusion, compared to 73% of extrusion with the equivalent volume of DMSO ($n = 7$). In the absence of light, OptoSrc cells had a similar extrusion rate with PP2 as with DMSO (15% and 17%, respectively, $n = 7$). Figure 4.12 shows the proportion of single OptoSrc cells extruded from the MDCK wt monolayer, with or without light stimulation. We note that larger statistics are required to draw definite conclusions, but the trend we observe is consistent with the results found in the literature [1, 117].

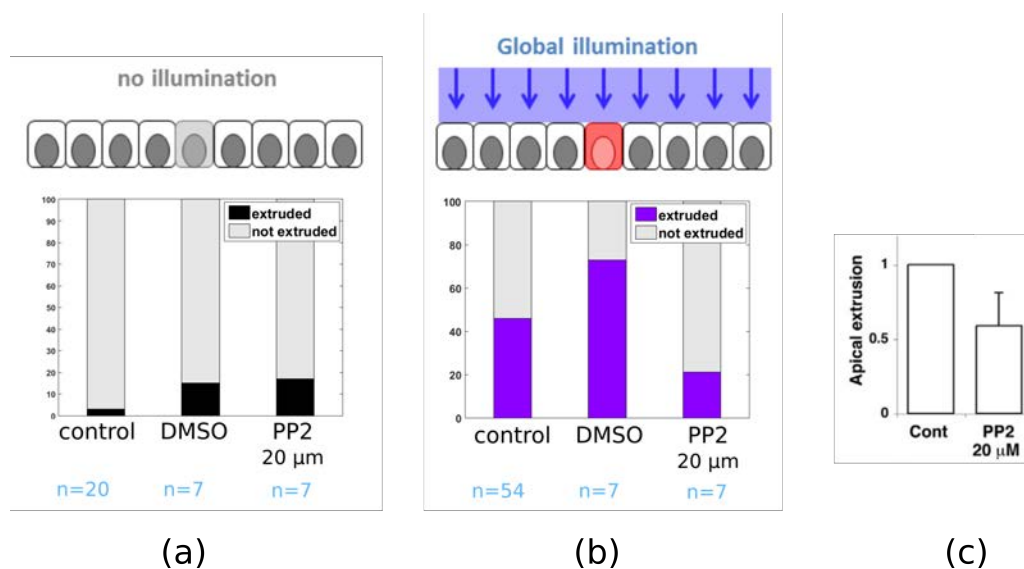


FIGURE 4.12: **Single OptoSrc cell in a monolayer of MDCK wt cells.** (a): In the absence of blue light, OptoSrc cells were not extruded from the monolayer. (b): When exposed to blue light, single OptoSrc cells were extruded from the monolayer in 46 % of cases. The extrusion rate of OptoSrc cells was halved in the presence of Src inhibitor PP2 ($20 \mu\text{M}$). (c): Kajita *et al.* also found a roughly 50 % decrease in the extrusion rate of single Src-transformed cells in a normal monolayer [117].

Kajita *et al.* have shown that single Src-transformed cells were apically extruded, when surrounded by normal cells [117], in 80% of the cases ($n = 90$). We have observed a similar trend with the MDCK OptoSrc single cell extrusions, albeit in lesser proportions. We note that the density of the cell monolayer can greatly impact the phenomenon of cell extrusion, as described by several groups [212–214]. Differences in cell density might thus be a source of variability in the extrusion rate observed in ours and others studies. Besides, in the study by Kajita *et al.*, the cells were cultured at 40.5°C and the activity of the Src mutant was triggered by a temperature shift to 35°C . The added stress induced by this unusual temperature of culture might then also explain the higher extrusion rate observed. Kajita *et al.* also found that the Src inhibitor PP2 ($20 \mu\text{M}$) reduced by half the apical extrusion of Src cells, which is consistent with our own data (Figure 4.12 (c)).

4.3.2 Group of OptoSrc cells in a wt monolayer

The same strategy was adapted to study groups of OptoSrc cells in a wt monolayer. In this case, we were careful not to shake the cells too much when dissociating them with trypsin, so that some clusters of OptoSrc cells remained cohesive. These partly dissociated OptoSrc cells were mixed with MDCK wt cells at a 3:100 ratio and seeded on a glass substrate.

A few groups of OptoSrc cells in the wt monolayer were submitted to a blue light stimulus. As in the single OptoSrc cell situation, some of these groups of cells were globally extruded from the normal monolayer, as seen on Figure 4.13. The extruded cells seemed to stick together on top of the monolayer. Out of ten groups comprising 4 to 26 cells, 4 groups were found to extrude from the monolayer. Other groups of cells (6 out of 10) were partly extruded, or not excluded at all. At first sight, no obvious link between the number of cells in the group and its extrusion transpired.

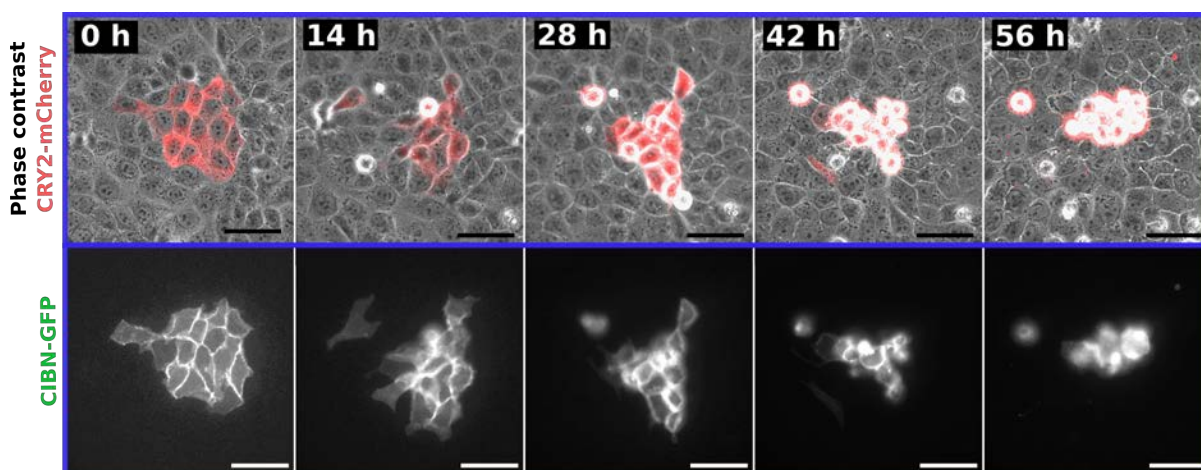


FIGURE 4.13: **Group of OptoSrc cells in a MDCK wt monolayer, under global illumination.** **Top:** A group of OptoSrc cells (mCherry-labelled, red) present in a wt monolayer is extruded from the monolayer **Bottom:** CIBN-GFP signal, showing the same group of Src-activated cells. Global blue-light illumination, 200-ms pulse every 5 minutes. Scale bar: 50 μm .

 [Movie 4.13](#)

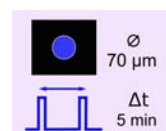
However, it should be noted that the groups of OptoSrc cells vary tremendously in size and shape, which makes it very difficult to make quantitative analyses using this statistical mixture technique. In order to study more precisely the effect of the size and shape of the interface between two cell populations, we need to create this interface in a reproducible manner *i.e.* we need a better control of the initial situation. To that extent, we can use a specific optical setup to pattern the light stimulus, and thus control spatially the activation of the oncogene.

4.4 OptoSrc & patterned light: optical control of local *Src* activation

The genetically modified MDCK OptoSrc cell line, containing the photo-activable oncogene *Src*, was then used with targeted illumination to select which cells to *Src*-activate.

4.4.1 Local *Src* activation in the OptoSrc monolayer

The **standard conditions of illumination** were set as a 200 ms-pulse of blue light every 5 minutes, for a 70 μm -diameter circular area (about 10 cells), and an initial density of ~ 2000 cells/ mm^2 .



Local illumination of the OptoSrc monolayer leads to a collective extrusion of cells

When a group of OptoSrc cells was illuminated using a circular pattern, cells from the illuminated area collectively came out of the monolayer and remained cohesive in an aggregate on top of the monolayer (Figure 4.14).

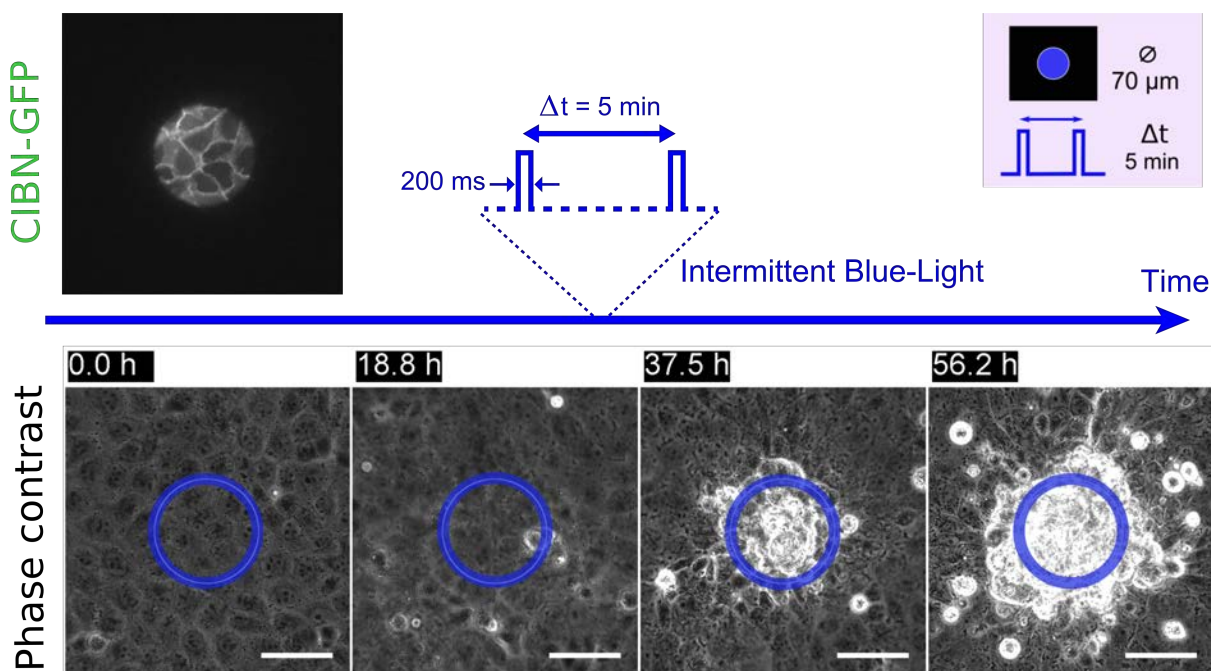


FIGURE 4.14: **Collective extrusion of a group of illuminated cells in an OptoSrc monolayer, in the standard conditions of illumination.** **Top:** CIBN-GFP signal, showing the illumination pattern (488 nm). The delay between two light pulses was set to 5 minutes. **Bottom:** Phase contrast images. The blue circle indicates the region of illumination. Scale bar: 50 μm . [Movie 4.14](#)

A word on the wording

We describe this phenomenon as a “collective extrusion” of the group of OptoSrc cells from the monolayer. However, this phenomenon is not an “extrusion” in the strict sense of the term: cellular extrusion is described as a mechanism to remove dying cells from an epithelium in order to maintain the integrity of the tissue [151]. In our case, we will see later that the cells escaping the monolayer are in fact not dying. We use the word “extrusion” as an extension of the behaviour observed for an isolated OptoSrc cell (section 4.3.1), but we specify it in the case of a group of cells by calling it a “collective extrusion”. There is no apparent reason to believe that it follows the same mechanism as the single cell extrusion.

Several clues, described later in detail, suggested that this was indeed a collective phenomenon, as opposed to multiple single cell extrusions:

- the cells escape the monolayer together, instead of being extruded individually.
- the 3D images show a mini-spheroid formed by the cells piled up together, with intact chromatin (Figure 4.20, page 91).
- a convergent flow of cells from the surrounding monolayer indicates a collective behaviour (Figure 4.22, page 93).
- when a flow of liquid was applied on the aggregate — for example when the cells were rinsed before PFA fixation — the cells remained cohesive and attached to the monolayer.
- when cell-cell junctions were disrupted with EGTA, the aggregate could not form (Figure 4.24, page 95).
- when cell dissociation was induced with trypsin — in the last step of the Traction Force Microscopy experiments, Chapter 5 — the cells from the aggregate took a long time to detach completely (1-2 hours), compared to the cells from the monolayer (which dissociated within about 30 minutes), showing that collectively extruded cells maintain cell-cell adhesions between them.
- we attempted to aspirate the aggregate using a micropipette, but we did not manage to detach it from the monolayer using only aspiration, suggesting that the spheroid was strongly attached to the monolayer.

Effect of the patterned light stimulus on MDCK wt cells

In order to evaluate the impact of the blue light on cells, we ran the same experiment on a monolayer of MDCK wt cells. We never observed any phenomenon resembling the collective extrusion previously described ($n = 20$). Figure 4.15 shows the evolution of a monolayer of MDCK wt cells subjected to the standard conditions of illumination, compared to an OptoSrc monolayer in the same conditions of illumination. This experiment acted as a double control. Not only did it show that the budding phenomenon was OptoSrc-dependent, but it also revealed that the dose of blue light irradiation delivered in the standard conditions of illumination was not toxic for the cells. Indeed, illumination towards the blue-UV side of the spectrum can turn out to be toxic for cells if it exceeds a certain dose² [203, 204].

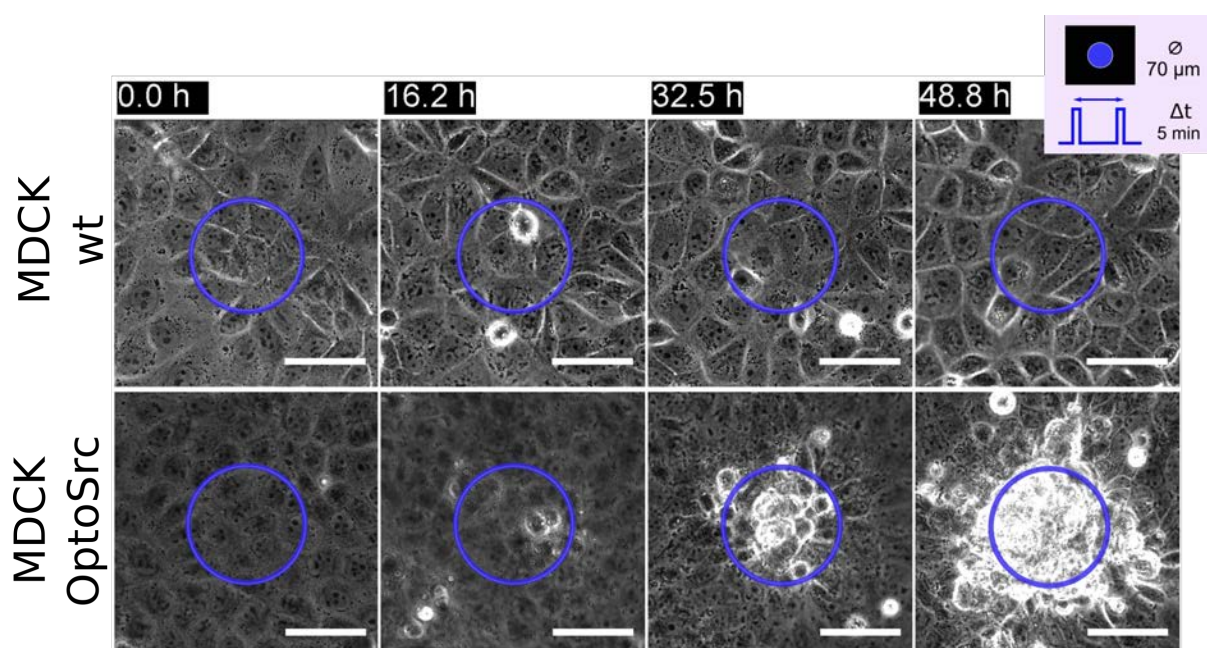


FIGURE 4.15: **Effect of the light stimulus on MDCK wt cells.** **Top:** MDCK wt monolayer subjected to the standard conditions of illumination. **Bottom:** An MDCK OptoSrc monolayer subjected to the same conditions of illumination gives rise to a collective extrusion. The blue circle indicates the illuminated area. Scale bar: 50 μm .

Effect of cell proliferation on the collective extrusion

To evaluate how cell division contributed to the collective extrusion, we ran this experiment either in the presence or absence of GlutaMAX, a supplement which stimulates cell growth. Cells were first seeded in normal medium (containing GlutaMAX), and grown into a monolayer overnight. Then, the medium was changed to either fresh GlutaMAX-containing media or FluoroBrite Media (Gibco), which does not contain GlutaMAX, and thus inhibits cell division. We

²This phototoxicity depends not only on the total dose of irradiation, but also on how exactly this dose is delivered (*e.g.* single occurrence of high intensity *vs* repeated instances of low intensity), as well as on the wavelength, and on the cell type.

observe that the collective extrusion was much larger in GlutaMAX-containing medium than in GlutaMAX-depleted medium, after 60 h of illumination (Figure 4.16). But we did observe the collective extrusion, even when cell growth was considerably slowed down. This revealed that cell proliferation clearly promotes the collective extrusion phenomenon, but that it is not the only mechanism involved.

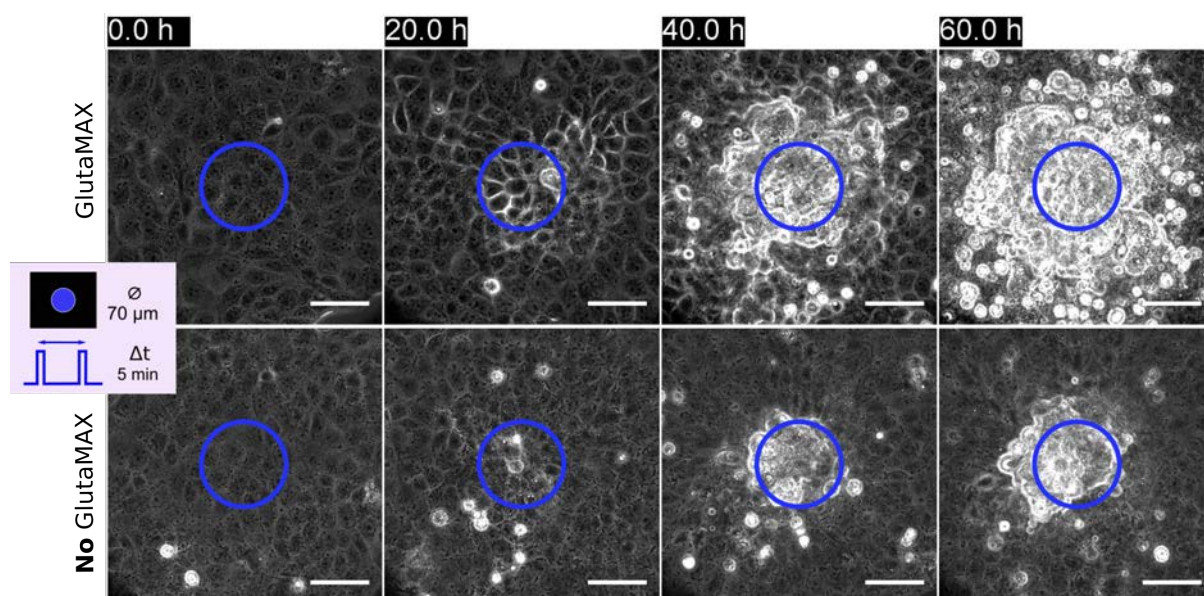


FIGURE 4.16: **Effect of cell proliferation on the collective extrusion.** **Top:** Monolayer of OptoSrc cells in normally supplemented medium, in the standard conditions of illumination. **Bottom:** An MDCK OptoSrc monolayer subjected to the same illumination conditions, in a GlutaMAX-depleted medium. The blue circle indicates the illuminated area. Scale bar: 50 μm .

In medium normally supplemented, we also noticed a considerable number of cell extrusions from the surrounding monolayer. Indeed, since we start this experiment with an already confluent monolayer, it reaches a very high density after 60 h, which favours cell delamination [212]. It then becomes difficult to discriminate between single cells that extrude because of the high density of the monolayer, and cells from the collective extrusion. Conversely, in the absence of GlutaMAX in the medium, the cell monolayer keeps a relatively stable cell density over 60 hours, and exhibits less single cell extrusions from the surrounding monolayer. The collective extrusion then appears more clearly in the monolayer, without the interference of cell delaminations all around. For this reason, we have decided to use FluoroBrite Media, which does not contain GlutaMAX and thus hinders cell proliferation, for all experiments on the collective extrusion.

The collective extrusion is Src-dependent

We submitted MDCK OptoSrc cells to the standard conditions of illumination in presence of two different Src inhibitors. The mechanism of action of these drugs is described in section 2.4. One of the most widely used inhibitor is PP2: a preferential, though not specific, inhibitor of the Src-family tyrosine kinases. When PP2 was added to the medium at a concentration of 10 μM , 2 h before the start of the experiment, illumination of a group of OptoSrc cells failed to induce the collective extrusion previously observed (Figure 4.17): $P_{bud} = 0\%$ ($n = 35$) — where the probability P_{bud} is defined as the number of collective extrusion events observed divided by the total number of targeted illumination experiments. We then used a more selective inhibitor: “Src inhibitor n°5”³. In the presence of this inhibitor at a concentration of 10 nM, no collective extrusion was observed (Figure 4.17): $P_{bud} = 0\%$ ($n = 9$). In the control conditions, *i.e.* when the same amount of vehicle was added to the medium (5 μL DMSO), the collective extrusion was observed with a probability $P_{bud} = 91\%$ ($n = 34$). These results show that no collective extrusion occurs if Src is overall inactivated.

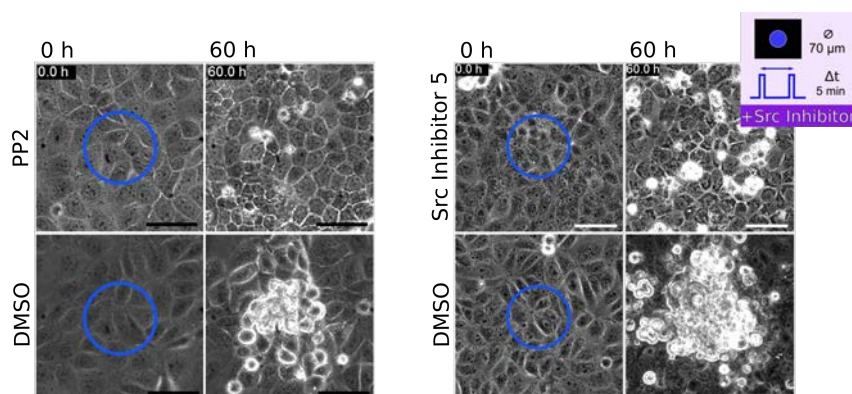


FIGURE 4.17: **No collective extrusion was observed in presence of Src inhibitors.** **Left:** Cells treated with PP2 at 10 μM (top) did not undergo a collective extrusion. Control: DMSO (bottom). **Right:** Cells treated with Src Inhibitor n°5 at 10 nM (top) also failed to form a collective extrusion. Control: DMSO (bottom). The blue circle indicates the region of illumination. Scale bars: 50 μm .

Src activation at the membrane is required for collective extrusion

Given that membrane recruitment enhances the ability of Src to phosphorylate its substrates, we tested two variants of the OptoSrc cell line devoid of either CIBN or CIBN-CAAX-GFP (Figure 4.18). These two constructs do not allow the recruitment of OptoSrc to the membrane: in the absence of CIBN, blue illumination cannot induce CRY2/CIBN dimerization, and by extension the recruitment of CRY2-Src at the membrane leading to its over-activation. Blue-light patterned illumination for these constructs did not result in a budding structure ($n = 36$ and $n = 10$ respectively) indicating that Src must be locally over-activated at the membrane to allow such a collective extrusion (Figure 4.18).

³4-(3'-Methoxy-6'-chloro-anilino)-6-Methoxy-7-(Morpholino-3-propoxy)-quinazoline

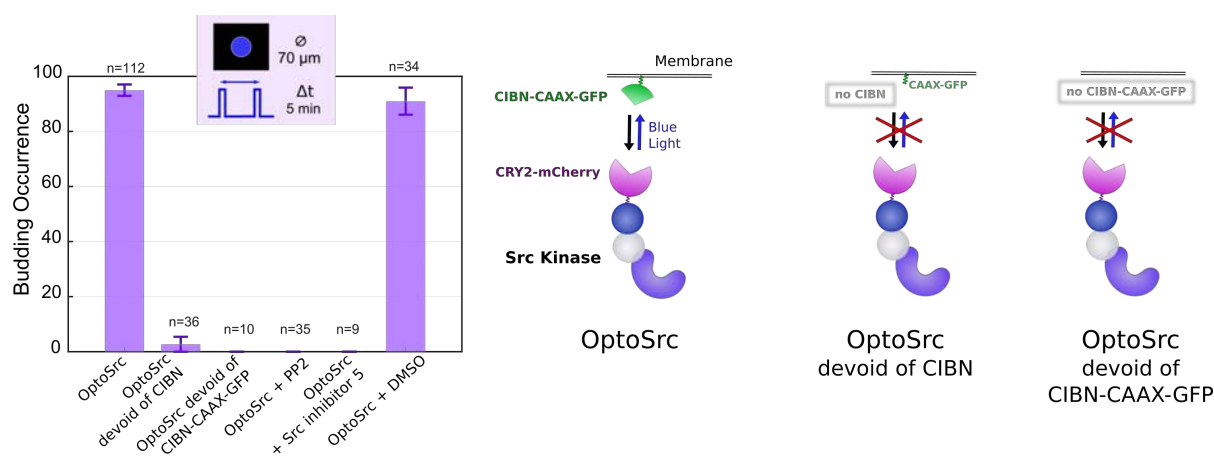


FIGURE 4.18: **Src activation at the membrane is required for collective extrusion.**

Left: Budding occurrence, in the standard conditions of illumination, for OptoSrc as well as the two constructs devoid of either CIBN or CIBN-CAAX-GFP, and for treatment with Src inhibitors (PP2 at 10 μ M and Src inhibitor n°5 at 10 nM). The error bars of the budding occurrence represent the uncertainty as described in section 2.8.3. **Right:** Schematic of the three different OptoSrc-based constructs used.

Live cell assays

Many normal cells undergo programmed cell death when they are detached from their underlying matrix support. This form of cell death was termed “anoikis” by Frisch and Francis [215]. Thus, the cells involved in the collective extrusion might be susceptible to anoikis. However, evidence suggests that Src influences the life or death decisions that cells make during many biological processes, and in particular the v-Src oncoprotein⁴ was found to protect epithelial cells from anoikis [216]. Indeed, v-Src-expressing cells are able to overcome the normal adhesion requirement of cell cycle progression and undergo anchorage-independent growth. Therefore, over-activating Src in the MDCK OptoSrc can actually make them more resistant and prevent them from undergoing anoikis.

We attempted several assays to check if the cells inside the budding structure were still alive, or if this collective extrusion phenomenon was related to cell apoptosis. Most of the classical viability assays are designed for flow cytometry, so they are not always adapted for adherent cell monolayers. Besides, the CRY2-GFP and CIBN-mCherry fluorescence of the OptoSrc cells limits our choice, in terms of wavelength, from all the available live/dead cell imaging reagents.

For instance, staining with a standard fluorescent marker of Caspase-3/7 activity (CellEvent Caspase-3/7 Green ReadyProbes, Invitrogen) was not practical since the fluorescent signal overlapped with the GFP signal in the OptoSrc cells.

⁴the viral homolog of the cellular c-Src oncoprotein

The strongest evidence of cell survival was obtained by performing Hoechst labelling of the cell nuclei. The budding structure was fixed with PFA after 60 h of exposure and labelled with Hoechst 33342 (NucBlue ReadyProbes, Invitrogen): this did not reveal condensed or fragmented nuclei, suggesting that extruded OptoSrc cells are not apoptotic (as illustrated on Figure 4.20).

Propidium iodide (PI) was used to stain the nucleus of apoptotic cells, since PI cannot cross the cell membrane of viable cells. The images showed the occasional nucleus staining, but almost none of the cells from the budding structure had their nucleus stained. Yet these results are made unclear by the fact that the cell membranes were also fluorescent. Since PI is not supposed to stain the cell membrane, and that the OptoSrc cell contain an mCherry labelling of CRY2-Src (localized at the cell membrane upon blue-light stimulus), we suspect that the membrane fluorescence likely comes from a cross-talk between the red (mCherry emission around 600 nm) and the far red channel (Cy5 emission filter: 625-775 nm). As such, we did not find this experiment definitely conclusive.

We then used 4-aminopyridine (4-AP), a K^+ channel inhibitor, which blocks the early stage of apoptosis in epithelial cells [151]. We found signs of toxicity after 48 hours for a concentration of 2 mM (contrary to [116,117]), so we used 4-AP at a concentration of 1 mM — for which the cells survived for at least 3 days, albeit looking slightly unwell. Addition of 4-AP did not block the formation of the collective extrusion with our standard conditions of illumination (Figure 4.19), suggesting that it is induced in an apoptosis-independent manner. However, 4-AP slowed down the formation of the collective extrusion, that appeared in about 37 ± 2 h (SEM, $n = 10$), compared to the average apparition time of 21 ± 1 h (see further for the definition of the appearance time).

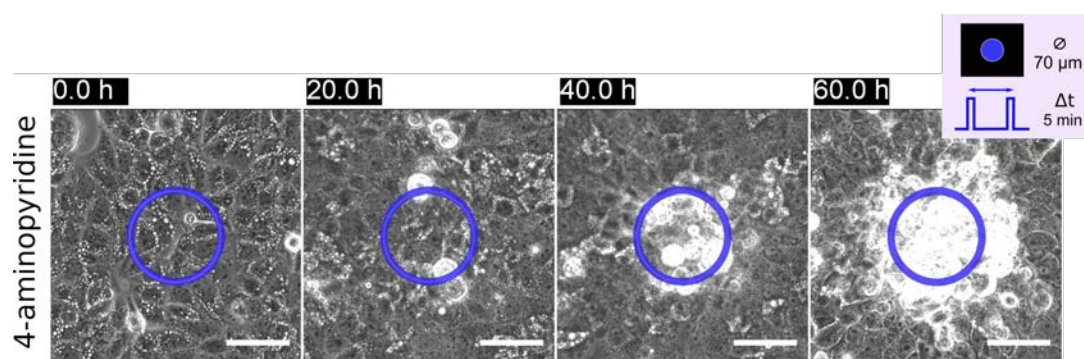


FIGURE 4.19: **Addition of 4-aminopyridine did not block the collective extrusion.** At this concentration (1 mM), the cells seem slightly unwell, but survive for at least 3 days. Standard conditions of illumination, the blue circle indicates the illuminated area. Scale bar: 50 μm .

Visualisation of the group of extruded cells in 3D

To view the appearance of the group of collectively extruded cells in three dimensions, we performed confocal microscopy after fixation. The 3D images revealed a cluster of extruded cells budding on top of the monolayer, at the location of the blue-light stimulation (Figure 4.20). These 3D images revealed that the cell monolayer is still intact underneath the extruded cells aggregate, in which the cells pile up in a seemingly random manner. Besides, the cells inside this structure appear rounder than the cells from the monolayer.

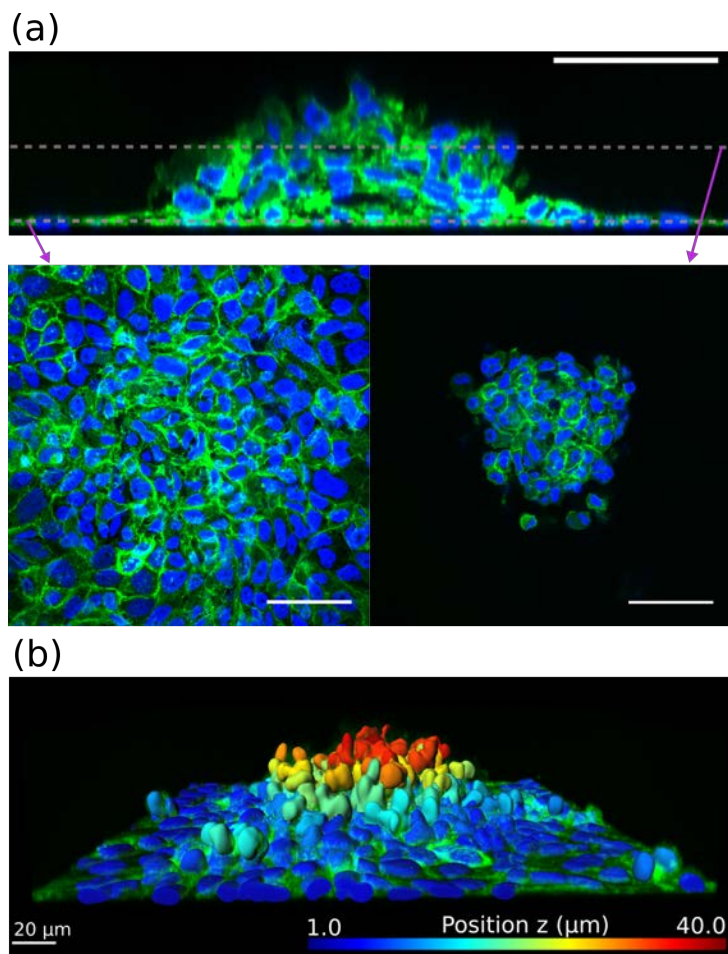


FIGURE 4.20: **Collective extrusion of a group of illuminated OptoSrc cells forms a bud-like structure.** (a) Confocal images of the 3D structure after 60 h of blue-light stimulation. The nuclei are labelled with Hoechst (blue), and the membranes are shown in green (CIBN-GFP label). **Top:** Side view **Bottom:** View of the structure at the surface underlying monolayer (left) and 25 μm above (right). Scale bar: 50 μm . (b) Cell nuclei, reconstructed with Imaris software, coloured by Z-position. Cell membrane labelled with GFP (green).

The **height** of the dome was measured to be $40 \pm 3 \mu\text{m}$ (SEM, $n = 12$, after 60 h of illumination), according to the nominal Z calibration of the confocal. The **number of cells** in a budding structure was estimated to be, on average, 210 ± 30 (SEM, $n = 6$, after 60 h of illumination). We thus estimated that the number of cells inside the area of illumination was multiplied by at

least 20 after 60 hours of illumination ($N_{in}(0) \approx 10$, $N_{in}(60 \text{ h}) \approx 210$), while the number of cells in the field of view outside the illuminated area was only multiplied by 3 ($N_{out}(0) \approx 80$, $N_{out}(60 \text{ h}) \approx 240$). One needs to bear in mind that cell proliferation is considerably slowed down in the absence of GlutaMAX in the medium, as previously mentioned, so this increase in the number of cells is not strictly attributed to cell division, but also to the recruitment of cells from around the field of view. This supports the fact that the formation of the bud does not simply arise by cell proliferation, but by an influx of cells towards this aggregate.

Definition of an “appearance time”

In order to study the dynamics of the collective extrusion, we defined the “appearance time” of the 3D structure. We chose to determine this appearance time by eye, because of a- the difficulty to set automated analyses using the phase contrast images, and b- the absence of obvious criteria to identify the collective extrusion from the monolayer, as opposed to isolated extrusions occurring normally in a cell monolayer.

To define the appearance time, we first ascertained the presence of such a structure within the 60 hours of the experiment; single cell extrusions were not considered. Likewise, cells starting to extrude from the monolayer and getting included back into the monolayer were not taken into account. Considering only a properly formed collective structure, we then worked backwards to establish the first frame for which its constituting cells started emerging together from the monolayer. This time was defined as the “appearance time”, and represents the very beginning of the collective extrusion. The spheroid takes its proper form several hours after this time, a fully-fledged structure taking about 36-48 hours to form. Figure 4.21 shows the frame of appearance of a 3D structure (middle image), as well as the monolayer one hour before and after this “appearance time”. We estimate the accuracy of this measurement to be ± 1 hour (*i.e.* 4 frames). In the standard conditions of illumination, the appearance time was measured to be, on average, 21 ± 1 h (SEM, $n = 130$).

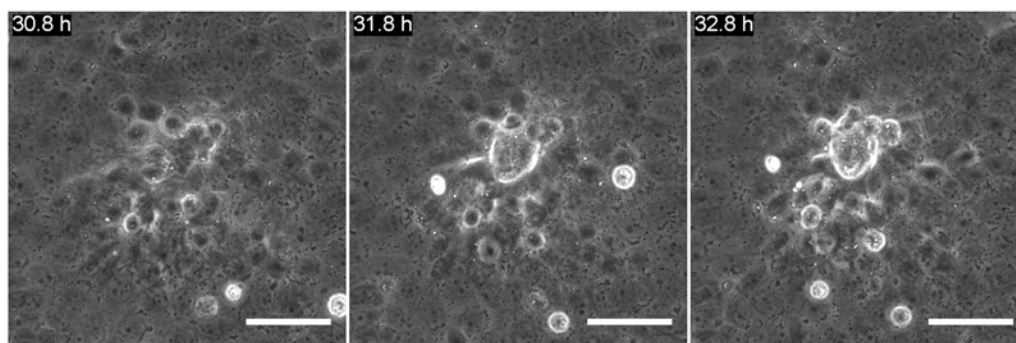


FIGURE 4.21: **Estimation of the bud appearance time.** On this example, the appearance time is estimated as 31.8 ± 1 h. Scale bar: $50 \mu\text{m}$.

Collective extrusion is preceded by a convergent flow of cells towards the illuminated area

Looking at the movies of collective extrusion, we observed an inward movement of the cells toward the illuminated area. We thus used Particle Image Velocimetry (PIV) to map the velocity field in the cell monolayer over time, and to quantify the convergence inside the region of illumination (ROI). Figure 4.22 shows the velocity field of the monolayer averaged over a period of 10 h. This velocity field is clearly directed towards the blue-light exposed area, suggesting that the surrounding monolayer acts as a reservoir of cells that feeds the collective extrusion phenomenon. We also plotted the value of the convergence, computed inside the ROI, towards the central area of illumination, as a function of time. Once the collective extrusion has started, the cells pile up on top of the monolayer, blurring the phase contrast signal in this area. Thus the velocity map cannot be computed in this region, which explains the decrease of the mean convergence value as soon as the collective extrusion occupies the entire ROI. But the velocity field outside of the ROI is still directed inwards.

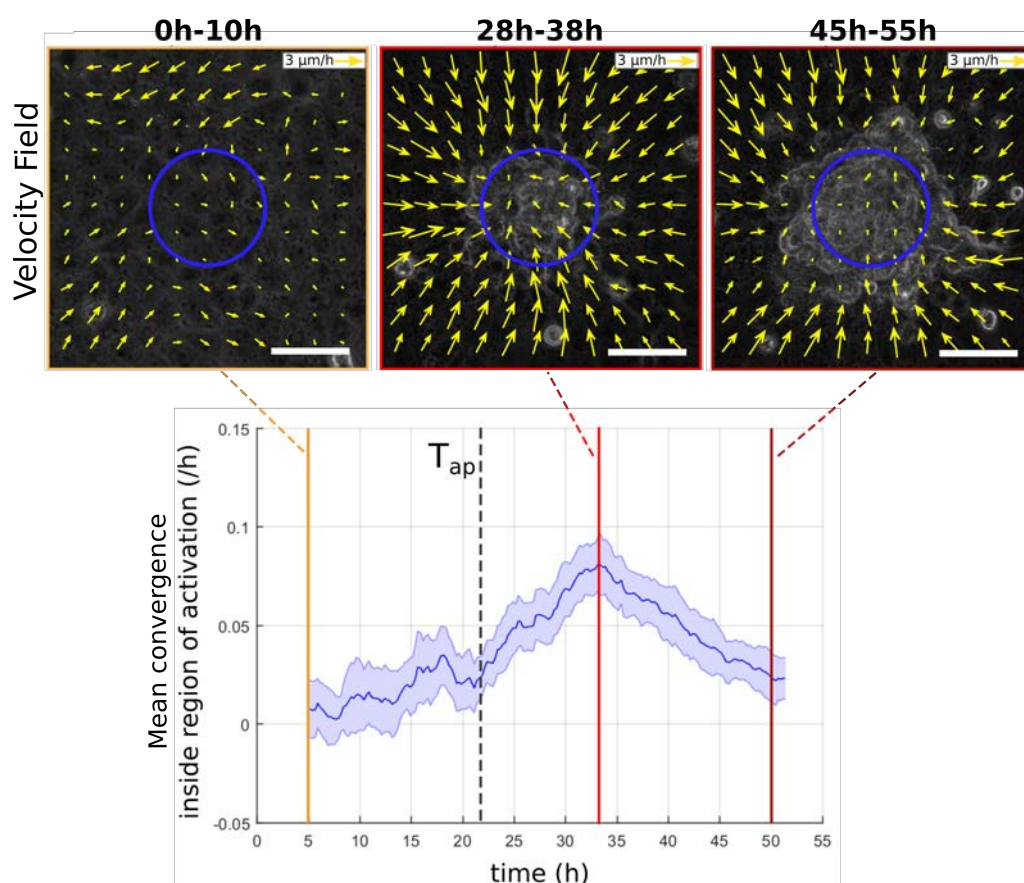


FIGURE 4.22: **Convergent flow of cells towards the illuminated area during collective extrusion.** **Top:** The velocity field (yellow arrows) is averaged over 10 hours. The blue circle delineates the region of illumination. Scale bar: 50 μm . **Bottom:** Mean convergence (the error bar is the standard deviation) inside the area of illumination, averaged over 10 hours: cells start to converge slightly before the appearance time.

In order to estimate the range of this convergent flow, we performed the same experiment at a lower magnification, using the 10x objective, to increase the size of the FOV. We estimated that a $70\ \mu\text{m}$ -diameter region of illumination induced a convergent flow in a $300\ \mu\text{m}$ -disk around the collective extrusion (Figure 4.23). From PIV measurements, we computed the radial velocity in the monolayer away from the center of the ROI, and averaged it over 10 hours. Then, we computed its angular average in the entire FOV, centered on the ROI. This showed that, at its peak, the convergence flow of cells was detectable up to $150\ \mu\text{m}$ away from the center of the ROI, in the standard conditions of illumination.

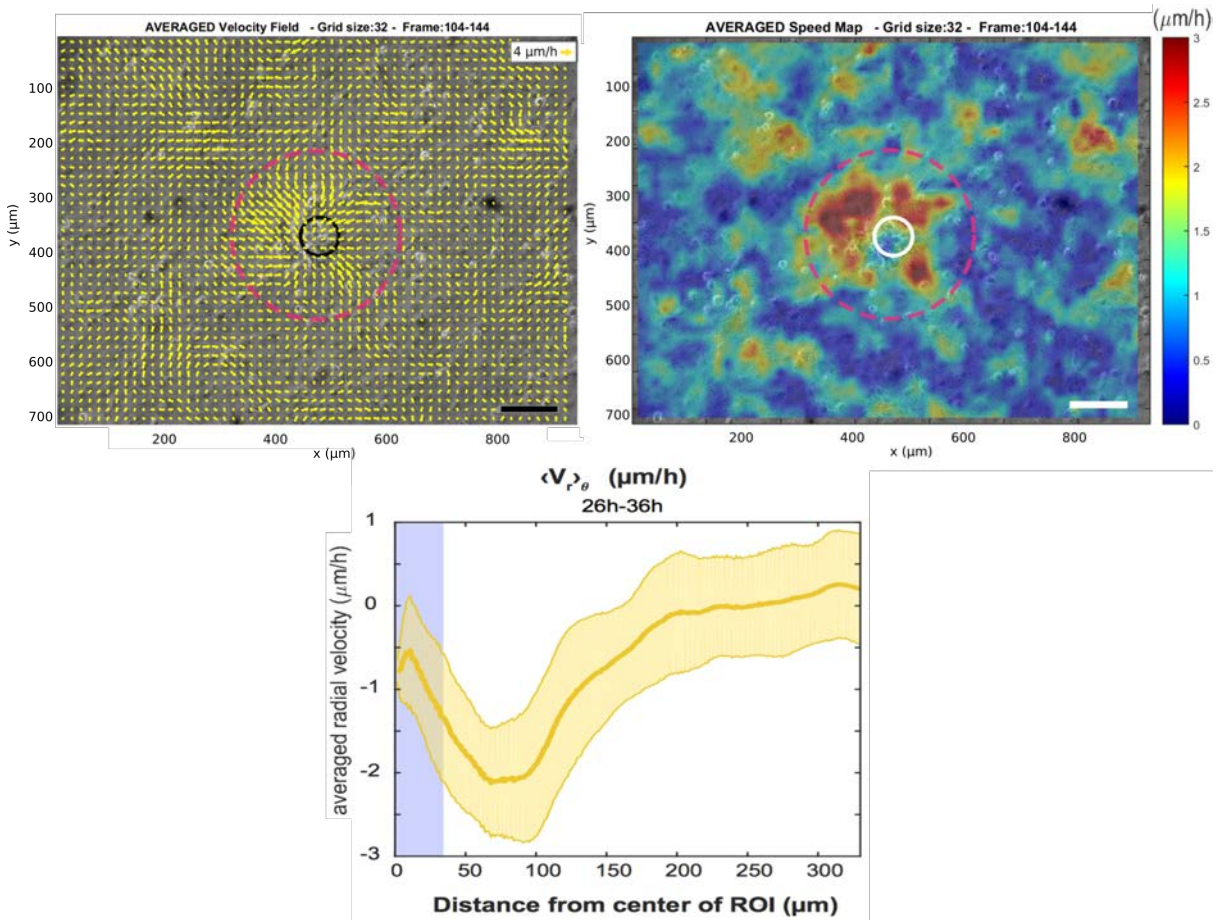


FIGURE 4.23: **Range of the convergent flow of cells towards the illumination area during collective extrusion.** **Top:** Velocity field (yellow arrows, left) and interpolated speed map (color-coded, right) of the monolayer averaged between 26 h and 36 h after the start of illumination. For this experiment, the appearance time is $T_{ap} = 28$ h. The black/white circle delineates the region of illumination (ROI diameter = $70\ \mu\text{m}$). The magenta circle indicates the area impacted by the convergent flow of cells (diameter $\sim 300\ \mu\text{m}$). Scale bar: $100\ \mu\text{m}$. **Bottom:** Angular average of the radial velocity component away from the center of the ROI, averaged between 26 h and 36 h (when the velocities in the monolayer are the highest). This indicates that the convergent flow reaches about $\sim 150\ \mu\text{m}$ from the center of the ROI.

Cells stay cohesive during the collective extrusion

The use of EGTA to disrupt cell-cell junctions prevented the formation of the budding structure (Figure 4.24). We noted that the overall extrusion rate of single cells in the surrounding monolayer seemed to increase in the presence of EGTA. Besides, activated OptoSrc cells seemed to be extruded more specifically from the region of illumination, but did not remain cohesive on top of the monolayer. Instead, they were detached and migrated freely in the medium. No convergent flow was measured towards the illuminated area in that case. This demonstrated that OptoSrc cells need to maintain intact cell-cell junctions to undergo a collective extrusion, and that the budding structure is not just made of individually extruded cells. This is additional evidence pointing to a collective phenomenon.

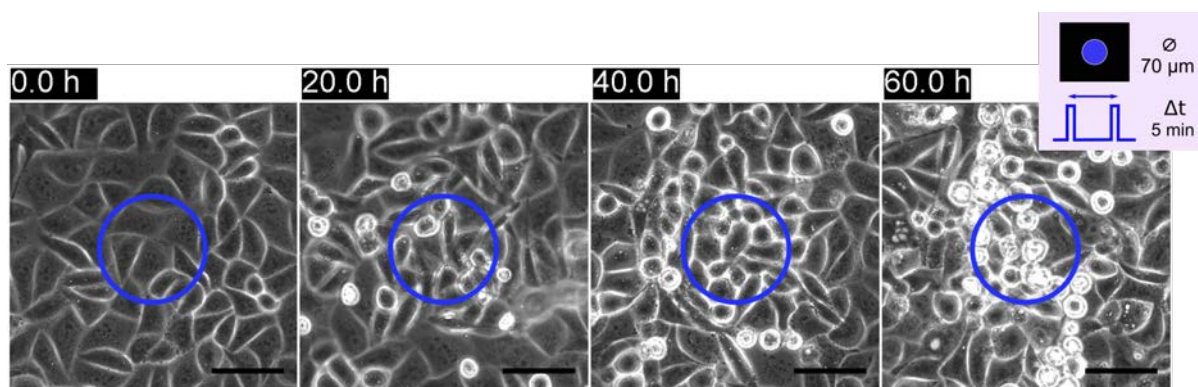


FIGURE 4.24: **EGTA disrupts cell-cell junctions and blocks the collective extrusion**, in the standard conditions of illumination. The blue circle delineates the ROI. Scale bar: 50 μm .

 [Movie 4.24](#)

4.4.2 Control, in space, of the collective extrusion

Varying the size of the ROI

The size of the illumination pattern could be modified within the range of the available area covered by the Mosaic (DMD). In our usual conditions for image acquisition (objective 40x/0.75 NA, field of view of the Mosaic: 160 x 120 μm^2), the diameter of the circular area spanned from 35 to 100 μm (which represents roughly 3 to 70 cells). Figure 4.25 shows the evolution of groups of cells of diameter 35, 50, 70, 85 or 100 μm (phase contrast images). Varying the size of the ROI clearly affected the size of the budding 3D structure. We determined the appearance time of this bud, as well as its underlying area, as a function of the ROI size. We estimated the area underneath the bud by thresholding the phase contrast images at the end of the experiment, *i.e.* after 60 h of illumination (Figure 4.26).

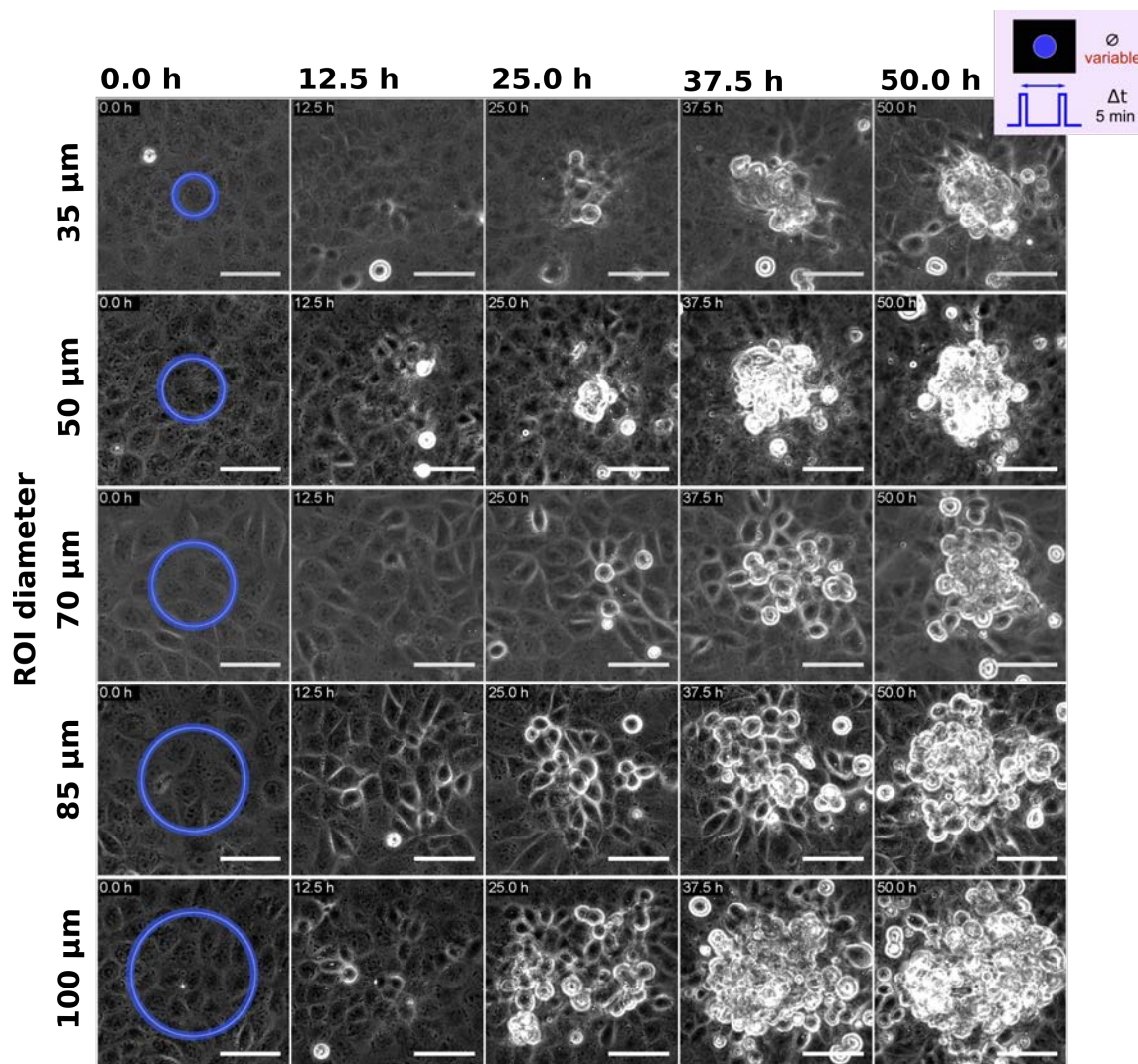


FIGURE 4.25: **Effect of the size of the ROI on the size of the bud.** Standard frequency of illumination but variable size of ROI (indicated by the blue circles). Scale bar: 50 μm .



FIGURE 4.26: **Determination of the bud area.** **Left:** Phase contrast image, 60 h after the start of illumination. **Middle:** Thresholding of the phase contrast image, giving the underlying area of the bud. Small regions corresponding to single cell extrusions or regions far from the ROI were not considered. **Left:** The red contour indicates the measured area of the bud. Scale bar: 50 μm .

The size of the illumination area influenced the size of the budding structure, without significantly modifying its appearance time (Figure 4.27). We noticed that, on average, the area of the aggregate was larger than the area of the ROI, by a factor of 1.25.

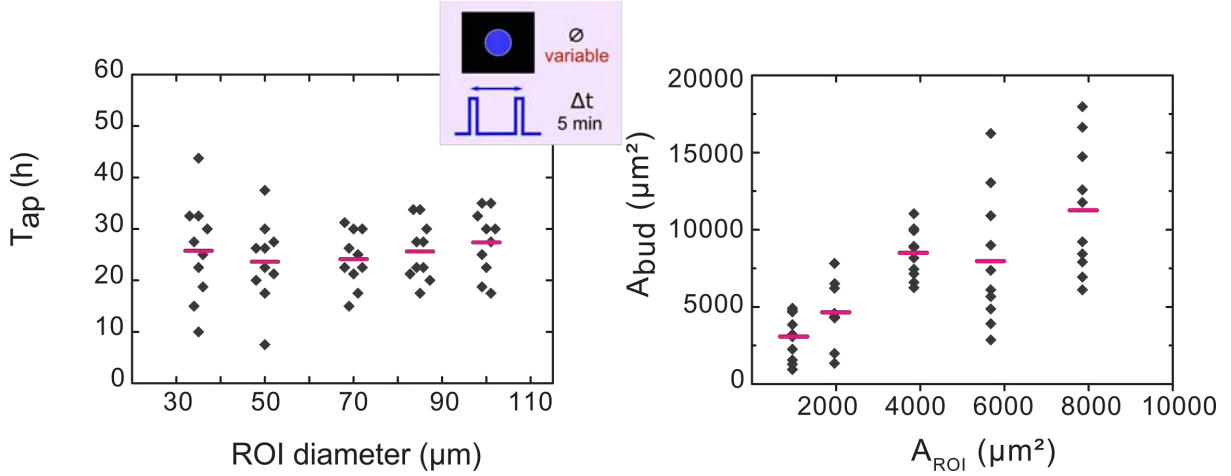


FIGURE 4.27: **Varying the size of the illuminated area.** This modified the area underneath the extruded structure (right) but not its appearance time (left). Each dot corresponds to one experiment for which we observed a bud. The pink line represents the average value.

These results show that we can control the size of the budding 3D structure, without modifying its appearance time, just by tuning the size of the illumination pattern.

4.4.3 Control, in time, of the collective extrusion

Effect of the illumination frequency on the collective extrusion

We can tune the level of activation of Src at the membrane by changing the illumination frequency ($1/\Delta t$): the less frequent the light pulses, the more freedom CRY2-Src has to diffuse to the cytoplasm, and the less time the kinase is able to phosphorylate its substrates. In the usual conditions, Δt was set to 5 minutes.

We have shown that varying the level of activation of Src had an impact on the evolution in time of the budding structure (Figure 4.28). The higher the level of Src activation, the faster the budding structure was formed. The appearance time of the bud as a function of the illumination frequency followed a saturation curve, that we fitted empirically by the following equation:

$$T_{ap} = T_{sat}(1 - k.e^{-\frac{\Delta t}{\tau}}) \quad (4.1)$$

with the saturating appearance time $T_{sat} = 47 \pm 3$ h, $k = 0.9 \pm 0.1$, and $\tau = 9 \pm 3$ min. Besides, the probability of budding P_{bud} decreased as the interval Δt increased. It could be fitted by: $P_{bud} = 1.1e^{-\frac{\Delta t}{\tau_{P_{bud}}}}$, with $\tau_{P_{bud}} = 29$ min. It can thus be described as a Poisson process, with a

characteristic time of 29 min.

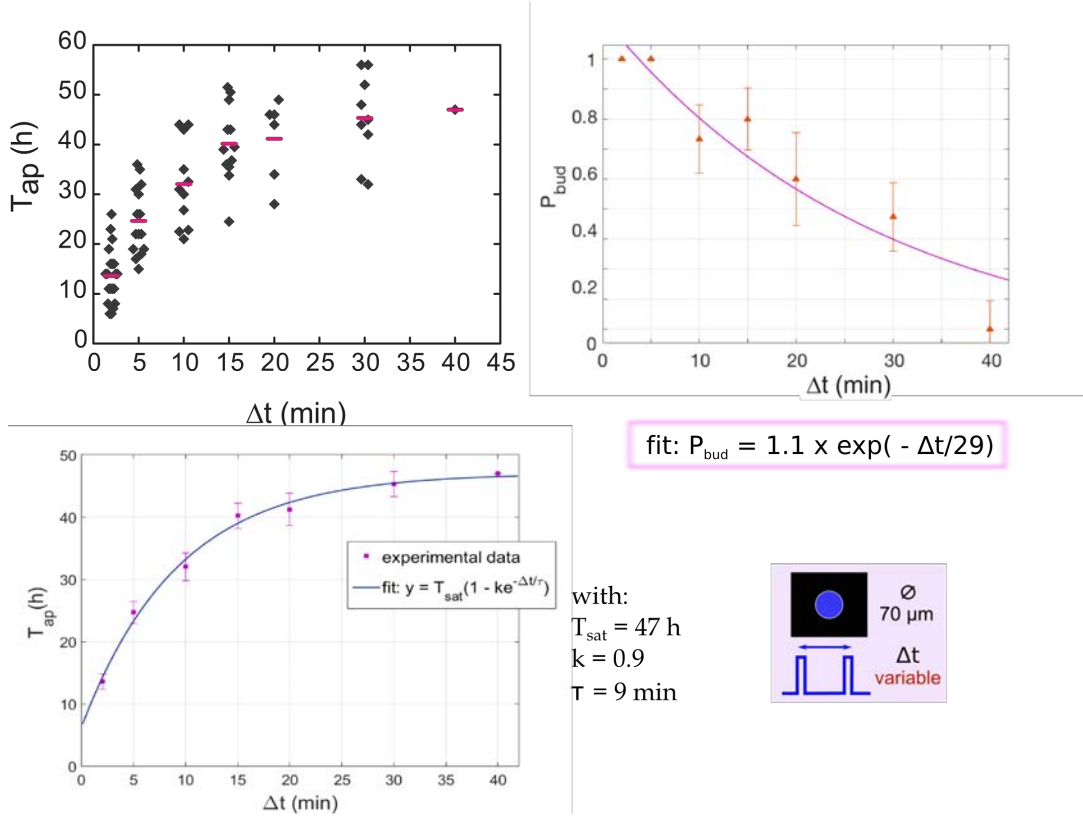


FIGURE 4.28: **Effect of the illumination frequency on the collective extrusion.** Appearance time T_{ap} (top left) increases as a function of the delay Δt between two light pulses, whereas the budding probability P_{bud} (top right) decreases. The error bars of P_{bud} represent the uncertainty as described in section 2.8.3. The appearance time T_{ap} as a function of the illumination frequency followed a saturation curve (bottom left). The illuminated area was a circle of diameter $70 \mu\text{m}$.

The data shown in Figure 4.28 allow us to draw several conclusions:

- The appearance time of the bud is delayed as the frequency of light pulses decreases. This suggests that varying the level of Src at the cell membrane has a direct impact on the dynamics of the collective extrusion.
- This slowed-down dynamics is accompanied by a decrease of the probability of budding P_{bud} , as the frequency of light pulses decreases. This means that P_{bud} clearly depends on the amount of over-activated Src at the membrane.
- The values of the appearance time from $\Delta t = 20$ minutes suggest a plateau for T_{ap} around $T_{sat} = 47$ h. It seems that if the collective extrusion hasn't occurred within 45-50 h of illumination, it is unlikely to happen at all. This consolidated our decision not to extend the experiments beyond 60 h.

- Light pulses as rare as one every 40 minutes still managed to give rise to a unique occurrence of budding (for $n = 10$ experiments), which in itself was quite surprising to us, since it is very spaced out compared to the dissociation time of CRY2 and CIBN of only a few minutes (see section 4.1.3).
- No collective extrusion was observed for intervals $\Delta t \geq 45$ minutes.

Is the collective extrusion reversible?

Since the recruitment of CRY2-*Src* to the membrane is reversible, in a matter of minutes (section 4.2.2), we wondered if the collective extrusion phenomenon was reversible as well. To check this, we stopped shedding light on the cells once the 3D structure was clearly visible, *i.e.* between 24 and 48 h after the start of stimulation.

When blue light illumination was stopped, the 3D structure collapsed over several hours. The time it took for the bud to disintegrate depended, of course, on its size at the moment when illumination was stopped. Most of the cells were then included back into the monolayer, while some others detached from the spheroid and floated individually in the medium. Figure 4.29 shows the formation of a budding structure over 36 h of illumination, followed by its collapse when the light was switched off, with the reintegration of cells into the monolayer.

For now, we have decided to describe only qualitatively the general situation that we observe. Indeed, the major difficulty in quantifying the reversibility of the collective extrusion is exactly the same as the reason that prompted us to adopt the optogenetic system in the first place: we do not have comparable initial situations. Indeed, after a certain duration of illumination, say 36 hours for example, some budding structures have been developing for 19 hours ($T_{ap} = 17$ h), and others for only 11 hours ($T_{ap} = 25$ h). Some already contain dozens of cells while others consist of only a few. Besides, in order to properly count the number of cells in the structure in real time, we would need to have access to a confocal microscope for several days in a row, which we do not currently have. It seems therefore particularly challenging to quantify the effect of stopping the illumination on an already-formed budding structure at a well-defined stage.

These experiments, albeit qualitative, have the merit of showing that the collective extrusion is indeed reversible when the light stimulation is stopped, even though we have not yet come up with a precise estimate for the proportion of cells that reintegrate the monolayer *versus* those that are ejected permanently. It is also important to note that the ability of the cells to reintegrate the monolayer is strongly conditioned by the local cell density. And as we have seen, the convergent flow of cells towards the illuminated area tends to increase the local density in that region, making that cell integration even more strenuous. The fact that some of the cells from the budding structure managed to take place in the monolayer when the illumination was

switched off is additional evidence that cells are indeed not dying while they are collectively extruded.

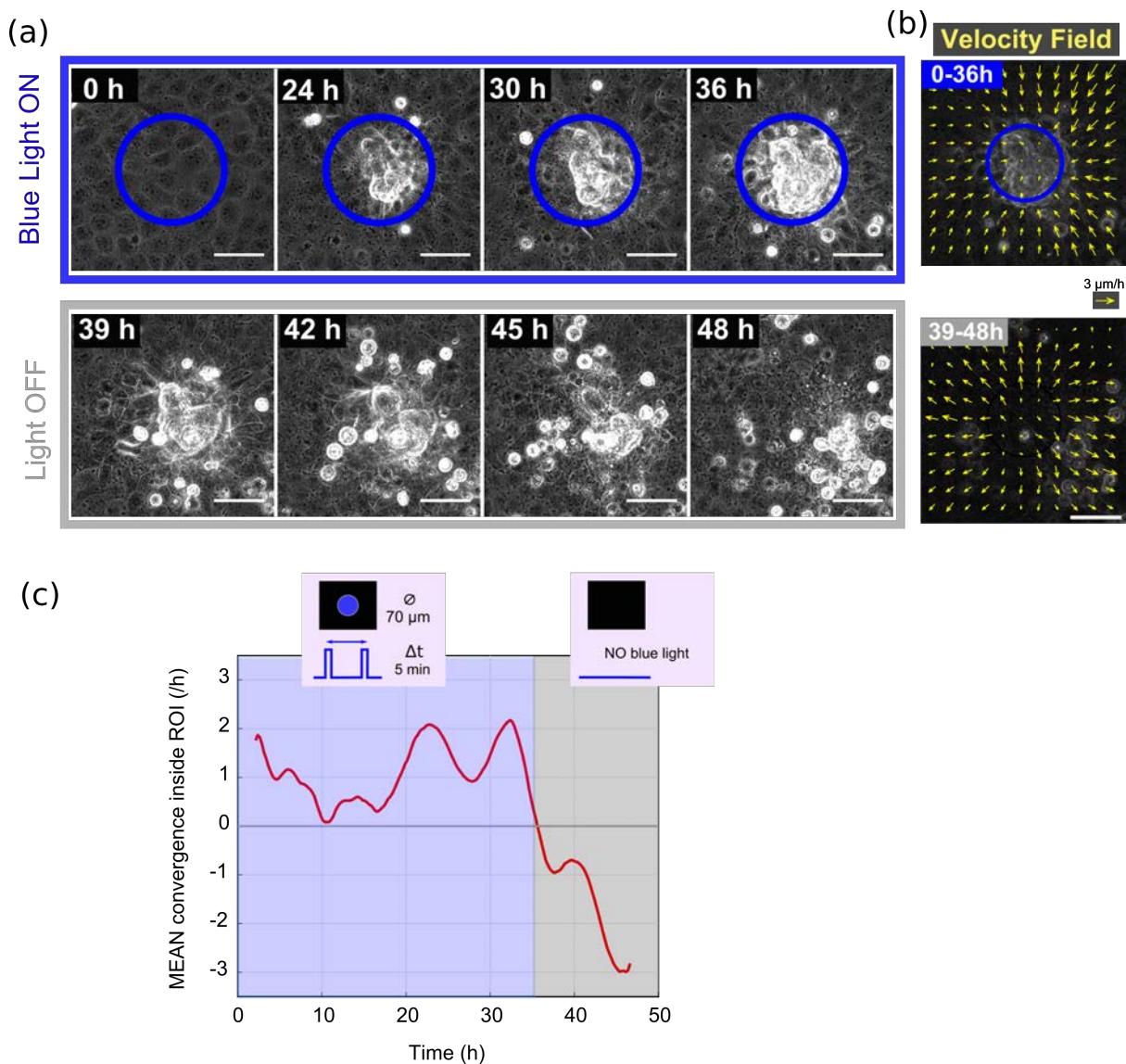


FIGURE 4.29: **The collective extrusion could be reversed by stopping the blue illumination.** (a) Phase contrast images. The cycle of illumination consisted of the standard conditions of illumination for 36 h (top panel, blue frame) followed by the absence of blue light (bottom panel, grey frame). (b) The convergent flow of cells observed during the collective extrusion under blue light stimulation was reversed when the illumination was stopped. The velocity field (yellow arrows) converged towards the ROI during the period of blue light illumination (0 - 36 h) and diverged away from the ROI after the illumination was stopped (36 - 48 h). (c) The mean convergence computed inside the ROI (as previously described) is positive upon the standard conditions of illumination, and becomes negative when the blue light is stopped. Scale bars: 50 μm . [Movie 4.29](#)

In particular, cells from the collective extrusion appeared to die when PP2 was added on an already formed budding structure. MDCK OptoSrc cells were submitted to the standard conditions of illumination in order to form a budding structure. After 48 hours, PP2 was added in the medium, and the standard conditions of illumination were maintained. The budding structure then disintegrated and its constituting cells appeared to be dying (Figure 4.30). The cells from the budding structure did not go back to the monolayer, and we did not observe a divergent flow of cells away from the budding structure, unlike what happened when the illumination was stopped, in which case the cells slowly entered the monolayer again. This is in accordance with the hypothesis that *Src* over-activation protects cells from undergoing anoikis, so that they end up dying when *Src* activation is suddenly blocked with PP2.

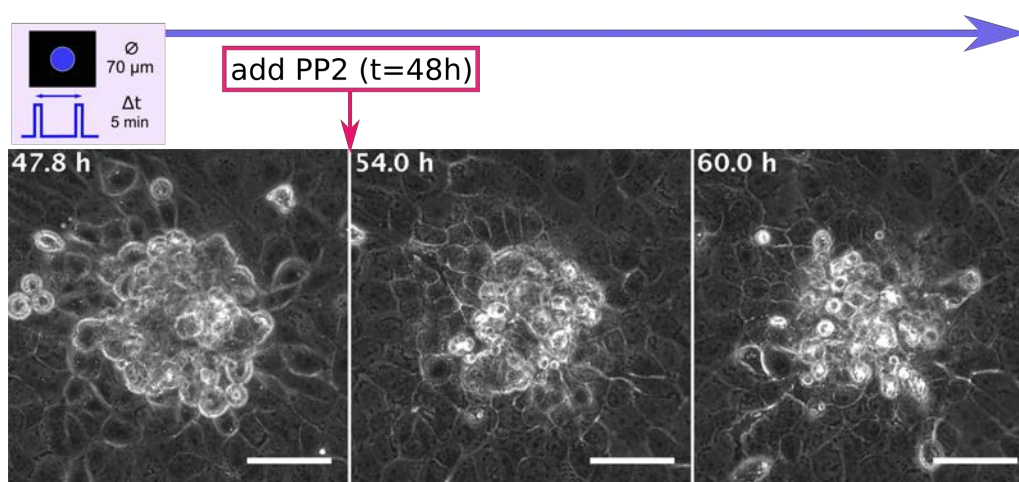


FIGURE 4.30: **The collective extrusion was not maintained when *Src* activity was blocked with PP2.** *Src* inhibitor PP2 was added on an already formed budding structure after 48 hours of illumination, which then started to collapse. Scale bar: 50 μm. [Movie 4.29](#)

4.4.4 Effect of the initial density on the collective extrusion

Cell density is one of the key parameters controlling collective cell behaviours [149, 217]. For instance, crowding has been shown to favour cell delamination in epithelial tissues: in *Drosophila* [213], as well as in zebrafish and MDCK monolayers [212]. Besides, it has been suggested that crowding-induced delamination could be involved in maintaining epithelial integrity (reviewed in [38]) and that mechanical stress induced by crowding could contribute to cell competition [218, 219]. In order to investigate the role of crowding in the collective extrusion phenomena, we computed the probability P_{bud} of observing the formation of a three-dimensional cellular aggregate within the first 60 h of stimulation, as a function of the density measured at the start of the blue-light stimulation. This initial density was measured by manually counting, on the phase contrast images, the number of cells in the field of view for each experiment. To give an idea of the variability in density, Figure 4.31 shows the phase contrast images of a monolayer

at different densities.

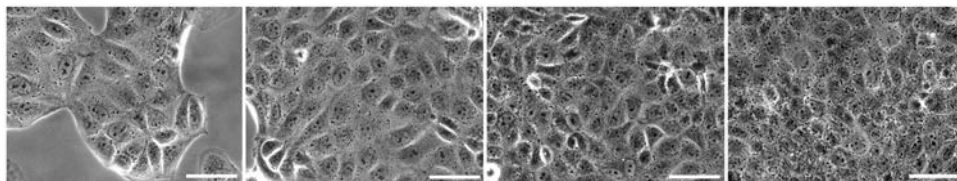


FIGURE 4.31: **Overview of MDCK OptoSrc monolayers corresponding to various initial densities.** From left to right, the initial densities are: 1000 - 2000 - 3000 - 4000 cells/ mm^2 . Scale bar: 50 μm .

For initial densities d_i corresponding to confluent MDCK OptoSrc cells monolayer ($1700 \text{ cells}/mm^2 \leq d_i \leq 3000 \text{ cells}/mm^2$), the budding probability P_{bud} was extremely high (95%, $n = 112$). If the monolayer of MDCK OptoSrc cells was initially too sparse ($700 \text{ cells}/mm^2 \leq d_i \leq 1700 \text{ cells}/mm^2$), P_{bud} dropped to only 70%, reinforcing the idea that a minimal reservoir of surrounding cells is needed. Surprisingly, when density was larger than 3000 cells/ mm^2 at the beginning of blue-light stimulation ($d_i \geq 3000 \text{ cells}/mm^2$), the probability of budding also dropped to 70% (Figure 4.32). This could be due to the mechanical strain exerted on the cells in a high density monolayer. Another explanation could be that high density favours the homo-dimerization of CRY2 (Figure 4.32 inset) to the detriment of the CRY2/CIBN dimerization, which would limit the recruitment and over-activation of Src at the membrane. But we do not observe this behaviour systematically in high density monolayers.

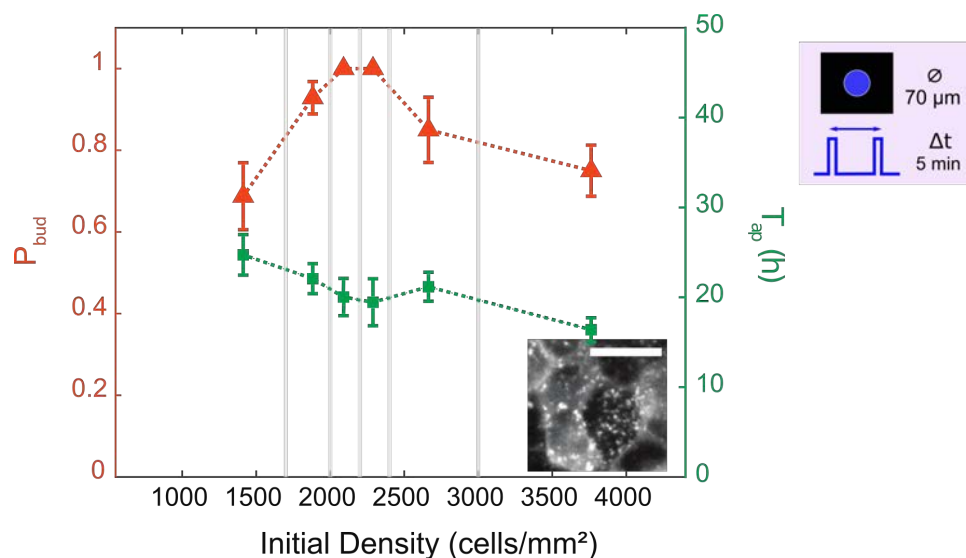


FIGURE 4.32: **Effect of the initial density on the collective extrusion phenomenon.** Budding probability P_{bud} (left axis, orange triangles) and appearance time T_{ap} (right axis, green squares) as a function of the monolayer density at the beginning of blue stimulation. Error bars represent the standard deviation for T_{ap} , and the uncertainty as described in section 2.8.3 for P_{bud} . Inset: example of crowded OptoSrc cells, in which CRY2-mCherry appears to homo-oligomerize (bright spots in the cells). Scale bar 20 μm .

4.4.5 Molecular basis of the collective extrusion

Effect of the substrate composition on the collective extrusion

We conducted the budding experiment on a substrate coated with fibronectin, that enhances the adhesion of cells to the substrate. In the standard conditions of illumination, the appearance of the collective extrusion was delayed on a fibronectin-coated substrate: $T_{ap} = 39 \pm 2$ h (SEM, $n = 10$), compared to the plain glass condition: $T_{ap} = 30 \pm 2$ h (SEM, $n = 10$) (Figure 4.33). This showed that an enhanced adhesion with the substrate acted against the collective extrusion of the Src over-activated cells from the monolayer.

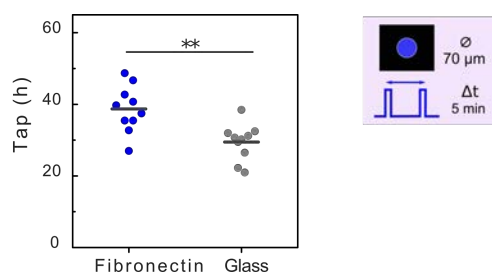


FIGURE 4.33: **Effect of substrate adhesion on the collective extrusion.** The appearance time T_{ap} of the bud is delayed on a fibronectin-coated substrate (blue points) compared to a plain glass substrate (grey points). $p = 0.002$

F-actin is recruited in the collective extrusion We used SiR-Actin to perform live imaging of F-Actin in the MDCK OptoSrc cells in the standard conditions of illumination. This revealed that F-actin strongly accumulated in the illuminated group of cells within a few hours of illumination (*e.g.* 6 hours on Figure 4.34). This suggests a correlation between recruitment of F-actin and the collective extrusion. Besides, confocal images of the budding structure after 60 hours of illumination revealed an F-actin accumulation at the multicellular scale in the underlying monolayer (Figure 4.34), suggesting that a contractile effect at the scale of the monolayer might be involved in the collective extrusion of activated Opto-Src cells. We do not detect a well-defined multicellular actin cable, though.

Cell contractility We next investigated whether cell contractility was correlated to the dynamics of the bud formation. Treatment with Calyculin A, which enhances cell contractility, resulted in a significantly faster budding ($p = 0.01$): $T_{ap} = 15 \pm 1$ h (SEM, $n = 28$), compared to $T_{ap} = 22 \pm 2$ h (SEM, $n = 30$) for the control condition (DMSO). The probability of budding P_{bud} slightly increased: 100% for Calyculin A, compared to 90% for DMSO. Conversely, treatment with the ROCK inhibitor Y-27632, that decreases cell cortical tension, resulted in a significantly slower budding ($p = 0.02$): $T_{ap} = 33 \pm 2$ h (SEM, $n = 55$), as opposed to $T_{ap} = 26 \pm 2$ h (SEM, $n = 24$) for the control condition (normal medium). This time, the probability of budding P_{bud} was decreased: 75% for Y-27632, compared to 83% in normal medium. Therefore, cell contractility does promote the collective extrusion phenomenon.

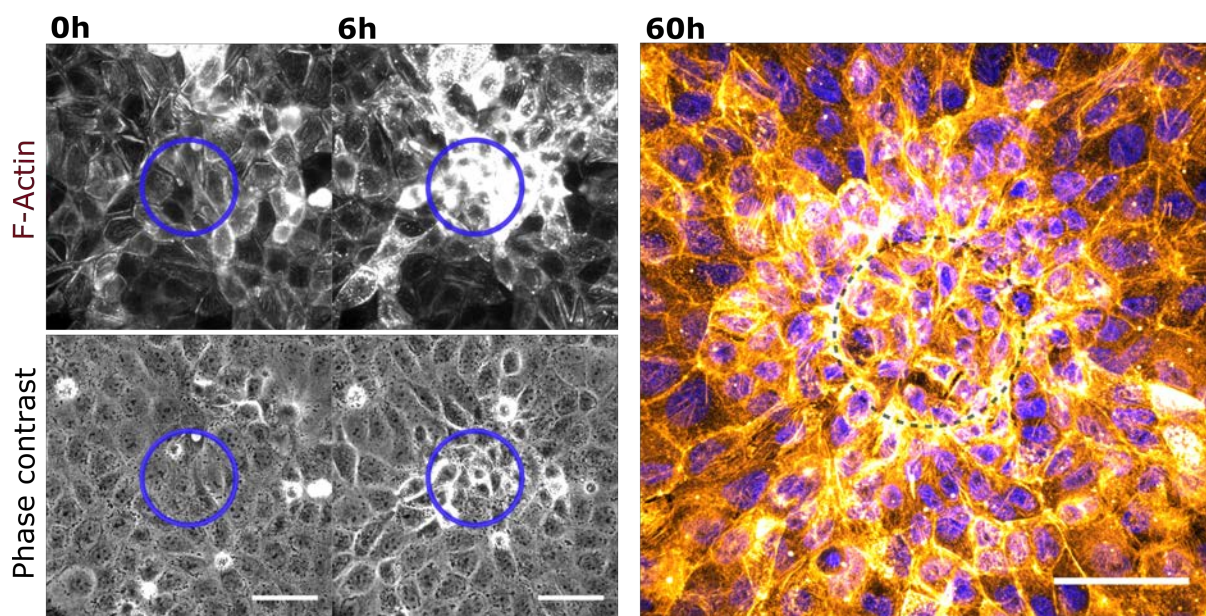


FIGURE 4.34: **F-actin is recruited in the group of illuminated OptoSrc cells**, within the first few hours of illumination (about 6 hours here). F-actin was stained with SiR-Actin (far-red fluorescence) in both live and fixed samples. **Left:** fluorescence (top) and phase contrast (bottom) images before illumination and after 6 h of illumination. **Right:** confocal images of F-actin (orange) and cell nuclei (blue) after 60 h of illumination (fixed sample). Scale bars: 50 μm .

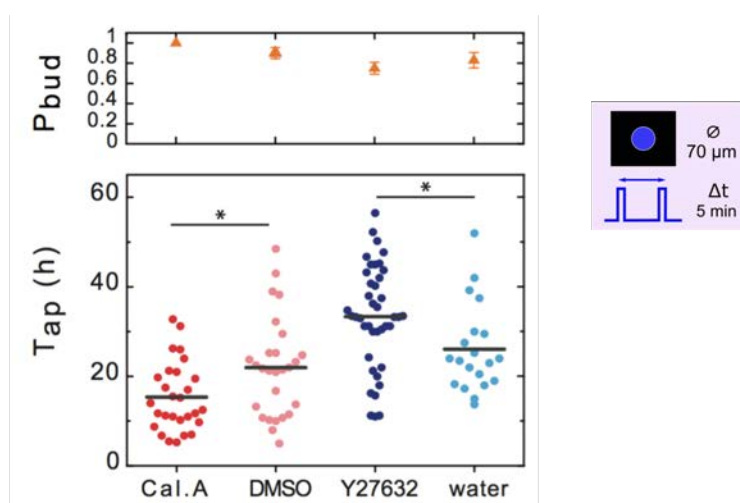


FIGURE 4.35: **Effect of contractility-modifying drugs on the appearance time T_{ap} (bottom) and probability of budding P_{bud} (top).** Calyculin A (1nM) decreases T_{ap} ($p=0.01$) and increases P_{bud} , while Y-27632 (10 μM) increases T_{ap} ($p=0.02$) and decreases P_{bud} . The error bars of P_{bud} represent the uncertainty as described in section 2.8.3.

4.4.6 Does the collective extrusion require a frontier between two distinct src-level populations?

Given that illumination of a whole monolayer of OptoSrc cells did not give rise to a collective extrusion phenomenon, we hypothesized that a frontier between two cell types was needed. In this case, the two cell types differ in their level of activation of Src. In order to evaluate the need for such a frontier, we created two situations in which the group of Src-activated cells was not surrounded by a normal monolayer.

First we seeded cells at low density, in order to obtain isolated groups of OptoSrc cells, and exposed them to blue light. In this case, we used the GFP channel to illuminate the whole field of view with 200-ms pulses of blue light every 5 minutes. The activated OptoSrc cells immediately – within 1 hour – spread out and started to migrate outward from the group of cells, eventually losing cell-cell contacts (Figure 4.36). After a few hours, the group of cells had completely broken apart. This is very far from the natural behaviour of normal MDCK cells, which are very cohesive and tend to stick together. Instead, this increased migration and individualisation is reminiscent of the phenotype of mesenchymal cells, suggesting that the over-activation of Src might be inducing an Epithelial-Mesenchymal Transition in the group of OptoSrc cells (discussed in the next section). In the context of the collective extrusion, this could imply that activated OptoSrc cells in the monolayer are indeed undergoing EMT, but do not have free space around them to migrate outwards, so they converge inwards and attempt to migrate out of the monolayer, resulting in a 3D “migration” that leads to the collective extrusion.

Second, in order to study a group of OptoSrc cells not surrounded by a normal monolayer, without this possibility of migrating outwards on a free surface, cells were confined on circular adhesive patterns of diameter $\varnothing = 100 \mu\text{m}$ (initial density $1700 \text{ cells}/\text{mm}^2 \leq d_i \leq 3000 \text{ cells}/\text{mm}^2$, $n = 10$). One must bear in mind that confining cells in an adhesive pattern also introduces geometrical constraints, and it is known that cells behave slightly differently under confinement [131, 220]. When all the cells in the pattern were illuminated (ROI $\varnothing = 100 \mu\text{m}$), almost no collective extrusion events were observed — $P_{bud} = 10 \%$, $n = 10$ — as opposed to the situation where the same $100 \mu\text{m}$ -area of an OptoSrc cell monolayer of similar initial density was illuminated — $P_{bud} = 84 \%$, SEM, $n = 19$ (Figure 4.36).

We see two possible explanations for this reduced occurrence of collective extrusion in a confined pattern. The first one is that the collective extrusion requires a frontier between two cells types, which is provided when activated OptoSrc cells are surrounded by normal cells. The second one is that the surrounding monolayer is needed to feed the collective extrusion. In particular, we have seen that the photo-activation of a group of cells induces a convergent flow of the surrounding monolayer towards the illuminated area. The surrounding normal cells then enter

the illuminated area, and are in turn *Src*-activated. In the case of a confinement pattern, the absence of a surrounding monolayer makes this convergent flow impossible. The fact that we mostly fail to see a collective extrusion might then also be attributed merely to the lack of a reservoir of cells to fuel the spheroid.

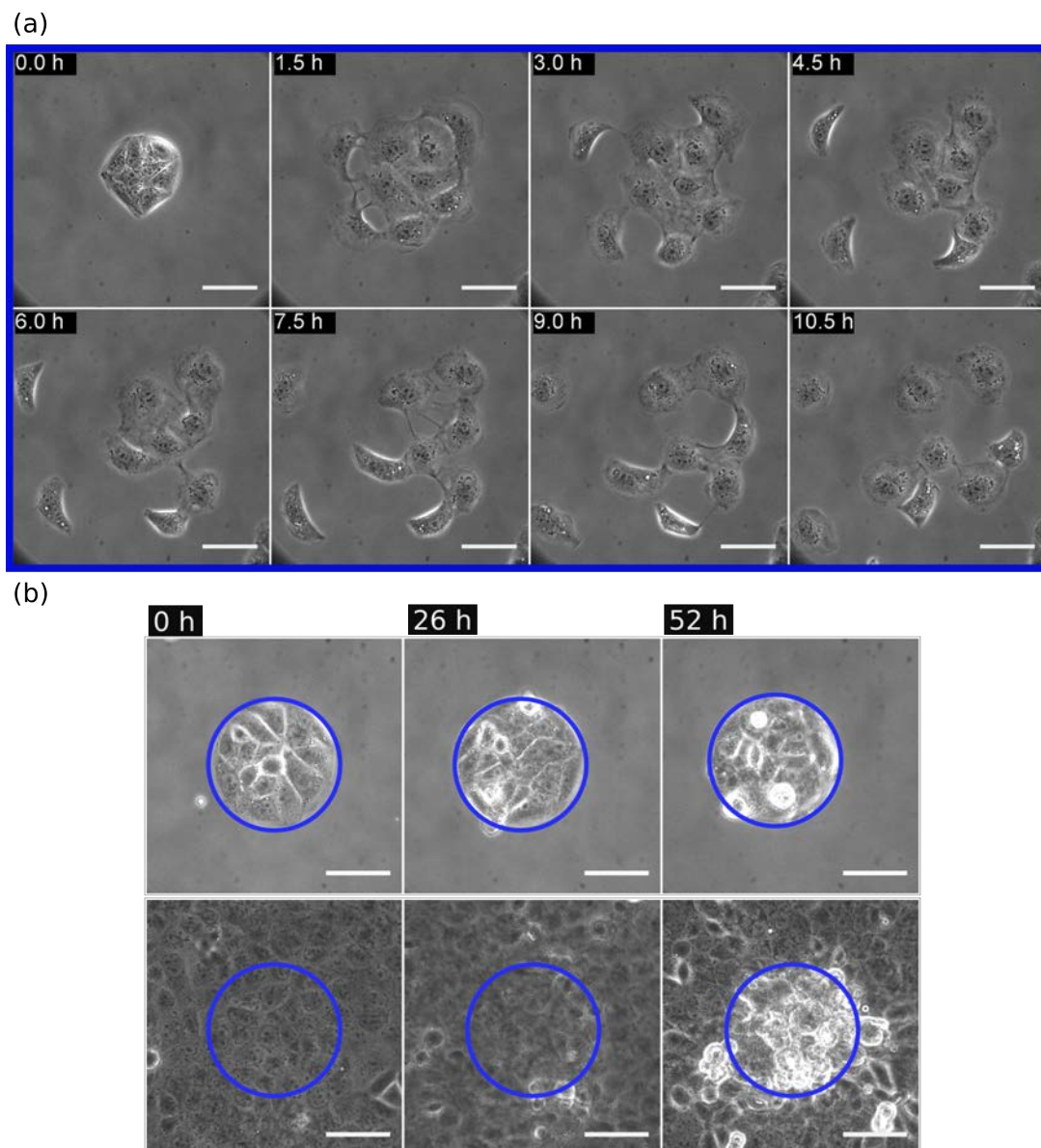



FIGURE 4.36: **Effect of the surrounding monolayer on the collective extrusion.** (a): An isolated group of OptoSrc cells upon blue illumination quickly spreads out and breaks apart. (b): Almost no budding was observed when cells were confined on an adhesive pattern whose area matches the region of illumination. **Top:** OptoSrc cells confined on a pattern and illuminated ($\varnothing = 100 \mu\text{m}$, $\Delta t = 5 \text{ min}$). **Bottom:** Monolayer of OptoSrc cell with the same illumination parameters. Scale bar $50 \mu\text{m}$.  [Movie 4.36](#)

4.4.7 Is the collective extrusion associated with an Epithelial-Mesenchymal Transition?

The epithelial-mesenchymal transition (EMT) refers to a complex process in which epithelial cells progressively lose their characteristic epithelial phenotype to become mesenchymal cells. The EMT phenomenon has been shown to be essential for germ layer formation and cell migration in the early vertebrate embryo [221], but it can also contribute to pathological events such as organ fibrosis and tumour progression [222,223]. Indeed, EMT induces the loss of epithelial polarity and intercellular junctions, and increases cell motility and invasiveness, thus promoting tumour invasion and metastasis [224]. It is now clear that EMT is not a binary process, in which cells are either in the full epithelial or the full mesenchymal state, but rather a spectrum of intermediary phases, and that cells can acquire a partial, or hybrid, EMT status [225]. This EMT “gradient” can be observed in tumours, in which the invasive front has completely undergone EMT, while cells from the tumour bulk remain largely epithelial [226].

In particular, Src activation has been found to be a trigger for EMT induction [71,227]. Plus, the behaviour of an isolated group of OptoSrc cells illuminated with blue light seemed to point to an EMT process (Figure 4.36). We thus investigated whether the MDCK OptoSrc were undergoing an EMT when Src was locally over-activated upon blue-light exposure in a cell monolayer, and if this could be linked to the collective extrusion phenomenon.

Various biomarkers have been used to identify EMT, some of which are acquired, while others are attenuated, during this transition [228]. For instance, cells undergoing EMT lose their typical epithelial markers such as E-cadherin and zonula occludens-1 (ZO-1), and acquire mesenchymal markers such as N-cadherin and vimentin. We first studied such markers in monolayers of MDCK OptoSrc either over-activated or not, using a global illumination. Whole monolayers of cells were either kept in the dark or exposed to a sequence of blue light pulses (200-ms pulse every 5 minutes for 24 hours) using the custom-made illuminator (section 2.7), then immunostaining was performed for E-cadherin, ZO-1, N-cadherin, vimentin, alpha-catenin, paxillin, and phospho-Myosin Light Chain. These preliminary experiments allowed us to identify the two markers that displayed the clearest differences between the lit and dark situations: the level of E-cadherin decreased, and that of vimentin increased, upon Src activation in OptoSrc cells (Figure 4.37). We thus decided to go forward with these two markers for the collective extrusion experiment.

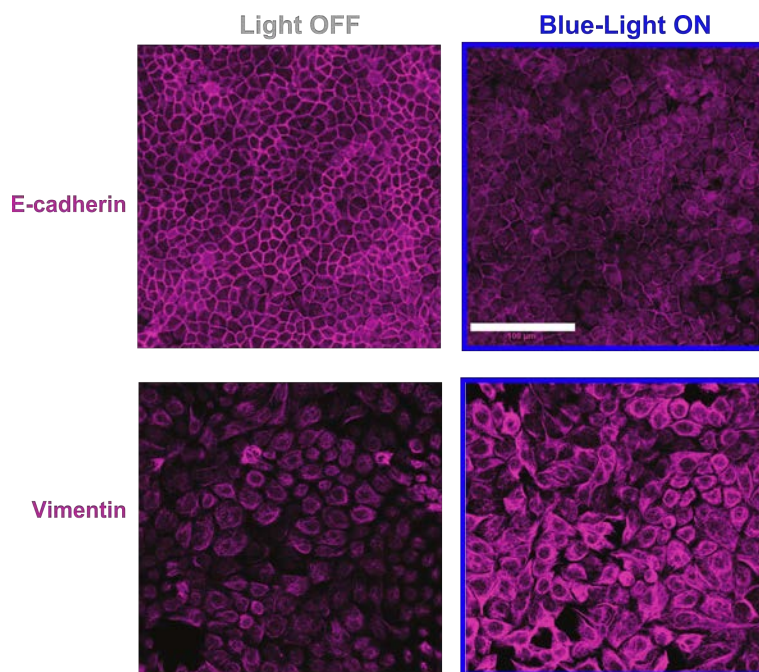


FIGURE 4.37: **Immunostaining of E-cadherin and vimentin in OptoSrc cells, exposed or not, to blue light for 24 h.** Cell monolayers were either exposed to blue light in the custom-made illuminator ($\Delta t = 5$ min), or kept in the dark for 24 hours. The confocal images of the E-cadherin and vimentin immunostaining were taken consecutively, with the same acquisition parameters. E-cadherin appears to be down-regulated, and vimentin up-regulated, in OptoSrc exposed cells, as opposed to non exposed cells. Scale bar: 100 μm .

We then created budding structures using the standard conditions of illumination for 60 hours, fixed them, and performed immunostaining of E-cadherin and vimentin on them.

E-cadherin The cell membranes, where E-cadherin is mostly localized, are easier to observe in the monolayer, where cells are spread on the substrate, than in the budding structure where cells are rounding up. We therefore focus on the underlying cell monolayer. Confocal images revealed that E-cadherin was depleted from the membranes of over-activated OptoSrc cells underlying the budding structure, compared to non-exposed cells from the surrounding monolayer (Figure 4.38 (a)). This shows that activated OptoSrc cells lose their typical epithelial cell-cell junctions as they undergo the collective extrusion. Yet, cells in the collective extrusion still remain cohesive, suggesting that cells either maintain E-cadherin junctions, albeit at low levels, or acquire a different type of cell-cell junctions.

Vimentin Confocal images revealed that vimentin was strongly expressed mostly in the cells at the top of the collective extrusion aggregate (Figure 4.38 (b)). These cells are likely the ones that have been illuminated the longest, *i.e.* the cells that are the most advanced in the collective extrusion process.

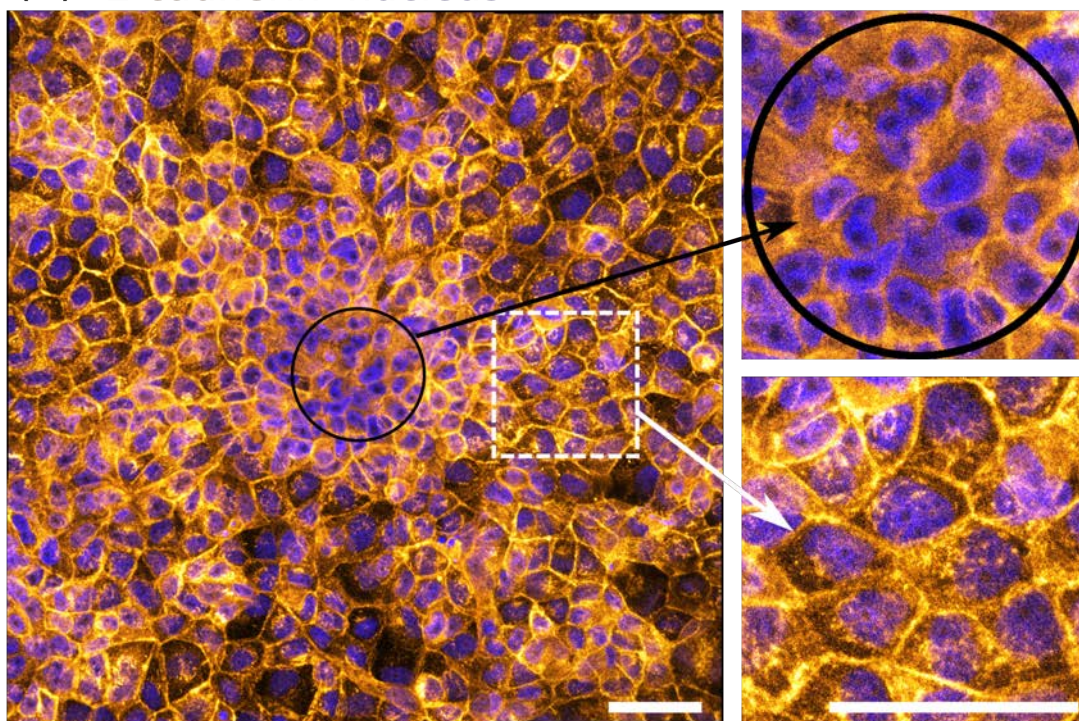
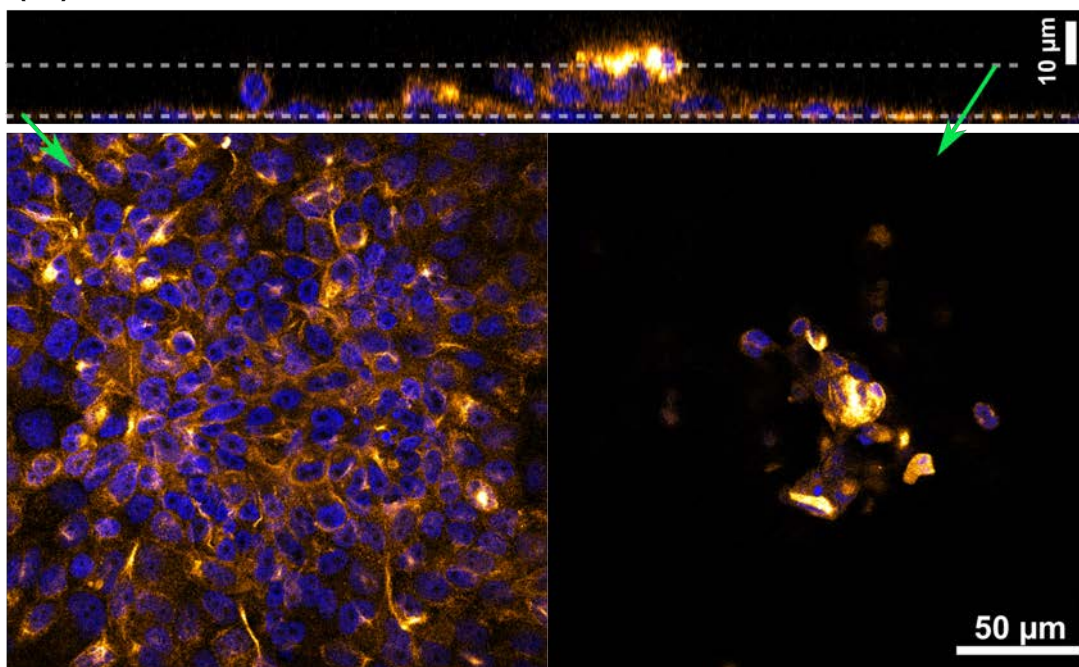
(a) E-cadherin nucleus**(b) Vimentin nucleus**

FIGURE 4.38: **Immunostaining of E-cadherin and vimentin in a monolayer displaying a budding aggregate.** A monolayer of MDCK OptoSrc cells was subjected to the standard conditions of illuminations for 60 h and fixed with PFA. **(a)** E-cadherin (orange) is depleted from the cell membranes of OptoSrc activated cells (black circle), compared to non-exposed cells from the surrounding monolayer. **(b)** Vimentin (orange) is strongly expressed in the cells at the top of the budding structure, compared to cells in the monolayer. Cell nuclei were stained with Hoechst (blue). Scale bars: 50 μm .

Altogether, the down-regulation of E-cadherin and up-regulation of vimentin in the OptoSrc activated cells of the budding structure suggest that these cells might be undergoing a partial EMT. Interestingly, these cells exhibit typical markers of an EMT, without displaying the usual phenotype of mesenchymal cells. Indeed, the cells in the aggregate remain cohesive with themselves as well as with the monolayer, instead of becoming more individualized, like mesenchymal cells.

In this chapter...

- We have introduced the OptoSrc system used during this thesis. We now have a stable cell line of MDCK cells in which Src is overactivated, reversibly, by exposure to blue light. We have then characterized this system: in particular, OptoSrc cells exposed to blue light display some characteristics of Src overactivation (membrane ruffling, increased migration, individualization), in a reversible manner.

- We have reproduced results previously observed in similar systems: a single activated OptoSrc cell gets extruded and detaches from a monolayer of normal cells.

- We then used an optical set-up to target blue-light illumination to a selected group of cells. We have shown that a circular group of such Src-activated cells undergo a collective extrusion from the monolayer, and these extruded cells stay cohesive in an aggregate. Src activation at the membrane is necessary for this collective extrusion. Besides, this phenomenon is preceded by a convergent flow of cells from the surrounding monolayer towards the illuminated area.

- We can control the collective extrusion both in space and time by tuning the illumination parameters, namely the illuminated area and the frequency of the blue-light pulses.

- The collective extrusion is reversible: when blue-light stimulation is stopped, the aggregate collapses and most of the extruded cells reintegrate the monolayer.

- The collective extrusion is context-dependent: a surrounding monolayer is needed to fuel the formation of the budding structure.

- The OptoSrc activated cells forming the collective extrusion could be undergoing a partial Epithelial-to-Mesenchymal Transition.

Chapter 5

Discussion

“It would be so nice if something made sense for a change.”

Alice in Wonderland,
by Lewis Carroll

Contents

5.1 MDCK OptoSrc cells' response to a light stimulus is context-dependent	112
5.2 Possible origins of the collective extrusion	113
5.2.1 Do cells follow the light?	114
5.2.2 The mechanical hypothesis	117
5.2.3 The molecular hypothesis	123

5.1 MDCK OptoSrc cells' response to a light stimulus is context-dependent

One particularly thought-provoking notion about OptoSrc cells is that their response to light-activation depends on their surroundings, as described in the previous chapter (section 4.4.6). In fact, if a group of OptoSrc cells at low density is exposed to blue light, it tends to spread out more than in the absence of light. In contrast, if a group of OptoSrc cells from a confluent monolayer is exposed to blue light, it tends to contract inwards.

The experiment shown in Figure 5.1 exemplifies this outwards *vs* inwards response to the same light stimulus when cells are in low *vs* high density, in a continuous manner: an isolated group of cells was illuminated with a circular pattern for at least 80 hours, so that we could witness the transition from an isolated situation to a confluent one. The first line shows the first two hours of illumination of the isolated group of cells, to which they responded by spreading out on the substrate (the velocity field is directed outwards). The second line (12 h to 24 h) shows the densification of the monolayer, until the initial group of cells becomes completely surrounded. At this point (around 24 h), the cells behaviour reverses from spreading out to contracting inwards (the velocity field is directed inwards). The third line (38 h to 66 h), shows that the collective extrusion finally occurs, as previously described. We have thus sequentially observed two separate responses of the same group of OptoSrc cells to the same light stimulus. This shows that the behaviour of the group of OptoSrc cells depends on its neighbourhood in a dynamic manner.

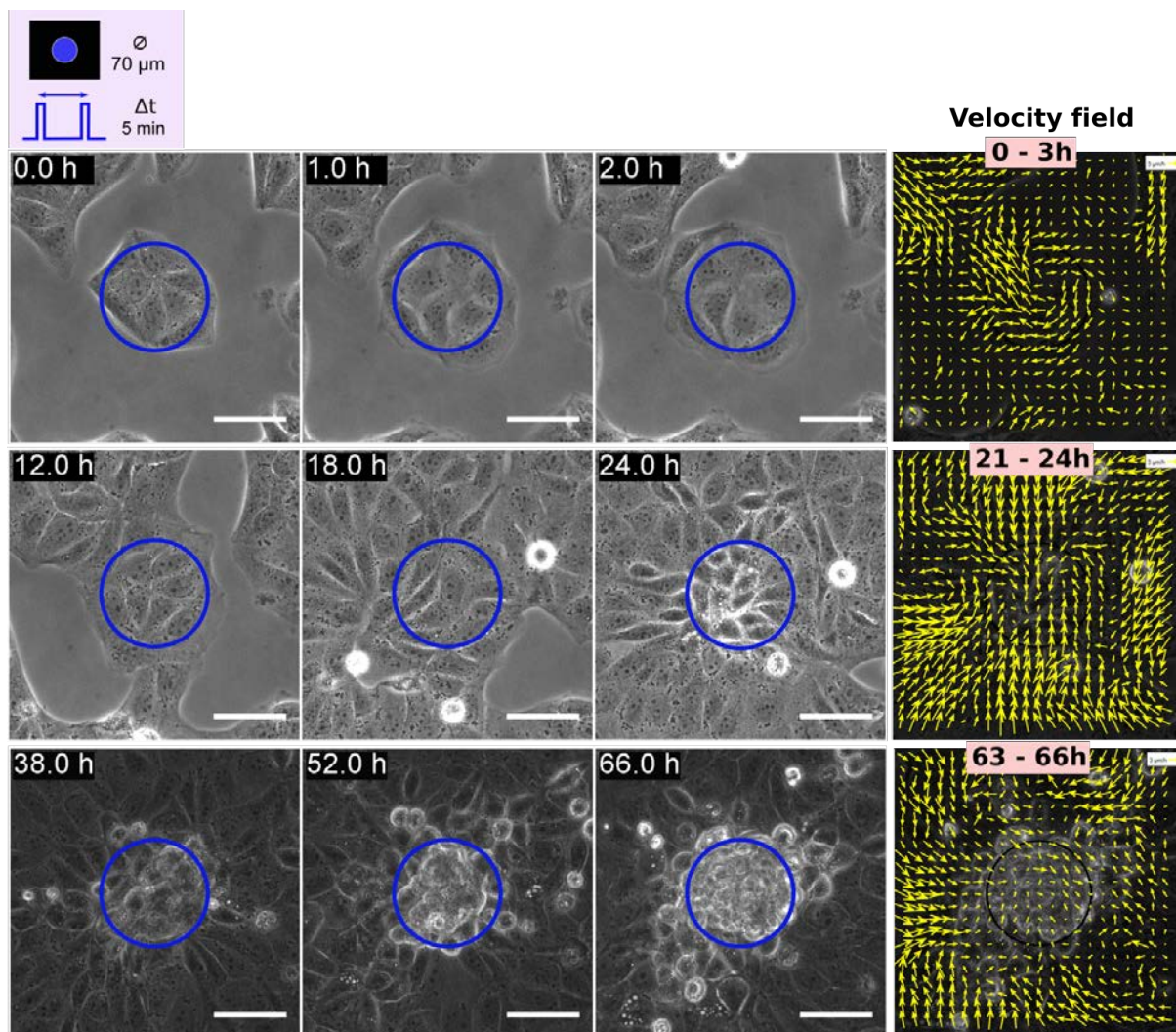


FIGURE 5.1: **Cell spreading followed by budding.** An isolated group of OptoSrc cells rapidly spreads on the substrate upon illumination (less than 1 hour). Only when it is surrounded with a confluent monolayer does it reverse this spreading behaviour into an inward contraction. Ultimately, the group of illuminated OptoSrc cells undergoes a collective extrusion as previously described. Standard conditions of illumination. Scale bar $50 \mu\text{m}$. [Movie 5.1](#)

5.2 Possible origins of the collective extrusion

We have seen that a group or Src-activated cells in a normal monolayer ends up extruding from the monolayer in a collective manner. Although we have identified several parameters that influence the formation of this 3D structure, we have yet to come up with a mechanistic explanation for this phenomenon. Here, we explore some of the hypotheses that could account for the collective extrusion.

5.2.1 Do cells follow the light?

Light-induced directed migration

We noticed that the collective migration of the OptoSrc cells could be directed using blue light. In this experiment, we illuminated a $70\ \mu\text{m}$ -circular area adjacent to a group of OptoSrc cells, so that the illuminated region overlapped with the border of the cells over a few μm (Figure 5.2). The cells then migrated to position themselves at the illuminated spot. Later, when the ROI was translated by $60\ \mu\text{m}$ to the right, the group of cells migrated once again to place themselves under the light. This is consistent with the fact that Src is involved in signalling networks regulating cell migration [72,229]. We had previously observed the formation of actin rearrangement and ruffles in Src-activated cells (section 4.2.2), which would indeed favour polarisation of the cells and migration to the illuminated region.

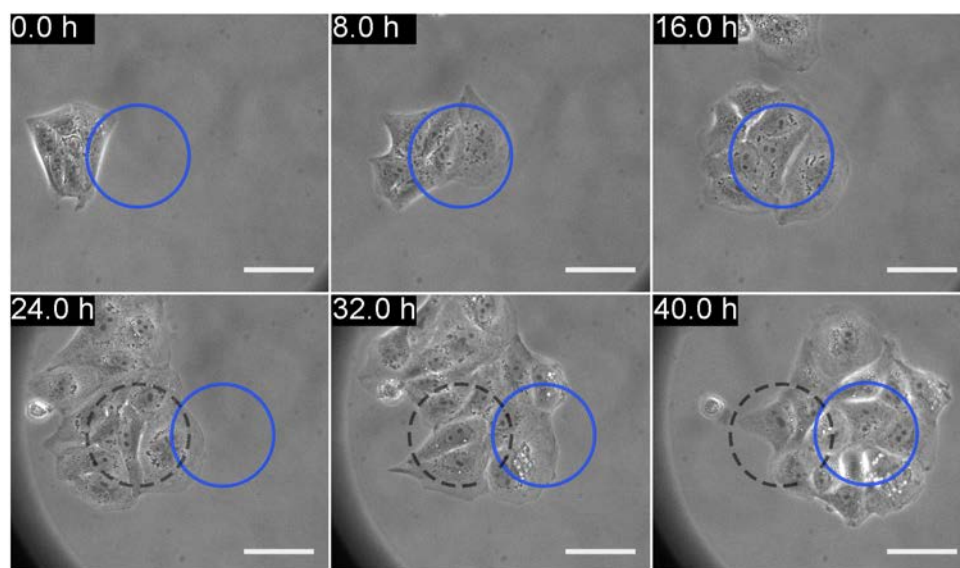



FIGURE 5.2: **Light-induced directed migration of a group of OptoSrc cells.** Cells migrate towards an illuminated area (blue circle). When the illuminated area is translated away from the group of cells after 24 h, cells migrate again towards the new illuminated area (blue circle, previous illuminated area in dashed black line). Scale bar: $50\ \mu\text{m}$.  [Movie 5.2](#)

A similar property was observed by Kim *et al.* [230], with cells containing an optically controlled Fibroblast Growth control Factor Receptor (called optoFGFR1). They use the light-inducible homo-oligomerization of CRY2 (in absence of CIBN) to control the regulation of FGFR1 in HeLa cells, and show that they can induce directed migration of these cells using light. They take advantage of this property to study different signalling pathways related to migration. Of note, it had previously been reported that Src is necessary for cell migration induced by Fibroblast Growth Factor 1 [231].

We therefore wondered if this light-induced migration could be the driving mechanism of the collective extrusion.

Translation of the ROI in the collective extrusion experiment

In order to better understand this light-attraction, we decided to translate the region of illumination after having formed a budding structure in a monolayer of MDCK OptoSrc cells. In this experiment, the region of illumination was translated by $90\ \mu\text{m}$ — *i.e.* $20\ \mu\text{m}$ away from the previous ROI — after 48 hours of illumination, by which time the collective extrusion had already started ($n = 14$). Figure 5.3 shows that the budding structure then reformed at the new spot of illumination. We noticed that the new budding structure was being fed by two complementary processes. First, as is usually observed in the collective extrusion phenomenon, the cells around the current ROI started to converge towards it. Second, the cells from the already formed bud migrated towards the new area of illumination to coalesce with the new spheroid.

These observations inspire several remarks:

- The cells from the first aggregate seem to be migrating on top of the monolayer towards the new illuminated region. This is reminiscent of the previously observed light-directed migration (Figure 5.2), although in this case the cells migrated on top of a cell monolayer instead of on a free glass surface.
- There might be some sort of communication, or at least adhesion, between cells, to attract cells from the first bud to the new area of illumination. This could be done through mechanical cues, for example if the cells from the first bud are being pulled physically towards the new budding area. Indeed, we have seen a recruitment of F-actin to the group of Src-activated cells (section 4.4.5), which could be involved in this mechanical pulling of the cells. Or it could also be due to chemical signaling between cells, as was previously suggested in the context of chemotaxis [232].
- We were surprised to see, in such an experiment, how fast the cells started to converge to a new spot of the OptoSrc monolayer. Figure 5.4 shows the averaged velocity field of the cells for the first 10 hours of illumination of the first and second (translated) ROI. The flow of cells towards the second ROI is already well under way during the first ten hours following the translation of the ROI, which is not the case for the first ROI. This likely means that the convergent flow towards the second ROI benefits from the convergent flow of cells towards the first ROI, that was already in place once the ROI was translated.

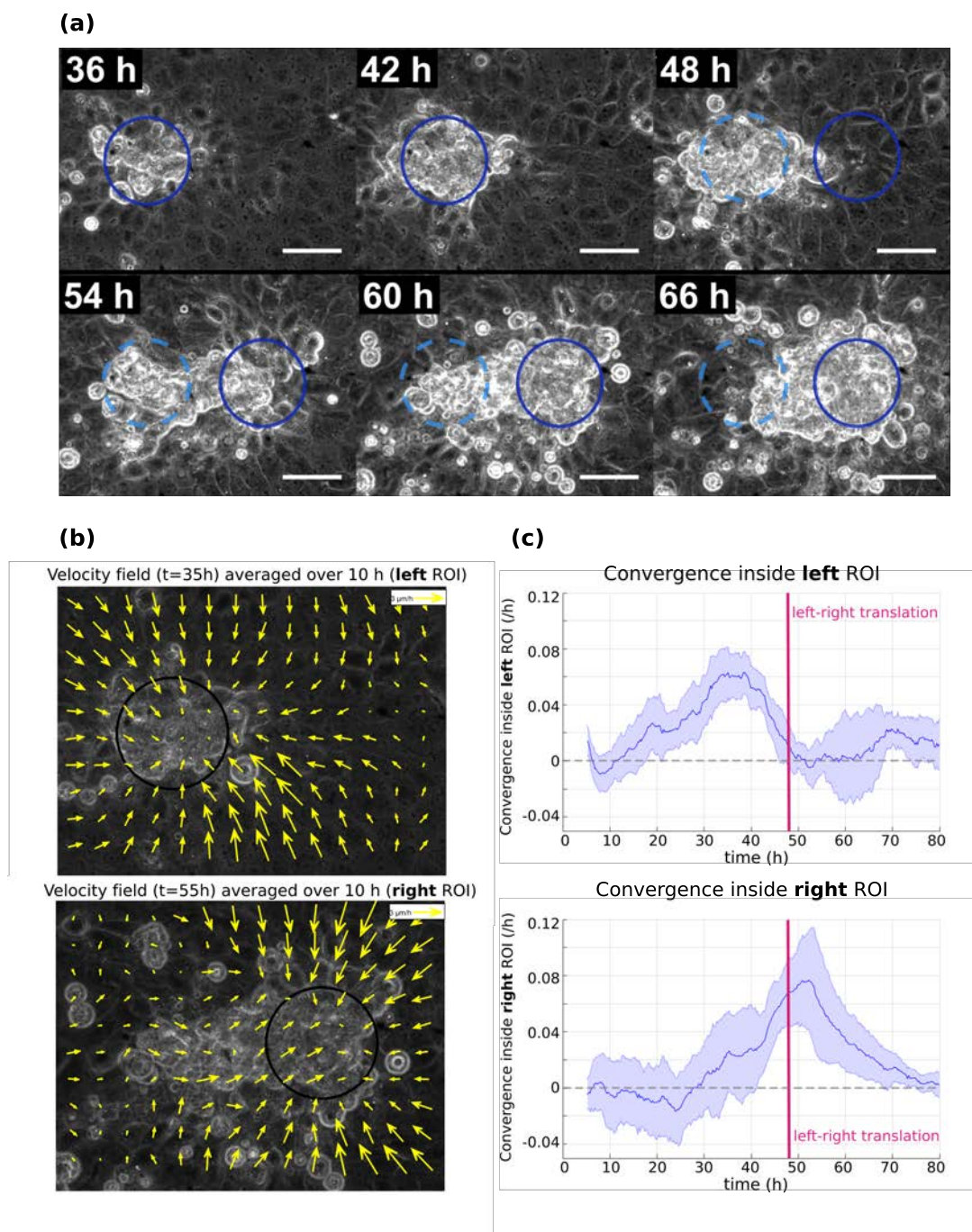


FIGURE 5.3: **Translation of the ROI once the budding structure is formed.** (a): Phase contrast images. A “new” budding structure emerges at the second illumination spot (on the right, solid blue circle), fed both by the monolayer around the illuminated area, and the budding structure that had been formed at the first ROI (dashed blue circle). The ROI is translated after 48 h of illumination. Scale bar 50 μm . (b): Velocity field obtained by PIV analysis and averaged between 30h and 40h for the first ROI (top), and between 50h and 60h for the second ROI translated to the right (bottom). (c): Convergence computed inside the first ROI (top) increases upon illumination of this region, and the second ROI (bottom) increases once the illuminated area is translated to the right. Error bars represent the standard deviation of the mean.

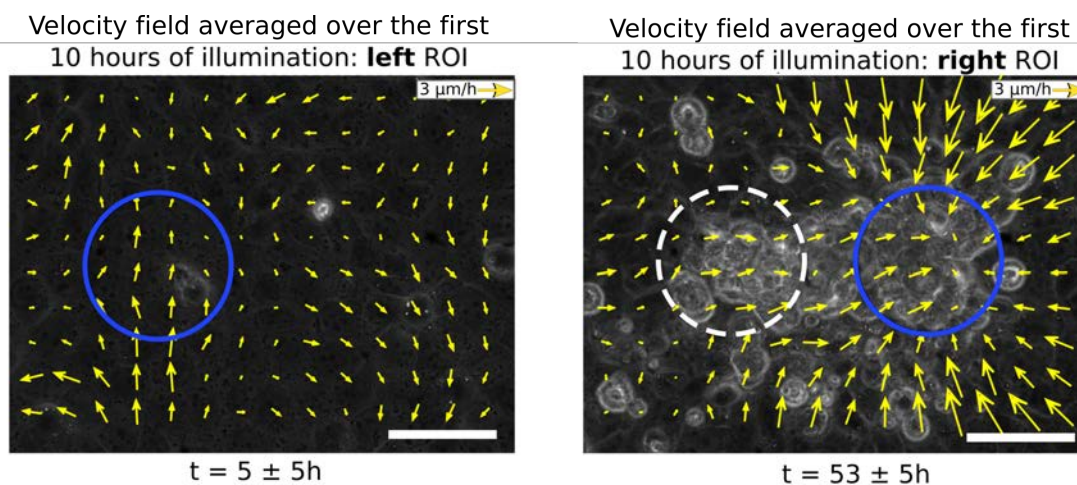


FIGURE 5.4: **The convergent flow of cells is faster after the translation of the ROI near an already illuminated area.** **Left:** The velocity field averaged over the first 10 hours of illumination of the first ROI does not reveal a convergent flow of cells towards this ROI (blue circle). **Right:** After translation of the illuminated area to the right, the average velocity field of the first 10 hours of illumination of the second ROI (48-58h) already reveals a convergent flow of cells, to which the first convergent flow of cells probably contributes. The white dashed circle delineates the first ROI, and the blue circle delineates the second ROI. Scale bar: 50 μm .

To further understand this phenomenon, we would then like to repeat the experiment by translating the ROI further away to see at which distance the budding structure can move or fail to migrate.

We have shown that blue light could be used to direct the migration of OptoSrc cells, and that this could be used to rapidly relocate the collectively extruded structure. The cell attraction to light could thus play a role in the formation of the budding structure. Yet, we have seen that the collective extrusion was hindered by confinement of the group of OptoSrc cells on a pattern (Figure 4.36), so this light attraction cannot be the only mechanism at play.

5.2.2 The mechanical hypothesis

The collective extrusion can originate from the balance of forces between the normal cells from the monolayer and the Src-activated cells. We have started to investigate this hypothesis by measuring the traction forces exerted by the cells on the substrate. In particular, we think that the direction of these forces can help to clarify the underlying mechanism of the collective extrusion.

We consider three potential scenarios, depicted on Figure 5.5:

(a) The illuminated OptoSrc cells contract, and pull on the surrounding monolayer. In this hypothesis, we expect a process close to a purse-string mechanism, in which a multicellular acto-myosin cable is formed at the interface between the group of OptoSrc cells and the monolayer, and draws in the surrounding cells by contracting inwards. Since this acto-myosin ring is part of the cytoskeleton, which is itself anchored to the substrate through focal adhesions, the contraction of the cable would then be transmitted to the substrate, and the traction forces generated would be directed inwards. Examples of this type of situation were found in studies of the gap closure of an epithelium over non-adherent circular patterns [233,234]. In these studies, the closure was driven by a purse-string mechanism, and the forces were directed inwards.

(b) The surrounding monolayer is actively pushing on the group of illuminated OptoSrc cells. Cells just outside the region of illumination would then exert forces on the substrate directed outwards, assuming the group of OptoSrc cells is opposing a resistance to this pushing behaviour.

(c) The activated OptoSrc cells are actively escaping the monolayer by “migrating” in the upper direction. They start to detach from the substrate, which prompts the surrounding cells to migrate inwards in order to maintain the integrity of the monolayer. This part of the process is then simply cell migration, in which cells extend lamellipodia to grab on the substrate and propel their body forward. In this case, the cells lamellipodia pulling on the substrate would generate forces directed outwards, which is what is commonly observed for cell monolayer migration [169,235].

These mechanisms are not mutually exclusive, and a combination of them is also possible.

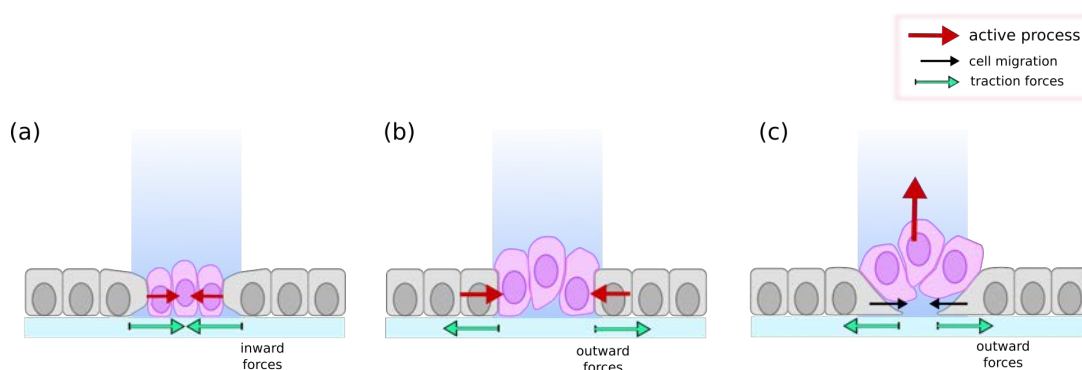


FIGURE 5.5: **Three possible mechanisms for the collective extrusion, and the direction of the traction forces associated.**(a): The illuminated OptoSrc cells contract and pull the surrounding monolayer inwards. The resulting forces on the substrate would be directed inwards. (b): The non-exposed monolayer is actively pushing on the group of activated OptoSrc cells. In this case, we expect the forces generated on the substrate to be directed outwards from the interface between the two cell types. (c): The group of OptoSrc cells is actively escaping the monolayer, which closes the resulting gap by migrating inwards. The forces generated are expected to be directed outwards.

Traction Force Microscopy

We used Traction Force Microscopy (TFM) to measure the traction forces that cells exert on the substrate during the collective extrusion [164,165]. The protocol is described in section 2.9.

Note that the TFM technique introduces several differences from the standard conditions of our experiments. First of all, the cell monolayer is grown on a soft substrate (acrylamide gel of ~ 10 kPa), instead of a rigid glass substrate ($\sim 70 \cdot 10^6$ kPa). We would thus need to characterize the impact of the substrate stiffness on the collective extrusion phenomenon. Our first observations suggest that the collective extrusion is slowed down on a soft substrate, and does not appear as well-defined as on a glass substrate. Plus, the acrylamide gel substrate is coated with fibronectin to enable cell adhesion, and we have already seen that the collective extrusion was slightly slower to appear on a fibronectin-coated substrate (Figure 4.33).

A monolayer of MDCK OptoSrc cells was grown on a fibronectin-coated soft substrate (10 kPa) containing fluorescent beads. A $70 \mu\text{m}$ -diameter disc was then exposed to 200-ms blue-light pulses every 2 minutes, in order to speed up the appearance of the collective extrusion. We then computed the traction forces from the displacement field of the beads using the TFM Package from the Danuser Lab [173]. We first note that the inversion step from the algorithm requires one to make an assumption about the sum of the forces: the net force of the whole field of view is set to zero. This is a reasonable assumption for isolated cells or groups of cells being entirely located inside the field of view, but it doesn't hold true when considering a monolayer, that extends further than the borders of the image. This induces a bias in the calculated forces on the border of the image. In order to circumvent this issue, we only consider the results in the center of the image (at least $50 \mu\text{m}$ from the border).

Figure 5.6 shows the traction forces obtained after 24 h of blue-light stimulation, *i.e.* around the time the budding structure starts to appear. First, we note that the traction magnitude is highest around the border of the ROI, showing that traction forces are indeed involved in the collective extrusion phenomenon. We see that the forces on the border of the ROI are directed outwards. We can thus eliminate the first scenario, in which the OptoSrc cells contract and pull the surrounding monolayer inwards through a purse-string-like mechanism. We cannot yet discriminate between the two remaining scenarios: whether the normal cells are pushing on the illuminated OptoSrc cells, or migrating into a gap left by the OptoSrc cells, remains unclear. To clarify this, we would like to compare the traction forces obtained for the collective extrusion to an OptoSrc cell population in two different situations: the migration of this cell population against a physical wall (*e.g.* PDMS [126]), and the closure of a monolayer around a circular gap by cell crawling [236]. Comparing the values of the traction forces to these two cases might then highlight which process is more likely to be involved in the collective extrusion phenomenon.

Of course, one must bear in mind that the process can also evolve over time, and it is entirely possible that the two different mechanisms both occur sequentially.

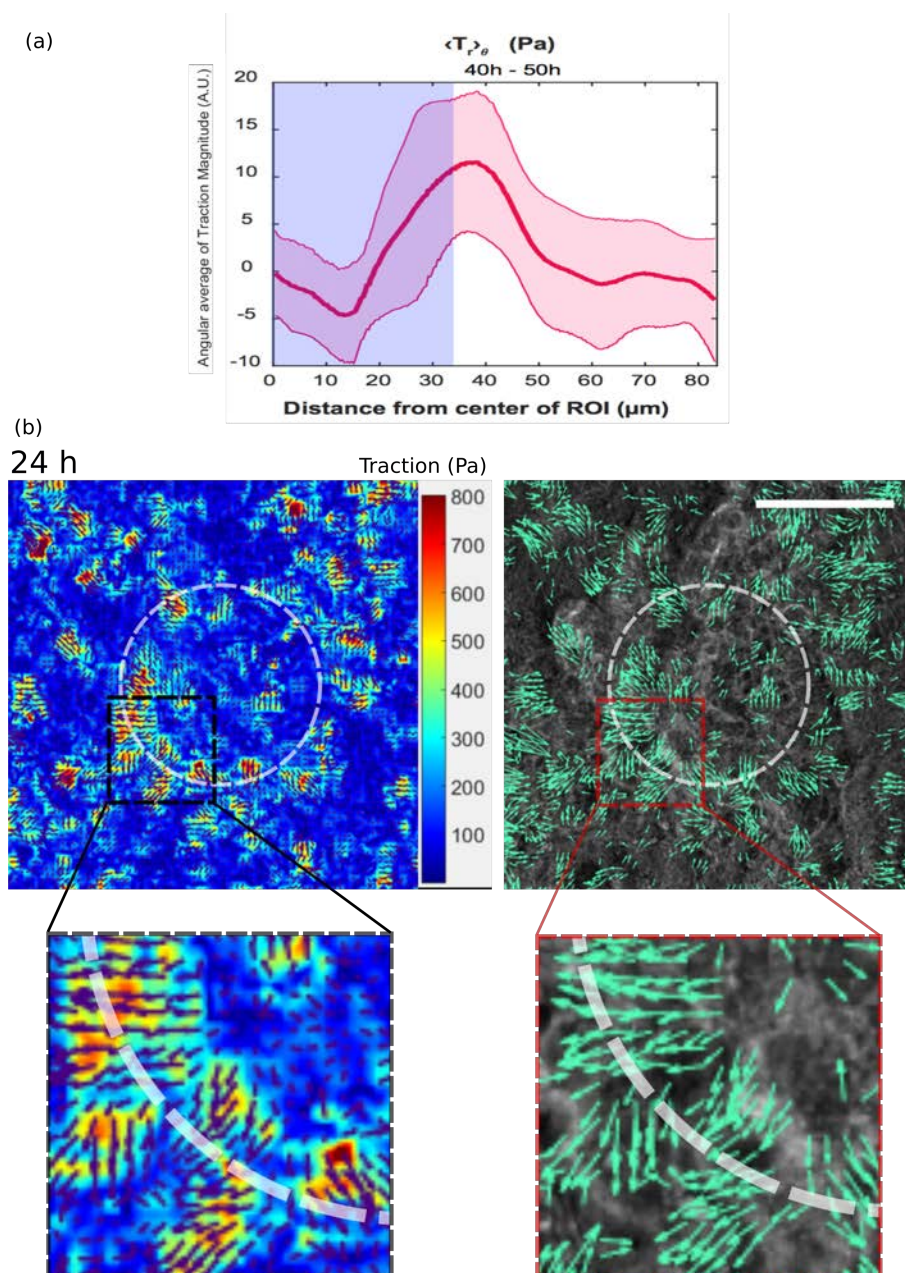


FIGURE 5.6: **Traction Force Microscopy experiment on the collective extrusion.** (a) Angular average of the traction magnitude, centered on the ROI at 24 ± 0.5 h (red line \pm orange lines). The traction magnitude reaches a maximum around the border of the ROI (radius $35 \mu\text{m}$). (b) **Left:** traction magnitude (Pa) and traction forces (arrows) in the monolayer after 24 h of blue-light stimulation. The white circle indicates the region of illumination. **Right:** traction forces (arrows) superimposed on the phase contrast images. The forces at the interface between the activated OptoSrc cells and the surrounding monolayer are directed outwards from the ROI. Scale bar: $50 \mu\text{m}$.

We have based our hypotheses on the study of gap closure in a cell monolayer, for which there are two major driving mechanisms: actin purse-string contraction [237] and cell crawling involving lamellipodia protrusion [236]. This question has been vastly studied in various systems *in vivo* and *in vitro*, and is still the source of some controversy [238]. In our system, there is an additional element to this already complex process: the surrounding monolayer is closing in on a group of Src-activated cells, not just on an empty space. It thus generates another scenario, in which one cell type is pushing on the other. We have already excluded the first scenario (a). It is now challenging to discriminate between the two possible situations (b) and (c). The main difference between these two situations is the origin of the forces. In (b), the surrounding monolayer is pushing on the group of activated OptoSrc cells, which are thus opposing a resistance. In (c), the activated OptoSrc cells are escaping the monolayer, and the surrounding cells merely follow their movement by migrating inwards. The underlying question is: are the OptoSrc cells opposing a resistance to the surrounding monolayer, or not? For one thing, measuring the internal stress might give a clearer view of the mechanical interaction in the collective extrusion experiment [239]. Besides, TFM only yields the traction forces exerted by the cells on the substrate, but does not give any information on what happens in 3D. In order to go further, we would thus like to probe the local pressure inside the aggregate. This can be done by introducing polyacrylamide microbeads in our 3D structure, that act as cell-like barometers to detect the local pressure of the tissue [240].

Antagonistic migration assay: MDCK wt vs OptoSrc

In the two previous chapters, we have described the two approaches we have used to study cell competition: the antagonistic migration assay between two cell populations and the creation of an interface *in situ* using a light-inducible oncogene. Of course, we also enquired about the combination of these two approaches: what would be the outcome of an antagonistic migration assay between MDCK wt and MDCK OptoSrc cells? In such an experiment, MDCK wt and OptoSrc cells were seeded in opposite compartments of a culture insert, which was then removed to start the AMA. The two populations were then subjected to a pulse of blue light every 5 minutes, using fluorescence illumination *via* the GFP channel, for the duration of the experiment. Figure 5.7 shows the progress of the assay with the phase contrast images and the GFP signal (only OptoSrc cells are labelled with GFP). Note that the timer was set to zero at the start of illumination, instead of the removal of the barrier (which was ~ 2 h prior to the start of illumination). Given that the MDCK wt cells were not fluorescently labelled, the kymographs based on the fluorescent signal could only be generated for the OptoSrc population. Instead, we chose to generate a kymograph using the phase contrast images, which gives at least a good account of the migration fronts.

First, these images enable us to directly compare the behaviour of MDCK wt and OptoSrc cells during the migration phase preceding the meeting. In particular, we can witness the spreading

of the cells on the edge of the OptoSrc population, as opposed to the cohesive migration front of the wt cells. The individualistic behaviour of OptoSrc cells is again exemplified by some cells detaching from the migrating front and exploring the free space on their own.

Second, the phase contrast kymograph shows that the MDCK OptoSrc migration front follows a shallower slope than that of MDCK wt cells, translating their higher front velocity. The two monolayers meet around 21 hours after the start of illumination, and then the wt population continues to migrate forwards while the OptoSrc population seems to move backwards. These are preliminary results ($n = 2$) and need to be repeated, as well as studied at longer times (at least 60 hours). But they are in line with the findings of Porazinski *et al.* [124], in which a population of MDCK Ras^{V12} cells was repulsed backwards by a population of MDCK wt cells in a similar confrontation assay.

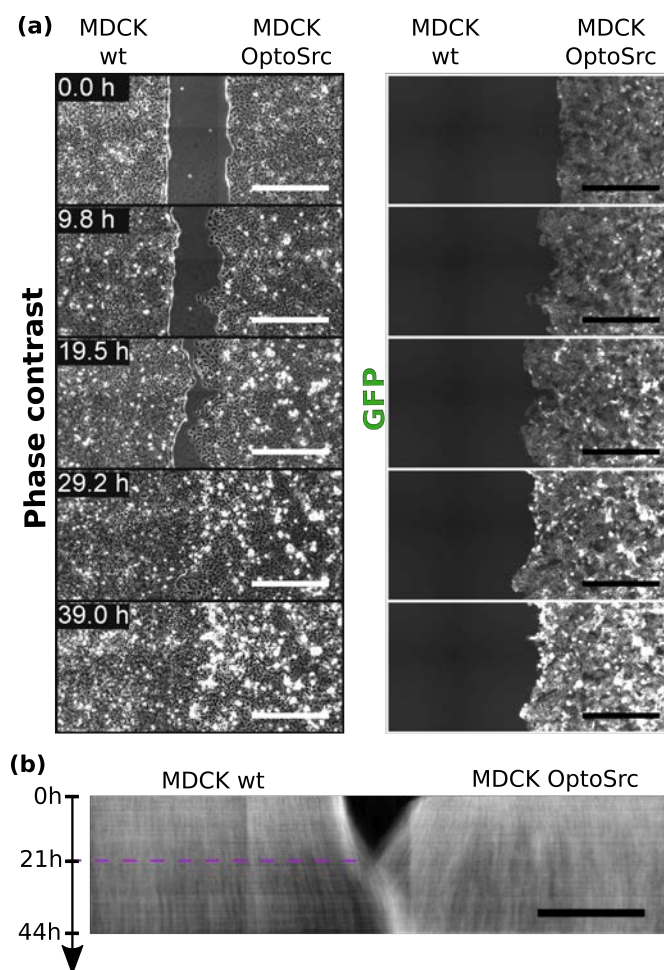


FIGURE 5.7: **Antagonistic migration assay between MDCK wt and MDCK OptoSrc cells.** (a) Phase contrast images (left) and GFP epifluorescence images (right) of the AMA. (b) Kymograph of the phase contrast images. After the first meeting (21 h on the kymograph), wt cells continue migrating forward while OptoSrc cells are repulsed backwards. Scale bar 500 μm .

More interestingly, this displacement of the OptoSrc cells by the wt cells is consistent with the collective extrusion phenomenon previously described. Indeed, in those experiments, the non-exposed OptoSrc cells — acting as the normal cells in the AMA — surrounding the area of illumination converge towards the group of activated OptoSrc cells, which seem to contract and move “backwards”, in this case towards the center. The recoil of the migration front that is observed in the linear geometry thus translates, in a circular geometry, to a recoil towards the middle and upwards of the monolayer, leading to the collective extrusion phenomenon.

5.2.3 The molecular hypothesis

In the study of Porazinski *et al.* previously mentioned, the authors propose an Ephrin-dependent mechanism, in which epithelial cells detect and respond to neighbouring cells overexpressing ephrins. The phenomenon they observe would thus result from a steep difference in ephrin expression levels between adjacent cells [124]. It might be interesting to evaluate the influence of ephrin levels in the outcome of our own system. In this respect, other molecules could potentially be involved in the identification of a frontier between two cell types, or cells of different Src levels.

We suspect that several mechanisms are involved in the collective extrusion. For instance, it can be due to the mechanical pushing of the normal cells on the Src-activated cells, to the attraction of OptoSrc cells towards the light, or to the difference in expression levels of a biological molecule, to name but three. A further question would then be: what enables cells from the budding structure to reintegrate the monolayer when blue light is stopped (Figure 4.29)? We are thus looking for either a reversible mechanism, or two separate mechanisms for the extrusion and the re-integration of cells in the monolayer.

Conclusion and Perspectives

In this PhD thesis, we have developed a new tool to study the interactions between normal and transformed cell populations. Using a photo-activable oncoprotein OptoSrc and an optical set-up to pattern light, we are now able to over-activate Src in a selected group of cells. We have seen that a circular group of activated OptoSrc cells in a monolayer is collectively extruded and forms a cohesive aggregate on top of the monolayer.

Based on our results, we have come up with a working model of this phenomenon:

- Localised exposure to blue light over-activates Src in the group of illuminated OptoSrc cells.
- Src over-activation induces actin remodeling in the cells (section 4.2.2), as well as increased migratory properties and individualisation of the cells (section 4.2.3).
- A convergent flow of cells then appears in the surrounding monolayer, and activated OptoSrc cells start to escape from the monolayer in a collective manner (section 4.4.1).
- The activated OptoSrc cells might be undergoing a partial EMT, as suggested by the down-regulation of E-cadherin at the membrane and the up-regulation of vimentin in the cells (section 4.4.7). Cells undergoing such an EMT cannot migrate outwards, as they do when they are isolated (section 4.4.6), so they migrate outside the monolayer in the upwards direction.
- OptoSrc cells start to pile up on top of the monolayer. Src activation can protect these cells against anoikis, in case they were not able to survive in the absence of contact with a substrate.
- As cells converge towards the illuminated area to fill the gap from the extrusion of OptoSrc cells, they enter the exposed region and are, in turn, Src-activated.
- The collective extrusion of OptoSrc cells grows, and is fueled by the convergent flow of cells from the monolayer.
- This process is reversible when the blue-light activation is stopped, and cells can even reintegrate the monolayer.

The main elements leading to the collective extrusion, induced by localised illumination of an OptoSrc monolayer, are summarized in a graphical conclusion (Figure 5.8).

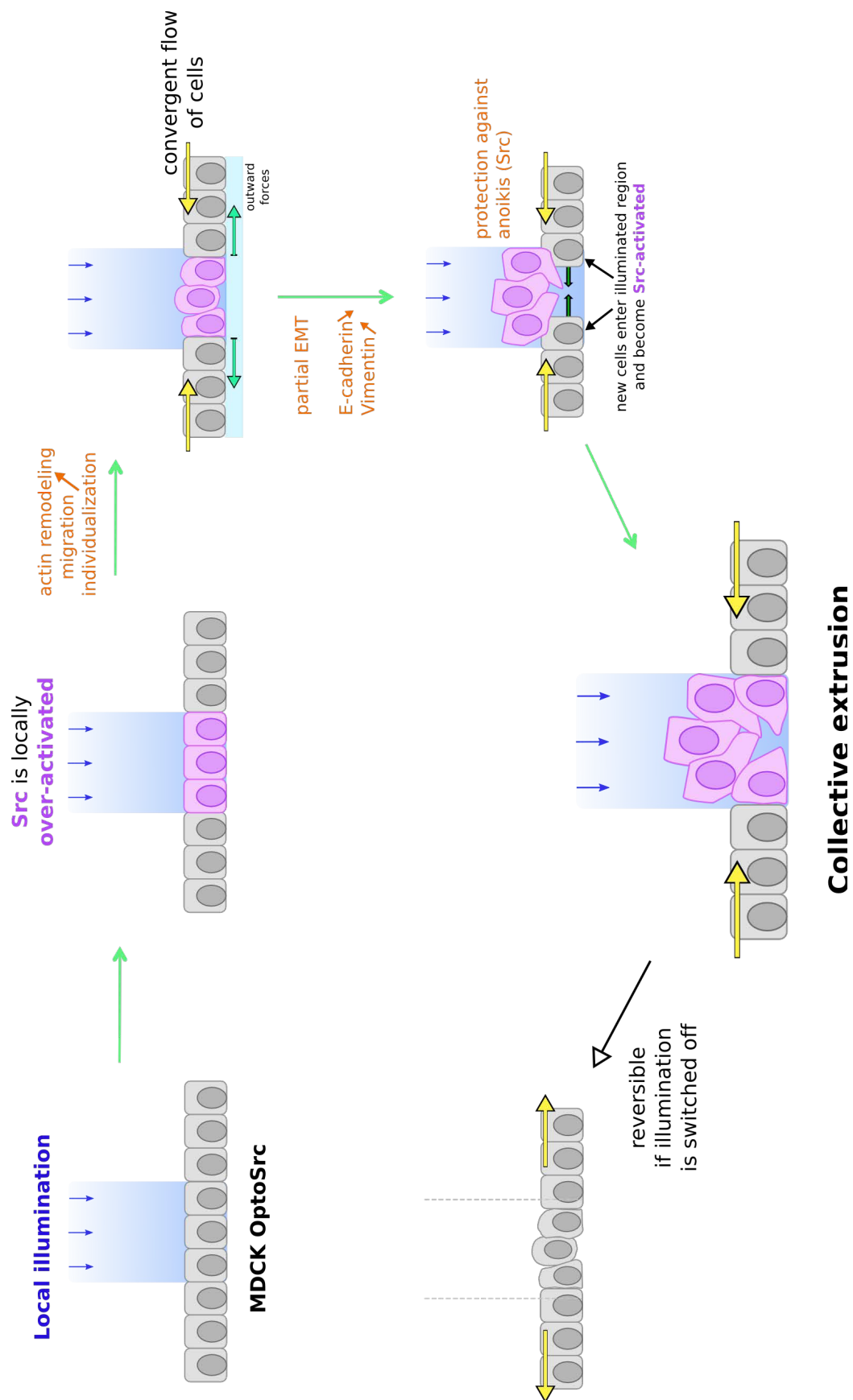


FIGURE 5.8: Graphical conclusion

Open questions

What happens in 3D?

In previous works on transformed cell extrusion from a normal tissue, cells were usually seen to extrude either apically [117] or basally [121], or both [116]. An interesting question that remains open is: what determines the apical *vs* basal extrusion? Could the activated OptoSrc cells collectively extrude in the basal direction, if given the chance? In that scope, studies of the collective extrusion on a thick layer of matrigel or collagen could help to address this question.

Interestingly, in the experiments of single OptoSrc cells in a wt monolayer, we have observed that some OptoSrc cells adopt an amoeboid-like migration (Figure 5.9). The term “amoeboid” refers to a rapid single cell crawling, during which cells change shape by rapidly protruding and retracting extensions, through various mechanical strategies [241]. It is one of the two main types of migration employed by migrating tumour cells, namely mesenchymal and amoeboid [242]. Figure 5.9 shows an example of amoeboid-like migration of an OptoSrc cell through a monolayer of wt cells. We thus wonder if we could observe more of this type of migration from OptoSrc cells if they were free to migrate in 3D.

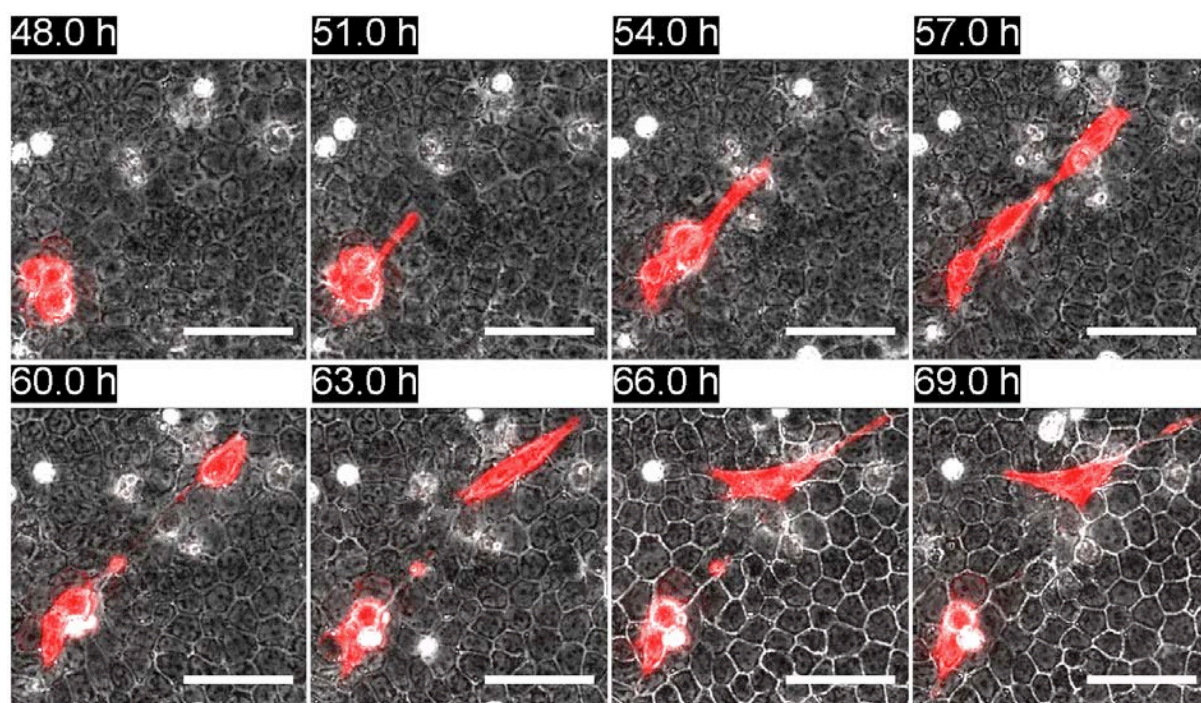


FIGURE 5.9: **Amoeboid-like migration of isolated OptoSrc cells (red) in a wt monolayer.** The timer refers to the duration of illumination. Scale bar 50 μm .

How is gene expression affected in activated OptoSrc cells?

In our experiments, we have chosen to use a disc of given diameter as our basic illumination pattern, and to keep this pattern constant over time. This has the crucial advantage of providing us with a repeatable perturbation of the monolayer. But it does not account for the movement of the cells in the monolayer: a cell can thus migrate in and out of the illuminated region and receive a discontinuous exposure to blue light. One way to deal with this would be to select a subset of cells to illuminate, and to follow them over time. One would need to adapt the software in order to control the ROI dynamically, and to be able to follow the cells that have already been illuminated. To that end, a new version of the OptoSrc construct expressing Dendra2, a green-to-red photo-switchable fluorescent protein [243,244], is currently being developed. Dendra2 can be photo-converted at the wavelength used for Src-activation (488 nm), and would provide us with a fluorescent marker to identify cells that have previously been illuminated, and cells that have not.

Besides, the ability to create a cluster of Src-activated cells in a healthy tissue using light appears as an opportunity to correlate genotypic and phenotypic alterations in the context of tumor progression. With this new Dendra2 construct, we will be able to follow the behaviour, over time, of Src-activated cells, and to purify them using FACS (Fluorescence Activated Cell Sorting). We will then study gene expression by transcriptomics at different time points, for different locations (in or outside the bud) as a function of the oncogenic stress (transformation level, cooperation with other oncogenes such as *ras* or *myc*).

What if we combine OptoSrc with other stresses?

In this project, we have so far studied the effect of only one oncogenic perturbation in a group of cells. But we know that tumorigenesis actually involves several factors. In particular, the multi-hit model of cancer induction (described in section 1.3.2) suggests that several different mutations need to accumulate in a cell to make it properly cancerous. In the future, we thus plan on studying the effect of the cooperation of OptoSrc with other oncogenes, such as *ras* or *myc*.

Another perspective will consist in evaluating the effect of a mechanical stress applied in the vicinity, or directly upon, cells expressing a mutated oncogene inside a normal monolayer. We would thus combine our optogenetic approach with *in vitro* techniques that allow the perturbation of the mechanical state within a monolayer: shear flow (using microfluidic devices), laser ablation, drugs (osmotic stress), micromanipulation (stretcher), to name a few. We should then be able to determine quantitatively the levels of stress that are necessary to induce a change in the phenotype of cells already bearing a mutated oncogene.

Clinical interests

As previously mentioned, during the first stages of carcinogenesis, some cells undergo genetic mutation making them precancerous. These cells then proliferate to form a precancerous lesion, or tumour field. Through additional genetic alterations, cells from this tumour field can ultimately acquire a malignant phenotype. These are the cells that can be clinically detected as cancers, due to their morphological abnormality. But the rest of the precursor cells surrounding these cancers often do not exhibit clear pathological abnormalities, and can easily be missed when the tumour is surgically removed. These are believed to cause local recurrence of cancer, or development of other primary tumours. There is currently no clinical method to identify these normal-looking transformed cells. Could it be possible to detect instead the boundary between normal and preneoplastic cells? If we could identify the molecules that play a role in intercellular recognition, or in the communication at the interface between normal and transformed cells, it could uncover biomarkers highlighting the frontier between normal tissues and precancerous fields. This would greatly help the early detection of cancers, as well as complete surgical tumour dissection.

Appendices

Appendix A

List of Movies

For the sake of simplicity, the movies bear the same number as their associated figure.

Movie 4.7: CRY2 relocalization upon blue light illumination in MDCK OptoSrc cells. In this experiment, 200-ms light pulses were induced every 20 seconds for 20 minutes, followed by 20 minutes in the dark. This cycle was repeated once more. The epifluorescence CRY2-mCherry signal shows the recruitment at the membrane of CRY2 (red arrows) in illuminated OptoSrc cells (blue rectangle). When left in the dark, CRY2 diffuses back to the cytoplasm (white arrows). Scale bar: 20 μm .

Movie 4.8: Membrane ruffling upon light activation of Src. **Left:** CIBN-GFP (left), Phase contrast (center) and CRY2-mCherry (right) images of cells going through two light/dark cycles. Scale bar 10 μm .

Movie 4.10: Phase contrast images of a wound healing assay on OptoSrc cells. **Left** Without intermittent blue light, the migration front is well defined, and the gap takes longer to close. **Right** With intermittent blue light (200-ms pulse every 5 minutes), Src activated cells display a less coherent migration front. Scale bar 200 μm .

Movie 4.13: Group of OptoSrc cells in a MDCK wt monolayer, under global illumination. **Left:** A group of OptoSrc cells (mCherry-labelled, red) present in a wt monolayer is extruded from the monolayer (phase contrast images). **Right:** CIBN-GFP signal, showing the same group of Src-activated cells. Global blue-light illumination, 200-ms pulse every 5 minutes. Scale bar: 50 μm .

Movie 4.14: Collective extrusion of a group of illuminated cells in an OptoSrc monolayer, in the standard conditions of illumination. **Left:** CIBN-GFP signal, showing the illumination pattern (488 nm) - The delay between two light pulses was set to 5 minutes. **Right:** Phase contrast images. The white circle indicates the region of illumination. Scale bar: 50 μm .

Movie 4.23: Range of the convergent flow of cells towards the illumination area during collective extrusion. **Top left:** Phase contrast images. Scale bar: 100 μm . **Top right:** Velocity field — resp. **Bottom left:** speed map — of the monolayer surrounding the collective extrusion, averaged over 10 hours (between 26 h and 36 h after the start of illumination). The black/white circle delineates the region of illumination ($\varnothing = 70 \mu\text{m}$). **Bottom right:** radial average of the radial velocity towards the center of the ROI, averaged over 10 hours.

Movie 4.24: EGTA disrupts cell-cell junctions and blocks the collective extrusion, in the standard conditions of illumination. Scale bar: 50 μm .

Movie 4.29: The collective extrusion could be reversed by stopping the blue illumination. The cycle of illumination consists of the standard conditions of illumination for 36 h followed by absence of blue light. Scale bar: 50 μm .

Movie 4.30: The collective extrusion was not maintained when Src was blocked with PP2. **Left:** The Src inhibitor PP2 was added on an already formed budding structure after 48 hours of illumination, which then started to collapse, with cells visibly dying. **Right:** Standard conditions were stopped after 48 hours. Cells from the budding structure started to reintegrate the monolayer. Scale bar: 50 μm .

Movie 4.34: F-actin is recruited in the group of illuminated OptoSrc cells, within the first few hours of illumination (about 6 hours in this movie). F-actin was stained with SiR-Actin (far-red fluorescence) in live samples. Phase contrast (left) and fluorescence (right) images of a monolayer in the standard conditions of illumination. Scale bar: 50 μm .

Movie 4.36a: An isolated group of OptoSrc cells upon blue illumination quickly spreads out and breaks apart. Scale bar 50 μm .

Movie 4.36b: Small to no budding was observed when cells were confined on an adhesive pattern whose area matches the region of illumination. **Left:** OptoSrc cells confined on a pattern and illuminated ($\varnothing = 100 \mu\text{m}$, $\Delta t = 5 \text{ min}$) **Right:** Monolayer of OptoSrc cell with the same illumination parameters. Scale bar 50 μm .

Movie 5.1: Cell spreading followed by budding. An isolated group of OptoSrc cells rapidly spreads on the substrate upon illumination (less than 1 hour). Only when it is surrounded with a confluent monolayer does it reverse this spreading behaviour into an inward contraction. Ultimately, the group of illuminated OptoSrc cells undergo a collective extrusion as previously described. Standard conditions of illumination. **Left:** Phase contrast images. **Right:** Velocity field (PIV) averaged over 3 h. Scale bar 50 μm .

Movie 5.2: Light-induced directed migration of a group of OptoSrc cells. Cells migrate towards an illuminated area (white circle). When the illuminated area is translated away from the group of cells after 24 h, cells migrate again towards the new illuminated area. Scale bar: 50 μm .

Appendix B

French Abstract

Au tout début de la carcinogénèse, une ou plusieurs cellule(s) subissent des mutations génétiques irréversibles. Les cellules ainsi transformées se retrouvent entourées de cellules normales. Or, lorsque des cellules tumorales sont présentes dans un tissu sain, elles sont en compétition (pour la nourriture, l'espace, ou plus généralement, les ressources) avec les cellules normales. Cette compétition peut donner lieu soit au développement de la tumeur, soit à sa régression si le tissu sain parvient à éliminer cette menace. Il est aujourd'hui admis que l'environnement des cellules mutées, mais aussi les interactions avec leurs voisines normales jouent un rôle dans le devenir des cellules transformées [1, 2]. Une question qui reste ouverte est : comment les conditions initiales jouent-elles sur la stabilité des cellules mutées ?

Pour apporter des éléments de réponse à cette question, nous avons mis en place des dispositifs *in vitro* permettant d'étudier les interactions entre des populations de cellules tumorales et de cellules normales, en relation avec leur environnement. Notre stratégie est de créer des situations contrôlées de co-existence entre deux types de cellules, qui se distinguent par l'expression d'un oncogène, et d'analyser leur évolution. Afin de réaliser de façon contrôlée et reproductible des interfaces entre deux populations de cellules, nous avons développé deux techniques complémentaires : la mise en contact de deux populations initialement séparées d'une part (I), et la création *in situ* d'une interface à l'aide d'une oncoprotéine photo-activable d'autre part (II).

I Compétition pour l'espace entre deux populations de cellules, normales et transformées

Nous présentons ici une première approche pour l'étude systématique d'une situation de mise en compétition entre deux populations. Nous avons utilisé pour ce travail des lignées HEK¹ (*Human Embryonic Kidney*) normales, ou wt (*wild-type*), et transformées (mutation *Ras*^{V12}), respectivement fluorescentes GFP et mCherry.

Les gènes *ras* encodent les protéines Ras, qui sont impliquées dans la régulation de la prolifération cellulaire, l'apoptose et l'organisation du cytosquelette [81, 82]. Ces gènes sont connus pour être l'objet de mutations dans de nombreux cancers [50, 79]. Les cellules que nous utilisons dans cette étude présentent la mutation appelée *Ras*^{V12}, mutation particulièrement répandue dans les tumeurs humaines.

Populations en co-culture

À l'inverse d'autres systèmes, la cohabitation entre cellules HEK normales et transformées ne donne pas lieu à une ségrégation des deux types cellulaires (*cell sorting*), y compris plusieurs jours après leur ensemencement. En effet, lorsque ces deux types cellulaires en suspension sont mélangés à nombre de cellules égal puis déposés sur un substrat, les cellules des deux types restent bien mélangées (Figure B.1 (a)). Nous nous sommes alors intéressés au cas où ces deux populations sont initialement séparées.

Expérience de migration antagoniste

On étudie la compétition pour l'espace entre les deux types cellulaires en utilisant une chambre à deux compartiments séparés par une barrière en silicone de 400 μm de large (Figure B.1 (b)). Chaque type cellulaire est cultivé jusqu'à confluence dans son propre compartiment, et la chambre amovible est retirée lorsque les deux populations sont confluentes. Les deux populations de cellules peuvent alors migrer sur la surface ainsi libérée, par le retrait de la barrière, à la manière d'une expérience modèle de cicatrisation de blessure.

On s'intéresse ici à la migration antagoniste des deux populations sur la surface libre qui les sépare (400 μm). Comme l'illustre la Figure B.1 (c), on observe qu'une fois la barrière enlevée, les deux populations cellulaires entament leur migration l'une vers l'autre jusqu'à entrer en contact. Lors de cette première phase de migration, dite "libre", on note que la population de cellules *Ras*^{V12} migre légèrement plus rapidement que la population de

cellules normales.

Lorsque les deux populations sont en contact, et que la surface libre est recouverte, on observe que les cellules transformées continuent leur avancée alors que les cellules normales reculent. La vitesse d'avancée de l'interface entre les deux types cellulaires est $V_{interface} = 3 \mu\text{m}/\text{h}$. Cette vitesse est non-négligeable, notamment dans la mesure où il ne reste plus de surface libre pour favoriser la migration (les cellules sont à confluence). Le déplacement de l'interface entre les deux populations, mesuré 30 h après le premier contact, varie de quelques micromètres à plus de $100 \mu\text{m}$, avec une moyenne de $76 \pm 18 \mu\text{m}$ (SEM, $n = 13$). La situation inverse où la population de cellules normales avance en faisant reculer la population de cellules transformées n'a pas été observée.

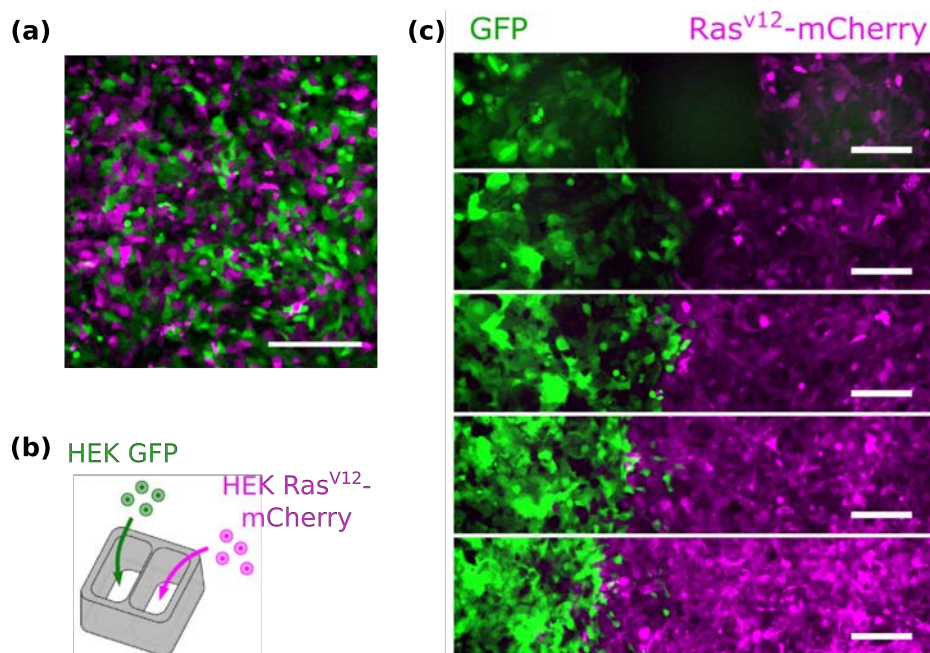


FIGURE B.1: L'interface entre des cellules HEK normales et transformées dépend des conditions initiales. (a) Les cellules HEK wt-GFP (vert) et HEK Ras^{V12} -mCherry (magenta) restent bien mélangées lorsqu'elles sont cultivées ensemble (ici 60 heures après le dépôt des cellules). Barre d'échelle : $100 \mu\text{m}$. (b) Pour réaliser des expériences de migration antagoniste, les deux types cellulaires sont cultivés dans deux compartiments séparés d'environ $400 \mu\text{m}$, à l'aide d'un insert de culture (Ibidi). (c) Exemple typique d'une expérience de migration antagoniste entre des cellules HEK wt-GFP (vert) et HEK Ras^{V12} -mCherry (magenta) : après la rencontre, les cellules transformées continuent leur avancée alors que les cellules normales reculent. La temps de référence $t = 0$ correspond au retrait de la barrière. Barre d'échelle : $200 \mu\text{m}$.

Analyse des images

Les cellules HEK wt et HEK Ras^{V12} sont associées à des marqueurs fluorescents différents — GFP et mCherry, respectivement — ce qui permet de les distinguer sur les images expérimentales, obtenues par microscopie en épifluorescence. Pour rendre compte de l'avancée des deux populations au cours du temps, nous avons réalisé des kymographes à partir des images de fluorescence. Nous avons travaillé à 1D : pour cela, chaque image est moyennée en y (axe perpendiculaire à la direction de migration) pour donner un vecteur-ligne correspondant à un temps donné. La concaténation de ces vecteurs-lignes permet ainsi de suivre l'avancée moyenne des fronts de migration au cours du temps (Figure B.2). Ces kymographes illustrent bien la migration des deux populations au cours du temps, et notamment l'avancée de la population des cellules transformées au dépend des cellules wt, après leur rencontre.

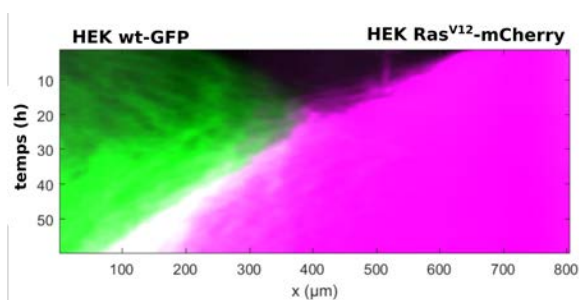


FIGURE B.2: **Kymographe d'une expérience de migration antagoniste** entre des cellules HEK wt-GFP (vert) et Ras^{V12} -mCherry (magenta). Ce kymographe est obtenu par moyennage en y des images de fluorescence d'une expérience de migration antagoniste (cf Figure B.1 (c)). On peut voir l'avancée de la population Ras^{V12} , et le recul de la population wt, après leur rencontre (vers 20 h).

Rôle de la densité sur la confrontation entre les deux populations de cellules HEK

Intuitivement, la densité cellulaire semble être un paramètre important dans ces expériences de migration antagoniste. On peut en effet imaginer qu'une différence de densités entre les deux populations favorise la population la plus dense à repousser la population la moins dense. Ainsi, nous avons mesuré la densité initiale de chaque population dans nos expériences.

De manière surprenante, ni les valeurs absolues des densités initiales des deux populations, ni leurs valeurs relatives (différence ou ratio), ne permettent de prédire le déplacement

de la frontière entre les deux tissus.

Influence de la largeur de l'interface sur la confrontation entre les deux populations

Le fait que les cellules HEK wt et Ras^{V12} restent mélangées lorsqu'elles sont en co-culture, mais forment une frontière à l'échelle d'une population cellulaire lorsqu'elles sont initialement séparées, suggère que la taille de la zone de contact entre les deux types cellulaires ait un rôle à jouer dans l'évolution du système.

Afin d'étudier le rôle joué par la taille de l'interface entre les deux populations, l'expérience de migration antagoniste a été réalisée avec des populations de cellules confinées latéralement. Un traitement anti-adhésif du substrat habituel permet de confiner les populations dans des motifs de taille et de géométrie contrôlées [130, 131] : nous avons choisi pour cette expérience de fabriquer des bandes adhésives de différentes largeurs, perpendiculaires au front de migration (Figure B.3). Ces expériences ont montré que le confinement latéral des populations favorise l'interpénétration des deux types cellulaires : lorsque les bandes adhésives sont suffisamment fines (moins de $200 \mu\text{m}$), on n'observe pas de frontière claire entre les deux populations comme dans la situation précédente "infinie". On n'observe donc plus ce phénomène de compétition où la population de cellules normales recule devant celle des cellules transformées. La taille de l'interface entre les deux populations semble donc bien avoir une influence sur la compétition cellulaire.

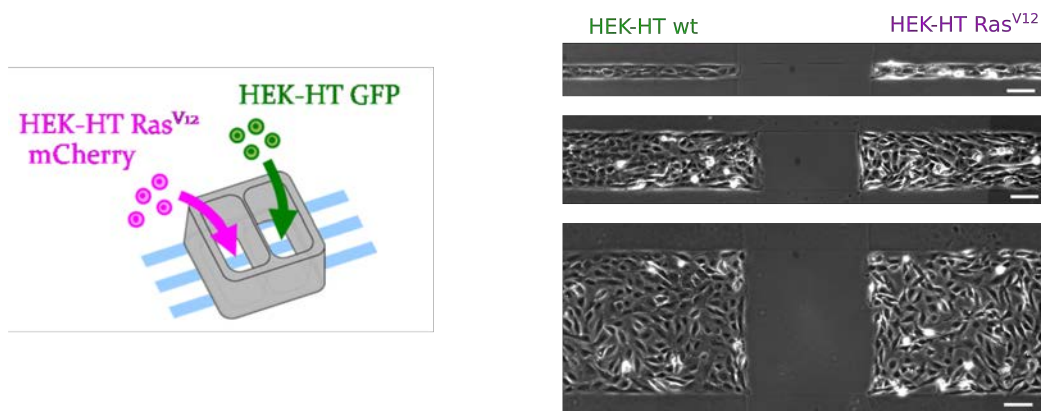


FIGURE B.3: **Confinement des populations de cellules HEK sur des bandes adhésives de largeur variable.** **Gauche :** Les cellules HEK wt-GFP et HEK Ras^{V12} -mCherry sont cultivées dans deux compartiments séparés, à l'aide d'un insert de culture (Ibidi) déposé sur des bandes adhésives. **Droite :** État initial d'expériences de migration antagoniste sur des bandes adhésives de différentes largeurs (50 , 200 et $500 \mu\text{m}$, de haut en bas) - barre d'échelle : $100 \mu\text{m}$

Conclusion L'expérience de migration antagoniste est un moyen pratique pour confronter deux populations. Elle a l'avantage d'être utilisable avec n'importe quel couple de populations cellulaires, en partant d'une situation initiale reproductible : deux populations séparées par un espace rectiligne de largeur donnée. Il est en outre possible de moduler cette situation initiale en confinant les populations latéralement, ce qui modifie la largeur du front de migration. Ces expériences ont montré que la taille de l'interface entre les deux populations joue effectivement un rôle dans le dénouement de la compétition qui s'y joue. Malheureusement, à ce jour, nous n'avons pas encore déterminé le ou les paramètres qui déterminent l'évolution du système, en particulier ceux qui permettraient de prédire la vitesse de déplacement de l'interface entre les deux populations. Nous avons ainsi décidé de développer un outil qui offrirait un meilleur contrôle de la situation initiale, et permettrait de s'affranchir de la phase de migration libre.

II L'optogénétique pour étudier la compétition cellulaire

MDCK OptoSrc: une lignée cellulaire exprimant un oncogène Src sous l'effet de la lumière

Par son approche combinée de la génétique et de la lumière, l'optogénétique permet un contrôle spatio-temporel direct de l'activité d'une protéine. L'oncogène Src, le premier à avoir été identifié, est connu pour être surexprimé dans de nombreux cancers humains [59].

Olivier Destaing (IAB, Grenoble) a développé la première construction permettant un contrôle spatio-temporel de la kinase Src : le système OptoSrc. Celui-ci utilise le système photo-sensible CRY2/CIBN : CRY2 et CIBN sont deux protéines issues de plantes qui se dimérisent sous l'effet de la lumière bleue, mais qui se dissocient en l'absence de lumière [157]. Dans notre cas, le fragment CIBN est ancré à la membrane *via* un groupement CAAX, et la partie CRY2 est couplée à une kinase Src mutée pour être dans le cytoplasme. Un stimulus de lumière bleue induit la dimérisation de CRY2/CIBN, ce qui a pour effet de recruter le fragment CRY2-Src à la membrane plasmique, où la kinase peut alors phosphoryler ses substrats naturels. On peut ainsi induire l'activation de la kinase Src dans une cellule à l'aide d'un stimulus de lumière bleue (Figure B.4).

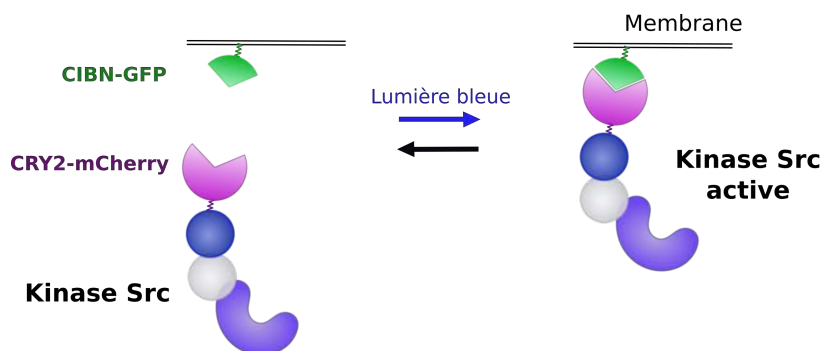


FIGURE B.4: **Principe du système OptoSrc.** La kinase Src est activée par son recrutement à la membrane, grâce au dimère photosensible CRY2/CIBN, sous l'effet de la lumière bleue.

Ce système OptoSrc a été exprimé de manière stable dans une lignée cellulaire épithéliale de rein de chien, appelée MDCK (*Madin-Darby Canine Kidney*) : la lignée **MDCK OptoSrc**. Les cellules de cette lignée surexpriment l'oncoprotéine Src et se comportent comme des cellules transformées lorsqu'elles sont éclairées dans le bleu ; non-éclairées, ces cellules gardent le phénotype des cellules MDCK normales. L'utilisation de ces cellules génétiquement modifiées combinée à un montage optique adéquat permet de créer des monocouches cellu-

lares dans lesquelles se cotoient des cellules normales et transformées, le motif des cellules mutées ayant été défini par le motif d'illumination.

Caractérisation du système OptoSrc

Le système OptoSrc a été validé par *western blot*, en montrant que la relocalisation de CRY2-Src à la membrane suffisait à augmenter la phosphorylation de p130 Cas, un substrat typique de Src [209]. Cet effet est bloqué par l'ajout d'un inhibiteur de Src, à savoir PP2 [133].

Nous avons ensuite vérifié que les cellules MDCK OptoSrc en culture formaient bien une monocouche épithéliale, et se comportaient comme des cellules MDCK "sauvages", ou wt (*wild-type*), en l'absence de lumière bleue. En revanche, lorsque ces cellules sont exposées à de la lumière bleue, elles présentent des caractéristiques typiques liées à l'activation de Src. On observe notamment l'apparition de réarrangements membranaires (*membrane ruffling*) dans les cellules en bordure de la monocouche, phénomène cohérent avec le rôle joué par Src dans le remodelage des sites d'adhésion [211]. Ces caractéristiques disparaissent en quelques secondes lorsque l'on cesse l'exposition à la lumière bleue. De plus, des expériences de blessures modèles (*wound healing* [123]) ont montré qu'une monocouche de cellules OptoSrc exposée à la lumière bleue migre plus rapidement, et de manière plus individuelle, qu'en l'absence de lumière bleue. Enfin, la présence de cellules *leaders*, habituellement observée au front de migration d'une monocouche de MDCK wt [123], n'a pas été observée pour les cellules MDCK OptoSrc illuminée avec de la lumière bleue.

Cellule OptoSrc isolée dans une monocouche de cellules wt

La stratégie la plus simple pour établir un contact entre des cellules MDCK wt et OptoSrc est de les mélanger puis de les illuminer. Pour cela, on réalise un mélange de cellules OptoSrc et wt dans une proportion 1:100, et on cultive ces cellules mélangées sur un substrat de manière à ce qu'elles forment une monocouche de cellules wt contenant quelques cellules OptoSrc isolées. Lorsque toute la monocouche est illuminée dans le bleu, seules les cellules OptoSrc sont sensibles au stimulus lumineux : on obtient ainsi des cellules transformées Src isolées dans un tissu wt.

Nous avons montré que les cellules OptoSrc isolées sont extrudées de la monocouche wt dans 46% des cas ($n = 54$), dans les 48 heures suivant le début de l'illumination (Figure B.5 (b)). En l'absence de lumière bleue, les cellules OptoSrc prolifèrent normalement dans la monocouche pendant au moins 48 heures, et ne sont extrudées que dans 3% des

cas ($n = 20$) (Figure B.5 (a)). Nos expériences préliminaires ont également montré que l'ajout d'un inhibiteur de Src, PP2 (à $20 \mu\text{M}$ dans du DMSO), diminue fortement le taux d'extrusion des cellules OptoSrc: seulement 21% d'extrusion, contre 73% dans la situation contrôle (ajout d'un volume équivalent de DMSO). En l'absence de lumière bleue, le taux d'extrusion des cellules OptoSrc avec du PP2 est similaire à celui avec du DMSO (15% et 17%, respectivement).

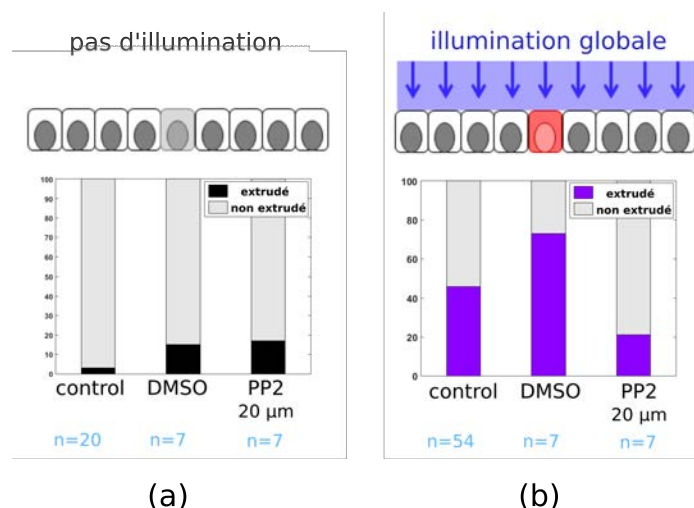


FIGURE B.5: **Extrusion de cellules MDCK OptoSrc isolées dans une monocouche de MDCK wt.** (a) En l'absence de lumière bleue, les cellules MDCK OptoSrc ne sont pas extrudées du tissu sain (3%). (b) Les cellules OptoSrc activées par la lumière bleue sont extrudées de la monocouche wt dans 46% des cas. L'ajout de PP2 (inhibiteur de Src) diminue fortement le nombre d'extrusion des cellules OptoSrc isolées (résultats préliminaires, $n = 7$).

Ces résultats sont en accord avec d'autres études basées sur des mélanges statistiques [116, 117]. Notamment, Kajita *et al.* contrôlent l'activité de Src dans des cellules par un changement de température, et montrent que des cellules isolées sur-exprimant Src sont extrudées d'une monocouche wt dans 80 % des cas ($n = 90$). Dans cette étude, l'utilisation de l'inhibiteur de Src PP2 à $20 \mu\text{M}$ réduit de moitié ce taux d'extrusion, ce qui est cohérent avec nos résultats.

Mise en place d'un montage optique pour contrôler le motif d'illumination

Au cours de cette thèse, nous avons établi le montage optique permettant de contrôler le motif d'illumination bleue sur les cellules. Celui-ci se base sur l'utilisation d'un DMD (*Digital Micromirror Device*): une matrice de micro-miroirs indépendants qui peuvent basculer en position "ON" ou "OFF" (Figure B.6). Chaque micro-miroir peut donc réfléchir, ou non, une lumière incidente. En contrôlant la position des micro-miroirs,

on contrôle donc le motif d'illumination qui sera envoyé sur l'échantillon placé dans le microscope.

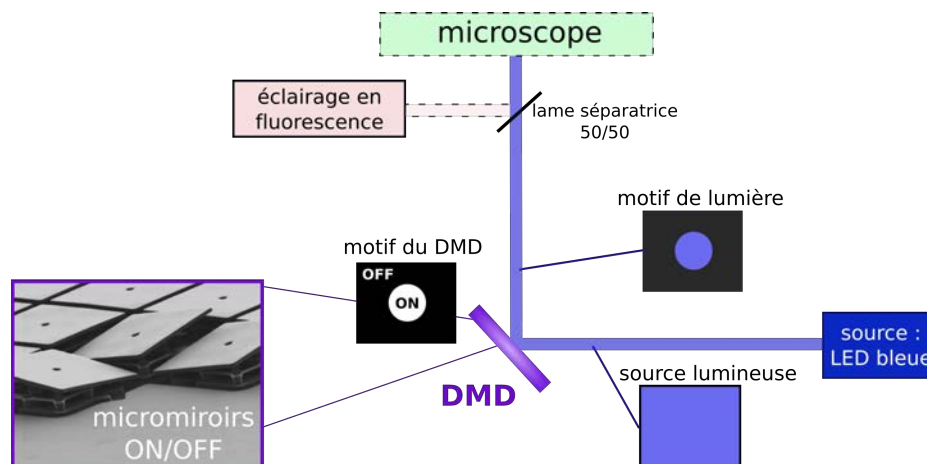


FIGURE B.6: **Contrôle du motif d'illumination à l'aide d'un DMD.** La lumière bleue venant de la source (LED) est réfléchi sur le DMD selon le motif des micro-miroirs en position "ON". Ce motif de lumière est ensuite envoyé vers l'échantillon placé dans le microscope. En parallèle, un éclairage en fluorescence classique peut être utilisé pour une illumination sans motif.

Suractivation localisée de Src dans une monocouche cellulaire

Une illumination ciblée a ensuite été utilisée pour sélectionner les cellules à transformer dans un tapis de cellules MDCK OptoSrc. Cette approche offre un meilleur contrôle et une meilleure reproductibilité de la situation initiale. La stratégie la plus directe pour utiliser ce système est d'illuminer un groupe de cellules au sein de la monocouche, et nous avons opté pour une géométrie circulaire.

∞ Un groupe de cellules OptoSrc photoactivées subit une extrusion collective

Nous avons choisi les conditions standards d'illumination suivantes : disque de diamètre $70 \mu\text{m}$, soumis à des impulsions lumineuses de durée 200 ms, espacées de $\Delta t = 5$ minutes. La densité initiale de la monocouche est d'environ 2000 cellules/ mm^2 . Lorsqu'un groupe de cellules OptoSrc est soumis à ces conditions d'illumination au sein d'une monocouche, nous observons une extrusion collective des cellules éclairées (Figure B.7).

Nous décrivons ce phénomène comme une "extrusion collective" du groupe de cellules OptoSrc activées hors de la monocouche cellulaire pour plusieurs raisons. Premièrement,

cette extrusion a lieu de manière simultanée dans le groupe de cellules OptoSrc éclairées. Ensuite, les images en 3D présentées par la suite (Figure B.8) révèlent, à l'endroit de la zone d'illumination, un agrégat de cellules cohésives attaché à la monocouche. D'autre part, cette structure tri-dimensionnelle résiste aux flux induits lors de rinçages successifs. Enfin, l'ajout d'EGTA, qui perturbe les jonctions intercellulaires, empêche la formation de cet agrégat. Ces différents arguments montrent que les cellules qui constituent l'agrégat sont bien cohésives entre elles et solidaires de la monocouche, d'où notre dénomination d'«extrusion collective».

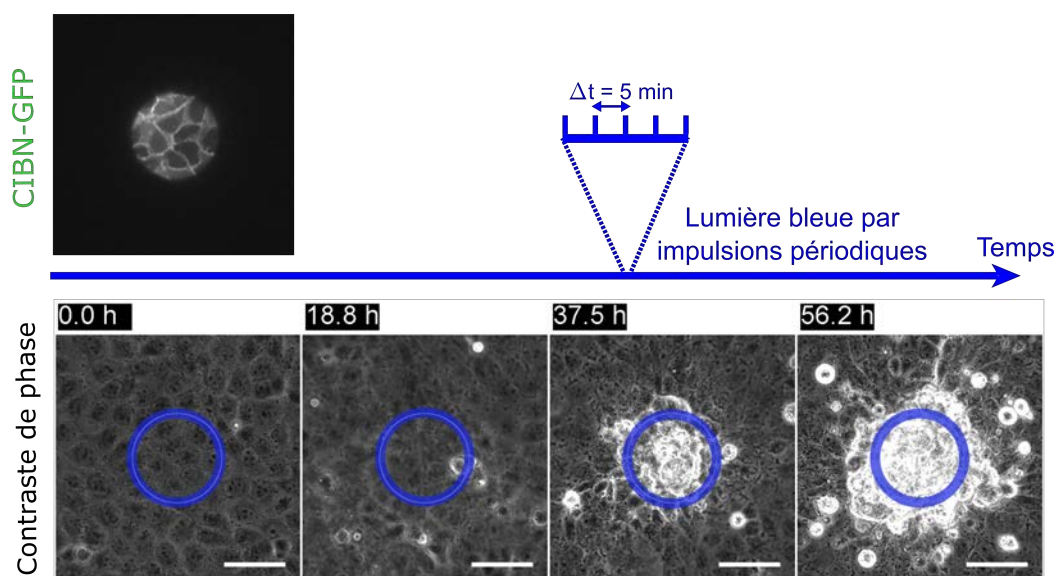


FIGURE B.7: **Extrusion collective d'un groupe de cellules OptoSrc illuminées au sein d'une monocouche de cellules OptoSrc.** Haut : Signal CIBN-GFP montrant le motif d'illumination (488 nm) : disque de diamètre 70 μm . L'intervalle entre deux impulsions de lumière bleue est fixé à 5 minutes. Bas : Images en contraste de phase de la monocouche OptoSrc. Le cercle bleu représente le contour de la région exposée à la lumière bleue. Les cellules extrudées apparaissent en blanc (car hors du plan focal). $t = 0$ indique le début de la stimulation. Barre d'échelle : 50 μm

∞ L'extrusion collective nécessite l'activation de Src à la membrane

Nous avons vérifié que les mêmes conditions d'illumination n'induisent pas d'extrusion collective dans une monocouche de cellules MDCK wt. Ainsi, le phénomène observé n'est pas dû à l'effet de la lumière bleue sur les cellules.

De plus, l'extrusion collective provoquée par l'illumination d'un groupe de MDCK OptoSrc au sein d'une monocouche n'a pas lieu en présence d'inhibiteurs de Src. Deux inhibiteurs de Src ont été utilisés : PP2 (Sigma, 10 μM) et Src inhibitor n°5 (Biaffin GmbH, 10

nM), et aucune extrusion collective n'a été observée dans ce cas ($n = 10$ pour chaque condition). Nous avons également testé deux constructions d'OptoSrc dépourvues respectivement de CIBN ou de CIBN-CAAX-GFP, dans lesquelles le fragment OptoSrc ne peut pas être recruté à la membrane sous l'effet de la lumière bleue. Ces deux constructions n'ont pas donné lieu au bourgeonnement d'un groupe de cellules exposé à la lumière bleue ($n = 36$ et $n = 10$, respectivement). Ces données suggèrent que Src doit être localement sur-activé à la membrane pour permettre la formation de l'extrusion collective.

∞ Visualisation 3D du groupe de cellules extrudées

Des images 3D des cellules extrudées ont été obtenues en microscopie confocale (Figure B.8). Ces images révèlent que le groupe de cellules extrudées prend la forme d'un dôme, ou sphéroïde, surplombant la monocouche cellulaire. On observe que le tapis de cellules est intact sous l'agrégat de cellules extrudées, qui semblent s'empiler de manière aléatoire.

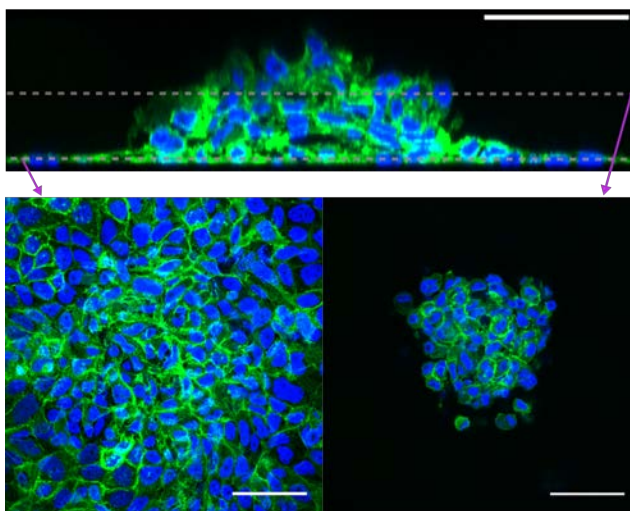


FIGURE B.8: **Visualisation 3D d'un groupe de cellules OptoSrc collectivement extrudées.** Images confocales de la structure 3D après 60 h dans les conditions standards d'illumination bleue. Marquage des noyaux en bleu (Hoechst) et des membranes en vert (CIBN-GFP). **Haut** Vue latérale. **Bas** Vue du dessus du tapis de cellules sous le sphéroïde, au niveau du substrat en verre (gauche), et 25 μm plus haut (droite). Barre d'échelle : 50 μm .

∞ Définition d'un “temps d'apparition” de l'agrégat de cellules extrudées

Nous avons défini un temps d'apparition T_{ap} pour cette structure tri-dimensionnelle. Celui-ci est déterminé en visualisant les films (temps entre 2 acquisitions en contraste de

phase : 15 minutes), car il est difficile de mettre en place des analyses automatisées sur des images de phase. Le temps d'apparition a été défini comme le moment où l'on observe les premières cellules qui bourgeonnent collectivement hors de la monocouche. Dans les conditions standards d'illumination, ce temps d'apparition a été mesuré en moyenne à 21 ± 10 h (SEM, $n = 130$).

∞ L'extrusion collective est précédée d'un flux convergent des cellules vers la région d'illumination

L'analyse en vélocimétrie par image de particules (PIV pour *Particle Image Velocimetry*) sur les images de phase de la monocouche cellulaire montre que les cellules hors de la région d'illumination migrent collectivement vers la région éclairée. Les champs de vitesse présentés en Figure B.9, obtenus par moyennage sur 20 h, illustrent ce flux convergent de cellules vers le motif d'illumination. Cette observation suggère que la monocouche cellulaire autour de l'aire illuminée sert de réservoir pour alimenter l'extrusion collective.

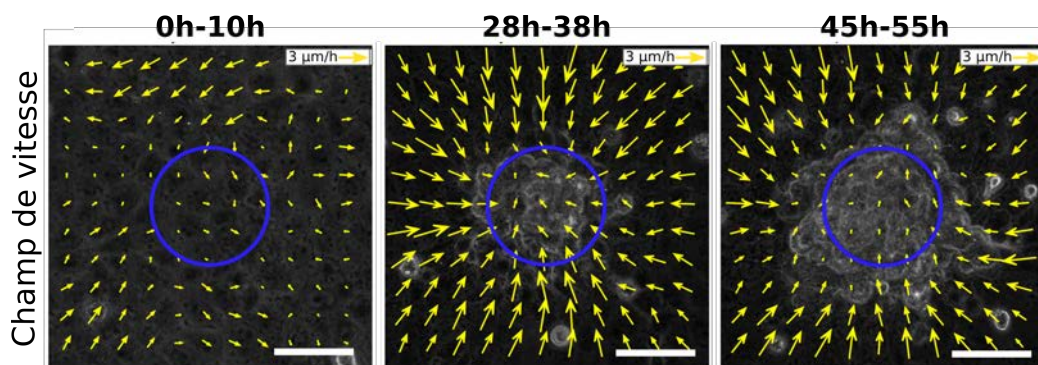


FIGURE B.9: **Flux convergent de cellules vers la zone d'illumination.** Le champ des vitesses (flèches jaunes, obtenu par PIV) est moyenné sur 20h. Le cercle bleu délimite la zone d'illumination. Sur cet exemple, T_{ap} a été mesuré à 22 h. Barre d'échelle : 50 μm .

∞ Contrôle spatial de l'extrusion collective

Nous avons ensuite varié l'aire du disque d'illumination bleue. Nous avons montré que la taille de la région illuminée influence directement la surface sous-jacente de la structure tridimensionnelle extrudée, sans modifier son temps d'apparition (Figure B.10-(a) et (b)).

∞ Contrôle temporel de l'extrusion collective

Grâce à la réversibilité naturelle du système CRY2/CIBN en l'absence de lumière bleue,

il est possible d'ajuster le niveau d'activation de Src dans les cellules MDCK OptoSrc en variant la fréquence d'illumination ($1/\Delta t$). En effet, plus les impulsions lumineuses sont espacées, plus le module CRY2-Src est libre de diffuser dans le cytoplasme, moins la kinase est susceptible de phosphoryler ses substrats à la membrane. Dans les conditions usuelles d'illumination, l'intervalle Δt entre deux impulsions de lumière bleue a été fixé à 5 minutes. Nous avons fait varier cet intervalle Δt pour moduler le niveau d'activation de Src. Nous avons ainsi montré qu'en variant le niveau d'activation de Src, la dynamique de l'extrusion collective était modifiée. Plus la fréquence d'illumination est haute (donc plus le niveau d'activation de Src est élevé), plus la structure tridimensionnelle se forme rapidement. En outre, la probabilité P_{bud} de former un bourgeon (définie comme le nombre d'extrusions collectives observées sur le nombre total d'expériences), décroît pour un Δt croissant (Figure B.10-(c) et (d)).

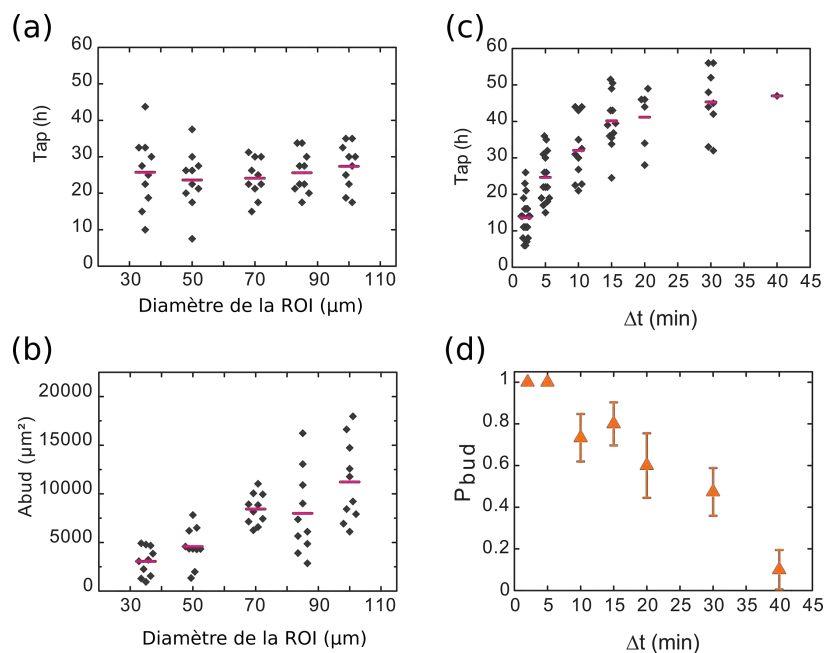


FIGURE B.10: **Contrôle spatiotemporel de l'extrusion collective** (a) Le temps d'apparition T_{ap} de l'extrusion collective ne varie pas en fonction de la taille de la région illuminée (ROI pour *Region Of Illumination*). (b) La taille de la ROI influence l'aire de l'agrégat de cellules extrudées A_{bud} . (c)-(d) L'intervalle Δt entre deux impulsions lumineuses permet de contrôler le temps d'apparition, ainsi que la probabilité P_{bud} de formation de cette structure.

∞ Effet de la contractilité sur le phénomène d'extrusion collective

Pour estimer le rôle joué par la contractilité des cellules sur le phénomène d'extrusion collective, les cellules ont été traitées avec deux drogues différentes : Calyculin A et

Y27632. L'ajout de Calyculin A, un inhibiteur des phosphatases connu pour augmenter la contractilité cellulaire, accélère le processus d'extrusion collective et augmente sa probabilité P_{bud} . À l'inverse, l'utilisation de Y27632, un inhibiteur de ROCK qui diminue la contractilité cellulaire, retarde sa formation et diminue P_{bud} . Ces résultats suggèrent que la contractilité cellulaire joue un rôle dans la formation de la structure tridimensionnelle.

∞ L'extrusion collective est réversible

Nous avons ensuite souhaité savoir si cette extrusion collective était réversible. En d'autres termes, ce phénomène nécessite-t-il une sur-activation permanente de l'oncogène Src dans les cellules ? Ou existe-t-il, au contraire, un seuil de sur-activation de Src au-delà duquel on induit une transformation irréversible des cellules ? Pour répondre à cette question, l'exposition lumineuse a été stoppée après 36 heures d'exposition dans les conditions standards d'illumination. Dans cette expérience, l'extrusion collective s'est arrêtée dès l'arrêt de la lumière bleue. La majorité des cellules a alors réintégré le tapis de cellules sous-jacent, les autres se sont détachées de la monocouche (Figure B.11). Il ne s'agit encore que de résultats préliminaires, mais ces observations montrent que le recrutement continu de Src à la membrane est nécessaire pour maintenir la cohésion entre les différentes cellules de l'agrégat, et sa stabilité au-dessus de la monocouche. Cela prouve également que les cellules constituant le bourgeon sont bien vivantes, puisqu'elles sont capables de réintégrer le tapis de cellules.

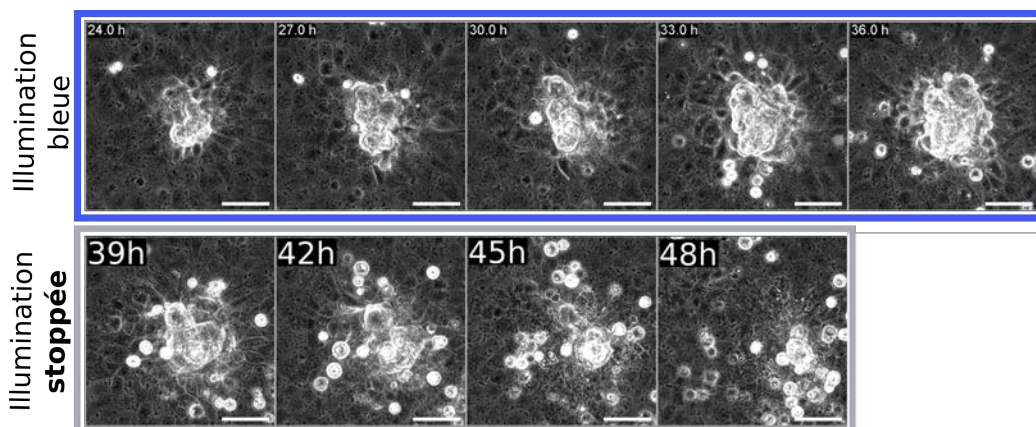


FIGURE B.11: **L'extrusion collective est réversible.** Images en contraste de phase. Le cycle d'illumination comprend une phase de 36 h dans les conditions standards d'illumination, suivi d'un arrêt de la lumière bleue. La plupart des cellules de l'agrégat réintègrent alors la monocouche. Barre d'échelle : 50 μm .

∞ Le comportement des cellules OptoSrc sur-activées dépend du contexte

Dans la mesure où l'activation d'une monocouche entière de cellules MDCK OptoSrc n'a pas donné lieu au phénomène d'extrusion collective, nous avons fait l'hypothèse que celle-ci nécessitait la présence d'une frontière entre deux types cellulaires. Nous avons ainsi étudié deux cas de figure dans lesquels le groupe de cellules OptoSrc sur-activées n'était pas entouré d'une monocouche de cellules non-activées.

Dans un premier temps, nous avons déposé des cellules à basse densité, afin d'obtenir des îlots de cellules OptoSrc entourés de substrat libre, et les avons soumis à un stimulus de lumière bleue. Les cellules OptoSrc ainsi activées ont immédiatement commencé à s'étaler et à migrer vers l'extérieur du groupe (Figure B.12 (a)). Après quelques heures, les cellules étaient complètement dispersées. Cette observation diffère du comportement des cellules MDCK normales, qui sont très cohésives et ont tendance à rester solidaires. En revanche, cette individualisation et cette augmentation de la migration rappellent le comportement de cellules mésenchymateuses : ceci suggère que la suractivation de Src induit une transition épithéliale-mésenchymateuse, ou EMT (*Epithelial-to-Mesenchymal Transition*), des cellules OptoSrc.

Pour tester la nécessité d'une interface entre les cellules OptoSrc activées et non activées, les cellules ont été confinées dans un motif adhésif circulaire et illuminées avec de la lumière bleue sur tout le motif adhésif. Nous avons observé peu d'extrusion du groupe de cellules photoactivées dans ce cas (Figure B.12 (b)). La présence de cellules "normales" autour du groupe de cellules sur-exprimant Src semble nécessaire pour déclencher l'extrusion collective.

On en déduit que le comportement des cellules OptoSrc sur-activées dépend du contexte : la présence d'une monocouche de cellules normales autour d'elles semble être importante pour le phénomène d'extrusion collective.

∞ L'extrusion collective est associée à une transition épithéliale-mésenchymateuse

La Transition Epithéliale-Mésenchymateuse (EMT), est un processus selon lequel les cellules épithéliales perdent leurs caractéristiques épithéliales et deviennent mésenchymales. L'activation de Src est connue pour induire une EMT [71, 227]. Nous avons souhaité savoir si cette transition était impliquée dans le phénomène d'extrusion collective observé avec notre système. Pour ce faire, nous avons utilisé la technique d'immunofluorescence sur cellules fixées. Nous nous sommes concentrés sur deux marqueurs de l'EMT : l'E-cadhérine

et la vimentine, dont la diminution (resp. l'augmentation) de l'expression dans les cellules témoigne d'une EMT. Nous avons effectivement observé une diminution de la quantité d'E-cadhérine aux jonctions inter-cellulaires des cellules dans l'agrégat de cellules extrudées, ainsi que l'apparition de la vimentine dans les cellules de la couche supérieure de la structure tri-dimensionnelle. Ces résultats suggèrent que les cellules OptoSrc photo-activées subissent une EMT partielle, qui pourrait être liée à l'extrusion collective.

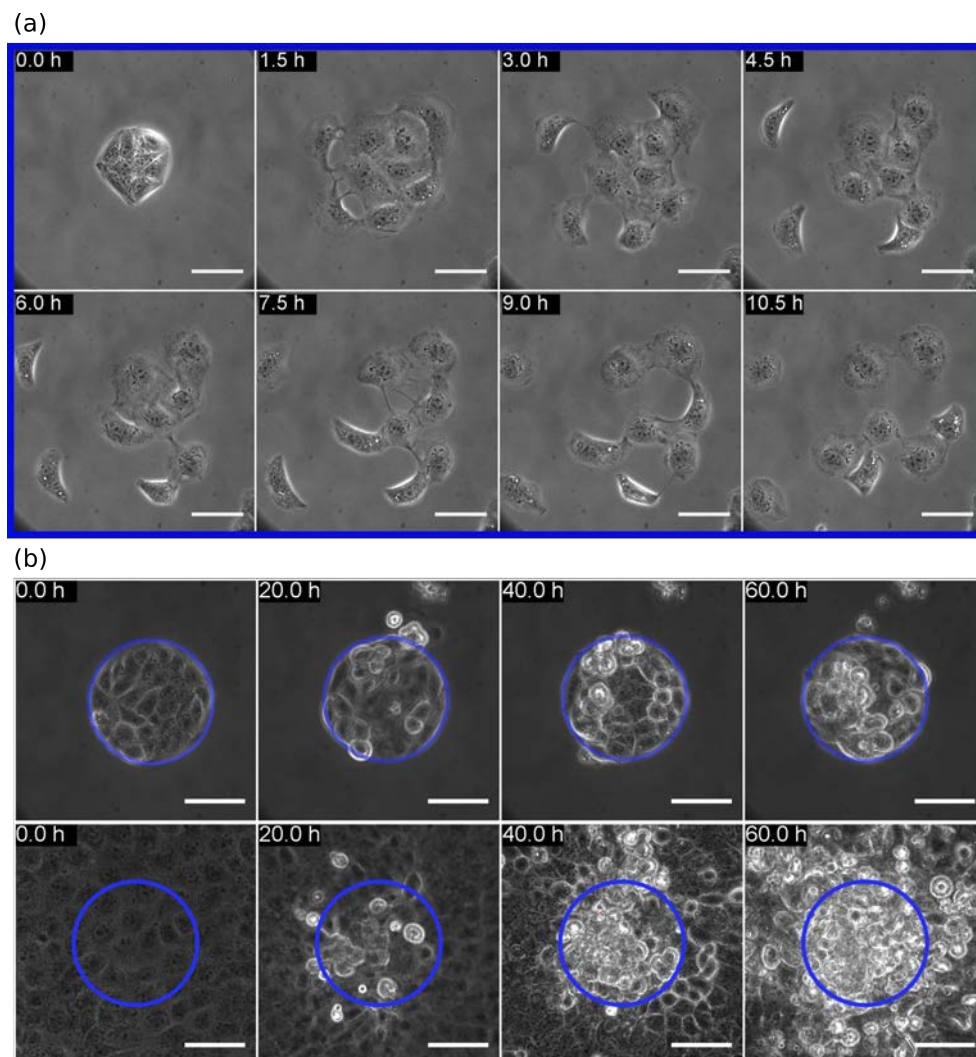


FIGURE B.12: Une frontière entre deux niveaux d'activation de Src est nécessaire pour induire l'extrusion collective. (a): un groupe de cellules OptoSrc isolé s'étale et migre individuellement sous l'effet de la lumière bleue. **(b) Haut :** cellules OptoSrc confinées dans un motif adhésif circulaire de diamètre $100 \mu\text{m}$. **Bas :** Un groupe de cellules OptoSrc dans les mêmes conditions d'illumination (zone éclairée de diamètre $100 \mu\text{m}$) s'extrude collectivement lorsqu'il est entouré de cellules non-éclairées. Barres d'échelle : $50 \mu\text{m}$.

Bibliography

- [1] C. Hogan, M. Kajita, K. Lawrenson, and Y. Fujita, “Interactions between normal and transformed epithelial cells: Their contributions to tumourigenesis,” *The International Journal of Biochemistry & Cell Biology*, vol. 43, pp. 496–503, apr 2011.
- [2] L. Wagstaff, G. Kolahgar, and E. Piddini, “Competitive cell interactions in cancer: A cellular tug of war,” *Trends in Cell Biology*, vol. 23, no. 4, pp. 160–167, 2013.
- [3] L. Blanchoin, R. Boujemaa-Paterski, C. Sykes, and J. Plastino, “Actin Dynamics, Architecture, and Mechanics in Cell Motility,” *Physiological Reviews*, vol. 94, pp. 235–263, jan 2014.
- [4] H. Herrmann, H. Bär, L. Kreplak, S. V. Strelkov, and U. Aebi, “Intermediate filaments: from cell architecture to nanomechanics,” *Molecular Cell Biology*, vol. 8, no. 7, pp. 562–73, 2007.
- [5] A. Akhmanova and M. O. Steinmetz, “Control of microtubule organization and dynamics: two ends in the limelight,” *Nature Reviews Molecular Cell Biology*, vol. 16, no. 12, pp. 711–726, 2015.
- [6] B. Alberts, D. Bray, K. Hopkin, A. Johnson, J. Lewis, R. Martin, K. Roberts, and P. Walter, *Essential Cell Biology*. Garland Science, 2014.
- [7] K. T. Patton and G. A. Thibodeau, *Anatomy and Physiology*. 6th ed., 2012.
- [8] C. Frantz, K. M. Stewart, and V. M. Weaver, “The extracellular matrix at a glance,” *Journal of cell science*, vol. 123, pp. 4195–4200, 2010.
- [9] P. Satir, L. B. Pedersen, and S. T. Christensen, “The primary cilium at a glance,” *Journal of Cell Science*, vol. 123, pp. 499–503, feb 2010.
- [10] N. Spassky and A. Meunier, “The development and functions of multiciliated epithelia,” *Nature reviews. Molecular cell biology*, vol. 18, no. 7, pp. 423–436, 2017.
- [11] V. S. LeBleu, B. MacDonald, and R. Kalluri, “Structure and Function of Basement Membranes,” *Experimental Biology and Medicine*, vol. 232, pp. 1121–1129, oct 2007.
- [12] E. Rodriguez-Boulan and I. G. Macara, “Organization and execution of the epithelial polarity programme,” *Nature Reviews Molecular Cell Biology*, vol. 15, no. 4, pp. 225–242, 2014.
- [13] M. Simons and M. Mlodzik, “Planar Cell Polarity Signaling: From Fly Development to Human Disease,” *Annual Review of Genetics*, vol. 42, pp. 517–540, dec 2008.
- [14] M. Lee and V. Vasioukhin, “Cell polarity and cancer—cell and tissue polarity as a non-canonical tumor suppressor,” *Journal of cell science*, vol. 121, no. Pt 8, pp. 1141–50, 2008.
- [15] C. Royer and X. Lu, “Epithelial cell polarity: a major gatekeeper against cancer?,” *Cell Death and Differentiation*, vol. 18, pp. 1470–1477, sep 2011.
- [16] C. Yoshida and M. Takeichi, “Teratocarcinoma cell adhesion: Identification of a cell-surface protein involved in calcium-dependent cell aggregation,” *Cell*, vol. 28, no. 2, pp. 217–224, 1982.
- [17] F. Nollet, P. Kools, and F. van Roy, “Phylogenetic analysis of the cadherin superfamily allows identification of six major subfamilies besides several solitary members,” *Journal of Molecular Biology*, vol. 299, no. 3, pp. 551–572, 2000.

- [18] J. L. Maître and C. P. Heisenberg, “Three functions of cadherins in cell adhesion,” *Current Biology*, vol. 23, no. 14, pp. 626–633, 2013.
- [19] E. Tabdanov, N. Borghi, F. Brochard-Wyart, S. Dufour, and J. P. Thiery, “Role of E-cadherin in membrane-cortex interaction probed by nanotube extrusion,” *Biophysical Journal*, vol. 96, no. 6, pp. 2457–2465, 2009.
- [20] N. Borghi, M. Sorokina, O. G. Shcherbakova, W. I. Weis, B. L. Pruitt, W. J. Nelson, and A. R. Dunn, “E-cadherin is under constitutive actomyosin-generated tension that is increased at cell-cell contacts upon externally applied stretch,” *Proceedings of the National Academy of Sciences*, vol. 109, pp. 12568–12573, jul 2012.
- [21] T. M. Rowlands, J. M. Symonds, R. Farookhi, and O. W. Blaschuk, “Cadherins: crucial regulators of structure and function in reproductive tissues.,” *Reviews of reproduction.*, vol. 5, pp. 53–61, jan 2000.
- [22] J. M. Halbleib and W. J. Nelson, “Cadherins in development: Cell adhesion, sorting, and tissue morphogenesis,” *Genes and Development*, vol. 20, no. 23, pp. 3199–3214, 2006.
- [23] F. Van Roy and G. Berx, “The cell-cell adhesion molecule E-cadherin,” *Cellular and Molecular Life Sciences*, vol. 65, no. 23, pp. 3756–3788, 2008.
- [24] B. Lodish, *Molecular Cell Biology*. Macmillian Learning, 8 ed., 2016.
- [25] V. Vasioukhin and E. Fuchs, “Actin dynamics and cell-cell adhesion in epithelia.,” *Current opinion in cell biology*, vol. 13, pp. 76–84, feb 2001.
- [26] B. Geiger, J. P. Spatz, and A. Bershadsky, “Environmental sensing through focal adhesions.,” *Nature reviews. Molecular cell biology*, vol. 10, no. 1, pp. 21–33, 2009.
- [27] P. Friedl and D. Gilmour, “Collective cell migration in morphogenesis, regeneration and cancer.,” *Nature reviews. Molecular cell biology*, vol. 10, pp. 445–57, jul 2009.
- [28] E. W. Esch, A. Bahinski, and D. Huh, “Organs-on-chips at the frontiers of drug discovery,” *Nature Reviews Drug Discovery*, vol. 14, no. 4, pp. 248–260, 2015.
- [29] H. P. Fischer, “Mathematical modeling of complex biological systems: from parts lists to understanding systems behavior.,” *Alcohol research & health : the journal of the National Institute on Alcohol Abuse and Alcoholism*, vol. 31, no. 1, pp. 49–59, 2008.
- [30] C. R. Gaush, W. L. Hard, and T. F. Smith, “Characterization of an Established Line of Canine Kidney Cells (MDCK).,” *Experimental Biology and Medicine*, vol. 122, pp. 931–935, jul 1966.
- [31] J. D. Dukes, P. Whitley, and A. D. Chalmers, “The MDCK variety pack: choosing the right strain,” *BMC Cell Biology*, vol. 12, p. 43, oct 2011.
- [32] M. Abercrombie and J. E. Heaysman, “Observations on the social behaviour of cells in tissue culture,” *Experimental Cell Research*, vol. 5, pp. 111–131, jan 1953.
- [33] C. Carmona-Fontaine, H. K. Matthews, S. Kuriyama, M. Moreno, G. A. Dunn, M. Parsons, C. D. Stern, and R. Mayor, “Contact inhibition of locomotion in vivo controls neural crest directional migration,” *Nature*, vol. 456, no. 7224, pp. 957–961, 2008.
- [34] R. Mayor and C. Carmona-Fontaine, “Keeping in touch with contact inhibition of locomotion,” *Trends in Cell Biology*, vol. 20, no. 6, pp. 319–328, 2010.
- [35] L. Petitjean, M. Reffay, E. Grasland-Mongrain, M. Poujade, B. Ladoux, A. Buguin, and P. Silberzan, “Velocity fields in a collectively migrating epithelium.,” *Biophysical journal*, vol. 98, pp. 1790–800, may 2010.
- [36] I. G. Macara, R. Guyer, G. Richardson, Y. Huo, and S. M. Ahmed, “Epithelial Homeostasis,” *Current Biology*, vol. 24, pp. R815–R825, sep 2014.

- [37] M. Stoker and H. Rubin, "Density dependent inhibition of cell growth in culture," *Nature*, vol. 215, pp. 171–172, 1967.
- [38] H. Katoh and Y. Fujita, "Epithelial homeostasis: elimination by live cell extrusion.," *Current biology : CB*, vol. 22, pp. R453–5, jun 2012.
- [39] M. Abercrombie, "Contact inhibition and malignancy," *Nature*, vol. 281, pp. 259–262, sep 1979.
- [40] D. Hanahan and R. A. Weinberg, "Hallmarks of cancer: The next generation," *Cell*, vol. 144, no. 5, pp. 646–674, 2011.
- [41] Y. Takai, J. Miyoshi, W. Ikeda, and H. Ogita, "Nectins and nectin-like molecules: roles in cell adhesion, polarization, movement, and proliferation.," *Nature Reviews Molecular Cell Biology*, vol. 9, pp. 603–15, may 2008.
- [42] Cancer Research UK, "Types of cancer."
- [43] D. Hanahan and R. A. Weinberg, "The hallmarks of cancer.," *Cell*, vol. 100, no. 1, pp. 57–70, 2000.
- [44] J.-S. Shin, A. Hong, M. J. Solomon, and C. Soon Lee, "The role of telomeres and telomerase in the pathology of human cancer and aging," *Pathology*, vol. 38, no. 2, pp. 103–113, 2006.
- [45] B. Vogelstein and K. W. Kinzler, "The multistep nature of cancer.," *Trends in genetics : TIG*, vol. 9, pp. 138–41, apr 1993.
- [46] N. Rhind and P. Russell, "Signaling Pathways that Regulate Cell Division," *Cold Spring Harbor Perspectives in Biology*, vol. 4, no. 10, pp. a005942–a005942, 2012.
- [47] R. P. Bissonnette, F. Echeverri, A. Mahboubi, and D. R. Green, "Apoptotic cell death induced by c-myc is inhibited by bcl-2," *Nature*, vol. 359, no. 6395, pp. 552–554, 1992.
- [48] A. Fanidi, E. A. Harrington, and G. I. Evan, "Cooperative interaction between c-myc and bcl-2 proto-oncogenes," *Nature*, vol. 359, no. 6395, pp. 554–556, 1992.
- [49] Khan Academy, "Cancer and the cell cycle," *Under license CC BY-NC-SA 4.0*.
- [50] I. a. Prior, P. D. Lewis, and C. Mattos, "A Comprehensive Survey of Ras Mutations in Cancer," *Cancer Research*, vol. 72, pp. 2457–2467, may 2012.
- [51] N. Rivlin, R. Brosh, M. Oren, and V. Rotter, "Mutations in the p53 Tumor Suppressor Gene: Important Milestones at the Various Steps of Tumorigenesis," *Genes & Cancer*, vol. 2, no. 4, pp. 466–474, 2011.
- [52] P. Rous, "Transmission of A Malignant New Growth By Means of A Cell-Free Filtrate," *Journal of the American Medical Association*, jan 1911.
- [53] G. J. Svet-Moldavsky, "Development of multiple cysts and of hemorrhagic affections of internal organs in albino rats treated during the embryonic or newborn period with Rous sarcoma virus.," *Nature*, vol. 7;180(4597), pp. 1299–1300, 1957.
- [54] C. G. Ahlström and N. Forsby, "Sarcomas in halsters after injection with Rous chicken tumour material," *The Journal of Experimental Medicine*, vol. 4, pp. 839–852, feb 1962.
- [55] R. A. Weiss and P. K. Vogt, "100 years of Rous sarcoma virus," *The Journal of Experimental Medicine*, vol. 208, no. 12, pp. 2351–2355, 2011.
- [56] K. Toyoshima and P. K. Vogt, "Temperature sensitive mutants of an avian sarcoma virus," *Virology*, vol. 39, pp. 930–931, dec 1969.
- [57] G. S. Martin, "Rous Sarcoma Virus: a Function required for the Maintenance of the Transformed State," *Nature*, 1970.
- [58] D. Stehelin, H. E. Varmus, J. M. Bishop, and P. K. Vogt, "DNA related to the transforming gene(s) of avian sarcoma viruses is present in normal avian DNA," *Nature*, vol. 260, pp. 170–173, mar 1976.

- [59] R. B. Irby and T. J. Yeatman, "Role of Src expression and activation in human cancer," *Oncogene*, vol. 19, pp. 5636–5642, nov 2000.
- [60] T. J. Yeatman, "A renaissance for SRC," *Nature Reviews Cancer*, vol. 4, pp. 470–480, jun 2004.
- [61] E. Ingley, "Src family kinases: Regulation of their activities, levels and identification of new pathways," *Biochimica et Biophysica Acta (BBA) - Proteins and Proteomics*, vol. 1784, pp. 56–65, jan 2008.
- [62] M. T. Brown and J. A. Cooper, "Regulation, substrates and functions of src," *Biochimica et Biophysica Acta - Reviews on Cancer*, vol. 1287, no. 2-3, pp. 121–149, 1996.
- [63] T. E. Kmiecik and D. Shalloway, "Activation and suppression of pp60c-src transforming ability by mutation of its primary sites of tyrosine phosphorylation," *Cell*, vol. 49, no. 1, pp. 65–73, 1987.
- [64] C. A. Cartwright, W. Eckhart, S. Simon, and P. L. Kaplan, "Cell transformation by pp60c-src mutated in the carboxy-terminal regulatory domain," *Cell*, vol. 49, no. 1, pp. 83–91, 1987.
- [65] H. Piwnica-Worms, K. B. Saunders, T. M. Roberts, A. E. Smith, and S. H. Cheng, "Tyrosine phosphorylation regulates the biochemical and biological properties of pp60c-src," *Cell*, vol. 49, no. 1, pp. 75–82, 1987.
- [66] G. S. Martin, "The hunting of the Src.," *Nature reviews. Molecular cell biology*, vol. 2, no. 6, pp. 467–475, 2001.
- [67] M. Hamaguchi, N. Matsuyoshi, Y. Ohnishi, B. Gotoh, M. Takeichi, and Y. Nagai, "p60v-src causes tyrosine phosphorylation and inactivation of the N-cadherin-catenin cell adhesion system.," *The EMBO journal*, vol. 12, no. 1, pp. 307–14, 1993.
- [68] W. Mao, R. B. Irby, D. Coppola, L. Fu, M. Wloch, J. Turner, H. Yu, R. Garcia, R. Jove, and T. J. Yeatman, "Activation of c-Src by receptor tyrosine kinases in human colon cancer cells with high metastatic potential," *Oncogene*, vol. 15, no. 25, pp. 3083–3090, 1997.
- [69] O. Destaing, A. Sanjay, C. Itzstein, W. C. Horne, D. Toomre, P. De Camilli, and R. Baron, "The Tyrosine Kinase Activity of c-Src Regulates Actin Dynamics and Organization of Podosomes in Osteoclasts," *Molecular Biology of the Cell*, vol. 19, pp. 394–404, jan 2008.
- [70] R. B. Irby, W. Mao, D. Coppola, J. Kang, J. M. Loubeau, W. Trudeau, R. Karl, D. J. Fujita, R. Jove, and T. J. Yeatman, "Activating SRC mutation in a subset of advanced human colon cancers.," *Nature genetics*, vol. 21, no. 2, pp. 187–90, 1999.
- [71] J. Behrens, "Loss of epithelial differentiation and gain of invasiveness correlates with tyrosine phosphorylation of the E-cadherin/beta-catenin complex in cells transformed with a temperature-sensitive v-SRC gene," *The Journal of Cell Biology*, vol. 120, pp. 757–766, feb 1993.
- [72] M. C. Frame, "Src in cancer: Deregulation and consequences for cell behaviour," *Biochimica et Biophysica Acta - Reviews on Cancer*, vol. 1602, no. 2, pp. 114–130, 2002.
- [73] J. J. Harvey, "An Unidentified Virus which causes the Rapid Production of Tumours in Mice," *Nature*, vol. 204, no. 4963, pp. 1104–1105, 1964.
- [74] W. H. Kirsten and L. A. Mayer, "Morphologic responses to a murine erythroblastosis virus.," *Journal of the National Cancer Institute*, vol. 39, pp. 311–335, aug 1967.
- [75] C. Shih, L. C. Padhy, M. Murray, and R. a. Weinberg, "Transforming genes of carcinomas and neuroblastomas introduced into mouse fibroblasts.," *Nature*, vol. 290, pp. 261–264, 1981.
- [76] M. Perucho, M. Goldfarb, K. Shimizu, and M. Wigler, "Human-Tumor-Derived Common and Different Cell Lines Contain Transforming Genes," vol. 27, no. December, pp. 467–476, 1981.
- [77] S. Pulciani, E. Santos, a. V. Lauver, L. K. Long, K. C. Robbins, and M. Barbacid, "Oncogenes in human tumor cell lines: molecular cloning of a transforming gene from human bladder carcinoma cells.," *Proceedings of the National Academy of Sciences of the United States of America*, vol. 79, no. 9, pp. 2845–2849, 1982.

- [78] C. D. Logsdon and W. Lu, "The significance of ras activity in pancreatic cancer initiation," *International Journal of Biological Sciences*, vol. 12, no. 3, pp. 338–346, 2016.
- [79] J. L. Bos, "ras oncogenes in human cancer: a review.," *Cancer research*, vol. 49, pp. 4682–9, sep 1989.
- [80] A. G. Gilman, "G Proteins: Transducers of Receptor-Generated Signals," *Annual Review of Biochemistry*, vol. 56, pp. 615–649, jun 1987.
- [81] F. McCormick, "Ras biology in atomic detail," *Nature Structural & Molecular Biology*, vol. 3, pp. 653–655, aug 1996.
- [82] J. Downward, "Ras signalling and apoptosis," *Current Opinion in Genetics & Development*, vol. 8, pp. 49–54, feb 1998.
- [83] D. P. Tabassum and K. Polyak, "Tumorigenesis: it takes a village," *Nature Reviews Cancer*, vol. 15, pp. 473–483, jul 2015.
- [84] V. Ayllón and a. Rebollo, "Ras-induced cellular events (review).," *Molecular membrane biology*, vol. 17, no. 2, pp. 65–73, 2000.
- [85] M. S. Steinberg, "Adhesion in development: an historical overview.," *Developmental biology*, vol. 180, pp. 377–88, dec 1996.
- [86] P. L. Townes and J. Holtfreter, "Directed movements and selective adhesion of embryonic amphibian cells," *Journal of Experimental Zoology*, vol. 128, pp. 53–120, feb 1955.
- [87] M. S. Steinberg, "Reconstruction of Tissues by Dissociated Cells," *Science*, vol. 141, no. 3579, pp. 401–408, 1963.
- [88] D. R. Garrod and M. S. Steinberg, "Tissue-specific Sorting-out in Two Dimensions in Relation to Contact Inhibition of Cell Movement," *Nature*, vol. 244, pp. 568–569, aug 1973.
- [89] E. Méhes, E. Mones, V. Németh, and T. Vicsek, "Collective motion of cells mediates segregation and pattern formation in co-cultures.," *PloS one*, vol. 7, p. e31711, jan 2012.
- [90] D. a. Beysens, G. Forgacs, and J. a. Glazier, "Cell sorting is analogous to phase ordering in fluids.," *Proceedings of the National Academy of Sciences of the United States of America*, vol. 97, pp. 9467–71, aug 2000.
- [91] D. Duguay, R. a. Foty, and M. S. Steinberg, "Cadherin-mediated cell adhesion and tissue segregation: qualitative and quantitative determinants.," *Developmental biology*, vol. 253, pp. 309–23, jan 2003.
- [92] S. Pawlizak, A. W. Fritsch, S. Grosser, D. Ahrens, T. Thalheim, and S. Riedel, "Testing the differential adhesion hypothesis across the epithelial mesenchymal transition," *New Journal of Physics*, vol. 17, no. 8, p. 83049, 2015.
- [93] M. S. Steinberg, "Does differential adhesion govern self-assembly processes in histogenesis? Equilibrium configurations and the emergence of a hierarchy among populations of embryonic cells," *Journal of Experimental Zoology*, vol. 173, pp. 395–433, apr 1970.
- [94] A. Nose, A. Nagafuchi, and M. Takeichi, "Expressed recombinant cadherins mediate cell sorting in model systems," *Cell*, vol. 54, no. 7, pp. 993–1001, 1988.
- [95] A. K. Harris, "Is cell sorting caused by differences in the work of intercellular adhesion? A critique of the steinberg hypothesis," *Journal of Theoretical Biology*, vol. 61, no. 2, pp. 267–285, 1976.
- [96] T. Lecuit and P.-F. Lenne, "Cell surface mechanics and the control of cell shape, tissue patterns and morphogenesis," *Nature Reviews Molecular Cell Biology*, vol. 8, pp. 633–644, aug 2007.
- [97] M. Krieg, Y. Arboleda-Estudillo, P.-H. Puech, J. Käfer, F. Graner, D. J. Müller, and C.-P. Heisenberg, "Tensile forces govern germ-layer organization in zebrafish," *Nature Cell Biology*, vol. 10, pp. 429–436, apr 2008.

- [98] J. Belmonte, G. Thomas, L. Brunnet, R. de Almeida, and H. Chaté, “Self-Propelled Particle Model for Cell-Sorting Phenomena,” *Physical Review Letters*, vol. 100, p. 248702, jun 2008.
- [99] X. Yang, M. L. Manning, and M. C. Marchetti, “Aggregation and segregation of confined active particles.,” *Soft matter*, vol. 10, no. 34, pp. 6477–6484, 2014.
- [100] G. Morata and P. Ripoll, “Minutes: Mutants of *Drosophila* autonomously affecting cell division rate,” *Developmental Biology*, vol. 42, pp. 211–221, feb 1975.
- [101] E. Moreno, K. Basler, and G. Morata, “Cells compete for Decapentaplegic survival factor to prevent apoptosis in *Drosophila* wing development,” *Nature*, vol. 416, no. 6882, pp. 755–759, 2002.
- [102] R. Levayer and E. Moreno, “Mechanisms of cell competition: themes and variations.,” *The Journal of cell biology*, vol. 200, pp. 689–98, mar 2013.
- [103] M. Amoyel and E. A. Bach, “Cell competition: how to eliminate your neighbours,” *Development*, vol. 141, no. 5, pp. 988–1000, 2014.
- [104] M. M. Merino, R. Levayer, and E. Moreno, “Survival of the Fittest: Essential Roles of Cell Competition in Development, Aging, and Cancer,” *Trends in Cell Biology*, vol. 26, pp. 776–788, oct 2016.
- [105] J. Menendez, A. Perez-Garijo, M. Calleja, and G. Morata, “A tumor-suppressing mechanism in *Drosophila* involving cell competition and the Hippo pathway,” *Proceedings of the National Academy of Sciences*, vol. 107, no. 33, pp. 14651–14656, 2010.
- [106] C. Rhiner, J. M. López-Gay, D. Soldini, S. Casas-Tinto, F. A. Martín, L. Lombardía, and E. Moreno, “Flower forms an extracellular code that reveals the fitness of a cell to its neighbors in *Drosophila*,” *Developmental Cell*, vol. 18, no. 6, pp. 985–998, 2010.
- [107] D. Hughes and D. I. Andersson, “Evolutionary consequences of drug resistance: shared principles across diverse targets and organisms,” *Nature Reviews Genetics*, vol. 16, no. 8, pp. 459–471, 2015.
- [108] A. Di Gregorio, S. Bowling, and T. A. Rodriguez, “Cell Competition and Its Role in the Regulation of Cell Fitness from Development to Cancer,” *Developmental Cell*, vol. 38, no. 6, pp. 621–634, 2016.
- [109] M. M. Merino, C. Rhiner, M. Portela, and E. Moreno, ““Fitness fingerprints” mediate physiological culling of unwanted neurons in *drosophila*,” *Current Biology*, vol. 23, no. 14, pp. 1300–1309, 2013.
- [110] J. M. Abrams, “Competition and compensation: Coupled to death in development and cancer,” *Cell*, vol. 110, no. 4, pp. 403–406, 2002.
- [111] E. Moreno and K. Basler, “dMyc transforms cells into super-competitors,” *Cell*, vol. 117, no. 1, pp. 117–129, 2004.
- [112] C. Rhiner and E. Moreno, “Super competition as a possible mechanism to pioneer precancerous fields,” *Carcinogenesis*, vol. 30, no. 5, pp. 723–728, 2009.
- [113] M. Basan, T. Risler, J.-F. Joanny, X. Sastre-Garau, and J. Prost, “Homeostatic competition drives tumor growth and metastasis nucleation.,” *HFSP journal*, vol. 3, pp. 265–72, aug 2009.
- [114] M. Kajita, K. Sugimura, A. Ohoka, J. Burden, H. Sukanuma, M. Ikegawa, T. Shimada, T. Kitamura, M. Shindoh, S. Ishikawa, S. Yamamoto, S. Saitoh, Y. Yako, R. Takahashi, T. Okajima, J. Kikuta, Y. Majima, M. Ishii, M. Tada, and Y. Fujita, “Filamin acts as a key regulator in epithelial defence against transformed cells,” *Nature Communications*, vol. 5, pp. 1–13, 2014.
- [115] S. Kon, K. Ishibashi, H. Katoh, S. Kitamoto, T. Shirai, S. Tanaka, M. Kajita, S. Ishikawa, H. Yamauchi, Y. Yako, T. Kamasaki, T. Matsumoto, H. Watanabe, R. Egami, A. Sasaki, A. Nishikawa, I. Kameda, T. Maruyama, R. Narumi, T. Morita, Y. Sasaki, R. Enoki, S. Honma, H. Imamura, M. Oshima, T. Soga, J.-i. Miyazaki, M. R. Duchon, J.-M. Nam, Y. Onodera, S. Yoshioka, J. Kikuta, M. Ishii, M. Imajo, E. Nishida, Y. Fujioka, Y. Ohba, T. Sato, and Y. Fujita, “Cell competition with normal epithelial cells promotes apical extrusion of transformed cells through metabolic changes,” *Nature Cell Biology*, vol. 19, no. 5, 2017.

- [116] C. Hogan, S. Dupré-Crochet, M. Norman, M. Kajita, C. Zimmermann, A. E. Pelling, E. Piddini, L. A. Baena-López, J.-P. Vincent, Y. Itoh, H. Hosoya, F. Pichaud, and Y. Fujita, “Characterization of the interface between normal and transformed epithelial cells,” *Nature cell biology*, vol. 11, pp. 460–7, apr 2009.
- [117] M. Kajita, C. Hogan, A. R. Harris, S. Dupré-Crochet, N. Itasaki, K. Kawakami, G. Charras, M. Tada, and Y. Fujita, “Interaction with surrounding normal epithelial cells influences signalling pathways and behaviour of Src-transformed cells,” *Journal of cell science*, vol. 123, pp. 171–80, jan 2010.
- [118] Y. Tamori, C. U. Bialucha, A. G. Tian, M. Kajita, Y. C. Huang, M. Norman, N. Harrison, J. Poulton, K. Ivanovitch, L. Disch, T. Liu, W. M. Deng, and Y. Fujita, “Involvement of Lgl and mahjong/VprBP in cell competition,” *PLoS Biology*, vol. 8, no. 7, 2010.
- [119] T. Bondar and R. Medzhitov, “p53-Mediated Hematopoietic Stem and Progenitor Cell Competition,” *Stem Cell*, vol. 6, no. 4, pp. 309–322, 2010.
- [120] S. S. Blair, “Genetic mosaic techniques for studying Drosophila development,” *Development*, vol. 130, no. 21, pp. 5065–5072, 2003.
- [121] M. Vidal, D. E. Larson, and R. L. Cagan, “Csk-deficient boundary cells are eliminated from normal drosophila epithelia by exclusion, migration, and apoptosis,” *Developmental Cell*, vol. 10, no. 1, pp. 33–44, 2006.
- [122] Y. Fujita, “Interface between normal and transformed epithelial cells: A road to a novel type of cancer prevention and treatment,” *Cancer Science*, vol. 102, pp. 1749–1755, oct 2011.
- [123] M. Poujade, E. Grasland-Mongrain, A. Hertzog, J. Jouanneau, P. Chavrier, B. Ladoux, A. Buguin, and P. Silberzan, “Collective migration of an epithelial monolayer in response to a model wound,” *Proceedings of the National Academy of Sciences of the United States of America*, vol. 104, pp. 15988–93, oct 2007.
- [124] S. Porazinski, J. de Navascués, Y. Yako, W. Hill, M. R. Jones, R. Maddison, Y. Fujita, and C. Hogan, “EphA2 Drives the Segregation of Ras-Transformed Epithelial Cells from Normal Neighbors,” *Current Biology*, vol. 26, pp. 3220–3229, dec 2016.
- [125] H. B. Taylor, A. Khuong, Z. Wu, Q. Xu, R. Morley, L. Gregory, A. Poliakov, W. R. Taylor, and D. G. Wilkinson, “Cell segregation and border sharpening by Eph receptorephrin-mediated heterotypic repulsion,” *Journal of The Royal Society Interface*, vol. 14, no. 132, p. 20170338, 2017.
- [126] P. Rodríguez-Franco, A. Brugués, A. Marín-Llauradó, V. Conte, G. Solanas, E. Batlle, J. J. Fredberg, P. Roca-Cusachs, R. Sunyer, and X. Trepát, “Long-lived force patterns and deformation waves at repulsive epithelial boundaries,” *Nature Materials*, no. September, 2017.
- [127] W. C. Hahn, C. M. Counter, a. S. Lundberg, R. L. Beijersbergen, M. W. Brooks, and R. a. Weinberg, “Creation of human tumour cells with defined genetic elements,” *Nature*, vol. 400, pp. 464–8, jul 1999.
- [128] W. J. Ashby, J. P. Wikswo, and A. Zijlstra, “Magnetically attachable stencils and the non-destructive analysis of the contribution made by the underlying matrix to cell migration,” *Biomaterials*, vol. 33, no. 33, pp. 8189–8203, 2012.
- [129] D. Who, R. Tyler, J. Harkness, D. Noble, A. Pond, R. Song, C. Oswald, and T. Master, “Control in Time And Really Definitely In Space of on oncogene using blue light,” *Journal of Psychic Papers*, vol. 10, no. 1, p. 388, 1989.
- [130] A. Tourovskaia, X. Figueroa-Masot, and A. Folch, “Long-term microfluidic cultures of myotube microarrays for high-throughput focal stimulation,” *Nature Protocols*, vol. 1, pp. 1092–1104, aug 2006.
- [131] M. Deforet, V. Hakim, H. G. Yevick, G. Duclos, and P. Silberzan, “Emergence of collective modes and tri-dimensional structures from epithelial confinement,” *Nature Communications*, vol. 5, p. 3747, may 2014.
- [132] M. Deforet, “Croissance et densification d ’ un épithélium en géométrie confinée,” *Thèse de Doctorat de l’Université Pierre et Marie Curie*, 2012.

- [133] J. H. Hanke, J. P. Gardner, R. L. Dow, P. S. Changelian, W. H. Brissette, E. J. Weringer, B. A. Pollok, and P. A. Connelly, "Discovery of a novel, potent, and Src family-selective tyrosine kinase inhibitor," *J Biol Chem*, vol. 271, no. 2, pp. 695–701, 1996.
- [134] P. A. Plé, T. P. Green, L. F. Hennequin, J. Curwen, M. Fennell, J. Allen, C. Lambert-Van Der Brempt, and G. Costello, "Discovery of a New Class of Anilinoquinazoline Inhibitors with High Affinity and Specificity for the Tyrosine Kinase Domain of c-Src," *Journal of Medicinal Chemistry*, vol. 47, no. 4, pp. 871–887, 2004.
- [135] R. Brandvold, M. E. Ste, C. C. Fox, and M. B. Soellner, "Development of a Highly Selective c-Src Kinase Inhibitor," *ACS chemical biology*, vol. 7, pp. 1393–1398, 2012.
- [136] J. Bain, H. McLauchlan, M. Elliott, and P. Cohen, "The specificities of protein kinase inhibitors: an update.," *The Biochemical journal*, vol. 371, no. Pt 1, pp. 199–204, 2003.
- [137] Z. A. Knight and K. M. Shokat, "Features of selective kinase inhibitors," *Chemistry and Biology*, vol. 12, no. 6, pp. 621–637, 2005.
- [138] Y.-p. Chong, K. K. Ia, T. D. Mulhern, and H.-c. Cheng, "Endogenous and synthetic inhibitors of the Src-family protein tyrosine kinases," *Biochimica et Biophysica Acta (BBA) - Proteins and Proteomics*, vol. 1754, pp. 210–220, dec 2005.
- [139] M. Kovács, J. Tóth, C. Hetényi, A. Málnási-Csizmadia, and J. R. Sellers, "Mechanism of Blebbistatin Inhibition of Myosin II," *Journal of Biological Chemistry*, vol. 279, pp. 35557–35563, aug 2004.
- [140] J. Kolega, "Phototoxicity and photoinactivation of blebbistatin in UV and visible light," *Biochemical and Biophysical Research Communications*, vol. 320, pp. 1020–1025, jul 2004.
- [141] A. Mikulich, S. Kavaliauskiene, and P. Juzenas, "Blebbistatin, a myosin inhibitor, is phototoxic to human cancer cells under exposure to blue light," *Biochimica et Biophysica Acta - General Subjects*, vol. 1820, no. 7, pp. 870–877, 2012.
- [142] M. Képiró, B. H. Várkuti, L. Végner, G. Vörös, G. Hegyi, M. Varga, and A. Málnási-Csizmadia, "Paranitroblebbistatin, the non-cytotoxic and photostable myosin II inhibitor," *Angewandte Chemie - International Edition*, vol. 53, no. 31, pp. 8211–8215, 2014.
- [143] S. Narumiya, T. Ishizaki, and M. Uehata, "Use and properties of ROCK-specific inhibitor Y-27632.," *Methods in enzymology*, vol. 325, no. 1998, pp. 273–84, 2000.
- [144] T. Ishizaki, M. Uehata, I. Tamechika, J. Keel, K. Nonomura, M. Maekawa, and S. Narumiya, "Pharmacological properties of Y-27632, a specific inhibitor of rho-associated kinases.," *Molecular pharmacology*, vol. 57, no. 5, pp. 976–983, 2000.
- [145] L. Chartier, L. L. Rankin, R. E. Allen, Y. Kato, N. Fusetani, H. Karaki, S. Watabe, and D. J. Hartshorne, "Calyculin-A increases the level of protein phosphorylation and changes the shape of 3T3 fibroblasts," *Cell Motility and the Cytoskeleton*, vol. 18, no. 1, pp. 26–40, 1991.
- [146] T. Kurisaki, R. G. Taylor, and D. J. Hartshorne, "Effects of the protein phosphatase inhibitors, tautomycin and calyculin-A, on protein phosphorylation and cytoskeleton of human platelets," *Cell Structure and Function*, vol. 20, no. 5, pp. 331–343, 1995.
- [147] J. Verweij and H. M. Pinedo, "Mitomycin C: mechanism of action, usefulness and limitations.," *Anti-cancer drugs*, vol. 1, no. August, pp. 5–13, 1990.
- [148] Y. Palom, G. Suresh Kumar, L. Q. Tang, M. M. Paz, S. M. Musser, S. Rockwell, and M. Tomasz, "Relative toxicities of DNA cross-links and monoadducts: New insights from studies of decarbamoyl mitomycin C and mitomycin C," *Chemical Research in Toxicology*, vol. 15, no. 11, pp. 1398–1406, 2002.
- [149] D. T. Tambe, C. C. Hardin, T. E. Angelini, K. Rajendran, C. Y. Park, X. Serra-Picamal, E. H. Zhou, M. H. Zaman, J. P. Butler, D. A. Weitz, J. J. Fredberg, and X. Trepap, "Collective cell guidance by cooperative intercellular forces.," *Nature materials*, vol. 10, no. 6, pp. 469–75, 2011.

- [150] S. A. Kim, C.-Y. Tai, L.-P. Mok, E. A. Mosser, and E. M. Schuman, "Calcium-dependent dynamics of cadherin interactions at cell-cell junctions," *Proceedings of the National Academy of Sciences*, vol. 108, pp. 9857–9862, jun 2011.
- [151] J. Rosenblatt, M. C. Raff, and L. P. Cramer, "An epithelial cell destined for apoptosis signals its neighbors to extrude it by an actin- and myosin-dependent mechanism," *Current Biology*, vol. 11, no. 23, pp. 1847–1857, 2001.
- [152] F. M. Hughes and J. A. Cidlowski, "Potassium is a critical regulator of apoptotic enzymes in vitro and in vivo," *Advances in Enzyme Regulation*, vol. 39, no. 98, pp. 157–171, 1999.
- [153] D. Choquet and H. Korn, "Mechanism of 4-aminopyridine action on voltage-gated potassium channels in lymphocytes," *The Journal of general physiology*, vol. 99, no. 2, pp. 217–240, 1992.
- [154] M. Ahmad, N. Grancher, M. Heil, R. C. Black, B. Giovani, P. Galland, Y. M. Road, M. A. Pennsylvania, P. G. Germany, and D. Lardemer, "Action Spectrum for Cryptochrome-Dependent Hypocotyl Growth Inhibition in Arabidopsis 1," *Plant physiology*, vol. 129, no. June, pp. 774–785, 2002.
- [155] R. Banerjee, E. Schleicher, S. Meier, R. M. Viana, R. Pokorny, M. Ahmad, R. Bittl, and A. Batschauer, "The signaling state of Arabidopsis cryptochrome 2 contains flavin semiquinone," *Journal of Biological Chemistry*, vol. 282, no. 20, pp. 14916–14922, 2007.
- [156] T. Instruments, "The pioneering work that led to the DMD."
- [157] M. J. Kennedy, R. M. Hughes, L. a. Peteya, J. W. Schwartz, M. D. Ehlers, and C. L. Tucker, "Rapid blue-light-mediated induction of protein interactions in living cells," *Nature methods*, vol. 7, pp. 973–5, dec 2010.
- [158] J. G. Rosas and M. Blanco, "A criterion for assessing homogeneity distribution in hyperspectral images. Part 1: Homogeneity index bases and blending processes," *Journal of Pharmaceutical and Biomedical Analysis*, vol. 70, pp. 680–690, nov 2012.
- [159] J. G. Rosas and M. Blanco, "A criterion for assessing homogeneity distribution in hyperspectral images. Part 2: Application of homogeneity indices to solid pharmaceutical dosage forms," *Journal of Pharmaceutical and Biomedical Analysis*, vol. 70, pp. 691–699, 2012.
- [160] J. G. Rosas, S. Armenta, J. Cruz, and M. Blanco, "A new approach to determine the homogeneity in hyperspectral imaging considering the particle size," *Analytica Chimica Acta*, vol. 787, no. October 2015, pp. 173–180, 2013.
- [161] T. Kanungo, D. Mount, N. Netanyahu, C. Piatko, R. Silverman, and A. Wu, "An efficient k-means clustering algorithm: analysis and implementation," *IEEE Transactions on Pattern Analysis and Machine Intelligence*, vol. 24, no. 7, pp. 881–892, 2002.
- [162] K. R. Poole, R. F. Taylor, and G. P. Wall, *Mixing Powders to Fine-scale Homogeneity: Studies of Batch Mixing*. AERE-R, UK Atomic Energy Authority Research Group, 1964.
- [163] M. Deforet, M. C. Parrini, L. Petitjean, M. Biondini, A. Buguin, J. Camonis, and P. Silberzan, "Automated velocity mapping of migrating cell populations (AVeMap)," *Nature Methods*, vol. 9, no. 11, pp. 1081–1085, 2012.
- [164] J. P. Butler, I. M. Tolic-Norrelykke, B. Fabry, and J. J. Fredberg, "Traction fields, moments, and strain energy that cells exert on their surroundings," *AJP: Cell Physiology*, vol. 282, pp. C595–C605, mar 2002.
- [165] R. W. Style, R. Boltyskiy, G. K. German, C. Hyland, C. W. MacMinn, A. F. Mertz, L. a. Wilen, Y. Xu, and E. R. Dufresne, "Traction force microscopy in physics and biology," *Soft matter*, vol. 10, pp. 4047–55, may 2014.
- [166] Y. Aratyn-Schaus, P. W. Oakes, J. Stricker, S. P. Winter, and M. L. Gardel, "Preparation of complaint matrices for quantifying cellular contraction," *Journal of visualized experiments : JoVE*, pp. 1–6, jan 2010.

- [167] J. R. Tse and A. J. Engler, "Preparation of hydrogel substrates with tunable mechanical properties.," *Current protocols in cell biology / editorial board, Juan S. Bonifacino ... [et al.]*, vol. Chapter 10, p. Unit 10.16, jun 2010.
- [168] A. Azioune, N. Carpi, Q. Tseng, M. Théry, and M. Piel, "Protein micropatterns: A direct printing protocol using deep UVs.," *Methods in cell biology*, vol. 97, pp. 133–46, jan 2010.
- [169] X. Trepap, M. R. Wasserman, T. E. Angelini, E. Millet, D. a. Weitz, J. P. Butler, and J. J. Fredberg, "Physical forces during collective cell migration," *Nature Physics*, vol. 5, pp. 426–430, may 2009.
- [170] L. Valon, A. Marín-Llauradó, T. Wyatt, G. Charras, and X. Trepap, "Optogenetic control of cellular forces and mechanotransduction," *Nature Communications*, vol. 8, p. 14396, feb 2017.
- [171] M. Moussus, C. D. Loughian, D. Fuard, M. Courçon, D. Gulino-Debrac, H. Delanoë-Ayari, and A. Nicolas, "Intracellular stresses in patterned cell assemblies," *Soft Matter*, 2014.
- [172] Q. Tseng, E. Duchemin-Pelletier, A. Deshiere, M. Balland, H. Guillou, O. Filhol, and M. Théry, "Spatial organization of the extracellular matrix regulates cell-cell junction positioning.," *Proceedings of the National Academy of Sciences of the United States of America*, vol. 109, pp. 1506–11, jan 2012.
- [173] S. J. Han, Y. Oak, A. Groisman, and G. Danuser, "Traction microscopy to identify force modulation in subresolution adhesions," *Nature Methods*, vol. 12, no. 7, pp. 653–656, 2015.
- [174] S. Garcia, *Maturation et mise en compétition de monocouches cellulaires*. PhD thesis, Université Pierre et Marie Curie - Paris 6, 2015.
- [175] J. Guck, S. Schinkinger, B. Lincoln, F. Wottawah, S. Ebert, M. Romeyke, D. Lenz, H. M. Erickson, R. Ananthakrishnan, D. Mitchell, J. Käs, S. Ulvick, and C. Bilby, "Optical Deformability as an Inherent Cell Marker for Testing Malignant Transformation and Metastatic Competence," *Biophysical Journal*, vol. 88, pp. 3689–3698, may 2005.
- [176] S. E. Cross, Y.-S. Jin, J. Rao, and J. K. Gimzewski, "Nanomechanical analysis of cells from cancer patients," *Nature Nanotechnology*, vol. 2, no. 12, pp. 780–783, 2007.
- [177] D. Wirtz, K. Konstantopoulos, and P. C. P. C. Searson, "The physics of cancer: the role of physical interactions and mechanical forces in metastasis," *Nature Reviews Cancer*, vol. 11, no. 512, p. 522, 2011.
- [178] R. W. Tilghman, C. R. Cowan, J. D. Mih, Y. Koryakina, D. Gioeli, J. K. Slack-Davis, B. R. Blackman, D. J. Tschumperlin, and J. T. Parsons, "Matrix rigidity regulates cancer cell growth and cellular phenotype," *PLoS ONE*, vol. 5, no. 9, pp. 1–13, 2010.
- [179] A. Fritsch, M. Höckel, T. Kiessling, K. D. Nnetu, F. Wetzels, M. Zink, and J. A. Käs, "Are biomechanical changes necessary for tumour progression?," *Nature Physics*, vol. 6, pp. 730–732, oct 2010.
- [180] S. C. Wei, L. Fattet, J. H. Tsai, Y. Guo, V. H. Pai, H. E. Majeski, A. C. Chen, R. L. Sah, S. S. Taylor, A. J. Engler, and J. Yang, "Matrix stiffness drives epithelial-mesenchymal transition and tumour metastasis through a TWIST1G3BP2 mechanotransduction pathway," *Nature Cell Biology*, vol. 17, no. 5, pp. 678–688, 2015.
- [181] "www.hek293.com."
- [182] M. Inada, G. Izawa, W. Kobayashi, and M. Ozawa, "293 Cells Express Both Epithelial As Well As Mesenchymal Cell Adhesion Molecules," *International Journal of Molecular Medicine*, vol. 37, no. 6, pp. 1521–1527, 2016.
- [183] J. Ranft, M. Aliee, J. Prost, F. Jülicher, and J.-F. Joanny, "Mechanically driven interface propagation in biological tissues," *New Journal of Physics*, vol. 16, p. 035002, mar 2014.
- [184] A. Yamada, R. Renault, A. Chikina, B. Venzac, I. Pereiro, S. Coscoy, M. Verhulsel, M. C. Parrini, C. Villard, J.-L. Viovy, and S. Descroix, "Transient microfluidic compartmentalization using actionable microfilaments for biochemical assays, cell culture and organs-on-chip," *Lab Chip*, vol. 16, no. 24, pp. 4691–4701, 2016.

- [185] M. Purschke, N. Rubio, K. D. Held, and R. W. Redmond, "Phototoxicity of Hoechst 33342 in time-lapse fluorescence microscopy," *Photochemical & Photobiological Sciences*, vol. 9, no. 12, p. 1634, 2010.
- [186] G. Lukinavičius, C. Blaukopf, E. Pershagen, A. Schena, L. Reymond, E. Derivery, M. Gonzalez-Gaitan, E. D'Este, S. W. Hell, D. Wolfram Gerlich, and K. Johnsson, "SiRHoechst is a far-red DNA stain for live-cell nanoscopy," *Nature Communications*, vol. 6, p. 8497, 2015.
- [187] G. D. O. Ramos, L. Bernardi, I. Lauxen, M. S. Filho, A. R. Horwitz, and M. L. Lamers, "Fibronectin Modulates Cell Adhesion and Signaling to Promote Single Cell Migration of Highly Invasive Oral Squamous Cell Carcinoma," *PloS one*, pp. 1–18, 2016.
- [188] A. F. Mertz, S. Banerjee, Y. Che, G. K. German, Y. Xu, C. Hyland, M. C. Marchetti, V. Horsley, and E. R. Dufresne, "Scaling of traction forces with the size of cohesive cell colonies," *Physical Review Letters*, vol. 108, no. 19, pp. 1–5, 2012.
- [189] C. Blanch-Mercader, R. Vincent, E. Bazellières, X. Serra-Picamal, X. Trepast, and J. Casademunt, "Effective viscosity and dynamics of spreading epithelia: a solvable model," *Soft Matter*, vol. 13, no. 6, pp. 1235–1243, 2017.
- [190] L. Cong, F. A. Ran, D. Cox, S. Lin, R. Barretto, N. Habib, P. D. Hsu, X. Wu, W. Jiang, L. A. Marraffini, and F. Zhang, "Multiplex Genome Engineering Using CRISPR/Cas Systems," *Science*, vol. 339, pp. 819–823, feb 2013.
- [191] K. Deisseroth, "Optogenetics," vol. 8, no. 1, pp. 26–29, 2011.
- [192] M. Yazawa, A. M. Sadaghiani, B. Hsueh, and R. E. Dolmetsch, "Induction of protein-protein interactions in live cells using light.," *Nature biotechnology*, vol. 27, pp. 941–5, oct 2009.
- [193] H. Liu, X. Yu, K. Li, J. Klejnot, H. Yang, D. Lisiero, and C. Lin, "Photoexcited CRY2 Interacts with CIB1 to Regulate Transcription and Floral Initiation in Arabidopsis," *Science*, vol. 322, pp. 1535–1539, dec 2008.
- [194] X. X. Zhou, H. K. Chung, A. J. Lam, and M. Z. Lin, "Optical Control of Protein Activity by Fluorescent Protein Domains," *Science*, vol. 338, pp. 810–814, nov 2012.
- [195] G. Guntas, R. A. Hallett, S. P. Zimmerman, T. Williams, H. Yumerefendi, J. E. Bear, and B. Kuhlman, "Engineering an improved light-induced dimer (iLID) for controlling the localization and activity of signaling proteins," *Proceedings of the National Academy of Sciences*, vol. 112, pp. 112–117, jan 2015.
- [196] D. Tischer and O. D. Weiner, "Illuminating cell signalling with optogenetic tools.," *Nature reviews. Molecular cell biology*, vol. 15, no. 8, pp. 551–8, 2014.
- [197] L. Valon, "Contrôle Optogénétique de la Polarité Cellulaire," *Thèse de Doctorat*, 2014.
- [198] O. Idevall-Hagren, E. J. Dickson, B. Hille, D. K. Toomre, and P. De Camilli, "Optogenetic control of phosphoinositide metabolism.," *Proceedings of the National Academy of Sciences of the United States of America*, vol. 109, pp. E2316–23, aug 2012.
- [199] D. L. Che, L. Duan, K. Zhang, and B. Cui, "The Dual Characteristics of Light-Induced Cryptochrome 2, Homo-oligomerization and Heterodimerization, for Optogenetic Manipulation in Mammalian Cells," *ACS Synthetic Biology*, vol. 4, no. 10, pp. 1124–1135, 2015.
- [200] L. J. Bugaj, A. T. Choksi, C. K. Mesuda, R. S. Kane, and D. V. Schaffer, "Optogenetic protein clustering and signaling activation in mammalian cells.," *Nature methods*, vol. 10, no. 3, pp. 249–252, 2013.
- [201] S. Lee, H. Park, T. Kyung, N. Y. Kim, S. Kim, J. Kim, and W. D. Heo, "Reversible protein inactivation by optogenetic trapping in cells," *Nature Methods*, vol. 11, pp. 633–636, may 2014.
- [202] A. Taslimi, J. D. Vrana, D. Chen, S. Borinskaya, B. J. Mayer, M. J. Kennedy, and C. L. Tucker, "Probing Protein Interaction and Function," *Nature Communications*, vol. 5, pp. 1–9, 2014.
- [203] V. Magidson and A. Khodjakov, "Circumventing Photodamage in Live-Cell Microscopy," in *Nano Letters*, vol. 6, pp. 545–560, sep 2013.

- [204] S. Douthwright and G. Sluder, “Live Cell Imaging: Assessing the Phototoxicity of 488 and 546nm Light and Methods to Alleviate it,” *Journal of Cellular Physiology*, no. September 2016, 2017.
- [205] Y. I. Wu, D. Frey, O. I. Lungu, A. Jaehrig, I. Schlichting, B. Kuhlman, and K. M. Hahn, “A genetically encoded photoactivatable Rac controls the motility of living cells,” *Nature*, vol. 461, pp. 104–108, sep 2009.
- [206] J. E. Toettcher, O. D. Weiner, and W. A. Lim, “Using Optogenetics to Interrogate the Dynamic Control of Signal Transmission by the Ras/Erk Module,” *Cell*, vol. 155, pp. 1422–1434, dec 2013.
- [207] Z. Feng, S. Nam, F. Hamouri, I. Aujard, B. Ducos, S. Vriza, M. Volovitch, L. Jullien, S. Lin, S. Weiss, and D. Bensimon, “Optical Control of Tumor Induction in the Zebrafish,” *Scientific Reports*, vol. 7, no. 1, p. 9195, 2017.
- [208] B. Kurien and R. Scofield, “Western blotting,” *Methods*, vol. 38, pp. 283–293, apr 2006.
- [209] R. Sakai, a. Iwamatsu, N. Hirano, S. Ogawa, T. Tanaka, H. Mano, Y. Yazaki, and H. Hirai, “A novel signaling molecule, p130, forms stable complexes in vivo with v-Crk and v-Src in a tyrosine phosphorylation-dependent manner,” *The EMBO journal*, vol. 13, no. 16, pp. 3748–3756, 1994.
- [210] L. Veracini, M. Franco, A. Boureau, V. Simon, S. Roche, and C. Benistant, “Two distinct pools of Src family tyrosine kinases regulate PDGF-induced DNA synthesis and actin dorsal ruffles,” *Journal of Cell Science*, vol. 119, pp. 2921–2934, jul 2006.
- [211] A. Hamadi, T. B. Deramandt, K. Takeda, and P. Rondé, “Src activation and translocation from focal adhesions to membrane ruffles contribute to formation of new adhesion sites,” *Cellular and Molecular Life Sciences*, vol. 66, no. 2, pp. 324–338, 2009.
- [212] G. T. Eisenhoffer, P. D. Loftus, M. Yoshigi, H. Otsuna, C.-B. Chien, P. A. Morcos, and J. Rosenblatt, “Crowding induces live cell extrusion to maintain homeostatic cell numbers in epithelia,” *Nature*, vol. 484, no. 7395, pp. 546–549, 2012.
- [213] E. Marinari, A. Mehonic, S. Curran, J. Gale, T. Duke, and B. Baum, “Live-cell delamination counterbalances epithelial growth to limit tissue overcrowding,” *Nature*, vol. 484, pp. 542–545, apr 2012.
- [214] R. Levayer, C. Dupont, and E. Moreno, “Tissue Crowding Induces Caspase-Dependent Competition for Space,” *Current Biology*, vol. 26, pp. 670–677, mar 2016.
- [215] S. M. Frisch and H. Francis, “Disruption of epithelial cell-matrix interaction induces apoptosis,” *J. Cell. Biol.*, vol. 124, no. 4, pp. 619–626, 1994.
- [216] D. Johnson, M. Agochiya, K. Samejima, W. Earnshaw, M. Frame, and J. Wyke, “Regulation of both apoptosis and cell survival by the v-Src oncoprotein,” *Cell death and differentiation*, vol. 7, no. 8, pp. 685–96, 2000.
- [217] T. E. Angelini, E. Hannezo, X. Trepat, M. Marquez, J. J. Fredberg, and D. A. Weitz, “Glass-like dynamics of collective cell migration,” *Proc Natl Acad Sci U S A*, vol. 108, no. 12, pp. 4714–4719, 2011.
- [218] B. I. Shraiman, “Mechanical feedback as a possible regulator of tissue growth,” *Proceedings of the National Academy of Sciences of the United States of America*, vol. 102, pp. 3318–23, mar 2005.
- [219] J.-P. Vincent, A. G. Fletcher, and L. A. Baena-Lopez, “Mechanisms and mechanics of cell competition in epithelia,” *Nature reviews. Molecular cell biology*, vol. 14, pp. 581–91, sep 2013.
- [220] S. R. K. Vedula, M. C. Leong, T. L. Lai, P. Hersen, A. J. Kabla, C. T. Lim, and B. Ladoux, “Emerging modes of collective cell migration induced by geometrical constraints,” *Proceedings of the National Academy of Sciences of the United States of America*, vol. 109, pp. 12974–9, aug 2012.
- [221] H. Aclouque, M. S. Adams, K. Fishwick, M. Bronner-Fraser, and M. A. Nieto, “Epithelial-mesenchymal transitions: the importance of changing cell state in development and disease,” *Journal of Clinical Investigation*, vol. 119, pp. 1438–1449, jun 2009.

- [222] R. Kalluri and E. G. Neilson, “Epithelial-mesenchymal transition and its implications for fibrosis,” *Journal of Clinical Investigation*, vol. 112, pp. 1776–1784, dec 2003.
- [223] J. J. Christiansen and A. K. Rajasekaran, “Reassessing Epithelial to Mesenchymal Transition as a Prerequisite for Carcinoma Invasion and Metastasis,” *Cancer Research*, vol. 66, pp. 8319–8326, sep 2006.
- [224] S. Heerboth, G. Housman, M. Leary, M. Longacre, S. Byler, K. Lapinska, A. Willbanks, and S. Sarkar, “EMT and tumor metastasis,” *Clinical and Translational Medicine*, vol. 4, no. 1, p. 6, 2015.
- [225] M. . Nieto, R. Y. Huang, R. A. Jackson, and J. P. Thiery, “Emt: 2016,” *Cell*, vol. 166, no. 1, pp. 21–45, 2016.
- [226] R. Y.-J. Huang, M. K. Wong, T. Z. Tan, K. T. Kuay, A. H. C. Ng, V. Y. Chung, Y.-S. Chu, N. Matsumura, H.-C. Lai, Y. F. Lee, W.-J. Sim, C. Chai, E. Pietschmann, S. Mori, J. J. H. Low, M. Choolani, and J. P. Thiery, “An EMT spectrum defines an anoikis-resistant and spheroidogenic intermediate mesenchymal state that is sensitive to e-cadherin restoration by a src-kinase inhibitor, saracatinib (AZD0530).,” *Cell death & disease*, vol. 4, p. e915, 2013.
- [227] B. Boyer, Y. Bourgeois, and M.-F. Poupon, “Src kinase contributes to the metastatic spread of carcinoma cells,” *Oncogene*, vol. 21, pp. 2347–2356, 2002.
- [228] M. Zeisberg and E. G. Neilson, “Biomarkers for epithelial-mesenchymal transitions,” *Journal of Clinical Investigation*, vol. 119, pp. 1429–1437, jun 2009.
- [229] S. J. Parsons and J. T. Parsons, “Src family kinases, key regulators of signal transduction,” *Oncogene*, vol. 23, pp. 7906–7909, oct 2004.
- [230] N. Kim, J. Kim, M. Lee, C. Kim, K.-y. Chang, and W. Heo, “Spatiotemporal Control of Fibroblast Growth Factor Receptor Signals by Blue Light,” *Chemistry & Biology*, vol. 21, pp. 903–912, jul 2014.
- [231] J. Liu, C. Huang, and X. Zhan, “Src is required for cell migration and shape changes induced by fibroblast growth factor 1,” *Oncogene*, pp. 6700–6706, 1999.
- [232] D. Ellison, A. Mugler, M. D. Brennan, S. H. Lee, R. J. Huebner, E. R. Shamir, L. A. Woo, J. Kim, P. Amar, I. Nemenman, A. J. Ewald, and A. Levchenko, “Cell-cell communication enhances the capacity of cell ensembles to sense shallow gradients during morphogenesis,” *Proceedings of the National Academy of Sciences of the United States of America*, vol. 113, no. 6, pp. E679–E688, 2016.
- [233] O. Cochet-Escartin, J. Ranft, P. Silberzan, and P. Marcq, “Border forces and friction control epithelial closure dynamics,” *Biophysical Journal*, vol. 106, no. 1, pp. 65–73, 2014.
- [234] S. R. K. Vedula, G. Peyret, I. Cheddadi, T. Chen, A. Brugués, H. Hirata, H. Lopez-Menendez, Y. Toyama, L. Neves de Almeida, X. Trepate, C. T. Lim, and B. Ladoux, “Mechanics of epithelial closure over non-adherent environments,” *Nature Communications*, vol. 6, p. 6111, 2015.
- [235] O. du Roure, A. Saez, A. Buguin, R. H. Austin, P. Chavrier, P. Silberzan, and B. Ladoux, “Force mapping in epithelial cell migration,” *Proceedings of the National Academy of Sciences*, vol. 102, pp. 2390–2395, feb 2005.
- [236] E. Anon, X. Serra-Picamal, P. Hersen, N. C. Gauthier, M. P. Sheetz, X. Trepate, and B. Ladoux, “Cell crawling mediates collective cell migration to close undamaged epithelial gaps,” *Proceedings of the National Academy of Sciences*, vol. 109, no. 27, pp. 10891–10896, 2012.
- [237] W. M. Bement, P. Forscher, and M. S. Mooseker, “A novel cytoskeletal structure involved in purse string wound closure and cell polarity maintenance,” *Journal of Cell Biology*, vol. 121, no. 3, pp. 565–578, 1993.
- [238] S. Begnaud, T. Chen, D. Delacour, R.-m. Mège, and B. Ladoux, “Mechanics of epithelial tissues during gap closure,” *Current Opinion in Cell Biology*, vol. 42, pp. 52–62, oct 2016.
- [239] V. Nier, S. Jain, C. T. Lim, S. Ishihara, B. Ladoux, and P. Marcq, “Inference of Internal Stress in a Cell Monolayer,” *Biophysj*, vol. 110, no. 7, pp. 1625–1635, 2016.

- [240] F. Ingremeau, M. E. Dolega, J. Gallagher, I. Wang, G. Cappello, and A. Delon, “Optical sensing of mechanical pressure based on diffusion measurement in polyacrylamide cell-like barometers,” *Soft Matter*, vol. 13, pp. 4210–4213, 2017.
- [241] T. Lämmermann and M. Sixt, “Mechanical modes of ‘amoeboid’ cell migration,” *Current Opinion in Cell Biology*, vol. 21, no. 5, pp. 636–644, 2009.
- [242] N. V. Krakhmal, M. V. Zavyalova, E. V. Denisov, S. V. Vtorushin, and V. M. Perelmuter, “Cancer Invasion: Patterns and Mechanisms,” *Acta naturae*, vol. 7, no. 2, pp. 17–28, 2015.
- [243] N. G. Gurskaya, V. V. Verkhusha, A. S. Shcheglov, D. B. Staroverov, T. V. Chepurnykh, A. F. Fradkov, S. Lukyanov, and K. A. Lukyanov, “Engineering of a monomeric green-to-red photoactivatable fluorescent protein induced by blue light,” *Nature Biotechnology*, vol. 24, no. 4, pp. 461–465, 2006.
- [244] D. M. Chudakov, S. Lukyanov, and K. A. Lukyanov, “Tracking intracellular protein movements using photoswitchable fluorescent proteins PS-CFP2 and Dendra2,” *Nature protocols*, vol. 2, no. 8, pp. 2024–2032, 2007.

Résumé

Lors du développement d'une tumeur au sein d'un tissu, les cellules cancéreuses se retrouvent entourées par les cellules saines. Les interactions entre ces deux types cellulaires, transformé et normal, jouent un rôle important dans le devenir de la tumeur, mais restent à ce jour mal comprises. L'objectif de cette thèse a été de mettre en place des systèmes *in vitro* qui permettent d'étudier les interactions entre une population de cellules normales et une population de cellules transformées.

Nous avons tiré profit d'une lignée de cellules épithéliales sensibles à la lumière, élaborée par Olivier Destaing (IAB, Grenoble). Lorsqu'elles sont exposées à la lumière bleue, ces cellules surexpriment la protéine Src, connue pour être surexprimée dans de nombreux cancers. Sinon, elles gardent un phénotype normal. L'utilisation de ces cellules, appelées « OptoSrc », combinée à un dispositif optique, permet de créer des tissus mosaïques dans lesquels le motif des cellules mutées est déterminé par le motif d'illumination bleue. Notre système présente plusieurs avantages : le contrôle dans le temps et dans l'espace du motif de cellules transformées, mais aussi l'activation graduelle et réversible de l'oncoprotéine.

Nous avons montré qu'en illuminant dans le bleu un îlot circulaire de cellules au sein d'une monocouche OptoSrc, les cellules activées s'extrudent collectivement, donnant naissance à un agrégat tri-dimensionnel cohésif surplombant la monocouche. Nous pouvons contrôler la taille et le temps d'apparition de ce sphéroïde en ajustant respectivement l'aire éclairée et la fréquence d'illumination. De plus, ce phénomène d'extrusion collective est réversible lorsque le stimulus de lumière bleue s'arrête. Finalement, nous avons montré que la formation de cet agrégat s'accompagne d'une diminution des E-cadhérines à la membrane, et de l'apparition de la vimentine, pour les cellules éclairées. Nos résultats suggèrent qu'un groupe de cellules surexprimant la protéine Src, au sein d'une monocouche de cellules normales, subit une transition épithéliale-mésenchymateuse partielle.

Mots Clés

Compétition cellulaire, oncogène Src, système optogénétique CRY2-CIBN, transition épithéliale-mésenchymateuse, comportements collectifs.

Abstract

During the development of a tumour in a tissue, the cancer cells are surrounded by healthy cells. The interactions between these two cell types, transformed and normal, play an important role in the tumour stability, but remain to this day poorly understood. The aim of this thesis was to establish *in vitro* assays to study the interactions between populations of normal and transformed cells.

We benefited from a light-sensitive cell line, constructed by Olivier Destaing (IAB, Grenoble). When they are exposed to blue light, these cells overactivate the protein Src, which is known to be overexpressed in many cancers. Otherwise, they keep a normal phenotype. Using these cells, called "OptoSrc", in combination with an optical setup, we are able to create mosaic tissues in which the pattern of mutated cells is determined by the blue illumination pattern. Our system has several advantages: a selective control in time and space of the group of transformed cells, and a gradual and reversible activation of the oncoprotein.

We have shown that when we illuminate a circular islet of cells from a monolayer of OptoSrc cells, the activated cells were collectively extruded, resulting in a cohesive three-dimensional aggregate on top of the monolayer. We can control the size and appearance time of this spheroid by tuning, respectively, the area and frequency of illumination. Besides, this collective extrusion is reversible when the blue light stimulation is stopped. Finally, we have shown that the formation of this three-dimensional aggregate coincides with the loss of E-cadherin at the membrane, as well as the apparition of vimentin, for the illuminated OptoSrc cells. Our results suggest that a group of cells overexpressing the protein Src, in a monolayer of normal cells, undergoes a partial epithelial-to-mesenchymal transition.

Keywords

Cell competition, Src oncogene, optogenetic system CRY2-CIBN, Epithelial-to-Mesenchymal Transition, collective behaviours